The Invisible Mediator: Systemic Depolarization Modulates Local and Rapid Transcription, Cellular Mitosis, and Stem Cell Fate

By:

Devon Charles Cardoso Davidian

B.S. (University of California, Merced) 2012

DISSERTATION

Submitted in satisfaction of the requirement for the degree of

DOCTORATE OF PHOLOSOPHY

in

QUANTITATIVE SYSTEMS BIOLOGY

in the

OFFICE OF GRADUATE STUDIES

of the

UNIVERSITY OF CALIFORNIA, MERCED

Principal Investigator: Nestor J. Oviedo

Committee Members: Michael Cleary
Ariel L Escobar
Richard Nuccitelli
Min Zhao

The Dissertation of Devon Charles Cardoso Davidian is approved by, and is accepted in the quality and form for publication on microfilm and electronically:

Dr. Min Zhao

Dr. Richard Nuccitelli

Dr. Ariel L. Escobar

Dr. Mike Cleary Committee Chairperson

University of California, Merced

Dedication

I would like to dedicate this body of work to my family, friends, and my fiancé. All of whom have stuck by me and have provided support and encouragements throughout the years. I would also like to acknowledge my Advisor Dr. Nestor Oviedo who has always been an excellent source of guidance and knowledge during both my undergraduate and graduate career. In addition, the members of my committee, Dr. Mike Cleary, Dr, Ariel Escobar, Dr. Richard Nuccitelli, and Dr. Min Zhao who have all provided welcomed advice and suggestions during my graduate research here at University of California Merced. I would like to conclude with an additional thank you to Dr. Ariel Escobar for his generous actions in allowing me to have access to resources and experimental technique that have substantially bolstered my research experience, data collection, and overall development during my studies as a graduate student.

Table of Contents

List of Figures/Tables

Chapter 1

Chapter 2

Chapter 3

Chapter 4

Personal CV

DEVON C DAVIDIAN

5200 N Lake Rd., Merced CA 95348 | 209-500-8919 | d2davidian@gmail.com

EDUCATION

BS in Bioengineering **January 2007 – January 2012**
University of California, Merced

Ph.D. in Quantitative Systems Biology **2012 – 2018**
University of California, Merced

AWARDS

Dean's Honor List **January 2010 – January 2011**
UC Merced Summer Research Fellowship **January 2013**
Outstanding research innovation (QSB Fall Retreat) **November 2014**

RESEARCH EXPERIENCE

Undergraduate Research
Lab/Principal Investigator: Dr. Nestor Oviedo **2010-2012**
Undergraduate research included bioelectric assays assessing planarian stem cell migration when exposed to physiological equivalent applied electric fields. During this program I developed an understanding of fundamental bioelectric and use of related data analysis software.

Quantitative Systems Biology Ph.D. Research
Lab/Principal Investigator: Dr. Nestor Oviedo **2012-2018**
My research focus was bioelectrical regulation of stem cells with an emphasis on gene regulation using low magnitude steady state applied electric fields. Domain over a wide array of electrophysiological techniques/assays, engineering/fabrication of electrophysiological devices (working closely with Dr. Ariel Escobar). In addition, I mastered and optimized an array of molecular based assays for the planarian model including: PCR, Electrophoresis, RNA Interference, immune-fluorescent labeling, In Situ Hybridization (fluorescent and chromogenic), bacteria and stem cell culturing Techniques, cDNA/Riboprobe Synthesis, and the use of various data analysis/graphic design software.

TEACHING EXPERIENCE

Teaching Assistant (Introduction to General Chemistry I)
University of California, Merced **August 2012 – December 2012**
Lead a discussion where students could pose questions about the material covered in class. I was also tasked with preparing lecture to reinforce material covered by the instructor. In addition, I created and graded all course assessments.

Teaching Assistant (Introduction to Biology I)
University of California, Merced **January 2013 – May 2013**
I oversaw conducting the wet lab experiments and insuring the experiments were done safely and properly through the semester. In addition, I created and graded all course assessments.

Teaching Assistant (Introduction to General Chemistry II)
University of California, Merced **August 2013 – December 2017**
I am tasked with conducting the wet lab experiments and insuring the experiments are done safely and properly through the semester. I graded and submitted all quizzes and lab reports.

Teaching Assistant (Tissue Engineering)

University of California, Merced **January 2014 – May 2014**

I held office hours once a week where students could pose questions about the covered material. I graded course work.

Teaching Assistant (Human Physiology)
University of California, Merced **January 2017 – May 2018**

I held office hours once a week where students could pose questions about the covered material. I graded course work.

PUBLICATIONS

TOR Signaling Distinguishes Planaria Stem Cell Populations and Control Localized and Organismal Growth
T. Peiris, T.H., Weckerle, F., Ozamoto, E., Ramirez, D., Davidian, D., García-Ojeda, M.E., and Oviedo, N.J.
Journal of Cell Science **2012**

Regional signals in the planarian body guide stem cell fate in the presence of DNA instability
T. Peiris, T.H., Ramirez, D., Barghouth, P.G., Ofoha, U., Davidian, D., Weckerle, F., and Oviedo, N.J.
Development **2016**

Direct Current Stimulation Induces Rapid Transcription and Enhances DNA Integrity in the Planaria
Davidian, D., Bargouth, P.G., Rojas, S., Ziman, B., Legro, M., Macial, E., Pham, I., Escobar, A.L., Oviedo, N.J.
Drafting for *Science* **2018**

ABSTRACTS AND PRESENTATIONS

TOR Signaling Distinguishes Planaria Stem Cell Populations and Control Localized and Organismal Growth
T. Harshani Peiris, Frank Weckerle, Elyse Ozamoto, Daniel Ramirez, Devon Davidian, Marcos Garcia-Ojeda, and Nestor Oviedo. Gordon Science Conferences in Tissue Repair and Regeneration, New London, NH USA. **2012**

Direct Current Electric Fields Mobilize Stem Cell Response during Wound Healing in vivo
Devon Davidian, Ariel L Escobar and Nestor J Oviedo. UC Merced Fall Quantitative Systems Biology Retreat 2014, Merced, CA USA. *(Judged and awarded for outstanding research innovation)* **2014**

Bioelectrical Regulation of Stem Cell Behavior in Planarians
Devon Davidian, Carolos Gomez, Ivy Pham, Ariel L Escobar and Nestor J Oviedo. 3rd North American Planarian Meeting 2015, Chicago, IL USA. **2015**

MEMBERSHIPS

Society of Developmental Biology

Acknowledgements

I would like to give thanks to my fellow graduate student colleagues who have helped me acquire much needed data in addition to providing me with exceptional companionship and many good memories over the years.

Abstract

The need for non-invasive therapies to address longstanding healthcare challenges is ever-present. Every year, cancer patients undergo harsh radiation therapies to combat the growth of aggressive tumors. Improving recovery periods of these patients is a challenge faced by healthcare professionals at large. Using the planarian model, we developed techniques to isolate adult planarian stem cells *in-vivo* and used this method to study the effects of steady-state direct current (DCS^S) in the complexities of the adult model organism. We discovered that exposure of transplanted planaria to DCS^S resulted in an overall resurgence of stem cell populations within distal irradiated tissues in manner which is sensitive to cytosolic Ca^{2+} influx. Within minutes of DCS^S exposure, planarian stem cell-specific gene expression can be seen returning to lethally irradiated tissue. Moreover, DCS^S activates DNA repair mechanisms leading to improved DNA integrity within cells exposed to γ-irradiation. However, the effects of DCS^S on planarian stem cells are not restricted to irradiated tissues as they were found to significantly impact planarian stem cell-specific gene expression and mitotic distribution within unirradiated planaria. This work demonstrates the capacity for DCS^S to effectively repopulate damaged irradiated tissues with cycling stem cells through mechanisms which are sensitive to Ca^{2+} regulation.

Bioelectric governance of stem cells using DCS^S is made possible by existing networks within stem cells which are designed to respond to naturally occurring bioelectric signals. A common endogenous steady-state electrical signal occurs during tissue injury by which the introduction of epithelial lesions consequently establishes a steady-state electric current. Thus, we sought to better understand the still obscure role of injury induced currents in the initiation and establishment of well-known wound response characteristics. To simulate injury induced currents without introducing physical injury, we developed new techniques to precisely expose planarian epithelial tissues to doses of the nonionic detergent, triton X-100 (trtx), resulting in local tissue depolarization. As a result, trtx-mediated tissue depolarization induced systemic mitotic responses from planarian stem cells while simultaneously generating transcriptomic responses of known planarian wound response genes, many of which closely resemble temporal patterns previously reported during actual tissue injury.

In contrast to DCS^S, whose cellular interactions are restricted to the outer cell membrane, pulsed direct current stimulation (DCS^P) is a common technique whose current effectively bypasses the highly resistive cell membrane and has been used by researchers as a tool to influence the behavior of cells. Exposure of planaria to DCS^P lead to dramatic changes in stem cell proliferation dynamics and strongly impacted the large-scale morphology of differentiated neural tissues. In addition, planarian DCS^P effectively reprogrammed tissue identity during planaria regeneration, resulting in complete anterior-posterior (AP) reversal. Surprisingly, signs of AP reprograming caused by DCS^P can be seen in the initial stages of planarian regeneration, where expression of anterior specific gene *smed-notum* is missing in the anterior and inappropriately expressed in the posterior of regenerating DCS^P planaria. In summary, we implemented a multifaceted approach that utilizes *in-vivo* techniques to demonstrate the potential for bioelectric signaling to mediate stem cell-related functions within the adult planaria model organism.

List of Abbreviations

Ca^{2+}	Calcium
Na^{2+}	Sodium
K^{+}	Potassium
Cl^{-}	Chloride
Ca_v	Voltage Gated Calcium Channel
Na_v	Voltage Gated Sodium Channel
K_v	Voltage Gated Potassium Channel
VGIC	Voltage Gated Ion Channel
RMP	Resting Membrane Potential
TEP	Transepithelial Potential
TEPD	Transepithelial Potential Difference
V_{mem}	Membrane Potential
DCS	Direct Current Stimulation
DCS^P	Pulsed Direct Current Stimulation
DCS^S	Steady-State Direct Current Stimulation
pDCS	Planarian Direct Current Stimulation
$pDCS^S$	Planarian Steady-State Direct Current Stimulation
$pDCS^P$	Planarian Pulsed direct Current Stimulation
AC	Alternating Current
DC	Direct Current
TENS	Transcutaneous Electrical Nerve Stimulation
ATP	Adenosine Triphosphate
NIC	Nicardipine
Thaps	Thapsigargin
EF	Electric Field
DCEF	Direct Current Electric Field
ACEF	Alternating Current Electric Field

EF_{IM}	Intermembrane Electric Field
V	Volts
C	Capacitance
R	Resistance
I	Current
I_C	Capacitive Current
I_R	Resistive Current
SERCA	Smooth Endoplasmic Reticulum Ca^{2+} ATPase
Na^+/K^+ ATPase	Sodium Potassium ATPase
cAMP	Cyclic Adenosine Monophosphate
IP_3	Inositol (1,4,5) triphosphate
PIP2	Phosphoatidylinositol (4, 5) Bisphosphate
PLC	Phospholipase C
DAG	Diacylglycerol
PI	Phosphoinositol
LMP	Low Melting Point Agarose
HMP	High Melting Point Agarose
IEG	Immediate Early Gene
PC2	Prohormone Convertase 2
DNA	Deoxyribonucleic Acid
RNA	Ribonucleic Acid
mRNA	Messenger Ribonucleic Acid
GJ	Gap Junction
DDR	DNA Damage Response
HR	Homologous Recombination
NHEJ	Non-Homologous End Joining
FACS	Fluorescent Activated Cell Sorting
IHC	Immunohistochemistry

Preface

Bioelectric signaling is a prominent regulator of cellular processes guiding cells during organismal development[1,2], adult tissue wound healing[3–5], large-scale regeneration[6–8]. Each cell, whether embryonic or terminally differentiated, is equipped with ion channels designed to generate and maintain what is known as a cellular resting membrane potential (RMP). Activities of transmembrane ion channels, and the ions they conduct, are governed by physical laws; making them sensitive to changes in the electrical landscape of their native microenvironments. Due to the rapid nature of bioelectric signaling, many cells have evolved to use this signaling paradigm to transmit information across long distances (i.e. neurons). Neurons transmit electrical signals while target cells are equipped to translate electrical stimuli into molecular responses, a process which altogether can be executed on a rapid time scale[9]. However, electrical signaling is not limited to neuronal circuits, tissues can experience changes in their endogenous electrical properties; changes which are then passed on to native cells within the tissue. This form of bioelectrical signaling is the focus within this body of work. We demonstrate that through the manipulation of large-scale and local endogenous bioelectric properties of tissues, we can achieve significant effects on the behavior of various cells.

Changes in the electrical properties of tissues occur naturally in several ways, one common example is injury. When injury occurs in a tissue (i.e. a cut or lesion) there is an immediate change in the electrical properties of the tissue at and around the injury site. More specifically, the introduction of a low resistance pathway (i.e. the lesion) between regions normally separated by healthy sheets of epithelial cells allows for the unrestricted flow of previously separated ions down their electrochemical gradients generating significant electrical currents/potentials[4,10]. These injury induced potentials are responsible for generating local changes in the electrical topography of tissue[4,10,11]. Interestingly, both excitable and non-excitable cells have reported responses to even minor electrical fluctuations in their local microenvironments. These responses can result in changes mitotic activity[12–15], guided cell migration[16–18], cellular differentiation dynamics[12,19,20], tissue specification/identity, organ morphology, and more. In addition to injury induced bioelectric signaling, tissues naturally modify their own endogenous bioelectric properties. This is most readily observed during embryonic development where substantial currents can be measured leaving the embryo at specific regions prompting specific developmental events[1,2,8]. Moreover, embryonic cells exhibit similar responses to changes in bioelectric landscapes as previously stated in adult tissues. Needless to say, bioelectrical signaling potentially regulates a multitude of cellular processes spanning many different cell types, not just electrically adept excitable cells.

The discovery of endogenous potentials, and their capacity to govern cell behavior, lead to the early development of techniques dating back to the late 1800s which use imposed electric currents to influence various biological processes[21]. Despite promising results, esteem for such techniques has, up until recently, been underwhelming. In the present day, a multitude of publicly available bioelectric devices have been developed to address several physical and psychological conditions. A common modality of electric stimulation used in these bioelectric devices is known as direct current stimulation (DCS). DCS can be in the form of steady state DCS (DCS^S) or pulsed DCS (DCS^P) each having their own unique effects on cell behavior. For example, devices administering DCS^S have been used to improve spinal cord injuries[22–24], chronic diabetic ulcers[25,26], Parkinson induced tremors[27,28], and a multitude of mental health conditions[28,29]. Likewise, pulsed direct current stimulation devices are being used to enhance healing nonunion bone

fractures[30–32], muscle growth[33,34], reduce muscle pain and fatigue[35–38], guide cellular differentiation[34,39,40], and much more. Although electrotherapy is a growing practice, little is understood in how these electrical currents interact and stimulate many of these reported cellular responses. Moreover, many documented effects are were gained from *in-vitro* analysis leaving much left to be understood in how these currents effect large scale *in-vivo* tissue networks. Using the planaria, *Schmidtea mediterranea*, we investigated the effects of DCS^{S} and DCS^{P} ($pDCS^{S/P}$) *in-vivo* and assess both organismal and cellular dynamics following each electric stimulation modality. From this work we discovered that using ***DCS^{S} we were able to reestablish neoblastic activity within tissues exposed to lethal doses of γ-irradiation which culminate in significant recapitulation of cell proliferation. Using membrane permeabilizing detergents we found the planarian neoblast, and characteristic wound response mechanics, are activated in response to regional tissue depolarization. In addition to steady state electrical influences, exposing planaria to pulsed DCS dramatically influences the natural distribution of dividing stem cells and reprogrammed endogenous anterior-posterior (AP) tissue identity during large scale anterior/posterior tissue regeneration.***

Chapter 2

Administering electric currents to tissues within a live animal is a challenging prospect as it requires methods of immobilization that are strong enough to inhibit gross mobility while gentle enough as to not introduce harm to the organism. In addition to this requirement, electrical stimulation requires full functionality of cells and thus, pharmacological or chemically induced anesthesia which may interfere with bioelectric signaling mechanisms were avoided. **In this chapter we describe the methods we have developed and implemented to achieve full-fledged planarian immobilization capable of housing the organism for brief (hours) or extended periods (days) of time.** We use a qualitative approach to assess the efficacy of our immobilization techniques which demonstrate that immobilized planaria are not negatively impacted and quickly recover their natural sensorial responses. In addition, we note that planaria subjected to agar immobilization are virtually indistinguishable from planaria who have not received treatment, indicating that immobilized planaria do not experience physical harm during or throughout the immobilization process. We believe these techniques have broad applications in planarian biology and can be used for a variety of studies which require healthy noninvasive means of planarian immobilization.

Chapter 3

In this chapter we explore various $pDCS^{S}$ induced transcriptional responses and elucidate **the hypothesis that the observed stem cell-specific $pDCS^{S}$ transcriptional activity is mediated by Ca^{2+} flux.** Using a specific L-type voltage gated calcium channel inhibitor (Nicardipine), we assessed the importance of Ca^{2+} flux through these channels and concluded it was vital in $pDCS^{S}$-mediated transcription. Ca^{2+}-mediated transcription was further supported by evidence demonstrating $pDCS^{S}$ induced transcription occurs on a rapid time scale and induces known immediate early genes. Immediate early gene transcription mechanisms are known to be regulated, in part, by changes in intracellular Ca^{2+} concentration; including those mediated by flux through L-type Ca_v. To investigate transcriptional responses within transplanted planaria exposed to $pDCS^{S}$ we assessed the origin of the transcriptional activity occurring within γ-irradiated tissues and discovered that neoblast specific gene expression (*smed-piwi-1*) originates from the irradiated host tissues. In the following chapter we elaborate on specific findings within chapter 3 and

explore the capacity for DCS to translate transcriptional responses into meaningful cellular activities.

Chapter 4

In this chapter we investigate the potential for DCS^S-mediated transcription of known DNA damage response (DDR) genes within irradiated tissues and their potential to enhance DNA repair/integrity. To test **the hypothesis that $pDCS^S$-mediated rapid transcription of DDR genes results in active DNA repair** we focused on the effects of 60min $pDCS^S$ transplanted planaria and restricted our analysis to hosts' tail tissues of the transplanted planaria. We evaluated expression levels of DDR genes and assessed their cellular localization following $pDCS^S$. It was found that, along with increased *smed-Rad51* expression, 60min of $pDCS^S$ significantly increased levels of nuclear RAD51 protein within cells from tail tissues. Propensity for DNA repair activities mediated by the observed increases in nuclear RAD51 following $pDCS^S$ was measured using COMET assay which revealed significant decreases in levels of DNA double stranded breaks within planaria subjected to 60min of $pDCS^S$. Looking beyond DNA damage, we addressed changes in cell cycle dynamics following $pDCS^S$ using FACS analysis and found that $pDCS^S$ exposure shifted the distribution of cycling cells from S phase arrest into G_2/M, which was supported by gene expression profiles of specific cyclin genes, regulators of cell cycle progression. Taking this a step further we found that $pDCS^S$ planaria exhibited the capacity to harbor mitotically competent neoblasts within these severely irradiated tissues as demonstrated by whole mount immunohistochemistry of phospho-histone H-3. The upcoming chapter assesses the effects of $pDCS^S$ exposure on intact homeostatic planaria who have received no treatment aside from agar immobilization.

Chapter 5

In this chapter we leave behind the transplanted planaria model to explore effects of systemic $pDCS^S$ exposure in the context of normal planarian homeostasis. To address potential bioelectric regulation of planarian stem cells, **we investigate the potential impacts that equivalent $pDCS^S$ exposures have on neoblast specific functions throughout the planarian body in the absence of exogenous manipulations such as irradiation/transplantation**. Interestingly, we found that $pDCS^S$ significantly redistributes normal endogenous mitotic activity leading to mitotic distributions patterns which favor lateral tissues over medial tissues. In addition to this finding we discover that $pDCS^S$ exposure can be used to effectively downregulate overall neoblast proliferation in a polarity specific manner. At the transcriptional level, $pDCS^S$ effectively redistributes endogenous *smed-piwi-1* gene expression to favor lateral tissues while effectively downregulating *smed-piwi-1* gene expression in a polarity dependent manner, resembling the effects of mitosis.

Later in this chapter, we leave the area of exogenous applied currents to investigate the role of tissue depolarization during the initiation of wound healing responses. To evaluate the role of injury induced tissue depolarization during wound healing initiation we devised a technique which allowed us to subjectively and precisely depolarize planarian tissue without inflicting physical injury or damage. Our technique involved localized exposure to concentrated detergent (triton X-100; trtx) to induce regionally cellular membrane depolarization to test **the hypothesis that dysregulation of regional cellular resting membrane potential will elicit characteristics of the planarian wound response.** To our excitement, regional tissue depolarization was enough to recapitulate planarian specific wound responses in the absence of physical

injury demonstrating effective uncoupling of physical injury and the subsequent wound response in planaria. More specifically, we found that neoblast mitosis following trtx exposure exhibits oscillatory response along the planarian AP axis, a response that is consistent and dependent on location of trtx exposure along the AP axis. Moreover, *smed-piwi-1* expression appears to resemble this mitotic response exhibiting unique AP dynamics which are dependent on trtx exposure locus. Interestingly, when measuring the expression of known planarian wound response genes, we found that trtx exposure induced characteristic transcriptional responses from these known wound response genes. Therefore, we conclude that trtx-mediated tissue depolarization is an adequate signal to mount tissue specific wound responses and acts on known wound induced mechanisms. In addition, we speculate that localized tissue depolarization exploits both local and long range signaling mechanisms to generate observed responses. In the remaining chapter we investigate the effects of pulsed direct currents on planaria tissue homeostasis and regeneration.

Chapter 6

In previous chapters, the focus of stimulation was restricted to a steady-state modality however, many devices and therapies utilize pulsed direct currents as a means to induce a desired biological effect. This is due to the properties of pulsed direct current allowing them to effectively penetrate the resistive cell plasma membrane and directly influence intracellular activities. Therefore, we dedicated this chapter to the investigation of pulsed direct current stimulation in the planaria ($pDCS^P$) and its potential govern various cellular functions. **We hypothesize that the stimulatory nature of $pDCS^P$ will impact neoblast specific signaling activity of planarian orthogonal muscle fibers ultimately leading to changes in neoblast specific behaviors such as cellular proliferation and large-scale regeneration.** To test this hypothesis, we first addressed the mitotic dynamics in planaria exposed to $pDCS^P$ and found that 6hrs of $pDCS^P$ resulted in systemic downregulation of proliferation, shifting the distribution of dividing neoblasts to substantially favor distal anterior tissues. In addition to this finding, $pDCS^P$ exposure over the course of regeneration rewires endogenous AP identity signaling resulting in planaria with flipped anatomical specification. These results were further supported by the discovery that $pDCS^P$ exposure reorients known anterior specific marker notum to regenerating tail regions of trunk animals within 6hrs, a persistent effect which ultimately lead to planaria perfect anatomical AP reorientation. Interestingly, the overriding nature of $pDCS^P$ are so potent that anatomical AP reorientation was observed within the non-regenerating differentiated tissue of the pharynx. Reorientation of the planarian pharynx was observed over the course of $pDCS^P$-mediated AP reversal during which the pharynx was forced to undergo large-scale morphological changes to resemble the new identity of regenerating planaria. This result reinforces our previous finding showing the significant morphological impacts $pDCS^P$ have on intact non-regenerating planaria.

All in all, this body of work encompasses interesting results which exhibit the potential for electrical stimulation to regulate cell behavior *in-vivo* in the adult planarian model. Results which potentially have far reaching applications in the development of non-invasive therapies to combat various degenerative diseases and improve the field of regenerative medicine.

CHAPTER ONE

BACKGROUND

Electrical Properties of Eukaryotic Cells

The human body, and its diverse cell populations, have evolved mechanisms to signal electrically. Bioelectric signaling is one of, if not the, most rapid signaling paradigms cells exploit to transmit stimuli across the body in mere fractions of a second. The importance of electrical signaling in cellular biology can be seen in its ever-present integration in fundamental aspects of cellular function. For example, rod cells in the eye constantly generate a steady current known as the 'dark' current which, being sensitive to absorbed light by rhodopsin, regulate cGMP levels, eventually leading to changes in vesicle secretion and signal transmission[41–43]. Series of neural networks send electrical signals across the body, packing and unpacking sequences of electrical data and then translating the various stimuli into cellular molecular responses[44–46]. Electrical signals tightly coordinate contraction of the heart, a vital process for all human beings[47,48]. The electrical signaling in this organ is so powerful, it can be measured on the surface of the skin, far from the heart, using an electrocardiogram[49]. Skeletal muscle, powering the movement of an otherwise immobile skeleton, function primarily through electrical signaling capable of translating neural input and relaying electrical signals throughout the long muscle fibers resulting in contraction[50–52]. Even prokaryotic like mitochondria, responsible for producing much of the energy within cells, in the form of ATP, rely on a powerful electrical field across the inner membrane to drive proton flux, thus producing ATP[53]. Dysfunction of these bioelectric processes, and functional ion channels conducting these signals, can lead to severe medical conditions termed channelopathies, many of which are severe and may lead to death[54–56]. The biological importance of endogenous electrical currents is difficult to understate.

Among the many fascinating characteristic properties of eukaryotic cells there is one, found in nearly all eukaryotic cells, which is grossly overlooked; their innate bioelectric properties. Eukaryotic cells are efficient, nearly perfect, batteries that function and respond dynamically to their ever-changing micro-environments[12,57,58]. The essence of a cells bioelectric properties is founded in its ability to separate and transport charged ions across the cell membrane phospholipid bilayer. Separation of charge across the phospholipid bilayer (i.e. electrochemical gradient), generated by the transport of ions through trans-membrane proteins, generates electric potential differences across the lipid bilayer[57]. Electric potential differences across the cell membrane at rest, a property shared by all living cells and organelles, is defined as the resting membrane potential (RMP)[57]. All cells in the body possess and maintain their own unique RMPs. With all cells possessing electric properties such as RMPs allows them to be sensitive to regulation by bioelectric signlaing networks. This understanding has driven research which has found that different cells utilize bioelectric currents in fundamentally different ways[6,8,12]. As such, bioelectric signaling is beginning to gain appreciation as is the impetus of a multitude of physiological processes including nutrient transport, osmotic regulation, respiration, and all cognition, to name a few[57].

Ion transport at the cell plasma membrane, which generates cellular RMPs, is governed by physical laws[57–59]. Characteristically, cell RMPs are governed by the electrochemical gradient of various ions across the plasma membrane and their relative permeabilities; which together describe the capacity for these ions to traverse the lipid bilayer through ion selective channels and transporters producing the cell RMP[58,59]. The energy source of ion movement is derived from the ionic concentration gradient across the membrane. Specialized ion pumps selectively transport ions across the membrane, utilizing energy from ATP hydrolysis, to establish and maintain cellular ionic concentration gradients[4,58,59]. These ionic concentration gradients create an electrochemical potential across the plasma membrane which directs ion flow in accordance to laws of diffusion and drift[57,59,60]. Regulation of the electrochemical gradient, and therefore the membrane potential, is a very dynamic and reactive process coordinated by an ensemble of transmembrane ion channels all responding to changes/deviations in the electrochemical gradient across the membrane from rest[57–59]. Fundamentally, the phospholipid bilayer is the root of all bioelectric potential within all cells being equipped with the ability to regulate ion specific transport and separate charged species[58]

Homeostatic RMP of cells are specifically calibrated across tissue types, geared towards specialized cell function within tissues composing an organism. For example, in the human body, neuronal cells typically have RMPs of -70mV[61,62] while skeletal muscle and epithelial cells have RMPs of -90mV[63] and -50mV respectively. The diversity in cellular RMPs echoes the dissimilar functions carried out by distinct cell types. In addition to the electrical properties at the cells membrane, nearly every aspect of the cell has its own passive electrical properties, enabling them to be influenced by imposed electrical currents[64,65]. For example, several amino acids are electrically charged, making complex proteins sensitive to incoming electric signals[58,66]. In addition to proteins of a cell, DNA and RNA that code these proteins are highly charged[66]. In short, cells naturally use these fundamental electrical properties to regulate a multitude of cellular processes enabling them to reliably respond to changes in endogenous/exogenous potentials in their surroundings.

Bioelectric properties of cell membranes

Before progressing towards topics regarding currents, membrane potentials, and how these properties regulate cell behavior, one must understand these bioelectric properties at the fundamental level. Much like how objects with mass gain or lose potential energy as they move up or down, charged ions travelling between points within a conductive medium experience changes in electrical potential energy. By convention, electrical potential differences are measured in volts (V). Most cells inhabit tissues encompassed by conductive salt rich mediums both intra- and extracellularly[67]. These mediums are highly conductive having minute changes in electrical potential difference between two given points. Therefore, the electrical properties of a cell can be attributed in large to the electrical properties of its membrane. In its most rudimentary form, a lipid bilayer is highly insulating, having a conductance of only 10^{-13} $\Omega^{-1}m^{-2}$ [68]. However, the measured conductance of biological membranes is far greater, by several orders of magnitude; this is due to the insertion of conductive pathways in the form of ion channels and transporters. Every living cell has its own innate electrical potential caused by the unique intra-/extracellular ion composition and the insulating plasma membrane endowed with a specialized set of ion channels/transports which permit the flow of ions across the membrane.

At the core of all bioelectricity are the ions which carry charge across the electrical barrier that is cell plasma membrane and the mechanisms by which cells achieve this feat. Firstly, in biological systems charge is carried by soluble ion species such as Na^+, K^+, Ca^{2+}, and Cl^- etc. These ions are differentially separated across the lipid bilayer creating concentration gradients between the intracellular and extracellular fluids. Differences in concentration across the membrane allow ions to travel down their concentration gradient, utilizing diffusional force, across the plasma membrane. However, these hydrated ions must traverse the hydrophobic plasma membrane to transmit signals within the cell thus, evolution has created pathways in the form of ion channels (passive transport utilizing diffusion), transporters (utilizing concentration gradients of specific ions to pump others), and pumps (active; utilizing ATP energy to transport ions against their concentration gradient) to enable the flow of ions across the membrane. Ion channels are specially designed to selectively transport specific ion species across the membrane. However, many of the channels tasked with transporting ions are gated such that they may be tightly regulated for specific cellular functions. Common gating mechanisms for ion channels are voltage gated (triggered by a change in membrane potential), ligand gated (triggered by the binding of a ligand) and stretch operated/mechanosensitive gated (triggered by a physical force/displacement such as stretch). To better understand how cells use changes in the electrical properties of their membrane to regulate the activity of various ion channels, we will elaborate on some basic electrical properties at the cell plasma membrane.

Biological membranes are barriers to the flow of polar solvents which, by consequence of the conductive salt solutions making up intra- and extracellular fluids, make biological membranes highly capacitive. Capacitance defined as the amount of charge (Q) needed to flow between two conducting mediums to create a given electrical potential ($C = Q/V$). The capacitance of a cell membrane is quite high ($\approx 1\mu F/cm^2$) and therefore very little voltage is required to generate charge separation across the cell membrane[59]. This high membrane capacitance causes charged ions to accumulate at the membrane interface and, as a consequence of this charge separation across the thin plasma membrane, a large intramembrane electric field (EF_{IM}) is generated across the membrane[59]. Electric fields are defined as the gradient of potential within space. In scalar, the electric field is defined as electrical potential over a given distance ($E = V/x$) and is generally reported in volts per centimeter (V/cm). To better understand the magnitude of EF_{IM} we will address them in the context of a cell at rest. Even though the RMP of cells range between -50mV to -100mV, low when compared to the magnitude of electrical potentials utilized by common household items, these bioelectric potentials are generated across the ultrathin plasma membrane (75Å) leading to substantially large EF_{IM} ($1x10^6 V/cm$). Having such an enormous EF_{IM}, any charged species either trapped within (charged protein subunits) or traveling through the membrane (ions) will experience the electrical force of the EF_{IM}.

Changes in RMP generate both resistive currents (I_R) caused by the flow of hydrated ions through transmembrane ion channels and capacitive currents (I_C) caused by changes in the separation of charged ions, across the membrane, at the membrane interface.

Resistive currents across the membrane are defined fundamentally by Ohm's Law as:

$$I_R = \frac{V_m}{R_m} \quad or \quad I_R = G_m V_m \tag{1}$$

Capacitive currents across the membrane are defined as:

$$I_C = C \cdot \frac{dV_m}{dt} \tag{2}$$

Thus, the total current traversing the plasma membrane of a cell is the sum of the prior:

$$I_T = I_C + I_R \tag{3}$$

$$\therefore\ I_T = C \cdot \frac{dV_m}{dt} + \frac{V_m}{R_m} \ \rightarrow\ I_T R_m - V_m = C R_m \frac{dV_m}{dt} \ \rightarrow\ \int_0^{V_m} \frac{dV_m}{I_T R_m - V_m} = \int_0^t \frac{dt}{C R_m} \tag{4}$$

$$-[\ln(I_T R_m - V_m)]_0^{V_m} = [\frac{t}{C R_m}]_0^t \quad \rightarrow \quad \frac{I_T R_m - V_m}{I_T R_m} = e^{\frac{-t}{C R_m}} \tag{5}$$

$$V_m = I_T \cdot R_m \left(1 - e^{\frac{-t}{\tau}}\right) \quad at\ rest\ t \gg \tau\ thus \quad V_m = I_T \cdot R_m \tag{6}$$

Electrical conductance of cells is reliant on ion channel composition of the membrane, activity of the channels, availability of ions to freely flow through the channels, and the resistance of the active channels. Albeit the flow of ions, and their direction, is dependent on the given ions electrochemical gradient. Resistive currents exemplify the passage of ions through conductive pathways within the cell plasma membrane such as ion channels and transporters (Fig 1). Capacitive currents occur when charge distribution at the surface of the inner/outer plasma membrane changes rapidly with respect to time. Sudden changes in ionic polarity at the surface of the outer plasma membrane induce changes at the surface of the inner plasma membrane, driven by laws of electroneutrality. Thus, the induced changes in membrane surface charge between the inner and outer plasma membrane generate said capacitive currents. Due to the large capacitance of the cell plasma membrane, cellular RMP is largely based on I_R because resting cells do not experience sudden changes in (intra-) extracellular ion concentration at the membrane interface making $\frac{dV_m}{dt} \rightarrow 0$ thus $V_m = I_R \cdot R_m$ as seen in equation (6). However, capacitive currents are utilized by researchers to study the responses of excitable and non-excitable cells to changes in membrane potential. This is achieved by electrically stimulating cells with rapidly changing currents, inducing I_C and effectively bypassing the large membrane

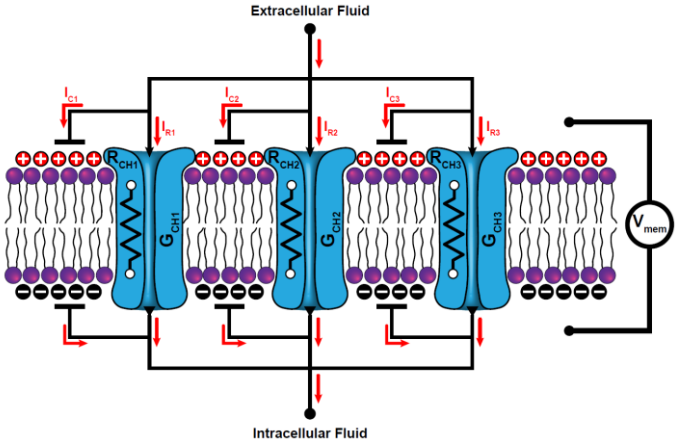

Figure 1. Illustration of ion currents entering plasma membrane phospholipid bilayer through ion channels (blue cylinders) with specific channel resistances. The illustration depicts capacitive currents (I_C), Currents through ion channels are given as (I_R), channel resistance (R_{CH}), and channel conductance (G_{CH}). The sum of the conductance ion channels in a cells plasma membrane, at any given time, is what give rise to the cellular membrane potential (V_{mem}) at that time.

resistance. Evolution has time and again utilized bioelectrical signaling in a multitude of cellular processes and due to its vast functionality specialized ion channels were developed early on to selectively govern the transport of a given ion.

Transmembrane Ion Channels and Transporters

Lipid membranes allow cells to compartmentalize reactions within distinct organelles and respond to changes in their local environment. The lipid bilayer of the cell is the first responder to all changes within the cells microenvironment. Therefore, the composition of the cell membrane is a pivotal characteristic in determining form and function of all eukaryotic cells. The composition of a membrane, with respect to its lipid composition and distribution of ion transporters, plays heavily into its ability to transport ions and thus effects its resting membrane potential. Specially designed trans-membrane proteins (channels and transporters) transport ions across the cell membrane allowing the cell to maintain specialized ionic concentrations across the lipid bilayer. Transport of unique ions allows these ions, such as Ca^{2+}, to have a dual role as signaling factors for many biological processes[69–72]. One of the most highly expressed proteins in the body is the Na^+/K^+ ATPase and accounts for nearly 1/5 of cellular energy expenditure[73,74]. Na^+/K^+ ATPase utilizes ATP energy to pump Na^+ and K^+ against their concentration gradients helping to maintain the Na^+ and K^+ concentration gradients across the plasma membrane. The Na^+/K^+ ATPase is an example of an electrogenic pump as its activity leads to a net exchange of 1 positive charge across the plasma membrane ($3Na^+$ out and $2K^+$ in); its activity helps establish a net charge differential across the plasma membrane[75]. There are many other ion pump ATPases, such as sarco/endoplasmic reticulum Ca^{2+} ATPase (SERCA), that utilize ATP energy to compartmentalize and store Ca^{2+} ions against their intracellular electrochemical gradient[75]. Other ion transporters use an ions electrochemical potential energy as fuel for rapid ion flux across the cell membrane. Cells are equipped with specialized ion channels called voltage gated ion channels (VGIC(s)) that can sense changes in the electrical properties of their surroundings and translate these electrical signals into cellular responses.

Voltage Gated Ion Channels

Ion channels are the primary mode of transport for ions across the plasma membrane. However, ion channels are not simply passive canals by which any ion can traverse the membrane. Ion channels are tightly regulated by the cell with specific membrane distribution and gene expression profiles varying with changing cell types and functions. In addition to this, many ion channels are both selective and gated meaning they selectively permit the transport of specific types of ions while tightly regulating the opening and closing of the pore. Whilst there is a huge diversity among known ion channels in regard to their function, selectivity, and if present, gating mechanisms; the focus of the remaining section will be on VGICs which are both selective and gated.

Ion Channel Structure and Function is Highly Conserved Across Species

VGICs are a unique family of ion selective channels which are equipped to respond directly and rapidly to changes in EF_{IM}. EF_{IM}s play a significant role in the gating mechanism for many ion selective channels. Changes in EF_{IM}, depending on the type of VGIC, will either activate or inactivate the channel[76–78]. VGICs utilize evolutionarily

conserved mechanisms for sensing and responding to changes in membrane depolarization. VGICs are complex proteins comprised of 4 protein domains each containing 6 α-helical protein subunits. The exact structure of a specific VGIC has been shown to vary minimally with evolutionary divergence with their fundamental properties remaining highly conserved[79–81]. While some primitive VGICs function through a single protein domain containing 6 α-helical subunits, many higher ordered eukaryotic VGICs have four identical protein domains whom together form the functioning VGIC[78,80–84]. These protein domains of eukaryotic VGICs are most commonly identical to one another and as such, elaboration on a singular domain is sufficient to address its partners.

Three of the major ions which have highly conserved VGICs associated with their regulated flow across the plasma membrane are Na^+, K^+, and Ca^{2+}. Nearly all cells in the body, excitatory or otherwise, express VGICs for one or more of these ionic species. With such diversity among VGICs come diverse ranges at which the channels can both sense changes in cellular RMP and respond to these changes with corresponding adjustments to their conductance's. A common misunderstanding associated with gated ion channel activity is that a channels conductance is absolute when in fact ion conductance through any given channel is stochastic[85–87]. When a VGIC is in an inactive state it will occasionally allow small amounts of ion current to slip through the conducting pore; owing to what is known as a low open probability[88,89]. VGIC conductance makes use of individual ions' electrochemical gradient, established at the plasma membrane, making for rapid, high volume ion conductance without the expenditure of energy. Moreover, when the channel is in the active state its open probability greatly increases leading to a large overall ion conductance[89,90]. Classifying ranges of RMP at which the open probability of a specific VGIC changes is crucial to understanding the threshold at which each channel will be found in an 'open' or 'closed' state.

Components of Voltage Gated Ion Channels

VGICs tasked with conductance of sodium (Na_v), potassium (K_v), and calcium (Ca_v) are structurally alike containing 4 protein domain subunits each having 6 α-helical transmembrane segments[76,77,81,83]. Within the 6 highly conserved transmembrane subunits of VGICs exists a voltage sensing domain (VSD) and a pore forming module (PM)[76,84,91]. Housed in the VSD is the transmembrane segment S4, an evolutionary conserved α-helix responsible for voltage sensing for the clear majority of VGIC family proteins[76,81,91,92]. The S4 segment is lined with charged amino acids which allow it to respond to changes in EF_{IM} following fluctuations in cellular RMP. More specifically the S4 segment of VGICs contain several positively charged amino acids (Arg and Lys) spanning the α-helix endowing it with voltage sensing properties[91,92]. Changes that occur to the cellular RMP, which in turn instantaneous modify EF_{IM}, impose electrical forces upon the charged voltage sensing S4 subunit of VGICs causing a physical displacement of the S4 subunit within the intramembrane space. VGIC tertiary structures contain a cavity specially designed to encapsulate the S4 helix allowing it to move freely along its z axis in response to changing EF_{IM}. During activation of VGICs, the S4 segment can move up to 15Å within the transmembrane VSD domain of the VGIC[82,92]. This large vertical displacement of the positively charged S4 α-helix creates what is known as a gating current[58,93,94]. All VSDs of VGICs generate gating currents measurable using modern electrophysiological techniques[93,95,96]. The dynamics of S4 sliding, within the tertiary structure of the VSD, has accumulated immense interest among scientific investigators. Rotational movement of the S4 α-helix during vertical movement within the VSD has been demonstrated and

supported by various biochemical and simulated models[78,92,97]. During helical revolution of S4 α-helix, the moving S4 segment is stabilized by neighboring S2 and S3 α-helices containing stabilizing negatively charged amino acids which act to neutralize adjacent positively charged S4 amino acids. The vertical movement of the S4 segment is then utilized to activate the VGIC. It is important to note that high resolution structures of the homotetrameric K_vs have been elucidated for decades[98–100] while high resolution analysis of Na_vs and Ca_vs have eluded scientists due to their lack of tetrameric symmetry[77,101,102]. Moreover, structural details and mechanisms for activation and inactivation of K_vs are well understood, permitting scientists to effectively inquire upon details regarding the intricacies of Na_vs and Ca_vs gating.

Conserved among K_vs, Na_vs, and Ca_vs is a α-helical structure which connects S4-S5 transmembrane subunits. The S4-S5 linker α-helix is fundamental for translating the physical displacement generated by the VSD into a rapid activation and/or inactivation response[77,82,92]. Due to the minute thickness of the plasma membrane, very small changes in the resting membrane potential of a cell translate into significant changes to the magnitude of the EF_{IM}. Physical displacement of the S4 α-helix, caused by changes in EF_{IM} magnitude, induces rapid conformational changes in the pore forming S5 and S6 subunits of VGICs which in turn opens or closes the pore[83,84,92,97]. Additional auxiliary cytoplasmic facing domains within VGIC tertiary structures can be modulated by intracellular proteins (PKC, CaMK, etc) introducing additional layers of regulation towards voltage sensitivity, activation thresholds, and inactivation[76,84,103,104]. Altogether, VGICs are diverse transmembrane proteins equipped to sense and respond to changes in EF_{IM} allowing cells to translate electrical input into molecular and cellular responses.

Inactivation of Voltage Gated Ion Channels

Many components involved in activation of VGICs play a part in the inactivation of VGICs however, VGIC inactivation varies between VGIC specialization. Inactivation of many VGIC family proteins involves vertical reconstitution of the S4 α-helix within the VSD conserved among all VGICs. However, VGICs can be inactivated either rapidly occurring within a few milliseconds or following depolarization while slow inactivation can take up to one-minute following depolarization to inactivate. Mechanisms VGICs employ to inactivate vary between the specialized VGIC families as well as inactivation response times.

K_v Activation and Inactivation

The crystal structure of *Streptomyces lividan* K_v, of whoms sequence is evolutionarily conserved, was discovered in 1998 enabling researcher's higher degrees of understanding of voltage gating mechanisms[100]. Since this ground-breaking discovery, there have been many detailed high-resolution K_v channel architectures generated for more complex organisms making the pursuit into understanding the intricacies of activation and inactivation mechanisms a fruitful endeavor. Currently there are three accepted mechanisms by which inactivation occurs in K_vs. Two of the three mechanisms involve conformational changes within the conduction pathway, one at the cytoplasmic pore opening and another within the selectivity filter that constrict the permeation pathway[92,99,104]. The final mode of inactivation involves plugging of the pore by means of a 'ball and chain' structure located at the cytoplasmic pore opening[105].

Inactivation and S6 Gating

Inactivation of K_vs by means of S6 hydrophobic collapse creates a lower voltage sensitive gate that closes the pore of the conducting K_v at the intracellular face when experiencing hyperpolarizing changes in RMP. The process of S6 gating involves all four VSDs of the K_vs which respond simultaneous to membrane hyperpolarization[92]. Membrane hyperpolarization changes the magnitude of EF_{IM} causing the voltage sensitive S4 α-helix to shift vertically downwards within the VSD domain. The S4 α-helix rotates 120 during its vertical displacement within the VSD resulting in the movement of all gating charges 15Å until the upper most charge (R1) reached the central hydrophobic VSD separator Phe233[78,92]. The force generated by the vertical displacement of S4 is exerted upon the S4-S5 linker leading to a 20Å lateral displacement of the VSD as well as hydrophobic deweeting of the intracellular K_v pore and pore closure of the lower gate by means of S6 α-helix gating[92]. Constriction of the intracellular pore opening by the S6 α-helices made possible by the bent configuration of the S6 α-helix created by a highly conserved proline aa sequence. In addition to this S6 α-helical bend, there is highly conserved hydrophobic PVP motif responsible for creating the lower S6 gate[92,104]. K_vs at rest are in their inactivated configuration described above.

Gating of the Selectivity Filter

Constriction in the conduction pathway of the selectivity filter is termed C-type inactivation as it is an alternative constriction of the permeation pathway with regard to N-type inactivation. C-type inactivation occurs at the extracellular facing pore of the K_v effecting kinetics at the selectivity filer[104,106]. C-type inactivation can occur independently of voltage dependent inactivation effecting the channels conductance in a state independent manner[104,106,107]. During C-type inactivation, the selectivity filter collapses due to the lack of K^+ interaction at a single site along the selectivity filter chain[108]. This vacancy at the selectivity filter allows for strong interaction between selectivity filter residues, inducing subtle conformational changes to the selectivity filter pathway which are then further stabilized by diffused water molecules that come from an inactivation cavity located behind the selectivity filter and stabilize the collapsed conformation[82,109]. This dramatically reduces K^+ conductance through the selectivity filter. Subsequent S6 pore closure at the cytoplasmic side cause the resident water molecules to diffuse back into the inactivation cavity allowing for recapitulation of the selectivity filter resuming its fully conductive conformation. Recapitulation of the selectivity filter following full S6 inactivation is crucial for proper K^+ conduction upon reactivation of K_v caused by changes in RMP.

Ball and Chain Inactivation

Ball and chain inactivation involves plugging of the cytoplasmic pore opening by the cytoplasmic N-terminal amino acids connected to the inner pore forming S6 alpha helix, owing to its alternative name ‘N-type inactivation’. N-type inactivation was coined 'ball and chain' inactivation as the amino acid chain tethered to an N terminal blocker was thought to resemble a ball connected to the S6 helix by a chain[59,104]. N-type inactivation only occurs following active channel conduction by S6 gate opening[59,110]. As such, this form of inactivation generates transient K^+ conduction by K_v followed by rapid inactivation. Though there is little sequence conservation at the N-terminus of K_vs capable of this form of inactivation, the presence of hydrophobic residues as well as positively charged residues at the N-terminus are important for all K_vs using N-type inactivation[111,112]. The

importance of residue interaction in this form of VGIC inactivation was solidified experimentally when researchers cleaved the N-terminus of drosophila shaker K_v and demonstrated inactivation can be recapitulated in these N-terminal deficient channels when stimulated in the presence of soluble N-terminal fragments[113]. Inactivation mechanisms involve S4 α-helices within the VSD as well as S4-S5 linker α-helices connecting voltage sensitive S4 α-helix to pore forming S5 segments of the K_v[92,114]. Rapid inactivation, following K^+ conduction, is caused by adjacent capacitive currents created by voltage-induced activation of the channel exerting an attractive force on the polarized inactivating ball of the N-terminus[58,59,93,112]. In the example of the voltage gated shaker K^+ channel of drosophila, it has been postulated that N-type inactivation occurs in response to gating currents generated by the movement of positively charged amino acids located within the voltage sensing S4 α-helix. Gating currents then generate an attractive force on negatively charged ions on the cytoplasmic facing membrane at the channels pore in turn attracts the positively charged 'ball' that then plugs the cytoplasmic pore opening effectively sealing and closing the channel.

Activation of K_vs

K_vs found in their resting state (inactivated) are sensitive to depolarizing voltages which activate the VGIC. Introduction of depolarizing RMPs causes simultaneous vertical displacement of S4 α-helices within VSDs and is the initial step of K_v activation[78,91]. Vertical displacement of the S4 α-helix pull on the S4-S5 linker α-helices which then destabilize the hydrophobic seal of the S6 gate[82,92]. These steps are the only steps in the activation process of K_vs that are voltage dependent as they summate the mechanisms occurring within the intermembrane space[92,95,104]. Destabilization of the hydrophobic seal of the S6 gate allow for diffusion of water within the intracellular pore cavity. Once the pore cavity has been fully rehydrated, complete pore opening occurs and introduction of K^+ ions into the pore cavity allow for ion conduction[92,115,116]. Thus, both S6 gate collapse and selectivity filter configuration stability permit full K^+ permeation across the plasma membrane.

Na_v Activation and Inactivation

Inactivation of these VGIC follow a voltage independent pathway involving what is termed generally as the 'ball and chain' inactivation mechanism. Amino acids composing the ball and chain machinery are located within a ~19 amino acid long chain connecting domains III and IV. Contained within this amino acid chain are highly conserved amino acids isoleucine (I), phenylalanine (F), and methionine (M) crucial for pore closure and inactivation[78,117,118]. Nav inactivation derives its voltage dependence from its coupling to the transmembrane S4 α-helix voltage sensor[83,118,119]. The inactivation motif is located at the intracellular face of the VGIC pore, outside of the intermembrane space, making it unable to respond directly to changes in EF_{IM}; as changes in the RMP do not directly exert forces on the inactivation loop and as such are not responsible for channel inactivation[78,117]. The ball and chain structure is connected directly to the S6 subunit bringing the IFM loop adjacent to the cytoplasmic opening of the ion pore. During inactivation of Na_v tyrosine residues in the cytoplasmic facing pore stabilize the IFM motif such that the phenylalanine residue protrudes and creates a hydrophobic seal[118,120]. Rapid inactivation mechanisms present in eukaryotic Na_vs are still poorly understood and as such is a significant area of investigation for many investigators. However, it has been found that the movement of the S4 α-helix within domains III and IV are crucial to rapid

inactivation of Na_v[121–123]. It has been discovered that hydrophobic residues, found within the intracellular end of IVS6 and within α-helices forming the S4-S5 linker, belonging to domains III and IV, form hydrophobic interactions with the IFM inactivation motif during depolarization induced inactivation. Rapid inactivation via IFM pore interactions has been further exemplified pharmacologically using toxins which uncouple activation from inactivation which operates by trapping the IVS4 segment which is permissive for activation but not inactivation[124,125]. Together, these hydrophobic interactions stabilize the hydrophobic seal generated by IFM interaction and are believed to be the sites forming the inactivation gate for rapid Na_v inactivation.

A very crucial aspect of VGICs structural complexity was discovered while investigating Na_vs; this was the discovery of VGIC auxiliary protein subunits. It was found that Na_vs associate with other proteins within the membrane which regulate their function and are in fact specific to individual classes of VGICs. Na_v only has a single family of protein subunits $Na_v\beta1$ and $Na_v\beta4$ whom, after being translated, embed in the plasma membrane and are found to interact specifically with Na_vs, modifying their behavior, playing a role in cell adhesion signaling and even being implicated in Na_v-related disorders[84,126–131].

Voltage Gated Calcium Channels

Voltage gated calcium channels (Ca_vs) are found within a plethora of cell types regulating crucial aspects of their function. Ca_vs are responsible for local influx of extracellular Ca^{2+} within the intracellular plasma membrane which then initiate a number of Ca^{2+} dependent cellular events. Ca_v activity in cardiac and smooth muscle is responsible for muscle contraction by elevating cytosolic Ca^{2+} concentration both directly and indirectly by activating Ca^{2+} sensitive ryanodine receptors within the SAR releasing stored Ca^{2+}[47,132,133]. Similar to cardiac and smooth muscle, Ca_vs within t-tubules of skeletal muscle allow for rapid muscle contraction. Skeletal muscle Ca_vs Increase cytosolic Ca^{2+} through extracellular Ca^{2+} influx and allosteric activation of ryanodine receptors directly activated by allosteric interactions with the activated t-tubule Ca_v[50,134]. Endocrine cells utilize Ca_vs to conduct Ca^{2+} entry initiating hormone secretion[135]. Neuronal Cavs located at the membrane of neural endplates regulate Ca^{2+} flux which initiates vesicle fusion and neurotransmitter secretion and synaptic transmission[136–138]. Moreover, a various cell types utilize Ca^{2+} influx from Ca_vs to regulate a number of cellular process from enzymatic activity to gene transcription[139]. It would be a challenge to overestimate the importance of Ca_vs and the breadth of cellular functions in which they participate.

Voltage gated calcium channels can be separated into 3 closely related yet distinct families. All known Cavs fall within 3 categorized protein families: Ca_v 1, Ca_v 2, and Ca_v 3[103,140]. Each family contains various structurally and functionally unique Cav subtypes which are delineated by changes in the hundredth position (Ca_v 1.1, Ca_v 1.2, etc). Ca_vs within each family have high sequence similarities (>70%) which decrease when compared across family lines (<25% to <40%)[141–143]. Generally, Ca_v families can be discerned based on their voltage dependent activation thresholds. Ca_vs requiring high levels of depolarization (L-type) make up all of Ca_v family 1. Next, the closely functionally related Ca_vs requiring intermediate to high levels of depolarization (P/Q/R and N-type) compose all of Ca_v family 2. Lastly, the most structurally distant to all other Ca_vs, Ca_v family 3, are composed of all Ca_vs which activate in response to low levels of depolarization (T-type). Each Ca_v family is specially designed to execute specific tasks, making their cellular distributions vary based upon cellular needs and responsibilities.

L-type Ca_vs

Cardiac, smooth, and skeletal muscle Ca_vs are defined by high depolarization requirements for activation and slow voltage dependent inactivation as well as cAMP-dependent Ca_v upregulation through PKA phosphorylation of Ca_vs. These calcium currents are conducted through L-type, referring to their long-lasting activation times, Ca_vs and are sensitive to dihydropyridines (DHP(s))[136]. L-type Ca_vs regulate excitation-contraction coupling where depolarizing action potentials activate L-type Ca_v conductance leading to increases in cytosolic Ca^{2+} and subsequent muscle contraction. Similarly, L-type Ca_vs regulate contraction of smooth muscle by elevation cytosolic Ca^{2+} generating muscle contraction. L-type Ca_vs are also found in endocrine cells and neurons stimulating release of hormones and neurotransmitters[135,136,139,144]. L-type Ca_vs were the first type of voltage dependent Ca^{2+} conducting channels discovered by electrophysiologists[76].

T-type Ca_vs

The next Ca_v to be discovered was the low voltage activating Ca_vs known as T-type Ca_vs. T-type Ca_vs are far more sensitive to depolarizing voltages being activated within negative RMPs and are transient in activity; owing to their characterization as T-type Ca_vs[145–147]. T-type Ca_vs are found in the peripheral nervous system, smooth muscle cells, bone, endocrine cells, and cardiac peacemaking cells being responsible for the repetitive firing regulating rhythmic heart beating[148,149]. Cardiac T-type Ca_vs found within sinoatrial node cells activate around -55mV which is only a 15mV depolarization from their resting -70mV potential[76,149].

N-type Ca_vs

N-type Ca_vs activate under intermediate depolarizations and inactivation kinetics in comparison to both L- and T-type Ca_vs. However, within neurons especially the voltage dependence of activation varies between cells considerably. Found predominantly in neurons functioning as a regulator for release of norepinephrine, which is where the classification of N-type was derived, N-type Ca_vs have been found function in both the kidneys and heart[150,151].

P/Q and R-type Ca_vs

P/Q and R-type Ca_vs are found most abundant in neurons and were discovered in Purkinje neurons and cerebellar granule neurons respectively[152–154]. P-type Ca_vs function as regulators of hormone and neurotransmitter release in excitatory and inhibitory neuronal synapses[155]. With the exception of cell type specific expression profiles and pharmacology's, the function of Q- and R-type Ca_vs still remain poorly understood[79,156,157].

Ca_v Activation and Inactivation

Tasked with the influx of a critical secondary messenger Ca^{2+}, Ca_v complexity is substantial having multiple functional subunits and a variety of binding domains for external protein regulation. As such, we will discuss fundamental properties of important Ca_v domains and discuss fundamentals of Ca_v activation and inactivation mechanisms. At

the most fundamental level, Ca_v activation and inactivation mechanisms occur similar to those within other eukaryotic VGICs like the previously described K_vs and Na_vs. However, research into Ca_v structure and function has unveiled a multitude of complexity within Ca_v protein tertiary structure including several auxiliary Ca_v subunits each with the capacity to impose regulatory roles governing Ca_v conductance.

High resolution images for Ca_vs do not exist as of yet however, structural models have been estimated from low resolution images of Ca_vs derived from skeletal muscle membranes[158–160]. In its complete form, Ca_vs are comprised of an alpha1 subunit with 4 domains (7 transmembrane alpha helices) much alike other VGICs, and auxiliary alpha2zeta dimer, gamma subunit, and beta subunit[161–166]. Of the auxiliary subunits, Ca_v alpha1, Ca_v gamma, and Cav delta are transmembrane proteins while Ca_v beta and Ca_v alpha2 reside on the intracellular and extracellular surface of the plasma membrane respectively[76,84,167–169]. To the benefit of the scientific community, researchers using X-ray crystallography were able to gain high resolution images of Ca_vB subunits[170,171]. Within this conserved Ca_vB subunit is are highly conserved protein binding domains (Src homology 3 and guanylate kinase MAGUK family) whose presence allow for not only external protein regulation fo Ca_v activity but stable Ca_v complex formation within the plasma membrane. The Ca_valpha1 subunit contains an alpha helix located within the linker of domains I and II (termed the alpha interaction domain (AID)) which bind within the Ca_vB subunit at the guanylate kinase domain which stabilizes Ca_vB and Ca_valpha1 interaction throughout the lifespan of the complexed Ca_v[172].

Ca^{2+} conduction requires only the pore forming Ca_v alpha1 subunit however, Ca_v alpha1 association with its auxiliary subunits alpha2zeta dimer and especially beta subunits exhibit more normal Ca_v voltage gating and Ca^{2+} conduction[173,174]. Thus, association of Beta subunits substantially regulates Ca_v behavior while alpha2zeta association has a lesser effect; gamma subunit association has an even less significant impact on Ca_v behavior[168,175]. In addition to Ca_v regulation by auxiliary protein subunits, a large amount of Ca_v regulation occurs at the carboxyl terminus (C-terminus) of the alpha1 pore forming subunit of mature Ca_vs. The C-terminus of Ca_vs contain 3 major sites for auxiliary protein interaction/regulation[76]. These sites are: EF-Hand motif which allow for Mg^{2+} and Ca^{2+} binding, IM motif (IQ-like motif) which permits Ca^{2+}-Calmodulin binding, and AKAP binding domain (ABD) motif which allows for AKAP15-PKA-mediated regulation. In short, these major C-terminal domains are known to regulate Ca^{2+} conductance, inactivation kinetics, Ca_v expression, and downstream functions of Ca_vs[176–181]. Moreover, the proteins tasked with C-terminal interaction are found downstream of Ca^{2+} signaling making them directly affected by Ca_v activity and subsequent changes in local cytosolic Ca^{2+}. With growing Ca_v diversity, understanding how each functional Ca_v subunit, including isomer variants, functionally regulates Ca_v behavior is a growing interest among researchers as Ca_v subunit introduced regulation within a single cell appears to be dynamic as an individual cell may express several isomers for a given regulator subunit[182,183]. With that aside, understanding how an individual VGIC can ascertain the ability to selectively isolate and conduct individual ions within a sea of diversity is a feat within itself.

Selectivity filter of VGICs and Ion Specificity

Ion specificity is key for ion specific transmembrane channels. Studies of voltage dependent ion channels, and their methods for rapid conduction and high ion selectivity, has allowed researchers to understand and discover specific amino acid sequences lining

the conducting pore whose existence enable VGICs to most effectively select and conduct specific ions in the face of a sea of diverse ionic counterparts. Pore selectivity towards a specific permeating ion is reliant on the amino acids lining the pore known as the selectivity filter. Potassium selectivity is grounded in a specific amino acid sequence which lines the inner pore of the K_v. Eukaryotic K_vs have evolved to utilize TVGYG[184–186]. The crucial amino acids required for Na_v selectivity contained in the inner pore forming loops are DEKA[187]. The outer ring of the Na_v pore forming selectivity filter, a fundamental determinant of Na^+ permeation rate through conducting Na_vs, contains amino acids EEDD[187–189]. The inner pore forming amino acids which are responsible for Ca_v selectivity is the sequence EEEE[190,191]. Ca^{2+} selectivity has been further illustrated by artificially creating a Ca_v from a Na_v through precise modifications in the amino acid sequence within the selectivity filter from DEKA to EEEE[192].

Some VGICs Respond to Minor Changes in RMP

Just as many VGICs are designed to respond to large changes in RMP, there are families of VGICs whom intermembrane protein structure and S4 amino acid composition allows for ion channel activation at far lower depolarization thresholds. These VGICs detect and respond with increased ion conductance in the presence of significantly smaller changes in cellular RMP. For example, T-type voltage gated calcium channels have a very high resolution of activation[84,148]. These channels are found to be activated when the RMP of the recipient cell depolarizes by 10 – 15mV leading to significant increases in channel conductance[58]. These VGICs are found to be expressed readily within cells that respond regularly to large depolarizing stimuli including nearly all types of excitable cells (skeletal/smooth/cardiac muscle and neural cells). As with all electrical stimuli, these VGICs are capable of sensing and responding to rapid changes in RMP, as long as these changes are sufficiently within the range at which the given channel is capable of sensing[76,84,91]. Without the existence of these highly efficient voltage sensing ion channels, it would be impossible for cells to transmit, relay, and decode electrical signals into molecular responses. These mechanisms enable the nervous system to receive stimuli in distal extremities of the body, relay this stimuli to the central nervous system, and subsequently respond and/or adapt to said stimuli in fractions of a second; a system that would be impossible to achieve in large multicellular organisms without robust bioelectrical signaling.

Cell Membrane Composition and its Impact on Bioelectric Processes

All electrical activities of a cell, be they passive or active, occur at lipid membrane interfaces. As such, the membrane of a cell, and its composition, are necessary elements in cellular bioelectric signaling. The fundamental principal of cellular lipid membranes is to create a barrier between intracellular and extracellular space. From an electrical standpoint, the plasma membrane of a cell can be viewed as a nonconductive boundary separating conductive fluids of the extracellular and intracellular space. Due to the necessity of electrical signaling within all cells, the cell creates conductive pathways, through membrane bound proteins (ion channels, transporters, and pumps), by which ions can traverse the nonconductive plasma membrane. Regulation of ion transport across the nonconductive plasma membrane is a fundamental aspect of all living cells, necessary for life. Plasma membranes, at the most fundamental level, are composed of lipids, carbohydrates, and proteins. However, there is much diversity in the realm of membrane

lipids; lipids can be categorized into phospholipids, glycolipids, and sterols. By weight, the membrane is split amongst protein (50%) and lipid (50%) with a small fraction attributed to glycolipids and sterols (5-10%). Phospholipids within the membrane create a hydrophobic barrier, by which its formation is entropically driven by water, within and around the cell. Phospholipids are amphipathic, containing a diacylglycerol backbone connected to a hydrophobic fatty acyl chains (being either saturated, monounsaturated, or polyunsaturated) and hydrophilic phosphate containing head esterified to either a choline (PC), ethanolamine (PE), serine (PS), inositol (PI), or simply phosphatidic acid (PA)[193,194]. Lipid membranes must be fluid structures, as such, lipid composition of membranes strongly depends on temperature. In mammals, with body temperatures of 37˚C, combinations of saturated and unsaturated fatty acyl chains are necessary to maintain fluidity of the membrane, avoiding the generation of rigid patches. Cells ensure a balanced distribution of saturated and unsaturated fatty acyl chains by generating lipids with one saturated chain and an unsaturated counterpart, pairing these two variations to a single phospholipid to safeguard even distribution of these hydrocarbon variations.

The abundance of the different types of phospholipids vary greatly across cell types and among organelles within a single cell. As membrane are the primary barrier for cells and intercept all extracellular inputs it has been postulated that the membrane itself may behave as a metabolic pacemaker of the cell[195,196]. Phospholipid composition within the membrane is dynamic and can change in response to variations in the cells microenvironment. Interestingly, it was found that various phospholipids interact with membrane bound proteins directly effecting their activity; these include ion transporters[194]. This lipid-protein binding interaction extends further with the discovery that various lipid groups nucleate into what are known as lipid rafts which can asymmetrically distribute and localize specific transmembrane proteins including ion channels and various signal transducers; this leads to signal nucleation and localization following a given stimuli[193,197–199]. Phospholipids are not only essential to the membrane but are often crucial elements in signaling following electrical stimulation or ion flux across the membrane. Asymmetric accumulation of specific protein species within the plasma membrane has been shown to be an important aspect to various cellular processes in which the cell coordinates an asymmetric response[200–203]. A variety of signaling pathways utilize membrane lipids for signaling, I will choose to delve into cell migration, neural transmission, and cell division to emphasize the important of membrane lipid asymmetry and its regulation.

Many signaling pathways involving flux of ions utilize unique phospholipids within the signaling cascade. Excitable cells regulate intracellular calcium through a Ca^{2+} induced Ca^{2+} release signaling pathway that involves PI phospholipids[204–206]. In this pathway phosphoatidylinositol (4, 5) bisphosphate (PIP2, a phosphorylated PI phospholipid) is cleaved by phospholipase C (PLC) to create the secondary messenger inositol (1, 4, 5) triphosphate which activated IP_3 receptors in the sarcoplasmic reticulum, releasing Ca^{2+} stores. PIP2 cleavage generates diacylglycerol (DAG) which acts as a protein docking site to facilitate protein localization to specific regions of the inner membrane leaflet[207]. The release of Ca^{2+} from intracellular stores is Ca^{2+} dependent; IP_3 alone is insufficient to garner robust Ca^{2+} release[208]. Thus, cytosolic Ca^{2+} regulation is a crucial aspect of signaling for many different cells and as consequence, the regulation of membrane phospholipids is essential as lipids share important roles within these pathways. Phosphorylation and dephosphorylation of PI phospholipids is carried out by a set of specialized kinases and/or phosphatases which specifically target positions 3, 4, and 5 within the inositol ring.

During neural transmission, fusion of presynaptic vesicles and subsequent release of neurotransmitter is regulated by Ca^{2+} flux and requires the presence of specific membrane phospholipids[209–211]. Although mechanisms of vesicle fusion are still somewhat unclear, it was found that synaptotagmin, a calcium sensing transmembrane protein that associates presynaptic vesicles with synaptic Ca_vs, binds to PIP2 in the inner leaflet of the presynaptic membrane[212,213]. PIP2 binding increases synaptotagmin affinity to Ca^{2+} binding within its C2 domain, which is necessary for Ca^{2+}-mediated attachment of synaptotagmin to PS lipids of the synaptic vesicle, priming it for membrane fusion[214]. Culminating with allosteric interactions of the SNARE complex and synaptic Ca_v allow for conformational changes in Ca_v, brought upon by pore binding of Ca^{2+}, to cause the SNARE complex to retract the synaptic vesicle, further priming the vesicle fusion with the synaptic membrane[214,215]. Accumulation of PIP2 is found in this inner leaflet of the synaptic membrane because the protein syntaxin sequesters both Ca_vs and PIP2 to the inner membrane of presynaptic terminals[216]. Dynamic membrane compositions found across various cell types illustrate the importance of membrane components and consequent cellular functionality.

Electrical Currents as Governing Mechanisms Behind Cellular Processes

Transepithelial potentials as bioelectric regulators

Ionic channels are distributed throughout cellular plasma membranes and in many cases, are done so asymmetrically. In epithelium, the single sheet like layer of cells encasing organs and embryos in humans and other organisms, asymmetric distribution of ion channels between the apical and basal membranes leads to differential ion flux across the epithelium generating transcellular currents. Cells making up the epithelium are held tightly together by adherens, tight junctions, and other cell-cell junctions which inherently create very resistive paracellular pathways in which these transcellular currents must traverse[3,4,6]. Thus, ionic currents traveling through the highly resistive pathways within the cell junctions of the epithelium are called paracellular currents and their existence create a transepithelial potential differences (TEP(s)) across all epithelium. The magnitude of TEPs depend on the resistance of the paracellular junctions and the amount of paracellular current. Many TEPs have been measured and they typically range from 10-60mV with respect to the basal layer[1,4]. Naturally, currents will always travel through the path of least resistance, as such, areas of the epithelial layer where cell-cell junctions are weak or by which the epithelial integrity has been compromised are then subject to experience high amounts of transepithelial electrical current.

Transepithelial ion currents are ever present in complex model organisms. These endogenous currents are implemented in numerous physiological processes, each unique to the next. The importance of transepithelial ion currents can be easily seen during early stages of embryonic development. In human oocyte fertilization, immediately following successful oocyte penetration by the spermatozoa, there is a large influx of Ca^{2+} which triggers a Ca^{2+} dependent inositol (1,4,5) phosphate (IP_3)-mediated RMP depolarization[217]. This fertilization current establishes the fertilization cone and ensures that subsequent attempts from neighboring spermatozoa are unsuccessful in created fertilization cones as they are unable to induce sufficient fertilization currents[218]. Following fertilization, the fertilized ovum must undergo several cycles of cellular mitosis, each taking 12-24hrs to complete, creating a blastomere (<16 cells) and eventually becoming a blastocyst containing 70-100 cells. Regulation of ion channel activity and distribution,

notably IP3r, along the blastomere cleavage sights have shown to be crucial for proper cell cycle progression and thus early developmental progression[2,219]. Following blastomere formation, when the blastomere reaches around 16 cells, cellular differentiation and left-right asymmetry establishment of the blastoderm begins. It has been found that proper left-right asymmetry establishment of the blastoderm, during these early embryonic stages, requires ion currents transmitted through gap junction and various ion channels[200,220,221]. The currents leaving the blastoderm during these crucial stages, contributing to the establishment of left-right asymmetry, generate disparities in TEP measured to be upwards of 20mV from left to right[200]. Embryonic gastrulation, marked by the formation of the primitive streak along the embryonic midline axis, is reliant upon the migration of endodermal progenitor cells from the endodermal layer into the primitive streak; forming the mesoderm. This stage of embryonic development initiates the transition from an embryo having 2 cellular layers to an embryo with 3 cellular layers comprised of an ectoderm, mesoderm, and endoderm. Interestingly, ion currents have been measured leaving the ectodermal layer at the primitive streak, by which cells are actively migrating into, generating TEPs ranging from 10 to 20mVs[222,223]. Epithelial to mesenchymal transition, seen at this critical stage of embryonic development, has been shown to be influenced by physiological electric fields[224,225]. Moreover, during stage 19 of neurula, the stage in which the neural crest is formed, ion currents have been implicated in the establishment of left-right patterning in vertebrate embryos[226,227]. Persistent ion currents have been measured, using a non-invasive vibrating probe technique, exiting the neural crest in axolotl embryos generating a constant trans epithelial potential upwards of 35mV[228]. In addition to the finding it has been found that neural crest cells from various vertebrate models migrate directionally under imposed electric fields[16,229,230]. Proper migration and guidance of neural crest cells to different regions of the vertebrate embryo is crucial as they are responsible for giving rise to many different neural, muscle, and connective cell types[231]. Modification or blockage of these endogenous ionic currents at specific stages of embryonic development are known to bring about developmental abnormalities[232,233]. Together these findings implicate endogenous ion currents as regulators of several stages of embryonic development overseeing and guiding cells through a variety of unique stages during development.

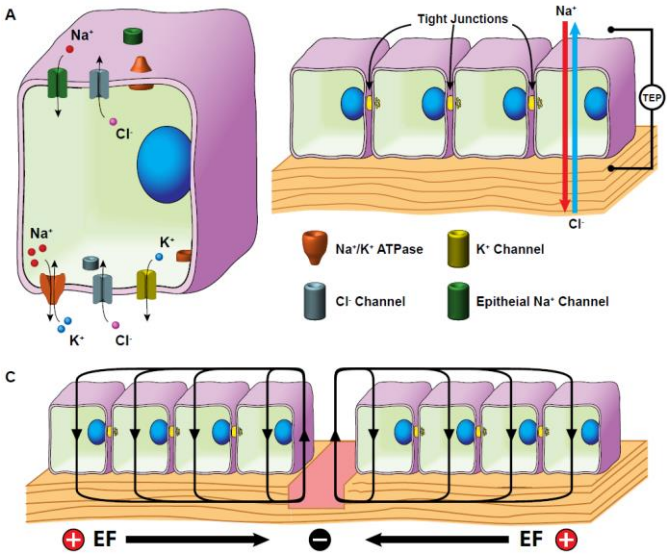

Figure 2. Schematic representation of electrogenic ion transport across epithelial cell sheets generating endogenous transepithelial potential (TEP). **A)** Simplified representation of ion transporters within the apical and basal membranes of epithelial cells generating electrogenic pumping of Sodium (Na^+) and Chloride (Cl^-). **B)** Wound induced epithelial sheet disruption causing TEP depolarization at the injury site which generate endogenous lateral steady state electric fields.

Cellular Migration Promoted by Electric Fields (Galvanotaxis)

Endogenous EFs are pivotal coordinators of many biological processes. Endogenous EFs are generated through regions of

depolarized tissue introduced among polarized tissues. EFs have been shown to play a significant role in promoting the migration of cells during early developmental stages, wound healing, and immune response to name a few. Induced migration of cells by an applied electric field is termed galvanotaxis. Typically, cells that illustrate galvanotactic responses do so in a directed fashion preferentially migrating exclusively towards one pole of the applied EF. Galvanotatic responses have been documented across a wide array of cell types derived from various species. Many galvanotatic cells are known to be involved in the wound healing process within their respective native tissues. Cellular galvanotaxis may be a natural cellular to endogenous injury potentials generated consequently through the rupturing of epithelia and subsequent TEP depolarization at the site of injury (Fig 2).

In fact, many responses seem to be biased towards a singular pole of applied EFs. Neurites of a neuron exposed to an applied EF will redirect cathodally and extended in this direction as long as the field is imposed[234–236]. This attraction to a singular pole of the applied EF that neurites growing in the cathodal direction show accelerated growth rates while neurites growing in the opposing direction experience slower growth rates than their counterparts[234]. These polar responses are caused by changes in the symmetrical protein composition of the lipid bilayer. Applied EFs induce asymmetry in transmembrane proteins causing stimuli reaching the cell membrane to be amplified in the regions enriched with these high levels of transmembrane receptors[236–238]. The mechanisms by which the EF causes membrane proteins to concentrate on specific polar faces of the membrane is still largely unknown however, there are a few working hypotheses.

Cellular growth guided by electrical currents (Galvanotropism)

Researchers have evidenced, for many years now, that organismal growth, in a variety of models ranging from plants to mammals, is in many cases sensitive to endogenous or artificially imposed EFs. Growth sensitivity to electrical fields is known as galvanotropism. Some of the earliest reports of galvanotropism occurred in the late 1800s where researchers Elfving and Müller independently found that electric currents could be used to guide the growth of seedling roots[21]. These works were supported by even earlier findings, reported in the mid to late 1700s, where electrified shrubs exhibited healthier and more accelerated growth rates than their unstimulated counterparts[21]. There has since been numerous reports of galvanotropism in a bacterium[239,240], plants[241–244], fish[245], various neuronal types[236,246–248], and even planaria[249]. Though still largely unknown, significant progress has been made in uncovering various cellular and environmental mechanisms which play a role in the galvanotropic response.

Mechanisms governing galvanotropic responses vary across species and cell types but there are several areas in which similarities can be drawn from responding cells. Firstly, galvanotropism for many cells comes in the form of a directed growth response to a specific pole of the applied or endogenous current. Directed response are believed to be governed by focal shifts in membrane components onset by electric field forces. Localization of membrane receptors as well as lipid rafts contained micro signaling domains have been shown to respond asymmetrically to imposed electric fields[17,237,250,251]. Although Ca^{2+} has been shown to be important for various cellular bioelectric responses[252–254] including galvanotropism[235,255], some galvanotropic events have been shown to be Ca^{2+} independent[256]. However, cyclic AMP and other GTPase-related signaling mechanisms hold significant domain over cellular sensitivity and responsiveness in cells exposed to galvanotropic inducing electric fields[256–258]. Much research is being dedicated to unveiling detailed regulatory networks underlying galvanotropic responses in

the hopes that they can be used to effectively improve therapies targeted at developmental abnormalities, neurodegenerative diseases, and other healing therapies in the future.

Electrical currents and their role in wound healing and tissue regeneration

Administration of electrical currents, for therapeutic means, has long been used in medical devices to assist in wound healing and regeneration of tissues. This practice is known as electrotherapy. The earliest recordings of electrotherapy date back to 1767 when Middlex Hospital implemented a special electrical apparatus which delivered electrical currents through tissues to accelerate wound healing in patients[259]. The majority of currents used in electro therapies in these times were direct currents. Direct currents (DC) were used anywhere from muscle stimulation therapy to accelerated wound healing. Later, in the mid-1850s, alternating current (AC) were found to be more effective in muscle stimulation, a quality attributed to their pulsing nature. AC was far more penetrant, capable of generating muscle contraction using much lower voltages[260]. Since these more primitive applications of electrical therapies, application of electrical currents have been found to be effective in the treatment of many conditions ranging from chronic pain relief to repair and regeneration of spinal cord injuries.

A very common application of modern electrotherapy is called transcutaneous electrical nerve stimulation (TENS). TENS uses surface electrodes on the patient's skin to deliver pulsing current through tissues stimulating subcutaneous nerves. The therapeutic potential of TENS was found by accident as TENS was initially developed to build patients tolerance to electrical stimulation preceding electrode implantation to treat spinal cord injury however, many patients receiving TENS reported pain relief from TENS alone, some even opted out of electrode implantation deeming TENS sufficient pain relief[261]. Modern day TENS is typically administered for extended periods of time over the course of several days, or even weeks, for continuous pain relief[262,263]. Since its serendipitous development as a therapeutic tool, TENS has been an effective tool to bring about pain relief in a variety of chronic pain conditions.

Electrotherapies have been controversial to say the least. Various literature reviews exist questioning the legitimacy of electrotherapies as therapeutic means for wound healing-related ailments[36–38,264–268]. Many of these studies address valid gaps in the understanding of how electrical currents and how they can be harnessed within the body as means to accelerate repair and recapitulation of tissues; concluding that more evidence is needed to illustrate the effectiveness of electrotherapies. Nonetheless, there is a surplus of evidence showing the existence of physiological electrical currents in variety organisms, including humans. Moreover, electrical currents generated at the site of injury have been exceedingly scrutinized and proven to be a crucial aspect in proper repair and wound healing. Despite these encouraging bodies of work using various electrotherapies, many of the mechanisms underlying these impressive results remain elusive. There have been several purposed mechanisms, with scientific validation, posited to describe the induction of plasma membrane asymmetry, generated by electric currents thought to be the cause for many of the unique galvanotactic responses.

Membrane Asymmetry Caused by Applied Currents

Applied electric currents have been shown to have the ability to redistribute cellular membrane lipids, transmembrane proteins and peripheral membrane proteins asymmetrically[251,252,269–277]. Many of these proteins are signal transducers influencing

numerous biological processes including cellular migration[251,252,269–272,272,273]. The resulting asymmetric properties of membranes under applied currents, generating DCEFs, are presented as possible mechanisms to explain the unique directedness observed during galvanotaxis[272,278–282]. However, the mechanism dictating the localization of signaling cascades, receptor, and overall response at the plasma membrane is a subject under ongoing debate. So far, there are three purposed theories explaining the membrane asymmetry and subsequent directed response during galvanotaxis. These posited mechanisms are DCEF induced 1) membrane electrophoresis, 2) electroosmosis and 3) electromechanical force transduction. All three theories agree there are polarized effects on cells during the galvanotactic response but present different mechanisms to explain how these effects are come to be.

Electrophoresis

As previously state, DCEFs have been shown to asymmetrically distribute membrane components. One of the purposed mechanisms behind this redistribution is electrophoresis (Fig 3 A). Electrophoresis is the forced migration of cell membrane components, based on their external charge, during exposure to DCEFs. Electrophoretic properties of membrane proteins describe both the direction and the rate at which these proteins travel in the presence of DCEFs. Redistribution of membrane components under applied DCEFs was shown to occur in both live cells and artificial lipid bilayers[234,237,251,253,275,276,278]. The rate at which these charged membrane proteins/lipids travel is dependent on both the magnitude of the DCEF and the viscosity of the lipid bilayer. It was shown that increasing the membrane viscosity through the addition of 25mol% of membrane cholesterol decreased the electrophoretic affect by nearly 50%[276]. Researchers, using fish epidermal cells, tested the efficacy of membrane electrophoresis as a model to explain cellular galvanotaxis. It was discovered that fish epidermal cell galvanotaxis was not dependent on extracellular Na^+, K^+, membrane potentials, or the transport of Ca^{2+}, Na^+, H^+, and Cl^- across their membranes[278]. However, cell migration was observed in the direction of applied forces by laminar fluid flow (electroosmosis). In contrast, the reversal of electroosmotic flow did not affect the galvanotactic response[278]. Though, slowing the migration of membrane components by increasing the membrane viscosity did slow the kinetics of the galvanotactic response[278]. In addition to this finding, PI3K inhibition reverses the galvanotaxis of these cells suggesting multiple downstream signaling pathways are being activated by DCEF application[278]. This shows that both membrane electrophoresis kinetics and signaling cascades effect the galvanotactic response. Electrophoresis is a known contributor to asymmetries found in the charged phospholipid of the lipid bilayer when exposed to DCEFs however, it has been shown that electroosmosis plays a key role in the asymmetries found among both transmembrane proteins and peripheral membrane proteins[274].

Electroosmosis

Electroosmosis is a physical force, exerted by laminar plug flow at the surface of the charged plasma membrane, displacing protruding proteins across the membrane in the direction of the flow (Fig *3C*). This laminar plug flow is generated by applied DCEFs and occurs at the surface of the cell membrane. Electroosmosis and electrophoresis occur simultaneous at the membrane surface under applied DCEFs however it has been shown that electroosmosis plays a more important role in the distribution effects of membrane

proteins[274]. Drift velocity (v_1) of a protein, relative to the plasma membrane, due to electroosmotic forces are governed by specific membrane properties; the dielectric constant of the aqueous phase (ε_r), permittivity of free space (ε_0), radius of protein in question (γ_1), radius of membrane phospholipid head group (γ_2), viscosity of aqueous phase (η_1) and the lipid membrane (η_2), and the zeta potential of both the protein in question (ζ_1) and the lipid bi layer membrane surface (ζ_2) (Fig 3 B, C)[275]. The direction in

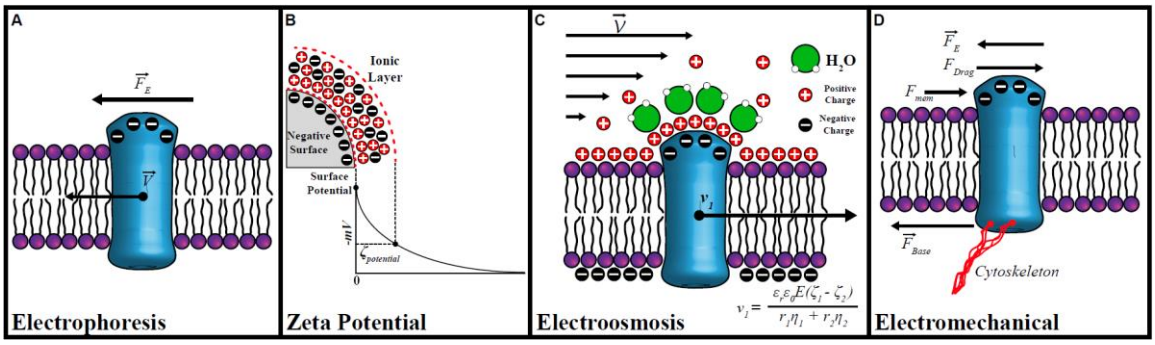

Figure 3. Illustrations describing each mechanism for membrane asymmetry. **(A)** Repulsion force generated by the electric field pushes the negatively charged membrane components to the positive pole of the field. **(B)** Describes what the zeta potential (ζ) is and how it is generated. **(C)** During electroosmosis, aqueous positively charged ions collect at the interface of the plasma membrane and membrane proteins generating a positively charged layer. Force, generated by the flow of polar water molecules, is then exerted on this layer pushing it towards the negative pole of the field. **(D)** Repulsion force (generated by the electric field), Drag force (generated by electroosmotic flow) and complimentary membrane forces act on protruding membrane bound proteins translating into a force at the cytoskeletal protein interface which is then felt intracellular.

which membrane proteins travel under the influence of a DCEF relies on this relationship between the zeta potential of the protein and the plasma membrane, $\zeta_1 - \zeta_2$. If $\zeta_1 - \zeta_2 > 0$, than the membrane protein will drift cathodally, if $\zeta_1 - \zeta_2 < 0$, the membrane protein will drift anodally[275]. This was confirmed experimentally using membrane bound, negatively charged, streptavidin and altering the zeta potentials to yield the two unique results; leading to the asymmetric drift of streptavidin both cathodally ($\zeta_1 - \zeta_2 > 0$) and anodally ($\zeta_1 - \zeta_2 < 0$)[275].

Electroosmosis of surface proteins have been tested on live cells. Using both embryonic muscle cells and *Xenopus* muscle cells researchers were able to control the drift direction of membrane proteins, under applied DCEFs, by modifying the charge at the cell surface through neuraminidase treatment[272,273]. Neuraminidase cleaves negatively charged sialic acid residues from the cells surface reducing the overall negative charge from the cell membrane (ζ_2)[283]. When HeLa cells and 3T3 cells, treated with neuraminidase, were subjected to DCEFs the asymmetric drift of membrane proteins was abolished and the directionality of migrating cells was decreased compared to untreated cells[284]. Electroosmosis provides another method at which electric fields asymmetrically reorient cell membrane proteins, many of which provide intracellular signals necessary for cell migration.

Electromechanical Model

Another mechanism to explain the galvanotactic response of cells is one solely generated by the mechanistic forces DCEFs exert on the protruding membrane proteins of cells. The electromechanical model describes that applied DCEF exert a physical torque on the negatively charged transmembrane glycoproteins resulting in a net force,

transmitted by the cytoskeleton (Fig 3 D), which can be felt throughout the cell, initiating the galvanotactic response[280,281,285,286]. This mechanism for galvanotaxis was testing by applying both steady state DCEFs and alternating current electric fields (ACEFs) simultaneously to keratinocytes. Maintaining the DCEF strength and changing the frequency of the ACEFs, which oscillates from a positive to negative value when applied, allows researchers to identify how cells are responding the DCEFs while the ACEFs are rapidly oscillating the polarization of the cell membrane[281]. In combining DCEFs and ACEFs at 160Hz, keratinocytes migrated directionally and more rapidly than their migration under DCEFs alone[281]. ACEFs at lower frequencies, 1.6Hz, when combined with DCEFs abolished the directedness of migration but did not influence migration rates[281]. Migration was not observed in ACEFs alone[281]. At high frequencies the force exerted by the DCEF to the membrane proteins is nearly constant allowing for keratinocytes to respond similarly to keratinocytes subjected to DCEFs alone[281]. However, reducing the frequency of the applied ACEF subjects the membrane proteins to forces that are oscillating in direction hindering the ability for keratinocytes to respond directionally[281]. The average applied electric field in all of the tested conditions was the same and under the electroosmotic and electrophoretic models it would be expected that membrane proteins would asymmetrically localize and thus directed migration would occur however, this was not the case when ACEFs of low frequencies were applied[281]. This work shows that the forces exerted at the intracellular junctions of transmembrane proteins and their cytoskeletal connections directly influence the direction of migration under DCEFs.

Once a cell reaches its target it must be able to receive stimuli from its surroundings, translate that stimuli into a response, and execute the called upon task by means of regulated gene expression. The expression of a gene is a tightly regulated, complex process that occurs constantly within every cell. Although every cell contains an identical, comprehensive DNA template; there is a huge diversity in genetic composition from cell type to cell type owing to their dynamic structure and functions.

Bioelectric Regulation of Gene Expression

Cells have long been known to respond to bioelectric stimuli such as incoming action potentials generated by peripheral stimuli. Excitable cells such as neurons or muscles trademark the capacity to translate bioelectric signals into cellular responses. These excitable cells traditionally respond by either generating an electrical response or through physical contraction[9,47,50,287] however, researchers have found these cells to also be capable of mounting transcriptional responses to these same stimuli[288–290]. However, excitable cells are not the only cell types which have been known to sense and respond to changes in the local electrical landscape. As mentioned previously, various stem cells and mesenchymal cells have been shown to both sense and respond to a range of electrical stimuli. As one would anticipate, many of the observable physical responses to these electrical stimuli are preceded by measurable changes in their unique transcriptomic profile[30,224,291–293]. This finding suggests that bioelectrical signaling executes action on cells by stimulating changes in the expression of certain genes to garner the physical responses observed by various researchers. Plasticity in gene expression is key to a cells survival and utility in the adult body; their new-found susceptibility to electric currents presents these instantaneous physical stimuli as potential key regulators of cell behavior. In addition to its important in natural cellular regulation, bioelectric governance over cellular gene expression opens new avenues for researchers to influence the behavior, fate, or function of cells in a local, systemic, and noninvasive way.

Immediate Early Genes (IEG)

At the fundamental level, cells are essentially compartmentalized units, separated by membranes, with designated functions which are determined by their specific protein architecture. Proteins in a cell are like parts composing a vehicle whereas gene transcription is like part manufacturing creating each unique component; together they build a working final product. Gene transcription is an essential dynamic cellular process, adapting and generating meaningful responses to changes in the cells environment. However, active gene transcription is complex function that requires the harmonious execution of many different moving parts; it is for this reason that active transcription, in general, is a process which can take hours to complete. For some cells, this window of time is simply too long as they must respond to rapidly changing stimuli. Therefore, cells have developed a method to mount active transcriptional responses to incoming stimuli; a class of genes found to exhibit exceptionally rapid transcriptional responses are known as immediate early genes (IEG)[294]. IEG transcription was first identified by researchers in 1972 in the context of viral infection where researchers discovered viral hijacking of transcriptional machinery resulted in rapid *de novo* RNA transcription within just minutes following viral integration[295]. Soon after this discovery it was found that many excitable cells, which readily respond to rapidly changing stimuli, possess the capacity to perform IEG transcription[288,289,296,297].

Though the level of understand regarding mechanisms regulating IEG transcription is readily expanding, several signaling cascades have been proven to mediate IEG transcription. Alike all transcriptional responses, incoming extracellular signals must be effectively transmitted from the cell plasma membrane all the way to the nucleus. In the case of IEG transcription, this process of signal transduction must happen at an extreme pace. IEG transcription has been shown to occur under the umbrella of a multitude of known signaling cascades such as RhoA-actin, ERK-MAPK, p38-MAPK, and more[294,298]. Many of these signaling pathways have a common denominator, sensitivity to changes in local intracellular Ca^{2+} concentration[298,299]. Independent studies have exposed IEG susceptibility to various forms of intracellular Ca^{2+} perturbation. For example, inhibition of L-type Ca_vs in excitable cells blocks rapid IEG transcription[300]. Not only is Ca^{2+} flux crucial for rapid cellular IEG transcription, increases in intracellular Ca^{2+} concentration mediates rapid transcription[299]. This was personified by the use of various Ca^{2+} chelators which clearly inhibit rapid transcriptional responses[301]. The importance of Ca^{2+} dynamics in rapid IEG transcription has stood the test of time and remains a fundamental regulator conferring stimuli into rapid active IEG transcriptional responses.

Planarian model organism:

Planaria have an amazing capacity to regenerate any lost or damaged tissue. Planarian regeneration is made possible by resident pluripotent stem cells called neoblasts. The planarian neoblast is still as much a mystery to modern science as it is an amazing cell with profound capacity to regenerate planarian tissues. The planarian neoblast is responsible for replenishing all cell types during normal homeostatic cellular turnover or large-scale tissue regeneration; owing to the organism's fortitude and longevity. Neoblasts can be identified genetically by screening for unique neoblast specific genes. A pan neoblast marker, known as *smed-piwi-1*, shows neoblasts spread throughout the body of the planaria, with two distinct exceptions: the pharynx and tissue

located above the photoreceptors. The ways by which neoblasts replenish their own stores, sense the need to replace missing tissues, and orchestrate complex regeneration is still unknown. However, there are several insights into this process.

Neoblasts make up 20-30% of all cells in the planarian body[302,303]. Neoblasts are found in the mesenchymal like space known as the parenchyma[302]. Neoblast populations can be selectively removed from the planarian body using γ-irradiation[302,304]. Irradiation sensitive neoblasts in the planaria can be separated into two groups: 'X1' which are dividing neoblasts in $S/G_2/M$ phase and contain high levels of DNA and 'X2' which are thought to be a mixture of G_1 neoblasts and neoblast progenitor cells. Following lethal irradiation, X1 and X2 neoblasts are completely removed from the planarian body with 24-48hrs[305,306]. A third population of neoblasts 'X3' are termed irradiation insensitive as it takes up to 96hrs to see a reduction in this population post-irradiation; this population is believed to be composed of differentiated neoblasts[307]. Molecular dissection of these populations of neoblasts can be achieved through the implementation of neoblast specific markers. There are many neoblast specific genes that can be used to label specific neoblast populations, many of these genes are either involved in the cell cycles (*H2B, PCNA, phospho-histone H3,* etc.) or are homologs of germ line specific cell markers within other model organisms (*smed-piwi-1, smed-bruli, smed-germline histone H4*, etc.)[302,305,306,308–310]. Among these markers, all planarian neoblasts, and flatworm neoblasts in general, express the Argonaute family member protein *smed-piwi-1*[311–313]. As such, *smed-piwi-1* expression is the current gold standard for planarian neoblast labeling. Delineation of neoblast development and function has been a premiere question in planarian biology for many research groups. Recent studies have been performed showing that neoblast populations, once thought to be homogeneous populations of stem cells, are in fact quite heterogenous encompassing diverse subpopulations that undertake different functions within the planarian body.

Regenerative competence of planarian tissues hinted at pluripotency among neoblast populations. Neoblast totipotency, and the establishment of naïve neoblast linage, was later illustrated when *Wagner et al.* injected single neoblast isolates into lethally irradiated tissues, effectively introducing competent self-renewing naïve neoblasts and restoring homeostatic tissue turnover within the irradiated tissues[313]. Neoblast progeny maturation occurs gradually. Pluripotent progenitor cells will cease to express *smed-piwi-1* yet, piwi-1 protein remains transiently as these cells travel towards their target differentiation site, gradually changing their genetic profile as differentiation begins[314–316]. However, determination of heterogeneity among the neoblast population was not fully elucidated by these results. Through the implementation of single cell transcriptomic analysis, heterogeneity among the X1 neoblast population has been discovered. As such, X1 neoblasts can be separated into 3 transcriptomically distinct subclasses: σ-, γ-, and ζ-neoblasts. Much like how mammalian stem cell niches are responsible for replenishing specific cell types within the local region, it has been found that these neoblast subtypes may tasked similarly, being responsible for renewal of specific cell types[317,318]. Interestingly, it is believed that the previously observed totipotent naïve neoblasts reside within the σ-neoblast populations as transplantation of ζ-RNAi into lethally irradiated hosts was sufficient to rescue complete regeneration. This is further supported by the purposed engendering role of γ-neoblasts for intestinal linage cells as they express the evolutionary conserved endodermal marker *gata 4/5/6*[317,319]*.* However, spatial positional cues (encoded by what are known as position control genes (PCGs)) act as a key determinants of tissue specific regeneration tasked with mapping, establishing, and maintaining anatomical polarity during planarian regeneration[320,321]. Interestingly, several labs have found that

systematic interferences of the bioelectric properties of regenerating planarian tissues during regeneration effectively reprograms these PCG regulators resulting in unique and consistent regenerative phenotypes[6,12,322,323]. These findings suggest endogenous bioelectric polarity may supersede known genetic tissue identity determinants, governing the positional dynamics of many of these genetic regulators during homeostasis and regeneration of planarian tissues.

Planaria are capable of complete regeneration of lost tissue within seven days following injury[305,324,325]. Proper regeneration of planarian tissue involves complex signaling dynamics capable of sensing exactly what tissues are missing and therefore, must be replaced. It has been demonstrated that specific genes coordinate neoblast driven regeneration towards specific tissue types. Specifically, genes within the Wnt-Frizzled pathway govern the fate of regenerative neoblasts in an anterior-posterior specific manner[326–330]. In parallel to genetic regulation, bioelectric signals exist within the planaria and have been demonstrated to hold important roles as regulators of regeneration and tissue identity, evidenced by their experimental disruption[322,323,331]. Endogenous bioelectric polarity is asymmetrically distributed along the anterior-posterior axis of the planarian body. Several studies have demonstrated that collective tissue polarity within the anterior is depolarized (more positive) with respect to posterior tissues[323,331,332]. Upon amputation, tissues adjacent amputated regions greatly depolarize as consequence of TEP dismantling due to loss of epithelial integrity, characteristic injury potential phenomena[322,331,332]. Disrupting planarian injury potentials leads to loss of regeneration as well as regenerative abnormalities[322,323,332], alike to those illustrated by other models subjected to bioelectrical interference during wound healing and development[10,11,233,333,334]. As such, bioelectrical signaling networks are powerful regulators guiding proper neoblast driven regeneration and these bioelectric networks may supersede accepted regulatory pathways known to modulate proper planarian regeneration such as PCG signaling. Modeling of bioelectrical properties of complex tissues, along with improvements upon single cell models, has been done revealing a vast network of pathways by which ion currents travel through collective cell tissues and convey patterning information[335–338]. Altogether, this body of work not only uncovers potential mechanisms governing electric regulation of planarian neoblasts but utilizes physical electric currents to predictively influence their genetic profile modifying and overriding (or hijacking) neoblast behavior.

SIGNIFICANCE

EFs play a critical role in mobilizing cells in response to injury or tissue loss. Migration of progenitor cells in response to injury is required to appropriately position cells to replace lost or missing tissues. Wound induced EFs play a significant role in cell migration and mobilization following injury[3,4,339]. These EFs are strongest at the site of injury and dissipate spatially as they travel away from the injured regions and temporally as the missing tissue is regenerated[3,5,340,341]. A variety of cells respond to electric fields, of physiological strength, by undergoing directional migration (galvanotaxis)[253,281,342,343]. The significance of wound induced EFs has been demonstrated through studies indicating: the galvanotactic response exhibited under applied EFs can override other known migratory signals[344,345]. Impaired re-epithelization following injury is characteristic of chronic wounds found in the elderly, diabetic ulcers and other similar regenerative deficiencies[346,347].

Tissues naturally regulate the flow of ions during wound repair. Regulation of injury induced ion flow must occur within the complex, highly ordered organismal tissues in which they are generated. Cells, and the tissues in which they compose, have developed highly ordered and efficient ways to control and regulate the ion fluxes and their innate 3D electrical resistances[2]. Regenerating tadpole tails have two critical phases with respect to the electrical currents exiting the tail stump. During the initial phase, first 8-10hrs, electrical currents are measured to be leaving the injured stump. Subsequently, the stump experiences an essential reversal phase at which the electrical current switches and flows inward for the remainder of the regenerative process[348]. Failure to induce this reversal phase in the regenerating stump results in the inability to regenerate the tadpole tail[348]. The ability for cells to regulate wound induced EFs illustrate its importance and utility during the regenerative process and its necessity for proper wound healing.

EFs influence wound healing and re-epithelization *in-vivo*. Reepithelization and wound closure is an essential part of the wound healing process in which EFs play a pivotal role[5,347]. In the newt for example, it was shown that enhancing the endogenous EF, generated by amputation, promoted reepithelization while abrogating the endogenous EF, using exogenous counter EFs, impede reepithelization[340]. In rat corneal injuries, pharmacological modifications to the TEP was enough to both increase and/or decrease the regeneration process by increasing or decreasing the lens corneal TEP[349]. In human corneal injuries, increasing the wound induced currents via aminophylline or chloride-free solution have a significant effect on the wound healing rates, offering easy non-invasive therapies for cornea-related injuries[333]. These studies provide evidence of endogenous EFs can be utilized to provide therapeutic care in accelerating and improving the wound healing process. There have been various studies investigating potential downstream molecular participants that may be targeted to impact the injury induced EF response.

Several downstream molecular/genetic regulators of EF responses have been identified *In-vitro*. Known regulators of cell migration also play roles in cellular galvanotaxis. Closure of wounds by migration, generated in lens epithelial cell (LEC) monolayers, was influenced by both applied EFs and the activation/inhibition of mitogen-activated protein kinase (MAPK) signaling, extracellular signal-related kinase (ERK1/2)[350]. LEC wounds facing the anode healed at normal rates while cathode facing wounds healed much slower[350]. Both wounding and applied EFs were found to independently increase

expression of ERK1/2[350]. Inhibiting MAPK signaling via U0126 prevented LEC wound edge migration irrespective of EF application[350]. Applied EFs beyond physiological wound induced EFs do not proportionally increase levels of ERK1/2 protein[350]. Though dramatically reduced, wound healing of LEC monolayers was not completely blocked via U0126 inhibition; indicating there are other signaling pathways promoting the wound healing response[350]. Wound healing and EF-mediated ERK1/2 activity was observed mouse keratinocytes and neutrophils[344]. Similar results were found when observing protein kinase B (AKT), Proto-oncogene tyrosine-*protein* kinase (Src), Mitogen-activated *protein* kinase (p38) and Janus kinase (JAK1) in responding mouse keratinocytes/neutrophils[344].

Molecular dissection of the galvanotactic response suggests large diversity associated with EF signal transduction. The galvanotactic response of human induced pluripotent stem cells (hiPS) were tested in 2D and 3D cultures as a means for improved therapeutic delivery of hiPS[18]. Cultured hiPS were found to be galvanotactic in both 2D and 3D environments with a response threshold of < 30mV/mm[18]. Inhibition of Rho-kinase reduced the directional response under applied EFs by 70-80%; indicating that the directionality of hiPS under applied EFs is dependent on Rho-kinase activity[18]. Phosphoinositide-3-kinase (PI3K) and its downstream targets have been shown to have direct effects on the directed migration observed during galvanotaxis[342,344,351–353]. PI3K is involved in a number of independent processes utilizing many unique downstream targets. In neural progenitor cells (NPCs) genetic disruption of PI3K hindered the galvanotactic response while EF application increased phosphorylation of AKT, a downstream target of PI3K, and increased/asymmetrically distributed intracellular PIP3[18]. Phosphatidylinositol-3,4,5-trisphosphate (PIP3), a downstream target of PI3K, plays a key role in the sensing chemotactic gradients[354–356]. During this chemotactic response, PIP3 expression is increased and concentrated at the leading edge of migrating cells[355,356]. EF exposure to NPCs markedly increased PIP3 expression as well as asymmetrically distributing intracellular PIP3 to the leading edge of migrating cells indicating it may also play important roles in the sensing and migration of galvanotactic cells[351]. These effects are seen both *In-vitro* and *ex vivo* NPCs[351]. Genetic deletion of phosphatase and tensin homolog (PTEN), a known inhibitor of PIP3, enhanced the galvanotactic response of mouse keratinocytes[344]. Phosphorylation of AKT was found to be dependent on levels of epidermal growth factor (EGF) and fibroblast growth factor-2 and was markedly decreased following inhibition of PI3K[351]. Modification of the PI3K pathway has been shown to also reverse the direction in which Dictyostelium cells migrate under applied EFs[352]. Genetically modulating of either guanylyl cyclase or cyclic guanosine (cGMP)-binding protein C concurrently with PI3K inhibition was found to mediate cathodal migration and anodal migration respectively[352]. This is in agreement with past findings implicating protein kinase C, cyclic AMP dependent kinase and cyclic GMP dependent kinase during cellular galvanotaxis[342,353,357]. This work not only shows the complexity in which signaling pathways mediate the galvanotaxis of cells but also elucidates the molecular dependencies observed during EF induced cellular responses. Studies like these show how specific genes can be targeted to modulate specific aspects of EF associated responses allowing for a researcher to use molecular approaches to modify the cellular translation of EF signaling.

The planarian neoblast. Classical studies in planarian biology, pioneered by T.H. Morgan and Margaret R. Murray performed in the early 1900's, demonstrated planarians

regenerative capacities that have since intrigued the scientific community. The regenerative powers of the planaria are made possible by the ever-so versatile planarian stem cell, the neoblast[324,358,359]. Planarian neoblasts can regenerate any organ within the planaria with such efficiency that a planarian fragment approximately 1/279th the planarian size can fully regenerate a new, functionally indistinguishable planaria[360]. The planaria maintains a ubiquitous homeostatic level of neoblasts utilized for cellular turnover and general tissue maintenance[359,361]. If injured or amputated, neoblasts will proliferate, migrate and differentiate to replace any and all of the lost or missing tissues. However, using lethal doses of γ-irradiation (3k – 6k rads) neoblast mitosis is permanently eradicated from the planaria, rendering it incapable of regeneration[324,358,359,362]. Since neoblast is the only dividing cell in the entire planaria γ-irradiation provides a useful tool to eliminate neoblast and study their function. Three general cell populations have been identified based on their sensitivity to γ-irradiation: X1, X2 and Xins. The X1 includes the proliferative neoblast population, while X2 and Xins are post-mitotic; represented by the early post-mitotic and differentiated progeny, respectively[363–365]. Lethally irradiated planaria die in within three weeks due to the inability to maintain homeostatic cellular turnover. Transplantation of healthy neoblasts through single cell transplantation or tissue transplantation can rescue otherwise terminal γ-irradiated planaria[358,362,366]. Being the only mitotic cell within the planaria, immunostaining using antibodies designed to label G_2/M phase phosphorylated histones (Phosphohistone H3) are used to label mitotic neoblasts within the planaria[367]. These tools allow us to assay the different neoblast populations as well as the mitotic behavior of neoblasts under any experimental condition within the adult planarian.

Planarian regeneration utilizes various ion transport pathways. Planarian regeneration can be greatly influenced through the inhibition of the natural flow of ions. Researchers at Tufts University using the voltage sensitive dye, DiBAC, showed that amputation causes large scale membrane depolarization of nearby cells. Pharmacological inhibition of H, K ATPase-mediated membrane depolarization using a highly specific H, K ATPase inhibitor, SCH-28080, revealed that planarian head regeneration and brain reformation requires tightly regulated tissue depolarization[322]. Furthermore, planarian regeneration can be greatly influenced by the dysregulation of other channel proteins. RNAi knockdown of planarian gap junctional (GJ) Innexin proteins (*Dj-Inx-5+13, −12)* lead to improper regeneration of bi-, tri-, and quadruple head regeneration phenotypes exemplifying the necessity for long range GJ communication for proper tissue specification during regeneration[368]. In fact, there is evidence suggesting that planaria exposed to varying current densities and fields, during regeneration, may succumb to regenerative abnormalities such as regenerative retardation, bi-polar heads and complete head/tail reversal[323,369]. Unfortunately, this classic experiment has yet to be reproduced. Collectively, this body of work shows compelling evidence for the influence of ion regulation during regeneration within the planarian model and thus ion-mediated neoblast behavior.

CHAPTER TWO

FINDING

Non-invasive techniques for long-term planarian immobilization and current delivery

2.1 Introduction

Full scale planarian immobilization is a technique which, over the years, has been has been achieved using several different approaches. However, to date, no prior techniques have been successful at large scale immobilization for periods greater than 6-24hrs without the use of pharmacological or molecular interference. For example, experiments have been performed in the past in which planaria have been encapsulated in agar for extended periods of time[370]. Traditionally these experiments were performed to graft planarian tissues from specimen to specimen or even interspecies engraftments[371]. Within these studies researchers successfully grafted tissue but did not quantify locomotion of planaria during or following the encapsulation process[371]. These methods were used to effectively 'glue' tissue together for extended periods while tissue healed. Aside from physical agar immobilization, we must address pharmacological and molecular approaches used to achieve planarian immobilization and the various drawbacks of such approaches.

Targeted RNAi of specific genes utilized by the planarian nervous system have been shown to effectively incapacitate the planaria. Selective knockdown of planarian prohormone Convertase 2 (*smed-PC2*), a neural peptide processor expressed throughout the planarian nervous system, leads to an overall loss of gross movement within 7 days[372–374]. *Smed-PC2* RNAi generates several physical phenotypes that may be undesirable during immobilization such as: ventral curling, ruffling of lateral epidermis, and the remaining capability of micro-movement[372]. The universal expression of *smed-PC2* within the planarian nervous system[373,375] suggests disruption of *smed-PC2* may have adverse effects, outside of locomotion, that may interfere with experimental results acquired by researchers. *Smed-PC2* has been found to play crucial roles in the development of germ line cells within sexual planaria and is required for the processing of various peptides and hormones within these planaria[376]. Nevertheless, It is believed that *smed-PC2* inhibition specifically influences muscle activity, although the effects of *smed-PC2* RNAi have yet to be explored more broadly[372].

Researchers have also implemented the use of low percent ethanol treatment to effectively immobilize planaria for extended periods of time[372]. Within this study, researchers soaked planaria in a planarian water solution containing 3% EtOH for 60min. This EtOH treatment ultimately lead to the inhibition of both gross and fine movements for up to 4hrs[372]. Furthermore, it was shown that this method of EtOH treatment effectively immobilized planaria through the temporary removal of ventral cilia, a planarians primary mode of transport[372]. Planarian locomotion is recovered after ~3hrs as the ventral cilia reform once EtOH is removed[372]. In addition to the short immobilization time, ethanol has

been found to have significant effects on cell membrane fluidity, with prolonged EtOH exposure proving capable of changing overall cell membrane composition in newly EtOH adapted cells[377–380]. Together, the effects of ethanol exposure to cell membranes make such treatments undesirable for bioelectric studies.

In addition to ethanol and RNAi techniques, the use of chloretone has proven effective in temporary planarian immobilization. Chloretone (Chlorobutanol; trichloro-2-methyl-2-propanol) was first introduced in the medical field as a local and systemic anesthetic used for a variety of applications in anesthesiology[381]. Implementation of the narcotic sedative chloretone has been used to immobilize planaria for various tissue augmentation procedures dating back to the 1920s[366,370,371]. Chloretone effectively depresses the central nervous system via active metabolization of trichloroethanol[382]. Typically, planaria are soaked in chilled 0.2% chloretone for several minutes causing them to become completely anesthetized for up to 10 minutes. We have observed that prolonged exposure to chloretone can cause adverse and destructive side effects to planarian tissues and therefore, this method of immobilization is suitable for quick, temporary applications only.

In the context of electrophysiological study, the polar nature of applied currents and the endogenous polarity of planarian tissues puts effective, long-term, planarian immobilization at center stage for required conditions. In addition to maintaining polarity of endogenous and exogenous electric properties, current delivery to planarian subjects was, in many cases, achieved through the implantation of glass microelectrodes on the ventral face of the planaria which, if planaria were not properly immobilized, would introduce large scale injury at the injection site. In summary, applied current experiments conducted within this work required the immobilization of gross locomotion, including micro-movement, for periods of up to 7 days. Many experiments also required substantive, ongoing, access to planarian tissues (i.e. microelectrode placement) and freedom to modulate and secure body axis as desired. Thus, we developed two distinct methods for moderate (up to 6hrs) and long-term (7+days) planarian immobilization.

2.2 Use of agar immobilization technique for moderate periods of suppressed gross locomotion while permitting body wide tissue accessibility and live viewing

Current delivery, used to generate body wide steady state EFs, was achieved through the injection of current beneath the planarian epithelial monolayer using precisely pulled glass capillary microelectrodes. To pass current using pulled glass microelectrodes, planaria must remain immobile for extended periods of time to ensure microelectrode placement remains constant and does not introduce large scale epithelial injury. Intact animals (~7mm in length) are first anesthetized, using chilled 0.2% chloretone, rinsed in planarian water, and placed atop a chilled glass microscope slide (75x50mm Corning: CLS294775X50). Then, complete submersion of planaria in liquified 1.0% low melting point agarose, near its gelation temperature, was used to incapsulate the planaria. Once planaria were relaxed and oriented properly, agar was solidified over ice with the planaria inside. Encapsulated planaria were then transferred to 35mm petri dishes and further secured with liquid agar on all sides. Once agar solidified atop ice, petri dishes containing immobilized planaria were secured within a custom build chilling station, planarian water was added to petri dishes and the current injection commenced (Fig 4 A).

To ensure that the agar immobilization process was not causing harm to the planaria, we immobilized planaria and quantified their response to light after long periods of immobilization (Fig 4 B, C). It is well known that planaria are photophobic and thus are

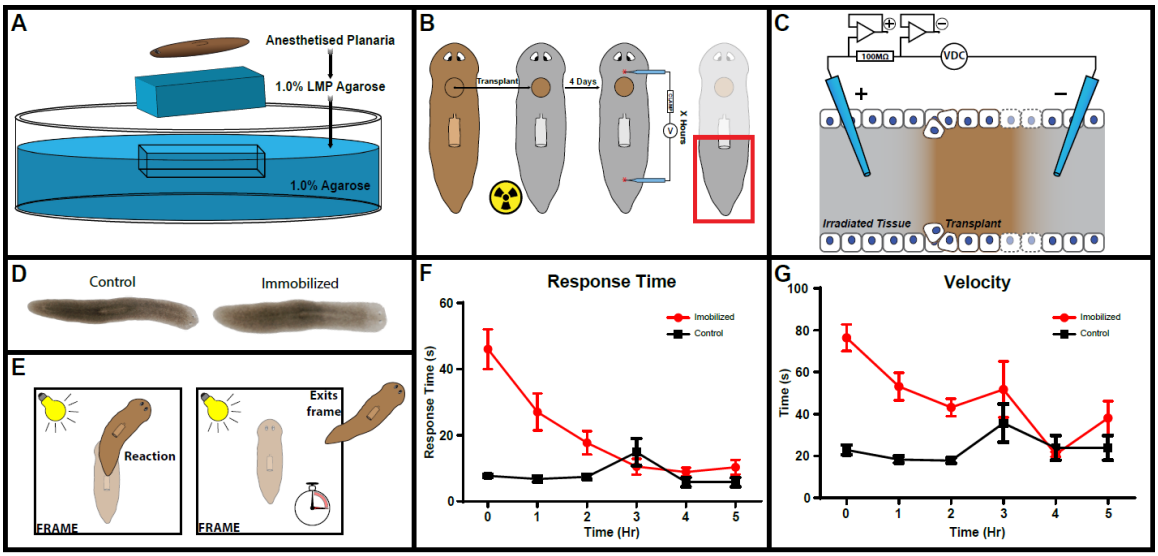

Figure 4 Agar imbedding of live planaria effectively immobilizes intact planaria for as long as 6hrs without negatively impacting planaria behavior or general health. **A)** Schematic representation illustrating the various steps in planaria agar immobilization; chloretone anesthetization to assist in embedding, submersion and embedding in 1.0% low melting point (LMP) agarose, transfer of embedded planaria into petri dish prepped with 1.0% agar. **B)** Transplantation procedure, wildtype planaria tissue are transferred and grafted into lethally irradiated host planaria, transplanted planaria are given 4 days and then subjected to $pDCS^S$ stimulation for designated stimulation periods, distal tail tissues are analyzed with modern molecular tools. **C)** Summary of circuit used to measure current traveling across 10MΩ clamp resistor consisting of two voltage follower op-amps to accurately measure voltage drop. **D)** Live images of wildtype and immobilized planaria after 6hrs of immobilization. **E)** Assessments used to measure photophobic responsiveness following immobilization; response time and travel velocity were measured. **F-G)** Response time Velocity assed each hour for control and immobilized planaria following 6hrs of immobilization.

repulsed by light[383]. Utilizing planarians natural photophobia, we quantified response time and velocity following intense light exposure. Response time was defined as the time it took for planaria leave its resting position when exposed to light. Velocity was defined as the amount of time it took for the responding planaria to travel from the position of origin to completely out of the frames field of view (1x1z) (Fig 4 C). It was observed that planaria, immobilized for 6hrs and then released, exhibited slower response times and velocities initially when gradually attenuated towards control (untreated) values within a 3hour period (Fig 4 D, E). Immobilization had no adverse effects on planarian behavior and thus results obtained with immobilized planaria are not adverse due to the planarian immobilization procedure.

2.3 Sustained long-term planarian immobilization for non-invasive electrical current stimulation designed to accommodate live viewing and close-proximity optical recordings

Due to the penetrant nature of pulsed electric currents, direct access to planarian tissues is not necessary. However, visual observation of planaria, throughout the course of current administration, was a necessity to allow for observation during regeneration. For these reasons, we developed a chamber that utilized our agar immobilization techniques, to create conductive pathways in which to administer electrical current and fresh pH_2O to isolated, immobilized, and visually accessible planaria. Nonconductive

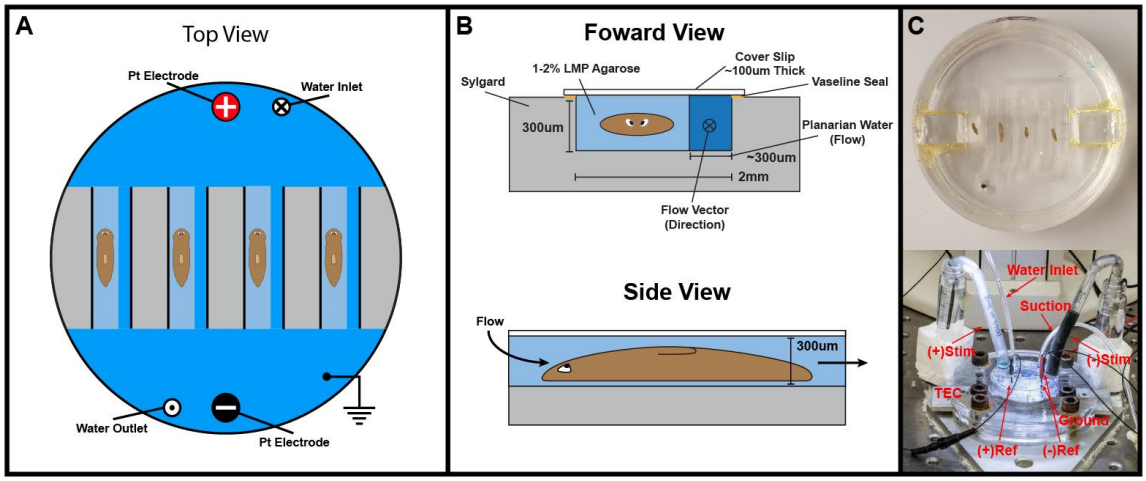

Figure 5. Long-term agar immobilization implemented for pDCS^{P}. **A)** Top view of planarian arrangement for long-term planarian agar immobilization. **B)** Forward and side views of planaria encapsulated in long-term immobilization chambers. **C)** Photo of 4 planaria immobilized in long-term immobilization chambers with and without stimulation setup.

sylgard was used to fabricate chambers equipped with 4 conducting channels, each having a depth of ~300µm, all contained within a 35mm petri dish (Fig 5 A). These channels were designed to house planaria ranging between 2-4mm in length and 100-200µm in depth for periods of up to 7days. Differing slightly from our standard agar immobilization technique described previously: following agar submersion, 4 x 6mm cut glass coverslips were placed atop gelling 1% LMP agarose, sealed on either side with vacuum grease, to create a clean, visually accessible, rectangular agar encapsulation chambers. Once planaria were successful encapsulated, pH_2O was added to the chamber, such that channels were hydrated yet not overflowing, and chambers were placed within our chilling stations (Fig 5 C). To ensure planaria remained hydrated with fresh flowing pH_2O throughout the course of immobilization, small inserts were cut from agar encapsulation rectangles and chambers to connected to gravity powered hydration inlets supplying fresh pH_2O for the duration of the experiment. To ensure water levels were maintained, liquid aspiration was activated opposite that of fluid introduction (Fig 5 A, C). Planaria undergoing these forms of immobilization showed no physical or regenerative abnormalities, attributed to immobilization alone, throughout the course of this study.

2.4 Discussion

Organismal immobilization is an important technique and has broad implications in numerous research disciplines. Immobilization is especially suited for the study of physiological change over time, in real time. Local and/or body wide suppression of gross locomotion is used in various applications from ensuring the safety of experimental subjects during surgical operation or real-time tracing of complex physiological processes to gain insight into the underlying phenomena. Short-term immobilization of many organisms can be achieved using pharmaceuticals to anesthetize the organism and perform measurements. However, significant drawbacks of using local or systemic anesthesia may arise from undesirable side effects the drug(s) may have, directly or indirectly, which have the potential to produce discrepancies within given data sets/observations. When venturing into the unknown, it is wise to reduce the number of variables when addressing a large complex question. As such, when experimental

procedures require local or system immobilization it is key to strive for a harmonious balance between adequate organismal immobilization while reducing the number of foreign environmental factors (drugs, stressors, etc) which may impair normal physiology of the subject.

Planarian immobilization has been achieved, using various techniques, for nearly a century to date[366,370–374]. However, the methods used for immobilization, in many cases, have physiological drawbacks on long-term form and function of planarian organ systems, epithelial tissues, and native plasma membrane proteins[376–380,382]. Therefore, we developed methodology which minimizes environmental stressors while permitting both intermediate (Fig 4 A) and long-term immobilization (Fig 5 B, A). Due to the electrical nature of our experiments, the integrity of epithelial membranes, and transmembrane proteins housed within cellular plasma membranes was of the utmost importance. The decision to implement an agar-based immobilization technique was founded in the need to physically restrain the planarian within a tight mold while simultaneously providing adequate hydration and access to tissues via glass microelectrodes. Agar is a porous substance which, depending on the temperature and agar density, can solidify to form porous, firm, gelatinous molds. The pore size of solidified agar molds, both high- (HMP) and low-melting point agar (LMP), is directly proportional to agar concentration[384]. Moreover, permeation of water and small molecules through agar is, as expected, also dependent on agar gelatinous concentration within its given solvent[385,386]. As such, we chose to use 1.0% LMP agar for planarian encapsulation due to its high resultant pore size and lower gelation temperatures which permit planarian submersion without introducing stress or causing tissue damage[384]. We found that once LMP agar was thoroughly gelled within planarian water temperatures could be dropped to 27-30°C for harmless planarian submersion and then quickly quenched atop ice for proper agar solidification. 0.8-1.0% HMP agar was used to firmly secure LMP encapsulated planarian at fixed locations within a given dish, ensuring planarian hydration and position for manual microelectrode manipulations (Fig 4 A).

Our technique for agar immobilization allowed for reduction of gross locomotion while introducing little to no changes/stressors to the natural planarian environment. We achieved both intermediate or long periods of immobilization with observed full recovery of planaria exhibiting no physical lesions and resuming normal behaviors shortly after encapsulation removal (Fig 4 B). Our immobilization technique also allowed for access of tissues for microelectrode penetration (Fig 4 A), close-proximity fiberoptic recordings of electrical stimulation (Fig 5 A), and even sustained long-term immobilization permitting normal planarian tissue regeneration all the while achieving near complete immobilization. These new immobilization techniques are dynamic and effective in immobilizing a large variety of planarian sizes ranging from 1-10mm. Changing planarian size for intermediate immobilization require slight changes in exposure times to chloretone for adequate anesthetization without any changes regarding agar prep or encapsulation procedure. However, long-term immobilization requires specialized chambers specific to a given planarian size range (Fig 5 A) and as these change, new chambers must be fabricated with larger lane depth, width, and lengths to accommodate planarian sizes.

In many ways, the planarian field needs long-term, efficient, and non-invasive immobilization techniques such as the one presented in this work. To date, both immobilization techniques presented in this work are the longest successful immobilization experiments of planaria without the use of gene knockdown or pharmacological interference. Prior to developing our new planarian immobilization methodologies, the most effective immobilization technique used 3% ethanol leading to a ~3hr immobilization

period[372]. Traditionally, tracking of physiological processes in planaria uses large populations of planaria, treated under the same conditions, which are then fixed at specific stages to assess the progression of a phenotype or process[304,358,365]. Techniques utilizing live tracking of physiological processes is an effective and informative technique gaining popularity in a number of model organisms[387]. However, live tracking within a singular planaria has yet to gain popularity in the planarian field, largely due to the lack of sufficient immobilization techniques. Two clear dilemmas facing the planarian field at large is 1) the in ability to perform transgenic experiments, forcing the expression of fluorescently labeled genes and 2) the capacity to immobilize the planaria for long periods of time and acquire live image tracing of various biological processes. The latter being resolved with this body of work. While planarian transgenics is brought up to speed, there are other forms of live imaging which can enhance our understanding of planarian biology. For example, the use of live potentiometric recordings during regeneration to visualize the tissue potential responses over the course regeneration. Live planarian potentiometric imaging techniques have been done prior to this work[322,331]. However, these potentiometric assessment were performed at various stages of regeneration[322,331], a process differing greatly to one capable of assessing ongoing live tracing of a single animal throughout the course of regeneration. Qualitative visualizations, such as those using potentiometric dyes, are areas in which planarian long-term immobilization can shine.

Despite clear evidence of immobilization and qualitative planarian health, more work must be done to evaluate details by which this immobilization technique effects planarian physiology, if any effect exists. For example, quantitative regeneration assays following long-term immobilization will provide evidence to address whether regenerative events remain consistent between immobilized and non-immobilized planaria. Preliminary results using long-term immobilization techniques demonstrate that regeneration during long-term immobilization retains similar pace to untreated planaria (this will be visited in upcoming chapters) suggesting agar immobilization does not, in any way, impede the planarians capacity to perform regeneration. Nevertheless, proper evaluations of fundamental aspects of planarian physiology such as neoblast function, ventral cilia, outer mucosal layer, and epidermal integrity should all be evaluated in future works to solidify this procedure as a safe and effective alternative to pharmacological or RNAi knockdown immobilization techniques currently in use in the field.

Altogether, these novel planarian immobilization techniques introduce new ways in which researchers can achieve suppression of gross locomotion, and for the first time, with high throughput capacities and immobilization periods exceeding 24hrs. Moreover, this opens the door for studies in planarian electrophysiology, during various biological processes, enabling researchers to attain detailed motion sensitive data such as live images/recordings in the planarian model. It is our hope that these immobilization techniques equip researchers with the tools to ascertain detailed time-lapse experimental data furthering our understanding in an array of research disciplines, including bioelectricity.

CHAPTER THREE

FINDING

Application of DCS^{S} induce rapid stem cell and DNA repair-related gene transcription in the presence of severe DNA damage

3.1 Introduction

To survive, cells must sense changes in their environment and, in response, deliver this information from the outside, to the nuclear transcriptional machinery inside, to alter gene expression. Generally speaking, cellular transcription is the process by which, in response to a given stimuli, cells engage in the formulation of coded RNA sequences, derived from their own genomic database. Transcribed RNA is later processed into either messenger RNA (mRNA), which is used to generate proteins in a processes known as translation[388–390], or will become functional noncoding RNA (ncRNA) units having critical roles in various cellular processes[391–393]. Commonly, gene transcription starts at the cell membrane where environmental cues are received and conferred to the intracellular space through various signaling cascades. This stimulus is then transmitted from the membrane to the nucleus where transcription is to occur. Once the signaling cascade has reached the nucleus, a transcription factor is activated and promotes polymerase binding to its respective promoter sequence within the DNA. Promoter binding is then followed by transcriptional activation by which full length RNA complimentary sequences are generated, these sequences are called pre-mRNA sequences. Pre-mRNA is then spliced at specific points to remove non-coding intron regions from the pre-mRNA, leaving coding exon regions, generating mature mRNA[394–397]. Mature mRNA is then translated into proteins by RNA/protein complex's known as ribosomes along with transfer RNAs (tRNA) which are forms of ncRNA[388–390]. Transcriptional processes are complex and require harmonious orchestration of signaling pathways to go from incoming stimulus to transcribed RNA. We have elected to remain general in our description of the complex process of cellular transcription however, further insight into transcription initiation and fundamental aspects coordinating the transcriptional processes can be found in these most thorough reviews[398–401]. Many cells in the body respond to split second stimulation (e.g. muscles, neurons, auditory cells, etc.) thus, cells have developed methods to respond to such rapidly changing stimuli and can modify their transcriptomic profiles within a matter of minutes.

Rapid changes in transcript abundance can come about in many ways, some of which are not through active transcription. The dynamics of transcriptomic modulation, in response to environmental cues, is a balance between active transcription and mRNA decay[402]. Regulation of mRNA decay allows cells to stabilize and sequester genomic transcripts into mRNA-protein complexes, creating distinct cytoplasmic processing bodies (PBs), that can be called upon in response to, and/or recovery from, changing impetus[402–404]. At any given time, as much as 50% of all polyadenylated mRNA within a cell is contained within these PBs[405,406]. It has been shown that mRNA stored within PBs can be

transferred to polysomes to undergo normal translation[404,407–410]. Stress induced mRNA sequestration can occur within 30 minutes, giving cells dynamic control of basal mRNA abundance[402,411,412]. In many cases, these mechanisms are designed to enhance translation, following environmental stress, by preferentially storing ribosomal mRNA[402,413]. In conjunction to these mRNA sequestering mechanisms, cells are equipped to rapidly respond to stimuli by means of active RNA transcription.

Instances of rapid transcription were first documented during viral infection where viral regulatory factors were rapidly transcribed in host cells within 2 minutes of infection; it was in this body of work were the phrase 'immediate early gene' (IEG) was born[295]. Following this discovery, biologists later adopted the phrase 'IEG' under a more broad context as it was found that many cells had the capacity to facilitate rapid transcription of genes, without the need for de novo protein synthesis, in response to a variety of extracellular stimuli[290,294,298,299,414–417]. Due to the discovery that many IEG transcripts peaked within 30 minutes of stimulation, the threshold for IEG transcription was extended to 60 minutes; encompassing a new array of cellular functions[418,419]. Presently, IEGs have been split into two major categories: rapid and delayed IEGs. This delineation was introduced when researchers noticed many IEGs were known transcription factors transcribed within minutes following stimulation, while others required >30 minutes, and were, in many cases, dependent on the production of their rapidly transcribed counterparts[294,420]. It is important to note that many genes classified as IEGs can be transcribed in a traditional fashion and are not restricted to mechanisms of rapid transcription. However, insight into the mechanisms governing IEG transcription remained elusive until researchers correctly postulated a poised/stalled RNA polymerase II (Pol II) as the trigger mechanism behind many IEG transcription events[294,411].

The time frame associated with rapid transcription calls for cells to adopt mechanisms poised and ready to respond to an array of biological stimuli. Researchers have discovered multiple mechanisms by which rapid transcription can be activated. Examples of these mechanisms include, but are not restricted to: excitation transcription coupling, induction via calcium influx, and poised stalled polymerase adjacent to transcription promoter regions[290,299,411,420,421]. The activation of neuronal IEGs has been observed in a variety of conditions such as: introducing an organism to a unique environment, exposure to electric stimulation, stress, and many other stimuli. It was eventually discovered that there are roughly 40 activity induced IEGs, many of which encode transcription factors[420]. However, some non-transcription factor IEGs, known as effector IEGs, encode unique proteins thought to influence signaling cascades outside the nucleus. IEGs have been studied extensively in neuronal cells as they play a significant roles in long-term memory, learning, behavior, and neural synaptic plasticity involved in neural circuit reorganization underling diverse physiological functions[294,422].

The promoter regions of known IEGs are unique in that, under basal conditions, they resemble promoter regions of actively transcribed genes. Moreover, histones encompassing IEG promoter regions are assembled with chromatin remodeled histone modifications (H3K4me3); promoters themselves are equipped with bound Pol II complexed with various activity dependent transcription factors all properties permissive for active transcription[420,423]. Our understanding of Pol II pausing and release mechanisms from IEG promotor regions is still segmented. However, some transcription factors have been implicated in directly regulating the pausing and release of Pol II. Researchers have found that negative elongation factor (NELF) and DRB sensitive inducing factor (DSIF) induce stabilized pausing of Pol II[411,424] while positive elongation factor b (P-TEFb) and

Myc (c-Myc) promote release and elongation of Pol II[419,425]. Yet, much remains unknown with regards to the active triggering mechanisms authorizing IEG transcription.

Local depolarization of cell membranes, in many cases, leads to influx of Ca^{2+} through voltage gated calcium channels (Ca_Vs). Magnitude of calcium flux, following stimulation, has been shown to be positively correlated with stimulus intensity[426–428]. Thus, weak stimuli leads to localized increases in Ca^{2+} concentration while more intense stimuli leads to elevated cytosolic and/or nuclear Ca^{2+} concentrations[429]. Subsequent calcium signaling results in what is known as Excitation transcription coupling (ETC); in which excitable cells engage in activity induced transcription. Local and/or nuclear elevations in Ca^{2+} concentration, owed to Ca_v activation, has been shown to lead to transcription; through cytosolic Ca^{2+} dependent signaling cascades or nuclear Ca^{2+}-mediated transcription factor activation[288,289,430–433]. Interestingly, many calcium dependent signaling molecules have been found in the immediate vicinity of Ca_Vs; allowing for an expeditious signaling response following Ca^{2+} influx through activated Ca_Vs[300,434–436]. Transcriptional activation of IEGs, brought upon by localized Ca^{2+} influx, is thought to be mediated by signaling cascades involving cyclic adenosine monophosphate (cAMP) and/or calcium dependent protein kinases[289,299,300,421,432,433,437]. Calcium has been implicated in the expression of IEGs due to observed transcriptional sensitivity to Ca_v inhibitors; complimented by live fluorescent tracing showing various signaling proteins being shuttled to the nucleus following synaptic activity (e.g. Ca_v activation)[299,438]. More specifically, Ca^{2+} flux has been shown to activate transcription of a variety of IEGs, among them is a gene known as early growth response gene-1 (*egr-1*).

egr-1, like many genes, is involved in a multitude of signaling cascades governing cellular functions such as cell proliferation, differentiation, wound healing, cancer tumor suppressor, etc[439–441]. Like other IEGs, expression of *egr-1* can be induced rapidly with its transcription found to be regulated by Ca^{2+} flux through Ca_v and sensitive to elevated intracellular Ca^{2+} concentrations[300,301,442]. More recently discovered, inducible through the influx of zinc (Zn^{2+}) through conducting Ca_Vs[296]. As mentioned previously, *egr-1* is a comprehensive gene having diverse functions within a variety of cell types. In neurons, *egr-1* is involved in the learning and memory; and in other mammalian cells, is utilized as a transcriptional regulator involved in cellular differentiation, mitogenesis, and even tumor suppression[297,439,440,443–445]. Interestingly, in planaria *egr-1* (*smed-egr-1*) is crucial for epidermal maturation and is found to be differentially expressed across neoblast subpopulations; enriched within ζ-type neoblast[317,446].

Active transcription often occurs in the presence of DNA torsion and actively introduces the formation of R-loops. Interestingly, studies have shown that DNA torsion may play a role in Pol II pausing[447,448]. R-loops are instances where mRNA binds to complimentary DNA sequences[449–451] however, due to intron splicing, creates unbound looped segments within the DNA which are susceptible to DNA damage[452–454]. Specialized proteins known as topoisomerases I/II (*topo I/II*) are responsible for hydrolyzing DNA to relieve torsion stress such as that introduced by R-loops. However, in doing so, *topo I/II* must introduce DNA double stranded breaks (DSBs) consequently creating DNA damage and incurring innate cellular DNA damage responses (DDR). Researchers have found that the promoter regions of genes transcribed via paused Pol II are enriched with DDR protein complexes, caused by nascent DSBs, shown to stabilize Pol II pausing and enhance both Pol II release and elongation[448,454]. It has been found that DSBs, within the promoter region of a subset of IEGs, including *egr-1*, is sufficient to induce their rapid expression in a *topo IIβ* independent manner[455]. Together, this work shows the unexpected importance of DSB and associated DDR proteins for IEG transcription.

For decades, it has been shown that an array of cell types manifest unique cellular responses in the presence of applied electric currents. Of the many responses, it has been observed that abundance of specific proteins become significantly enriched following electric stimulation[456–458]. Consequently, it was found that many of these EF dependent protein enrichments were superseded by EF induced active RNA transcription[458,459]. Since these findings, numerous studies have established that application of EFs can induce RNA transcription in a variety of cell types[458–461]. Furthermore, genes induced by applied EFs are known to be involved in a multitude of signaling pathways regulating everything from cellular differentiation, mitogenesis, apoptosis, and migration[458,460]. Interestingly, electric induction of known proponents to IEG transcription has been observed in neuronal and non-neuronal cells which, following exposure to applied EFs, experienced differential expression of *c-fos* and *MAPK*[458–460]. While it has been known that electric stimulation of neuronal cells induces Pol II-mediated transcription of IEGs[288,289,294,299], transcriptional activation via applied EFs within non-neuronal, non-excitable cells, is a novel observation[459,460]. Moreover, applied EFs have been shown to induce transient increases in cytosolic Ca^{2+}[457,462], a known mediator of IEG transcription[299–301,430]. Interestingly, EF induced gene transcription was observed to be most abundant at early stages of EF exposure, in some cases as rapid as 30min post-EF initiation[458–460,462]. Thus, we aim to specifically implicate mechanisms of rapid IEG transcription with EF-related transcriptional activity and illustrate how applied EFs can predictively induce rapid transcription of stem cell-specific genes altogether furthering the understanding bioelectric regulation of gene transcription.

3.2 pDCS^S activates stem cell-specific gene expression within lethally irradiated tissues

Neoblasts were isolated within the planarian body by transplanting a healthy cylindrical WT tissue insert, measuring ~800µm in diameter, into lethally γ-irradiated (6K rads) tissue; all experiments were carried out four days post-transplantation (4DTP) (Fig 6 A). pDCS^S, generated by injecting 7µA across the pre- and post-pharyngeal region, to immobilized transplanted planaria caused significant increases in mRNA levels of the neoblast specific marker *smed-piwi-1*. To quantify *smed-piwi-1* expression profiles during pDCS^S we performed a time course of pDCS^S from 15mins to 60mins assessing mRNA levels every 15mins. It was observed that pDCS^S caused a significant increase in *smed-piwi-1*$^+$ cells within the host tissue throughout the time course,

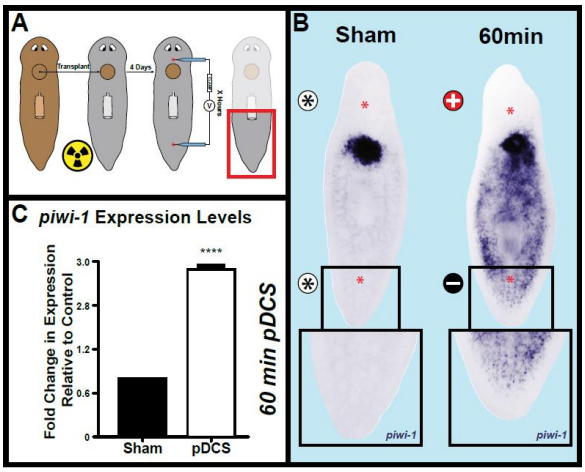

Figure 6. pDCS^S induce rapid transcription of neoblast markers. **A)** Schematic representation of planarian transplantation where healthy unirradiated tissue is transplanted into lethally γ-irradiated tissue. Four days post-transplantation (4DTP) planaria are subjected to weak steady state electric stimulation through the injection of current (7µA) via pulled glass microelectrodes, of approximately 1MΩ resistance, clamped over a 10MΩ resistor. Currents are applied for varying times and planaria are then fixed and analyzed through different molecular techniques. **B)** *In-situ hybridization* of *smed-piwi-1* illustrating *smed-piwi-1*+ induction at 60 minutes compared to a transplanted planaria without applied current (control). **C)** *Smed-piwi-1* expression levels measured in transplanted tail tissues by qPCR analysis against housekeeping gene *UDP glucose*. Values are illustrated as foldchange of sham vs 60min pDCS^S planaria.

most notably in distal posterior tissues (Fig 6 B). Interestingly, qPCR analysis of *smed-piwi-1* mRNA levels at each time point showed the most elevated levels of *smed-piwi-1* transcripts at 15mins with an 18-fold increase in *smed-piwi-1* expression; this progressively decreased reaching a 1.5-fold increase at 60min pDCS^{S} (Fig 6 C). This rapid transcriptional response was indicative of a process known as immediate early gene transcription (IEG). It was also noted that expression of neoblast markers *smed-cyclin-B* and *smed-PCNA* followed the same trend as seen with *smed-piwi-1*. This data suggests that neoblast genes were being rapidly transcribed in response to applied EFs. However, expression within distal posterior host tissue, in such a short period of time, begged the question of whether cells expressing these genes originated from the donor or the host tissue.

3.2.1 pDCS^{S} initiates a robust, rapid transcriptional response within lethally irradiated tissues

It is well known that certain cells can respond to stimuli with rapid transcription. This is most likely out of necessity, with rapid incoming stimuli cells must adapt and respond with a rapid form of gene transcription so that they may change their diverse genetic profile. One known mechanism for rapid gene transcription is called immediate

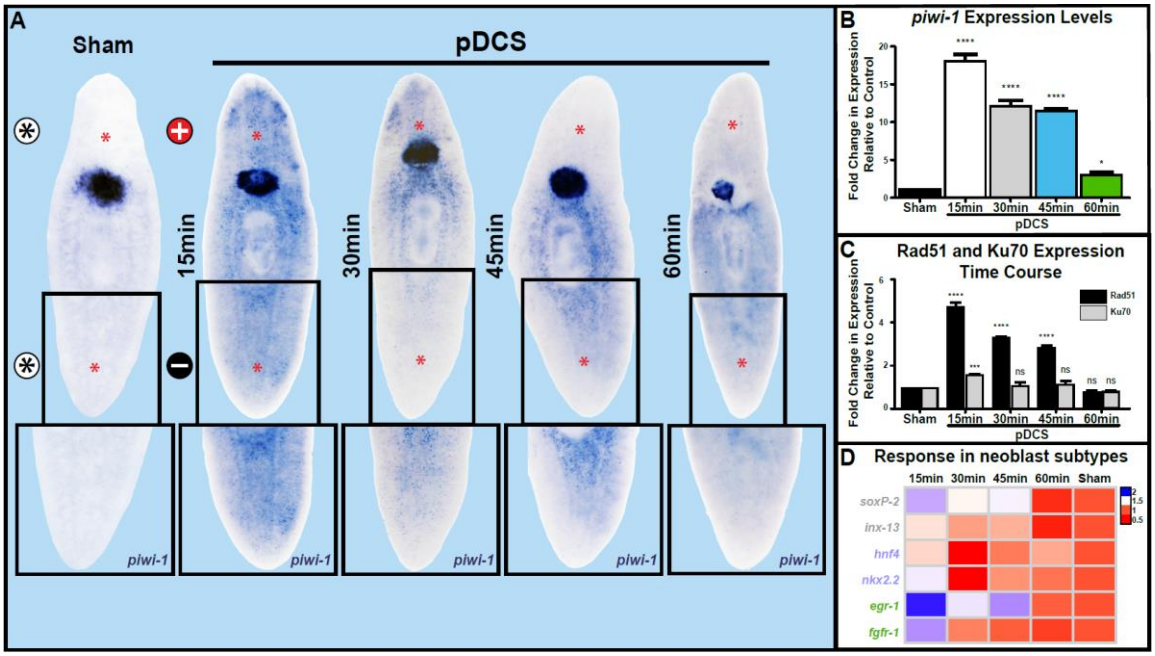

Figure 7. pDCS^{S} induces rapid transcription of neoblast markers. 4DTP planaria are subjected to weak electric currents through the injection of current (7μA) via pulled glass microelectrodes of approximately 1MΩ resistance. pDCS^{S} application is performed for 15, 30, 45, and 60min; planaria are then fixed and analyzed through different molecular techniques. **A)** *In-situ hybridization* of *smed-piwi-1* illustrating *smed-piwi-1*+ induction at 15, 30, 45, and 60 minutes compared to a transplanted planaria without applied current (control). **B)** *Smed-piwi-1* expression levels as measured by qPCR analysis against housekeeping gene *UDP glucose*. Values are illustrated as foldchange of sham compared to pDCS^{S} planaria. **C)** *smed-Rad51* and *smed-Ku70* expression levels within the tail fragment of +/-pDCS^{S} transplanted planaria, as measured by qPCR analysis against *UDP glucose*. **D)** Time course analysis of neoblast subpopulation genes for σ-type (*smed-soxP-2, smed-Inx-13*) γ-type (*smed-hnf4, smed-nkx2.2*), and ζ-type (*smed-egr-1, smed-fgfr-1*) as represented by a heatmap. P<0.005**, P<0.0005***, P<0.0001**** and ns= no significance, One/Two-Way ANOVA. Three independent replicates 5 animals/experiment.

early gene transcription (IEG)[294,298]. Neurons have been the primary cells in which these mechanism are heavily investigated, being cells that constantly respond to µs changes in stimuli, genomic plasticity is a fundamental property of neural cells playing crucial roles in dynamic processes such as learning[139,294,296,420]. There are two prominent categories of IEG transcription delineated by their temporal timeframes; rapid (active within 0 to 30 minutes) and delayed (active within >30min) IEG transcription[294,411]. Delayed IEG transcription, requires transcription factors in the nucleus to recruit RNA Pol II and chaperon this transcription complex to the promoter site to initiate transcription. This mechanism of IEG transcription requires more time and as a result, transcript level changes can be seen between 30-60 minutes[294,298]. The second form of IEG transcription is termed rapid IEG transcription. Rapid IEG mechanisms relies on poised RNA Polymerase II which is actively stalled on the promoter site by negative elongation factor (NELF)[411]. Once a stimulus is received, the stalling protein, NELF, is inhibited, releasing RNA Pol II to actively begin transcription. Genes following rapid IEG can be detected as early as 2 minutes following a stimulus[411,463]. As described previously, we observed changes in transcription as early as 15mins after stimulated with pDCS^S (Fig 7). However, changes in gene expression persist for as long as 60mins, suggesting that pDCS^S engage in both rapid and delayed mechanisms to induce gene expression within these resident cells. Therefore, we set to explore regulatory networks underlying rapid pDCS^S using known regulatory networks underlying IEG transcription as guidelines.

It is known that Ca^{2+} influx through L-Type voltage gated calcium channels (Ca_v) can directly lead to IEG transcription in some IEG inducible cells[300]. We tested the role of L-Type Ca_vs in the IEG transcription we observed using pDCS^S. We enlisted the pharmacological inhibitor nicardipine (NIC) to block the activity of L-Type Ca_vs in the adult planaria. Dihydropyridine (DHP) Cav antagonist NIC was chosen over other DHP antagonists like nifedipine or nimodipine due to its established superiority in platyhelminth Cav inhibition. Planaria Ca_vs have conserved variation at specific amino acid residues located within the DHP binding pocket (in rat:Q1043 and M1161 to Q/E/V1043 and I1161 in planaria) which confer decreased affinity/sensitivity to DHP inhibition[464,465]. Mutations at these residues in the DHP pocket have been shown to decrease DHP affinity 10-fold[466]. NIC overcomes these site variations and effectively inhibits planarian Ca_vs due to its ionizable alkylamino group on the 5-position of the pyridine ring which has been shown to interact with residues outside of the DHP binding site[467]; it is this interaction, unique to NIC, that is thought to be responsible for planarian Ca_v inhibition via NIC[464]. The effectiveness of NIC over other DHPs has been proven experimentally in planaria[464,468–470].

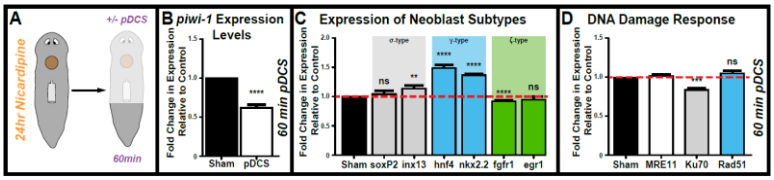

Figure 8. Nicardipine (NIC) effectively attenuates pDCS^S induced transcription within the tail post-60 minutes application. **A)** Schematic representation of experimental design showing a 4DTP planaria soaked in 5µM NIC for 24hours and then subjected to (+/-)pDCS^S for 60minutes, for analysis we focused on tail fractions. **B)** qPCR analysis showing gene expression levels of *smed-piwi-1* in (+/-)pDCS^S 4DTP planaria respectively, soaked for 24hr in 5µM NIC planarian water. We observed a significant decrease in *smed-piwi-1* expression in NIC soaked pDCS^S planaria compared to sham. **C)** qPCR analysis showing gene expression levels of neoblast subtypes (σ-type, γ-type, and ζ-type) showing varied responses to pDCS^S application in the presence of NIC. **D)** qPCR analysis showing no significant response in DNA damage repair genes in pDCS^S planaria compared to sham in the presence of 5µM NIC. P<0.005**, P<0.0005***, P<0.0001**** and ns= no significance, One/Two-Way ANOVA. Three independent replicates 5 animals/experiment.

To effectively inhibit L-Type Ca_vs with nicardipine, we soaked transplanted planaria in 5uM NIC planarian water for 24hrs, prior to $pDCS^S$ exposure. Planaria were then rinsed with fresh planarian water and immobilized as described previously (Fig 8 A). In NIC exposed planaria we found that, even after 60min $pDCS^S$, there was a notable decrease in *smed-piwi-1* expression when compared to the NIC control (Fig 8 B). This is due to effective NIC inhibition of L-type Ca_v blocking the flux of Ca^{2+} into stimulated cells. This is further demonstrated by the lack of induced transcription of neoblast subpopulation markers (Fig 8 C) as well as the consistent DDR transcriptional response (Fig 8 D). All previously seen transcription activity was effectively blocked by the L-type Ca_v inhibitor NIC. When looking at single cell RNAseq data for L-type Ca_vs it is shown that γ-type neoblast subpopulations are not enriched in L-type Ca_v expression[317], consistent with our results showing NIC inhibition have little effect on γ-type gene expression within $pDCS^S$ planaria (Fig 8 C).

Egr-1 is a well characterized and established IEG[296,471–473]. In the planarian model, *egr-1* is a gene marker for the ζ-type subpopulation of neoblasts[317,474,475]. *Egr-1* consistently responds to $pDCS^S$ in nearly all $pDCS^S$ conditions in which we impose upon transplanted planaria. As would be expected of an IEG, *egr-1* exhibits its highest expression levels within 15min of $pDCS^S$ (Fig 7 D). We strongly believe this response from planarian *egr-1* is indicative of IEG transcription onset rapidly by $pDCS^S$. In addition to the response from egr-1, all other neoblast subtype genes (*soxP-2, inx-13, hnf4, nkx2.2, and fgfr-1*) exhibit their highest levels of expression at 15min $pDCS^S$; suggesting this transcriptional response is influencing a wide variety of signaling pathways (Fig 7 D). Interestingly in the presence of NIC, IEG transcription is inhibited showing no significant increase in egr-1 transcription (Fig 8 C). This transcriptional impotence, with regards to *egr-1*, was also observed when transplanted planaria, exposed to 60min $pDCS^S$, contained no healthy neoblasts within the body (Fig 9 M, O). These data strongly suggest IEG mechanisms are behind the observed transcriptional response to $pDCS^S$.

3.2.2 $pDCS^S$ induced gene expression originates within the lethally irradiated host tissues yet requires the presence of healthy transplanted neoblasts

To test the ancestry of *smed-piwi-1*$^+$ cells found in the tail of transplanted planaria treated with $pDCS^S$, we setup a series of transplantation conditions to deduce the origin of *smed-piwi-1* expressing cells. We set to confirm prior observations using the original transplantation conditions, WT to IRR, and performing $pDCS^S$ for 60mins (Fig 9 A). Consistent with our prior findings, *smed-piwi-1* expression was significantly increased post-$pDCS^S$ (Fig 9 B). Interestingly, $pDCS^S$ significantly increased a variety of neoblast subtype specific genes as well as genes associated with DNA damage response (DDR) (Fig 9 C, D). It was noted that among the DDR genes measured by qPCR, *Smed-Rad51*, which is vital for homologous recombination, was significantly increased following 60mins of $pDCS^S$ (Fig 9 D). To test whether *smed-piwi-1*$^+$ cells were coming from transplanted tissues we removed *smed-piwi-1* expression from donor planaria via *smed-piwi-1* RNAi and transplanted *smed-piwi-1* RNAi into lethally irradiated host tissue (Fig 9 E). *Smed-piwi-1* RNAi only inhibits neoblasts from expressing *smed-piwi-1* but in no way influences their behavior or ability to operate as full-fledged neoblasts[363]. After measuring *smed-piwi-1* expression, via qPCR, within the tail of the host we found that *smed-piwi-1* expression remained elevated post-60min $pDCS^S$ (Fig 9 F). Interestingly, gene expression of neoblast subpopulations (Fig 9 G) and DDR genes (Fig 9 H) were elevated by $pDCS^S$ application

similar to WT to IRR transplant pDCS^S conditions. To confirm the hypothesis that *smed-piwi-1*$^+$ cells are resident to host tissues we performed *smed-piwi-1* RNAi to host tissues

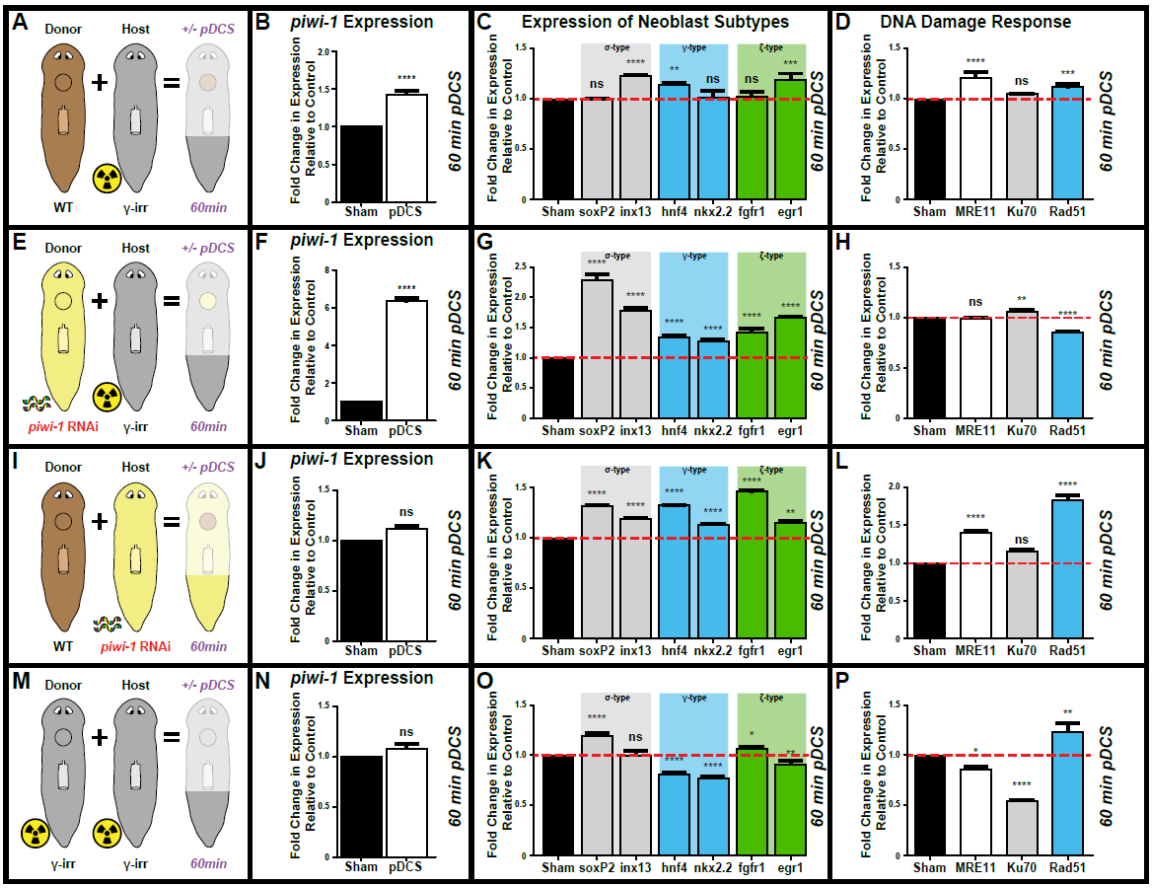

Figure 9. It was concluded that resident host cells within the tail region, and not transplanted neoblasts, respond to pDCS^S and required the presence of healthy transplanted neoblasts. **A)** Schematic representation of planarian transplantation where healthy unirradiated tissue is transplanted into lethally γ-irradiated (6k rads) tissue. 4DTP planaria are subjected to pDCS^S through the injection of current (7μA) for 60 minutes. RNA is then extracted from tails fractions for qPCR analysis. **B)** *qPCR analysis of* of *smed-piwi-1* showing a significant increase at 60 minutes pDCS^S compared to sham. **C)** qPCR panel measuring genes indicative of neoblast subtype populations σ-type, γ-type, and ζ-type after 60 minutes of pDCS^S. **D)** Transcriptional response following 60minutes of pDCS^S of genes known to play significant roles in DNA damage repair whether it be indicators of DNA repair initiation (*smed-MRE11*), nonhomologous end joining (NHEJ; *smed-ku-70*) or homologous recombination (HR; *smed-Rad51*). **E)** Replicate experimental procedure and analysis as shown in (A) however the donor tissue is originating from an *smed-piwi-1* RNAi planaria while the host is lethally γ-irradiated. **F, G)** qPCR analysis of genes of interest show significant increases post-60 minutes of EF application however the **H)** DNA damage repair genes are showing mild or decreased responses in gene expression. **I)** Replicate experimental procedure and analysis as shown in (A) however the donor tissue is wild type while the host tissue is *smed-piwi-1* RNAi. **J)** qPCR analysis showing no significant changes in *smed-piwi-1* expression. **K)** Significant increases are still found in neoblast subtypes as well as **L)** DNA damage repair genes after 60 minutes of pDCS^S. **M)** Schematic representation of planarian transplantation where donor and host tissues are lethally γ-irradiated (6k rads), given 4DTP, and exposed to 60 minutes of pDCS^S. **N)** qPCR analysis of *smed-piwi-1* showing no significant changes in expression. **O)** Expression levels of neoblast subpopulation genes vary indiscriminately after pDCS^S. **P)** Expression levels of DNA damage repair genes following 60 minutes of pDCS^S showing increases in NHEJ while HR-related genes are reduced. P<0.005**, P<0.0005***, P<0.0001**** and ns= no significance, One/Two-Way ANOVA. Three independent replicates 5 animals/experiment.

and transplanted WT tissue in the pre-pharyngeal region (Fig 9 I). As expected, *smed-piwi-1* expression was attenuated to control levels even with 60min pDCS^{S} (Fig 9 J). This suggests that *smed-piwi-1*$^{+}$ cells are in fact resident cells expressing *smed-piwi-1* in the presence of severe DNA damage following pDCS^{S}. Under these conditions, resident cells were still able to express neoblast subpopulation markers (Fig 9 K) as well as DDR genes, most notably *smed-Rad51* (Fig 9 L). However, in experiments where both donor and host tissue was lethally irradiated (Fig 9 M), *smed-piwi-1* mRNA was negligible (Fig 9 N). This result indicates that somehow, pDCS^{S}-mediated transcription within host tissue requires the presence of transplanted neoblasts. In fact, transcription of neoblast subclass markers were varied in response to pDCS^{S}, with both increased and decreased levels with respect to control (Fig 9 O). Interestingly, DDR genes responded to pDCS^{S}, with a notable increase in *smed-Rad51* gene expression (Fig 9 P). From these experiments we believe that resident, γ-irradiated, cells are sensitive to pDCS^{S} and respond with elevated transcriptional activity. The transcriptional response involving *smed-Rad51* is very interesting because it may be a mechanism by which these cells, possibly resident neoblasts, are actively repairing their damaged DNA thus regaining competence in the presence of severe DNA damage.

3.3 Discussion

Epithelialized tissues have long been known to generate endogenous TEPs that influence local cellular function. These TEPs have been shown to play crucial parts in the formation of anatomical parts during regeneration, neural guidance and growth, and can influence cellular migration among a wide array of cell types to name a few impacts of endogenous bioelectricity. Moreover, single cells are functionally dependent on self-generated RMPs utilizing these bioelectrical phenomenal in a plethora of signaling cascades. It comes to no surprise that bioelectrical signaling is largely engrained in cellular and organismal function. As such, manual manipulation using exogenous applied electric fields presents itself as a powerful tool to predictively modulate form and function at both the cellular and organismal level. Utilizing the planarian model due to its simplistic anatomical modality and evolutionarily conserved signaling mechanisms, we explored the effects of applied electric fields on stem cell behavior focusing on cellular transcription and subsequent gene expression modulation.

Common instances of regional sustained bioelectrical depolarization occur during epithelial wounding. Injury sustained by epithelial tissues effectively short circuits the TEP at the injury site generating adjacent lateral electric fields[3,4,234,291,292,476]. These generated electric fields depolarize cell plasma membranes which can have profound effects on membrane composition and resulting cellular function[3,4,7,237,279,282,291,335]. The presence of depolarizing injury induced endogenous TEP depolarization within amputated planaria has been demonstrated using voltage sensitive potentiometric dyes[322,374]. Furthermore, these depolarizing potentials generate endogenous EFs which are felt within planarian tissues. These injury potentials have been shown to guide normal planarian regeneration as disruption or manipulation of these injury potentials, pharmacologically or through exogenous current injection, results in regenerative abnormalities[322,323,368]. The ability for planaria to properly and completely regenerate lost or damaged tissues, with a nearly boundless capacity, remains poorly understood. However, it is well known that complex transcriptional patterning underlie the planarian regeneration; governing the fate, architecture, and location of regenerating tissues[326,359,367,477]. Complete, large scale, planarian regeneration requires 5 to 7 days[304,365]. However, the underlying gene

expression profiles change rapidly upon onset of injury, exhibiting differential expression as early as 60 minutes post-amputation[324,327,365,477]. However, the connection between genetic regulation of stem cell behavior during regeneration/tissue reconstitution and depolarizing electric fields has not been directly addressed experimentally in planaria. Moreover, bioelectrical regulation of stem cells during tissue regeneration and normal cellular turnover is, in large part, grossly overlooked when investigating stem cell-mediated phenomena.

3.3.1 pDCS^{S} promotes neoblast specific gene expression within lethally irradiated tissues via host cell stimulation

To study bioelectrical regulation of neoblast gene expression we designed an experimental model which enabled us to isolate healthy neoblasts within the planarian body to dissect their genetic response to electrical stimulation both spatially and temporally (Fig 6 A). Healthy neoblasts were transplanted into lethally irradiated tissues to effectively isolate neoblasts within irradiated tissues and dissect their response to applied electric fields generated thought he injection non-oscillating currents (Fig 6 A). After substantial vetting of a range of current magnitudes, we found that 7μA-10μA of non-oscillating current injection was near maximal capacity for planarian tissues before causing tissue damage (Fig 6 A). As mentioned previously, planarian tissue amputation induces rapid genetic responses within neoblasts and differentiated tissues alike[319,477]. Yet, this genetic response has not been investigated with respect to bioelectrical depolarizations experienced by planarian tissues as consequence of tissue amputation. By injecting 7μA across the transplanted planarian body we found that within 60mins of pDCS^{S} there was a large increase *smed-piwi-1*$^{+}$ cells, a neoblast specific marker (Fig 6 B). The expression of a neoblast specific marker suggests not only the presence of healthy neoblasts but that they can be found within distal regions of lethally irradiates host tissues (Fig 6 B). Further confirmation through qPCR analysis shows a significant increase in piwi-1+ cells within irradiated tissues following current stimulation (Fig 6 C). Most striking about this finding is the shear displacement between healthy transplanted neoblasts and *smed-piwi-1*$^{+}$ cells observed within lethally irradiated tissues 3-5mm away from the transplant. Moreover, this response is achieved with 60mins of current stimulation, observed and quantified immediately after stimulation. Begging the question, is this expression the result of transplanted neoblasts rapidly migrating to repopulate irradiated tissues in the presence of pDCS^{S} or is this the result of resident cells expressing neoblast specific markers despite severe DNA damage received from lethal irradiation and if so, what cells type specifically?

A series of planarian transplantation conditions were designed to dissect the origin of cell expressing neoblast markers following 60mins of pDCS^{S}. To control the origin of *smed-piwi-1*$^{+}$ expressing cells, we designed transplantation models using dsRNA silencing techniques to nullify *smed-piwi-1* expressing cells within specific tissues (Fig 9 E, I). First, we repeated the standard transplantation condition with stimulation as a baseline for pDCS^{S} stimulated neoblast specific gene expression (Fig 9 A). Following the standard model, we transplanted tissue from a *smed-piwi-1* deficient (*smed-piwi-1*$^{-}$) donor into a lethally irradiated host absent *smed-piwi-1* expression (Fig 9 E). Subsequent *smed-piwi-1* expression, following pDCS^{S}, within this *smed-piwi-1*$^{-}$/γ-irr model would, by deduction, must originate in cells absent *smed-piwi-1* dsRNA and as such be resident cells within the γ-irr host. It was shown, through qPCR analysis, that piwi-1 expression remained at elevated levels following pDCS^{S} (Fig 9 F). In addition to this finding, gene markers for neoblast subpopulations also exhibited elevated expression patterns following

pDCS^{S}, like that of our standard transplant model (wt/γ-irr) (Fig 9 C, G). These analyses show clear evidence of resident cells responding to pDCS^{S} disregarding aberrant levels of DNA damage. To confirm our hypothesis that pDCS^{S} stimulated *smed-piwi-1* gene expression originates within the lethally irradiated host tissues, we generated a transplant model in which wildtype donor tissue was transplanted into a *smed-piwi-1*$^{-}$ host (wt/*smed-piwi-1*$^{-}$) (Fig 9 I). As expected, gene expression of piwi-1 within host tissues was insignificant (Fig 9 J). Gene expression related to neoblast subpopulations remained sensitive to pDCS^{S}, illustrating the presence of healthy neoblasts within *smed-piwi-1*$^{-}$ host tissues capable of responding to pDCS^{S} yet incapable of mobilizing a *smed-piwi-1* specific response. Interestingly, transplant models in which both donor and host tissues received lethal doses of γ-irradiation (γ-irr/γ-irr) pDCS^{S} was incapable of generating a stem cell-related gene expression response (Fig 9 M, N, O). This finding suggests the planarian body requires the presence of healthy, functioning, neoblasts to mobilize stem cell-related transcriptional responses to pDCS^{S}.

3.3.2 DNA damage repair genes are elevated within irradiated tissues following pDCS^{S}

Our methods of pDCS^{S} clearly resonate throughout the planaria. However, discovering that these effects are directly dependent on host tissues introduces new and exciting possibilities for electrotherapy. Reason being, both active RNA transcription and cellular mitosis rely on sufficient levels of DNA integrity[478–480], levels which are seemingly out of reach within the lethally γ-irradiated tissues of the host planaria. In the planaria, it has been shown that exposure to sublethal doses of γ-irradiation causes DNA DSBs and induces a subsequent systemic DDR[481]. When exposed to sublethal doses of γ-irradiation, planarian neoblasts are quickly wiped out however, after several days, neoblast populations recover and normal homeostatic cellular turnover ensues resulting in organismal recovery[482,483]. These studies fail to elaborate on the status of genomic integrity throughout this recovery period even though it has been clearly shown that DDR is quickly initiated within sublethal γ-irradiation planaria. Nevertheless, recovery of neoblast populations following lethal doses (>4000rads) of γ-irradiation is a feat no planarian researcher has yet to accomplish. For the first time, we show evidence that populations of neoblasts can be stimulated to resume normal neoblast specific activities despite lethal doses of γ-irradiation.

Similar to the rapid induction of *smed-piwi-1* gene expression during pDCS^{S}, DDR specific gene *Rad-51* is rapidly induced by pDCS^{S}; resembling the same characteristic decline with increasing stimulation times observed in *smed-piwi-1*(Fig 7 C). This pDCS^{S} induced DDR phenomena is one which has received little to no attention among the community of researchers investigating various electrotherapies. However, we believe these responses are regulated by rapid changes in intracellular Ca^{2+} ion concentrations induced by pDCS^{S}. This hypothesis is supported by research linking rapid DDR with increased intracellular Ca^{2+} concentration. A known contributor to rapid DDR is poly ADP-ribose polymerase 1 (PARP-1). PARP-1 is a nuclear protein which rapidly nucleates at site of DNA damage (within 1-2min) and recruits DDR proteins to proceeded with proper DNA repair[484,485] and is an important step in the initiation of cell survival and avoidance of programmed cell death[485,486]. Interestingly, it has been shown that PARP-1 activation, in response to DNA damage, directly stimulates the activation of various Ca^{2+} ion channels of the transient receptor potential ion channel (TRP) protein family[487,488]. Moreover, increased concentration in intracellular Ca^{2+} is crucial to the survival of cells latent with

DNA damage as it serves to facilitate the shuttling of phosphorylated nuclear ATM into the cytosol to activate NF-kB leading to the execution of a cell survival pathway. Not surprisingly, the cell survival pathway onset by NF-kB activation requires activated PARP-1[486,489]. Thus, rapid DDR and cellular resilience in the presence of surmountable DNA damage are processes which are heavily reliant on intracellular Ca^{2+} concentrations. Moreover, we demonstrated inhibition of cellular influx of Ca^{2+} via L-type Ca_v significantly reduced the rapid increases in DDR gene expression following $pDCS^S$ (Fig 8 D). Together, this data provides for the first time a link between bioelectrical signaling and rapid induction of DDR genes crucial for securing cell survival in the presence of DNA DSBs. Although further experiments are required to generate substantial casual links between $pDCS^S$ induced Ca^{2+}/PARP-1-mediated rapid DDR and subsequent cell survival within the γ-irradiated tissues of the transplanted host, these data show promising links between already known regulators of these important cellular pathways fueling the curiosity for future study of these conserved mechanisms in the planarian DNA damage model.

3.3.3 Rapid transcription induced through $pDCS^S$ is mediated by Ca^{2+}, a known regulator of rapid IEG transcription

One of the most significant findings of this work was the ability for $pDCS^S$ to induce transcription of neoblast specific genes within lethally irradiated host tissues. Initial findings of 60min expression prompted interest in the temporal dynamics of *smed-piwi-1* expression in the presence of $pDCS^S$. To our surprise, $pDCS^S$ induced the most robust *smed-piwi-1* expression within 15min $pDCS^S$ (Fig 7 A, B), completely eclipsing the initial observation of *smed-piwi-1* expression at 60min (Fig 6 B, C). However, other model systems have demonstrated the capacity to initiate rapid gene expression following a given stimulus. One mechanism, rapid IEG transcription, caught our interest as we found that *egr-1*, a known IEG[471–473], exhibited rapid expression during $pDCS^S$ exposure (Fig 7 D). In addition to egr-1, all measured genes delineating the three neoblast subtypes, as well as DDR gene *smed-Rad51,* exhibited the highest expression levels at 15min, consistent with measured piwi-1 expression. Although these genes are having yet to be characterized as IEGs, we demonstrate their susceptibility to Ca^{2+} flux, a known regulator of rapid IEG transcription. As the potential mechanisms for $pDCS^S$ induced rapid *smed-Rad51* transcription have been discussed previously, we will focus on the expression dynamics of neoblast specific genes.

One of the most common cell types to partake in rapid IEG transcription are excitable cells. A variety of muscle and neural cell types have been shown to have the capacity to mount rapid IEG transcription following endogenous or exogenous electrical stimulation in a process known as excitation transcription coupling[288,289,433]. Interestingly, intracellular Ca^{2+} concentration has been shown to regulate the capacity for these cells to mount these rapid transcriptional responses even in the presence of saturating stimuli[139,299–301,490]. In the planaria, muscle cell excitation is initiated by Ca2+ influx through L-type Ca_vs[491] and L-type Cav inhibition in planaria has been shown to impact the expression of various genes required for proper tissue regeneration[468,469]. To elaborate on this, we subjected transplanted planaria to L-type Cav inhibition via 5µM nicardipine soaking for 24hrs and then proceeded to subject these planaria to equivalent $pDCS^S$ exposure for 60min. We found that NIC inhibition was sufficient to completely abrogate $pDCS^S$ induced gene expression of *smed-piwi-1, smed-Rad51*, and most neoblast subtypes including IEG *egr-1*. Although more experiments are required to sufficiently implicate the prominent secondary messenger Ca2+, we believe these experiments

demonstrate some of the first documented instances of IEG expression in planaria and display the capacity for DCS^S to generate rapid, significant responses within otherwise hopeless irradiated tissues. With further understanding of mechanisms permitting DCS^S induced neoblast responses, we believe DCS therapies can be utilized to rapidly and effectively initiate stem cell activity in tissues where significant levels of DNA instability is rampant such as cancer patients receiving radiation therapies or patients suffering from various age-related ailments.

CHAPTER FOUR

FINDING

DCS^S enhances DNA damage repair, influences cell cycle behavior, and induces mitotic activity within lethally irradiated tissues

4.1 Introduction

Ionizing radiotherapy is a common cancer therapy target toward the destruction of proliferative cancer cells through the introduction of aberrant levels of DNA damage. However, in some cases, radiotherapies are insufficient and result in incomplete cancer removal as some ionized cancer cells prove radio-resistant and overcome severe DNA damage, evading programmed cell death[492,493]. Understanding how cancer cells can overcome such severe DNA damage may provide insight into mechanisms of rapid and efficient cellular DNA repair. Interestingly, unique ion channel activity has been shown to contribute towards intrinsic and acquired cancer cell radio-resistance[494,495]. Of the ion channels attributed with radio-resistance is the nonselective cation channel member 2 of the melastatin family of transient receptor potential channel (TRPM2). TRMP2 expression is found in a variety of cancerous growths including insulinomas, hepatocellular carcinomas, lymphomas and many others. TRPM2 has two means by which it is activated: 1) activation through reactive oxygen species[487] or, through its principal activator, 2) ADP-ribose (ADPR)[487,496]. ADPR is generated by either the mitochondria or produced through the release of ADPR from ADPR polymers by glycohydrolayses[497]. Interestingly ADPR polymers are formed during DNA repair by poly ADP-ribose polymerases (PARPs)[484,494]**.** PARPs recruit ALC1, a known DDR protein, of whom role is to remodel chromatin to facilitate DNA damage repair[484]. The onset of DNA damage triggers TRPM2 activity causing influx of cations, including Ca^{2+}, resulting Ca^{2+} overload and subsequent programmed cell death[494]. However, many cancer cells express a mutated form of TRPM2 which contains a truncated, non-functional, conductance pathway effectively silencing TRPM2 activity[498]. In addition to this finding, TRPM2 has been found to regulate the formation of nuclear phosphorylated histone H2AX (γH2AX) foci[488]. Nuclear γH2AX is responsible for initiating and orchestrating repair of DNA double stranded breaks (DSBs) by serving as a docking point for DNA damage repair molecules[499]. From these data it has been speculated that ion flux through TRPM2, and other TRP family ion channels such as TRPV1, is directly influenced by the introduction of DNA DSBs and are paramount in the formation of DNA damage repair complexes[494].

DDR requires cell cycle arrest to allow cells time to assess the damage and undergo active repair. It has been shown that, in addition to TRP family ion channels, voltage gated K^+ channels (K_v) have been implicated in the orchestration of cell cycle arrest and allowance of DNA repair[488,495,500]. Ca^{2+} conductance through TRP ion channels depends heavily on K_v activity. Leukemia cell survival following irradiation rely heavily on the Influx of Ca^{2+}, by means of nonselective ion flux, and thus K_v activity. It was found that

influx of Ca^{2+} and interim K_v activity permits G_2/M cell cycle arrest through a CaMKII-mediated inhibition of cdc25B. Inhibition of K_v activity via RNAi blocked G_2/M cell cycle arrest leading to decreased cell proliferation and increased cell death[495,500]. Once the cell has effectively entered an arrested state, DDR proteins must nucleate at the appropriate sites of damage and engage in active DNA repair. As discussed, γH2AX nucleates at DNA lesions and promotes the localization of DNA repair machinery. The process of DNA damage response involving γH2AX is complex and deserves further elaboration.

The key regulator for the formation of DNA lesion foci is γH2AX. The H2A variant, H2AX, comprises roughly 10-15% of all cellular histones as a core component of nucleosomes and disruption of its phosphorylation compromises DDR nucleation resulting in increased DNA DSBs[501,502]. In eukaryotes, γH2AX is created through the serine phosphorylation of H2AX at the carboxyl-terminal SQE motif by ataxia-telangiectasia mutated kinase (ATM:DNA DSBs) and ataxia-telangiectasia Rad3-related kinase (ATR:DNA SSBs)[502,503]. Introduction of DSBs trigger the binding of γH2AX, encompassing the DSB, along the DNA. γH2AX binding is crucial for DDR as it recruits DSB recognition and repair proteins to the site of the DNA DSB allowing the cell to properly asses and repair the DNA lesion[478,479]. Typical DDR foci colocalization events are limited to singular foci of Rad51 and Mre11 per γH2AX foci; indicating γH2AX calls for a singular DSB repair complex and does not mediate a compound homologous recombination event at a single DSB[501,504]. Moreover, the formation of phosphorylated γH2AX and establishment of these DDR foci is crucial for maintaining cell cycle arrest and to allow for proper DDR to occur[479,505]. However, disassembly of these DDR foci is also crucial for the readmittance and signaling of completion of DNA repair. Dephosphorization of γH2AX by nuclear serine phosphatases allows cells to recover from G_2/M cell cycle arrest and renter cell cycle[506].

Planaria are formidable models in the study of DNA damage and its subsequent effects on cellular proliferation. With their abundant population of dividing stem cells[358,364,365] and conserved DNA repair mechanisms[481], planarian DNA damage models are helping researchers better understand both stem cell- and anatomical regional-specific signaling mechanisms contributing to DNA repair response mechanisms[481,507]. Interestingly, the lethality of irradiation can be combatted by the transplantation of healthy stem cells, via injection or tissue engraftment, into the lethally irradiated host tissue[304,358]. Rescue of these planaria is achieved by the intervention of newly introduced pluripotent neoblasts which progressively repopulate the irradiated tissue and restore normal cellular turnover[304]. However, this restorative process takes weeks and relies on the introduction of foreign stem cells to support and revitalize irradiated tissues. In addition, these studies do not explore the possible impact of transplantation on the recapitulation of damaged stem cells within host tissues. By implementing novel approaches, we sought to improve neoblast repopulation within the transplantation model by introducing stimulation direct currents to enhance the repopulation process. What we found was quite astonishing; not only did $pDCS^S$ enhance neoblast repopulation, it did so at an astonishing rate. Moreover, the systemic nature of $pDCS^S$ significantly impacted cells within the lethally irradiated host, stimulating them to undergo active DNA repair and even participate in active cellular expansion via mitosis. In this chapter we will explore the impact of $pDCS^S$ on neoblast repopulation and their significant effects on host cells.

4.2.1 $pDCS^S$ induces rapid expression of DNA damage repair genes resulting in active DNA repair within lethally irradiated tissues

The standard transplantation model (wt/γ-irr) was used to isolate healthy neoblasts populations to dissect their responses to applied electrical current stimulation. As described previously, pDCS^S elicit a rapid and robust transcriptional response within lethally irradiated tissues (Fig 6, 7). Surprisingly, along with increased levels of stem cell-related genes, it was found that *Smed-Rad51* displayed similar rapid induction in expression levels associated with pDCS^S exposure (Fig 7 C). Expression levels of *smed-Rad51*, like that of *smed-piwi-1*, were found to be most elevated within only 15mins of electrical stimulation, attenuating as time passed (Fig 7 C). *smed-Rad51* expression remained slightly elevated at 60mins of pDCS^S within the tissue of the lethally irradiated host (Fig 7, 10). Together, this rapid and sustained transcriptional DDR suggests that subsequent translation may lead to active DNA repair in within lethally irradiated host tissues of planaria subjected to electrical current stimulation. This mechanism may assist in transcription of neoblast-related genes and help reestablish resident neoblasts into a competent functional form.

Rad51 must be present in the nucleus to perform its task of homologous recombination to repair double stranded DNA breaks[481,508]. We measured levels of nuclear vs cytosolic *smed-RAD51* using α-RAD51 antibodies on fixed single cell homogenates. Application of pDCS^S for 60 min significantly increased the levels of nuclear *smed-RAD51* when compared to control - pDCS^S 4DTP planaria (60% to 40% respectively) (Fig 10 B). During quantification, *smed-RAD51* co-expression with DAPI was considered nuclear while RAD51 expression outside the DAPI perimeter was considered cytosolic (Fig 10 B). To confirm the increase in nuclear *smed-RAD51* with an increase in actual DNA repair, we measured DNA damage directly using COMET analysis. DNA damage levels were quantified using a standardized COMET scale in which nuclei with extended comet tails are scored as cells having high levels of fragmented (damaged) DNA while small or no comet tails are scored as cells containing little to no DNA damage (Fig 10 C). It was evidenced that 60mins of applied pDCS^S greatly decreased the overall levels of DNA damage compared to the - pDCS^S 4DTP control (Fig 10 D). These data illustrate a direct connection between pDCS^S and their ability to influence cells to actively participate in DNA repair, even in the presence of tremendous amounts of DNA damage.

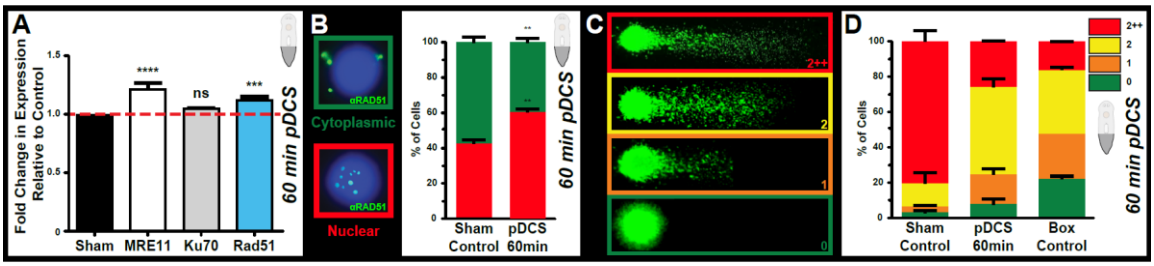

Figure 10 pDCS^S induces active DNA repair in the γ-irradiated tail region of 4DTP planaria **A)** qPCR analysis showing gene expression profiles for known DNA repair proteins post 60 minutes pDCS^S (7μA); both *smed-MRE11* and *smed-Rad51* show increased levels of gene expression compared to sham. **B)** First, photographic representation of cytoplasmic vs nuclear *smed-RAD51* as indicated using αRAD51 immunostaining on homogenized, single cell samples derived from tail fractions of transplanted planaria. Quantification of nuclear and cytoplasmic *smed-RAD51* among sham transplant fractions and pDCS^S transplant fractions represented as percentages. **C)** Photographic representation of COMET scale used to quantify levels of DNA damage within samples; largest comet tails indicate highest levels of DNA damage. **D)** Quantification of COMET DNA damage assay within unmodified box control tail fractions, sham 4DTP tail fractions, and +60 min pDCS^S 4DTP tail fractions as represented by %of cells exhibiting respective levels of DNA damage. P<0.005**, P<0.0005***, P<0.0001**** and ns= no significance, One/Two-Way ANOVA. Three independent replicates 5 animals/experiment.

4.3.1 pDCS^{S} permits mitotic activity within distal irradiated tissues by overriding cell cycle regulators and enhancing DNA integrity

To understand how electric fields can influence cellular mitosis, we must first understand the underlying bioelectric properties of the cell cycle. The cell cycle is divided into four distinct points: growth phase 1 (G_1), synthesis phase (S), growth phase 2 (G_2), and mitosis (M)[67,75,480,509,510]. Aside from these four cell cycle phases there are two additional phases, interphase (I) and quiescence (G_0), in which the cell is either gathering nutrients in preparation for cell division or is mitotically dormant[67]. The initial growth phase G_1 is characterized by an increase in cellular protein synthesis, growth of organelles, and a general increase in size. G_1 is followed by DNA replication, S phase, in which the cell duplicates its DNA to carry down to its progeny. In G_2 phase, occurring after complete DNA replication, the cell undergoes a final bout of growth in preparation for cellular division. Finally, the cell divides, in a process known as mitosis (M phase), separating its DNA, organelles, plasma membrane, and cytosol, creating a replicate daughter cell. However, to undergo the various phases of the cell cycle, evolution has designed a system of checks and balances set in place to safe guard improper cellular replication.

Cell cycle progression is regulated by two key regulatory protein types, cyclins and cycling dependent kinases (CDKs). Unique cyclin-CDK complexes regulate each phase of the cell cycle and cyclin-CDK dynamics conduct proper cell cycle progression. In short, there are three major cell cycle checkpoints: G_1/S, G_2/M, and M checkpoint; failure to pass any of these three checkpoints can cause cell cycle arrest or even trigger apoptotic cell death[480,509,510]. However, there are known bioelectric phenomena underlying the complex process of cellular mitosis. Actively proliferating cells tend to have slightly depolarized RMPs compared to their quiescent counterparts[12,13,511,512]. As such, depolarization of cellular RMP, through pharmacological or genetic modification of ion channels, is capable of coaxing quiescent cells into a proliferative state[13,513–515]. Once the cell has entered the cell cycle, progression through cell cycle check points has been shown to be associated with distinct changes in RMP. Specifically, initiation of cell cycle corresponds with RMP depolarization; progression through G_1/S checkpoint corresponds with RMP hyperpolarization. Hyperpolarized RMP persists through S phase, permitting proper DNA replication. Conversely, RMP begins to depolarize upon completion of S/G_2 phase and this depolarized RMP state coincides with proper G_2/M phase progression[12,13,512]. In final, cells undergoing the M phase are found to be in their most depolarized state, illustrating the significance for a depolarized RMP and proper M phase initiation/progression[12,512]. Changes in polarized states, during the cell cycle, correspond with changes in expression of specific ion channels, is known to directly influence the cellular RMP[13,516,517]. Together, this work introduces the complex orchestration of ionic flux during cellular proliferation exhibiting bioelectrical regulation of cell cycle and its progression. Interestingly, cancer cells with mounted DNA instability persist through DNA cell cycle checkpoints and successfully divide. We investigate the effects of direct current stimulation cells containing significant DNA instability, induced through ionizing γ-irradiation, and observe significant effects on cellular propensity to divide under this genome stress.

A unique attribute of proliferative cancer cells is their propensity to continuously proliferate in the face of DNA damage, avoiding programmed cell death. Cancer cells incur DNA damage in many ways and yet, these cells often continue to divide and grow into aggressive metastatic cancers. In fact, improper repair of damaged DNA, through common cellular repair mechanisms, is at the forefront of many cancers. However, the

ability to stall cell proliferation, activate DNA repair, and avoid programmed cell death has potential as a therapeutic tool for non-cancerous cells exposed to DNA damage inducing chemotherapies used to treat cancer. Chemotherapy has been an effective way to treat a multitude of cancers for many years however, it is not without its shortcomings, including the severe damage of surrounding healthy tissues. To ensure proper treatment of cancerous growths, patients must be subjected to chemotherapies implementing DNA damage inducing techniques that target both cancer cells and the surrounding tissues. In many cases, these treatments have severe side effects that persist long past treatment, ailing the treated patients. Many of the side effects can be attributed to consequential death of healthy tissues exposed to chemotherapy treatments. In coming results, we introduce an effective way to stimulate active DNA repair in tissues exposed to lethal doses of ionizing γ-irradiation, reporting for the first time a novel outcome of applied currents *in-vivo*; further illustrating the abundant therapeutic potential of applied EFs.

4.3.2 pDCS^S reduces *p53* expression permitting increased mitosis within lethally irradiated tissues

Due to the rapid resurgence of stem cell-specific gene expression we proceeded to further assess changes in the behavior of stem cell-specific functions within these irradiated tail fragments. One essential function of the planarian neoblast is being the sole propriety for cell turnover as it is the only planarian cell capable of undergoing normal proliferation. Interestingly, we discovered that irradiated tail tissues exposed to 60min of pDCS^S exhibited significant responses in the expression of cell cycle-related genes (Fig 11 B, C). We performed a general assessment of cell cycle specific genes by measuring gene expression levels of known cyclin regulators responsible for mediating passage through conserved cell cycle checkpoints (Fig 11 A). It was found that 60min of pDCSS lead to an overall decrease in the expression of *smed-cyclin-D, -E*, and *-A* (Fig 11 C). These three cyclins are known for mediating cell cycle entry, passage into S phase, and G_2/M phase transition

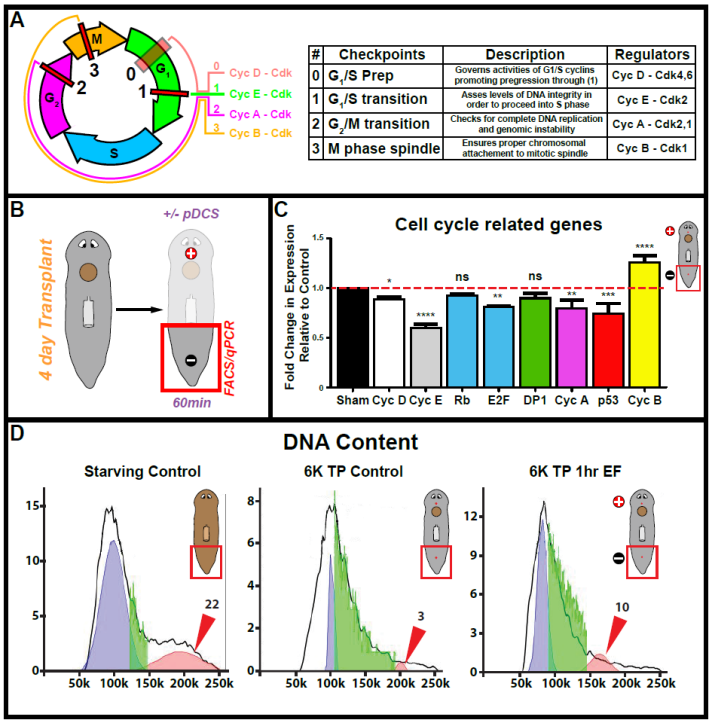

Figure 11. pDCSS mediates M phase checkpoint clearance leading increase in mitotic events within lethally irradiated host tissues. **A)** Cell cycle summary including cell cycle checkpoints and the respective cyclin-cdk complex's responsible for their regulation. **B)** Experimental design for cell cycle FACS and qPCR analysis. 4DTP planaria were subjected to 1hr pDCSS and then tail tissues from these planaria were isolated for both FACS and qPCR analysis. **C)** Quantitative PCR result for various regulators of the cell cycle showing varied responses to 60min pDCSS exposure. **D)** FACS analysis of tail fragments showing an increase in M phase cells in exposed irradiated tissues. P<0.005**, P<0.0005***, P<0.0001**** and ns= no significance, One/Two-Way ANOVA. Three independent replicates 5 animals/experiment.

respectively[480,509,510,518]. Conversely, 60min pDCS^S lead to marked increases in *smed-cyclin-B*, responsible for permitting entry into active cellular mitosis[509,510,518]. In addition to this increase in *smed-cyclin-B*, expression levels of *smed-p53* were reduced in pDCS^S planaria, a gene tasked with initiating cell cycle arrest in either G_1/S or G_2/M phase transitions in the presence of significant DNA damage[518,519]. No significant impact in gene expression was observed in *smed-Rb* or *smed-DP1*; associated proteins of transcription factor E2F with inhibitory[520–522] and complimentary[523,524] functions respectively (Fig 11 C). The expression of planarian *smed-E2F* is shown to be decreased in pDCS^S planaria compared to sham control (Fig 11 C). Transcription factor *E2F* is known to be maximally expressed during G_1/S phase as it plays a role in G_1/S transition[520]. Thus, reduction in *smed-E2F* expression is supported by the clear shift from S phase towards M phase in host tissue cells onset by 60 min pDCS^S (Fig 11 D). To further asses the effects of these changes in cyclin expression we performed FACS analysis on the same isolated tail fragments and measured cell cycle dynamics.

Moderate exposure to pDCS^S was sufficient to significantly impact cell cycle dynamics within the irradiated tail tissue of 4DTP planaria. As a baseline measurement of cell cycle activity, we assessed cell cycle dynamics in tail fragments of sham control planaria. We found that under normal conditions cells are grouped accordingly: 56 ± 3% G_1 phase, 14.5 ± 1.5% S phase, and 22 ± 0% G_2/M phase (Fig 11 D). However, pDCS^S experiments are performed in transplanted planaria whose tails are subjected to lethal doses of γ-irradiation which will significantly impact the homeostatic distribution of cycling cells. As such, significant amounts of DNA damage, introduced by γ-irradiation, a large percent of cells are expected to be arrested in S phase as the G_2/M transition checkpoint will thwart all attempts for the cell to proceeded into active mitosis with insufficient genomic integrity (Fig 11 A). As anticipated, the vast majority of cells within tail tissues of sham control planaria were found to be within S phase (48.5 ± 1.5%) with a minute percentage of cells found in G_2/M phase (3 ± 1%) and the remaining cells were found in G_1 (15.5 ± 1.5%) (Fig 11 D). As hinted by qPCR results, 60min of pDCS^S resulted in a significant increase in the percentage of cells found in G_2/M phase increased from 3 ± 1% to 10 ± 1% (Fig 11 D). In addition to this finding there was a significant reduction in the number of cells found in S phase, decreasing by nearly 10% in pDCS^S planaria (Fig 11 D). With these results demonstrated within 60min of pDCS^S we later assessed if larger periods of pDCS^S exposure impacted levels of mitotic events.

Transplanted planaria, under normal circumstances, do not exhibit cell proliferation within distal regions of the hosts' irradiated tissue even after several weeks[366,525]. However, 6hrs of applied pDCS^S induced cellular proliferation in severe irradiated distal tissues only 4 days post-transplantation (Fig 12 C). The ability to create mitotic events within tissues riddled with severe DNA damage, otherwise absent of such things, is extraordinary. Six hours of pDCS^S, generated by the injection of 7μA across the body of the transplanted planaria, was sufficient to significantly increase mitotic events outside of the transplanted tissues (Fig 12 B). Interestingly, application of pDCS^S alone was sufficient to increase mitotic events within irradiated host tissues (Fig 12 B, C). Polarity influences not the number of dividing cells found within irradiated tissues, but the location in which these mitotic events are most readily found. pDCS^S with polarity complimentary to that of the endogenous planarian polarity ([-]H [+]T) saw an increase in mitotic events in both the head and the tail with significantly more mitotic events found in the anterior region than any other condition, including control (Fig 12 B). Complimentary to this finding, switching the polarity of the pDCS^S ([+]H [-]T) causes a shift in the distribution of mitotic events (Fig

12 B, C). These results suggest the instances of mitotic events follow a bias favoring depolarized [-] regions.

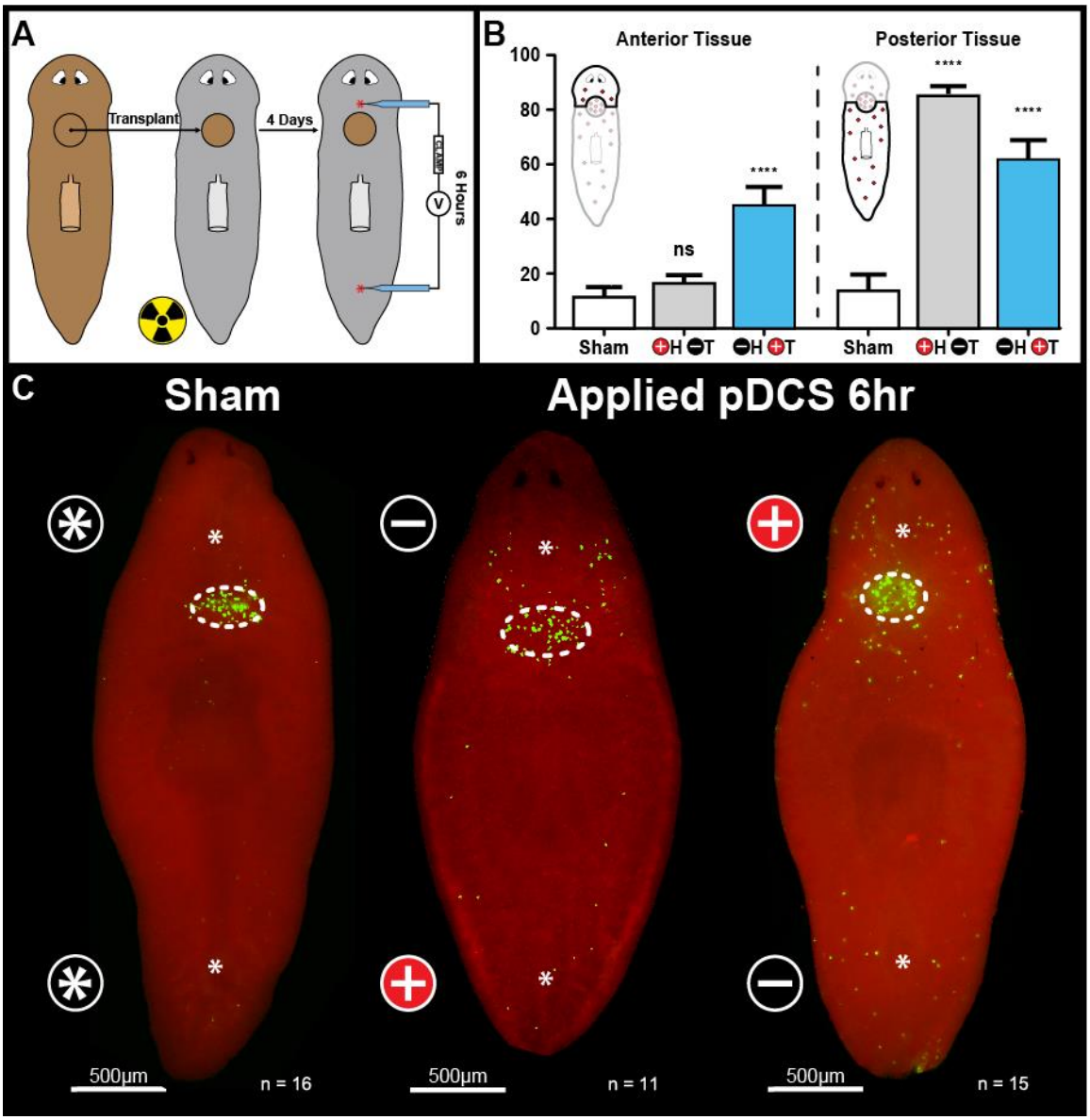

Figure 12. 6hr pDCS^{S} induces cellular mitosis within distal irradiated tissues in a polarity driven manner. **A)** Schematic representation of planarian transplantation where healthy unirradiated tissue is transplanted into lethally γ-irradiated tissue. Four days post-transplantation (4DTP) planaria are subjected to 6hrs of pDCS^{S}. **B)** Percent of quantified cells found dividing outside of the transplant within either the anterior or posterior irradiated tissues of the transplanted planaria in planaria subjected to [+]H [-]T pDCS^{S} planaria. Anterior and posterior delineation is set at the center of the transplant. **C)** Percent of quantified cells found dividing outside of the transplant within either the anterior or posterior irradiated tissues of the transplanted planaria in planaria subjected to [-]H [+]T pDCS^{S} planaria. **D)** Immunostaining of H3P in pDCS^{S} planaria of both polarities compared to sham control. Lastly, H3P staining in lethally irradiated planaria without transplantation, subjected to 6hr pDCS^{S}, exhibiting null H3P^{+} Cells. P<0.005**, P<0.0005***, P<0.0001**** and ns= no significance, One/Two-Way ANOVA. Three independent replicates 5 animals/experiment.

4.4 Discussion

An outstanding global health issue is combating DNA damage causing agents, environmentally and pharmacologically driven, which severely damage tissues which can be very difficult to revitalize. The ability to activate mitotic activity of native pluripotent stem cells within these tissues riddled with DNA damage would be an all-powerful tool to help restore these tissues. Here we present evidence, within the lethally irradiated planarian tissues, that passing low magnitude, body wide, steady state electrical currents through damaged tissues is an adequate method to restore mitotic activity of γ-irradiated neoblasts. In addition to this we show that these electrical currents suppress the known cell cycle regulator *p53*, which causes cell cycle arrest at the S phase checkpoint, likely allowing for these γ-irradiated neoblasts to enter M phase; requiring only 6hrs of current stimulation. Moreover, cells exposed to these low magnitude electrical currents exhibit rapid levels of DNA repair which assisting in the ability for these cells to enter M phase. Together, this data introduces electrical current stimulation as a power tool to enhance DNA repair and repopulate native stem cell populations *in-vivo* having tremendous potential as a therapeutic tool for a number of applications.

4.4.2 pDCS^{S} upregulates DNA damage repair response resulting in active DNA repair reported by increased DNA integrity

Cells are in a constant standoff against DNA damage and subsequent genomic instability. With age comes inherent DNA damage from metabolic processes, creating reactive oxygen species, and environmental stresses generating DNA damage and genomic instability[508,526–528]. Genomic instability and subsequent mutations are key attributes of cellular transformation from normal proliferating cells to proliferating cancer cells[492,526,529]. DNA damage elicits a complex cellular response which may result in cell cycle arrest, cellular senescence, and programmed cell death through apoptosis[530,531]. Induced cellular senescence is a powerful tool used by a multitude of cancer chemotherapies designed to force proliferating cancer stem cells into a state of senescence, which can lead to programmed cell death and eventual immune clearance[530,532]. However, it has been shown that proliferative cancer cells coerced into cellular senescence have the potential to become more potent tumorigenic proliferating cancer stem cells[533,534]. These studies are in line with evidence showing initial effectiveness with cancer chemotherapies and subsequent rapid tumorigenesis when relapse occurs. In cases of tumorigenic relapse, proliferative cancer cells become more aggressive, developing drug resistances and increased metastatic behavior[534]. A key question remains as to whether aggressive tumor formation is a result of 1) a subpopulation of proliferating cancer cells which have evaded cellular senescence or are a result of 2) previously senescent cells, induced pharmacologically or due to aberrant levels of DNA damage, escaping cellular senescence and reengaging in cellular proliferation.

It has been demonstrated that programmed cell death is induced upon lethal doses of ionizing irradiation in the planarian model[535]. Moreover, lethal irradiation in planaria causes significant amounts of DNA double stranded breaks (DSBs) generating a robust DNA damage response and upregulation of DNA repair genes[481,536]. Lethal irradiation in planaria leads to eventual organismal death. However, if transplanted with healthy neoblasts, either through neoblast injection or through complete tissue transplantation,

lethally irradiated tissues can be rescued within weeks[304,358]. This rescue of irradiated tissue is made possible by populations of pluripotent neoblasts capable of giving rise to every cell type within planarian tissues[358]. Interestingly, cell cycle and cellular senescence has been shown to be regulated by fluctuations in resting membrane potential as consequence of ion channel activity[6,13,512,537]. In harmony with these studies, for the first time we have illustrated data that shows the potential for low magnitude steady-state direct currents have the potential to elicit a cellular DDR and subsequent cellular mitosis within lethally irradiated tissues.

It is well known that DNA damage induces a DDR within planaria[481]. However, application of oscillating currents have been shown to cause damage DNA leading to programmed cell death[538–540] while non-oscillating currents, as used in these experiments, have not been examined in regards to DNA damage and DDR. Interestingly, we found that when subjecting transplanted planaria (wt/γ-irr) to low magnitude pDCS^S we observed a rapid increase in DDR when compared to sham control (Fig 7 C). Increased gene expression of *smed-Rad51*, a conserved DDR in planaria[481], is rapidly enhanced by pDCS^S, being most pronounced at 15mins of pDCS^S and tapering off within 60mins of pDCS^S. The shear time scale of this finding is astonishing, to see such profound expression of DDR onset by pDCS^S. Planarian homolog *Rad51-A* (*Smed-Rad51*) is expressed throughout the adult body and is preferentially found within irradiation sensitive neoblasts while also showing moderate levels of expression in irradiation insensitive differentiated cells[481]. Due to its abundance in neoblasts, *smed-Rad51* expression within 4-day post-irradiation tissue is expected to exhibit strong down regulation. However, pDCS^S exposure induces a strong *smed-Rad51* response (Fig 7 C). Induced pDCS^S DDR gene expression levels of *smed-Rad51* may originate from either differentiated or neoblast cells. As it is shown that pDCS^S reengage neoblast specific gene expression within the posterior irradiated tissues, it is plausible these same 'neoblast' cells are also engaging in active DDR onset by pDCS^S exposure.

To assess active DNA damage repair within pDCS^S exposed irradiated tissues, we addressed accumulation of phosphorylated H2AX (γH2AX) and subsequent nuclear Smed-RAD51 foci of cells within these pDCS^S exposed irradiated tissues. Generation of DNA damage loci, as reported by formation of γH2AX, accumulate with increasing levels of DNA damage acting as anchoring points for DDR machinery[499,502,541]. When investigated in the context of pDCS^S, we see no significant increase in nuclear γH2AX after 60mins of pDCS^S (Fig. 10).D As anticipated, these results are indicative of the equivalent severity of DNA damage, and subsequent γH2AX foci, received by the irradiated tissues of both +/-pDCS^S planaria. Interestingly, even with equivalent levels of nuclear γH2AX, we saw distinct differences in the recruitment of nuclear *smed-RAD51* between pDCS^S and non- pDCS^S γ-irr tissues. Within the 60-minute window of pDCS^S exposure, we see an increase of 20% of cells expressing nuclear *smed-RAD51* (Fig. 10 B). This clear increase in nuclear *smed-RAD51* may be a direct consequence of rapid elevation of *smed-Rad51* mRNA exhibited in γ-irr tissues exposed to equivalent pDCS^S (Fig 7 C). Moreover, pDCS^S induced DDR resulted in decreased levels of DNA lesions as measured by COMET assay (Fig 10 D). pDCS^S of 60mins shows both increases in *smed-RAD51* nuclear localization which may directly regulate the observed decrease in DNA fragmentation through the repair of DNA DSBs; incurred by lethal doses of γ-irr experienced by these tissues. The potency and effectiveness of pDCS^S exposure as a potential therapeutic tool to stimulate and rapidly enhance the cellular DDR and DNA damage repair mechanisms is illustrated by its clear effects within the lethally γ-irr tissues of this transplanted planarian model.

Potential mechanisms contributing to the observed increase in planaria DNA repair following $pDCS^S$ may be explained through the robust secondary messenger Ca^{2+}. We have previously illustrated a clear Ca^{2+} dependence of observed $pDCS^S$ responses through the inhibition of planarian L-type Ca_vs via NIC (Fig 8 B, D). It is important to note that increased cytosolic Ca^{2+} concentration through L-type Ca_v activity results in increased nuclear Ca^{2+} is still a topic of debate[430,542]. Ca^{2+} has been implicated in a number of crucial aspects of homologous recombination DSB repair including Rad51/Rad54 complex activity[543], stability of single strand nucleoprotein Rad51 filaments[544], sensitivity of DDR[487,488], and more. In concert with increased mRNA expression of *smed-Rad51* following $pDCS^S$ application (Fig 7 C), increased nuclear smed-RAD51 protein following 60min $pDCS^S$ application (Fig 10 B) may be attributed, in part, to increase cytosolic/nuclear Ca^{2+} concentration prompted by L-type Ca_v activity. In support of the role of Ca^{2+} in promoting DSB repair, increased cytosolic and nuclear Ca^{2+} concentration has been observed following radiation and other DSB inducing procedures[545–547]. DSB induced Ca^{2+} mechanisms have likely developed due to the functional role Ca^{2+} plays during DSB repair having assistive roles in Rad51 nucleoprotein stability and Rad54-Rad51 complex activity[543,544]. The formation of Rad51 nucleoprotein filaments is dependent on proper accumulation of DNA damage sensor proteins such as breast cancer gene 2 (BRCA2) yet, the stability of these nucleoprotein filaments is dependent on Rad51 ATPase activity[548] and Rad54-Rad51 complex formation[543,544]. Nucleoprotein Rad51 filaments have increased stability in their ATP-bound state thus, slowing Rad51s' inherent ATPase activity promotes filament stability. Interestingly, elevated intracellular Ca^{2+} concentration was proven to reduce Rad51 ATPase activity increasing Rad51 nucleoprotein stability[544]. Another contributor to Rad51 stability is the DNA damage repair protein Rad54. In yeast, researchers found that Rad54 not only enhanced Rad51 nucleoprotein filament stability but also promoted Rad51-mediated strand exchange. Intriguingly, the function of Rad54, which, in addition to previously mentioned roles, primarily acts to shuttle nucleosomes across dsDNA in order to grant access to DNA repair complexes, was shown to become enhanced when complexed with Rad51[549,550]. Interestingly, this function in the eukaryotic Rad54 homolog has been shown to be conserved[548]. In addition to its surprising role in Rad51 filament stability, the same group of researchers demonstrated Ca^{2+} works to promoting enhanced Rad54-Rad51 complex-mediated DNA strand exchange leading to increased DNA repair via homologous recombination[543,544].

Collectively, increases in intracellular Ca^{2+} onset by $pDCS^S$ may function to enhance the observed DNA damage repair process increasing its effectiveness and accelerating its temporal kinetics in severely irradiated planarian tissues. The ability to increase enhance DNA repair in such short periods of time (60 min) may be attributed to enhanced sensing mechanisms in the presence of $pDCS^S$. A known first responder to DNA damage in both ssDNA and dsDNA is PARP1[551]. PARP1 binds to DNA damage loci and promotes the formation of DNA repair complexes promoting DNA repair and cell survival[484,485]. PARP1 is one of the most abundant nuclear polypeptides having roughly 2 million molecules per nucleus, this makes it an extremely effective scanner of DNA damage; capable of detecting DNA lesions within minutes[552,553]. Interestingly, PARP1 sensory mechanisms for detecting γ-irradiation induced DNA damage have been shown to activate Ca^{2+} influx through conducting ion channels of the TRPM family[488]. Thus, enhancing Ca^{2+} influx via $pDCS^S$ may have complimentary effects on the DNA damage repair kinetics accelerating and enhancing overall DNA DSB repair.

Much of this is speculative and more work must be performed to justify such hypotheses. For example, modulation of both intra- and extracellular Ca^{2+} concentrations

during $pDCS^S$ application will provide insight on the Ca^{2+} dependencies suggested by observed Ca_v dependence. Additionally, measuring the activity of key proponents such as *smed-Rad54* and *smed-PARP1,* both of which are conserved within the planarian genome, in the presence of $pDCS^S$ using IHC and western blotting techniques in conjunction with DNA damage assays such as COMET will provide functional relevance to the mechanisms conferring $pDCS^S$ influence over DNA DSB repair. Moreover, deducing specific cell populations capable of performing such feats in DNA repair may elucidate populations of cells with increased resilience to DNA damage. Further dissection of such seemingly radio-resistant cells has the potential to provide fundamental knowledge regarding cellular transformation in cancer. Despite clear limitations in the presented work, there is clear evidence of enhance DNA repair and such interactions with electric currents and induced ion flux inspire new avenues for investigation in seemingly unexplored mechanisms of DNA repair.

4.4.3 $pDCS^S$ induced DNA repair and *p53* suppression promotes cellular mitosis

Cell cycle and membrane potential have shown to be intertwined, exhibiting codependency in a variety of model organisms. Details behind the connection between cellular RMP and cell proliferation/cycle regulation have been extensively reviewed[12,13,512]. It is evident that bioelectricity plays a significant role in the onset of cellular proliferation and predictively fluctuates as various stages of the cell cycle are engaged. However, there is little evidence showing a connection between bioelectricity and recovery of tissues exposed to significantly damaging levels of radiation. We present data illustrating the effectiveness of $pDCS^S$ to reinforce cellular mitosis in tissues exposed aberrant levels of DNA damage and cell cycle arrest induced by significant doses of ionizing irradiation.

Annually, a significant number of patients undergo ionizing radiation therapy in conjunction with chemotherapy designed to target and eradicate malignant cancer cells. The effectiveness of radiation therapy is undisputed, having the potential to save up to 50% of the roughly 14 million yearly patients diagnosed with cancer[554,555]. However, radiotherapy unbiasedly targets all cells within the penetrant tissues, including healthy normal cells. Several studies have shown increased sensitivity of cancer cells, latent with DNA damage, to ionizing radiation when compared to normal cells, as normal cells are better equipped to repair damaged DNA[556–558]. Doses of irradiation in treatment are optimized to levels that are sublethal to surrounding normal cells such that recovery can ensue. Yet, in some cases, aggressive relapse occurs despite proper chemotherapy/radiotherapy[526,530]. Here we present a potential modality in which extreme doses of γ-irradiation can be combated by administration of local $pDCS^S$ with the capacity to both enhance cellular DDR and increase proliferation of healthy normal cells.

Direct current stimulation, of magnitudes reflecting the currents generated endogenously by injury or epithelial rupture, have been shown to have a multitude of effects on many different cell types[3,4]. However, many of these studies regarding non-oscillating electric fields focus on tropic phenotypes exhibited by exposed cells such as guided migration (galvanotaxis) or directed axonal growth (galvanotropism) of neurons[16,20,248,559]. Interestingly, it has been shown that physiological DCS directly influence cellular proliferation in a polar fashion. In the presence of applied currents, cultured corneal epithelial cells orient their mitotic axis perpendicular to the generated electric field lines[560]. In addition to this control over cellular mitosis, it has been shown that enhancing wound induced injury potentials can speed up the wound healing process[333,340,349,354]; a complex process requiring many cellular processes including

cellular proliferation[347,561]. Application of low magnitude exogenous oscillating electrical stimuli has been shown to has the potential to have the capacity to enhance cellular proliferation of a variety of cell types[15,562]. There is mounting evidence showing the proliferative impact of electrical stimuli can be both positive or negative depending on both the type of electrical stimulation (oscillatory or steady state) and the magnitude of stimuli imposed on cells[348,538,562–564]. Within our transplantation model (wt/γ-irr) we demonstrate that low magnitude pDCS^S can enhance the mitotic capacity of cells exposed to lethally irradiated tissues.

Initiation, progression, and overall cell cycle regulation is mediated by specific protein complexes known as cyclin-cdk complexes. Due to surmountable levels of DNA damage, induced by γ-irradiation, mitosis within the host of transplanted planaria is near impossible due to the heavy reliance on DNA integrity during the cell cycle[358,366,480]. Using external stimuli, we were able to activate neoblast specific gene expression within these otherwise barren tissues; naturally, the possibility of inducing mitosis within these newly neoblast harboring tissues was explored. In the presence of pDCS^S, we found that gene expression of various cyclins, tasked with regulating cell cycle checkpoints, displayed promising responses to pDCS^S. Expression of *smed-cyclins-D, -E,* and *-A* all exhibit slight downregulation in the presence of pDCS^S (Fig 11 C), a result suggesting increased instances of G_2/M phase cycling cells. This is supported by research showing these cyclins (D, E, A) are downregulated during onset of M phase cyclin, cyclin B[510,518,519]. In ordinance with this line of thinking, the discovery that *smed-cyclin B* shows significant upregulation in the presence of pDCS^S suggesting pDCS^S promotes cell cycle progression all the way through to G_2/M. In addition to significant effects on cyclin gene expression, FACS analysis of pDCS^S planaria supported described cyclin dynamics. As anticipated, cells within sham control tail tissues were found to be arrested within G_1/S phase due to insufficient DNA integrity. However, 60min of pDCS^S exposure slightly remedied this imposition with over 3-fold increase in cells participating in G_2/M phase and 10% less cells found in S phase (Fig 11 D). Progression through G_1/S phase has been previously reported to regulated by applied currents[565]. Clearly, pDCS^S enhances neoblast presence within lethally irradiated host tissues leading to increases in mitosis promoting properties. With mounting evidence that bioelectric signaling plays a significant role in cell cycle regulation, having potentially overriding regulatory capabilities[12,13,512,565], the observed effects are in line with electrical regulation of mitosis yet novel for their capabilities to promote mitosis despite significant levels of DNA damage. Moreover, promoting mitotic activity within lethally irradiated tissues is a significant feat achieved by pDCS^S and data suggests it may execute action through the downregulation of *p53*.

A known proponent of aberrant cellular proliferation is the dysregulation or loss of tumor suppressor *p53*[508]. *p53* is a known tumor suppressor whose activity leads to cell cycle arrest, cellular senescence, and programmed cell death[526,529–531]. In planaria, downregulation of the planarian homolog *smed-p53* leads to increases mitosis, even in the presence of significant DNA DSBs[481]. Planarian exposed to pDCS^S show subsequent downregulation of *Smed-p53* generated during 60mins of pDCS^S (Fig 11 C). This decrease in *smed-p53* mRNA may lead to decreased *p53* activity within arrested cells, allowing them to escape cell cycle arrest and reengage in cellular mitosis (M phase). In addition to reduced *p53* expression, DNA integrity shows marked improvement following pDCS^S (Fig 10 D). Although oscillating DCS induced cell death has been shown to operate in a *p53* dependent manner[14], the intricacies between low magnitude non-oscillating DCS and *p53*-mediated mechanisms remain open for elucidation. Similar to our observed effects of pDCS^S, keratinocytes within human tissue explants exhibited accelerated tissue closure

with marked increases in proliferation and simultaneous reductions in p53 gene expression following DCS^S treatment[566]. It was found that apoptosis regulatory protein Siva (SIVA1) was upregulated by DCS^S treatment ultimately leading to reduced p53 via ubiquitination and degradation[566]. In concert with overall promotion of cellular mitosis is the evident reduction in expression of *smed-E2F, smed-cyclin-D, -E, and -A* (Fig 11 C). As levels of mRNA are evaluated against tissue of transplanted sham control planaria whose cell cycle profile exhibit increased percentage of S phase cells (Fig 11 D), suggestive DNA damage induced S phase arrest. Due to the cyclic nature of their expression, decreased levels of *smed-E2F* (highest in S phase[520,522,567])*, smed-cyclin-D* (S)*, -E* (G_1/S)*, and -A* (G_2)[480,510,518] demonstrates clear propensity for $pDCS^S$ to promote exit from arrest and enter G_2/M phase as shown via FACS (Fig 11 D). Although these collective responses are intriguing, outstanding questions remain: is $pDCS^S$ induced DNA repair adequate to independently promote cellular reengagement into the cell cycle, leading to the observed reduction in *smed-p53* expression or are $pDCS^S$ directly reducing *smed-p53* expression leading to cell cycle reentry? Potential dynamic $pDCS^S$ regulation of *smed-p53* is an intriguing avenue which deserves further investigation. This mechanism has not been adequately explored within the scope of this body of work and subsequent experiments must be performed to implicate *p53* activity in regulation of cellular mitosis of these damaged cells. To date, little is known regarding steady state DCS and governance over cell cycle regulators described above. However, it is well known that various stages of the cell cycle are bioelectrically regulated through distinct changes in membrane potential of a dividing cell[12,13,512]. Additionally, elevated intracellular Ca^{2+} transients has been demonstrated central to G_1/S phase transition[568,569] and M phase activity[570,571] as well as dependence on calcium-calmodulin activity during S phase transition[572,573]. Known Ca^{2+} cell cycle regulation and apparent L-type Ca_v activity within $pDCS^S$ planaria suggest possible Ca^{2+} involvement in the regulation of cell cycle within $pDCS^S$ planaria. This connection between resting membrane potential and cellular proliferation is key in establishing the link between $pDCS^S$-mediated influence over cell cycle progression in DNA damaged cells yet, much work is needed to decipher mechanisms permitting these responses.

With only qPCR data to support the action of *smed-p53* in $pDCS^S$-mediated neoblast mitosis, there is clear opportunity to expand on this claim. Potential future experiments to address limitations in the present data could focus on changes in *p53* expression at the protein level. Using IHC and western blots, *p53* protein levels and anatomical distribution could be assessed following 60min $pDCS^S$ to address functional regulation of *p53* by $pDCS^S$ application. Additionally, $pDCS^S$ application in planaria containing functional knockdown of *smed-p53* would be useful in determining the necessity of *p53* activity in observed $pDCS^S$ driven mitosis within lethally irradiated tissues. Such an experiment would resemble that performed in Fig. 9 where either host or donor tissue would be selectively treated with *smed-p53* RNAi and then subjected to tissue transplantation and subsequent $pDCS^S$ and assessed for neoblast mitosis using both IHC and FACS analysis. To address potential Ca^{2+}-mediated $pDCS^S$ cell cycle regulation, implementation of Ca^{2+} chelators such as BAPTA-AM and EGTA-AM can be used to implicate changes in intracellular Ca^{2+} concentration and observed $pDCS^S$-mediated increases in mitotic cells. Additionally, pharmacological inhibition of SERCA via thapsigargin can be used to deplete intracellular Ca^{2+} stores to as an additional means to implicate changes in intracellular Ca^{2+}. The potential crosstalk between biophysical $pDCS^S$ responses and mitotic genetic/ionic regulators such as p53 and Ca^{2+} are interesting concepts that deserve further investigation.

Intermediate application of steady-state pDCS^S within lethally irradiated tissues exhibit a propensity towards increased mitosis. This was demonstrated with 6hrs of constant current injection of 7μA across the planarian body of wt/γ-irr transplanted planaria showing significantly increased proliferation outside of the transplanted tissue (Fig 12 C-D). Without pDCS^S there is little to no mitosis within the surrounding irradiated host tissues 4 DTP (Fig 12 C-D). Interestingly, the increased mitosis within these irradiated tissues seems to be more prolific within the posterior regions of the planaria (Fig 12 B, C). This may be related to both the pDCS^S-related up regulation of neoblast specific gene expression (*smed-piwi-1*) alongside increased DDR (Fig 7 and Fig 10) as well as recently discovered anterior-posterior differences in the regulation DDR genes[481]. Like many other steady-state pDCS^S-related responses, induced cellular mitosis within irradiated tissues appeared to have an inherent polarity bias favoring the cathodal regions of the pDCS^S; showing significant enhancement in anterior mitosis when the polarity of the pDCS^S was reversed caused the anterior to at the cathodal pole of the pDCS^S (Fig 12 C). pDCS^S induced cellular mitosis within γ-irradiated host tissues may have reaching applications in the recovery of tissues damaged by varying levels of irradiation used during radiation cancer therapies or in patients suffering from significant levels of DNA damage produced naturally through aging.

CHAPTER FIVE

FINDING

Effects of steady-state direct current stimulation on homeostatic planarian tissues

5.1 Introduction

As of yet, this study has focused primarily on steady-state direct current stimulation and their effects on the transplanted, DNA damage, planaria model. In addition to these remarkable results, we have found that the same magnitude steady-state direct currents have profound and rapid effects on intact homeostatic planaria. Similar to the transplanted planarian model, $pDCS^S$ directly affect the expression of neoblast specific gene *smed-piwi-1* while also significantly influencing the mitotic activity of neoblasts.

Intact homeostatic planaria have very characteristic distributions of neoblasts and their mitotic events[481,574–576]. Planarian neoblasts are found within mesenchymal tissues, nearly spanning the entirety of the planarian body. There are however, two major regions of tissue absent of neoblasts, these regions are: the pharynx and tissue above the photoreceptors[365,525,576]. Thus, upkeep of these neoblast deficient tissues requires the migration of pluripotent progeny capable of reaching and replacing burdened cells located within these tissues[365,577,578]. However, it is still unknown what signals guide cells to their proper destination and, upon arrival, instruct these cells to properly differentiate despite complex body asymmetry. For insight, we look to endogenous electrical cues found within many complex organisms.

It has been shown that body polarity dictates many biological processes, especially during development and regeneration[234,236,333,564,579–584]. However, not much has been shown with respect to body polarity and regulation of body homeostasis. EFs have been shown to contain instructional cues for cells and it has been shown that the physical EF, and signals they carry, propagate and penetrate collective cell bodies, tissue, and/or organs[335,337]. In the planarian model, previous work illustrated that within an intact, non-regenerating planaria, the anterior portion of the planaria is relatively depolarized in comparison to the posterior tissues[585–587]. We have found that when this innate polarity is altered through the application of an external $pDCS^S$, resident neoblasts begin to behave differently than they would under standard homeostatic conditions.

5.2.1 6-hour $pDCS^S$ redistributes homeostatic neoblasts in a polarity dependent manner

At rest, planarian neoblasts are found undergoing mitosis throughout the body except for tissues above the photoreceptors and surrounding the pharynx. The relative distribution of these dividing neoblasts slightly favors anterior tissues across the anterior-posterior axis and no difference has been reported across the left-right axis[359,481,588]. Overall, large intact planaria exhibited modest overall proliferation values of ~140cell/mm^2

(Fig 13 A, D). Moreover, there was no statistically significant difference in mitosis across the left-right axis comparing lateral and medial mitotic density, each displaying values around 200cells/mm^2 (Fig 13 C). However, after pDCS application for 6hrs the distribution and density of proliferating neoblasts change quite dramatically. For these experiments, planaria ranging from 5-7mm were starved for seven days and then exposed to pDCS with a magnitude of 7mA of injected current across the entire body. Electrodes were carefully placed beneath the ventral epithelial below the eyes and just above the tip of the tail to ensure the clear majority of the planarian body was subjected to pDCS application. When the polarity of the pDCS^S compliments/enhances that of the endogenous natural

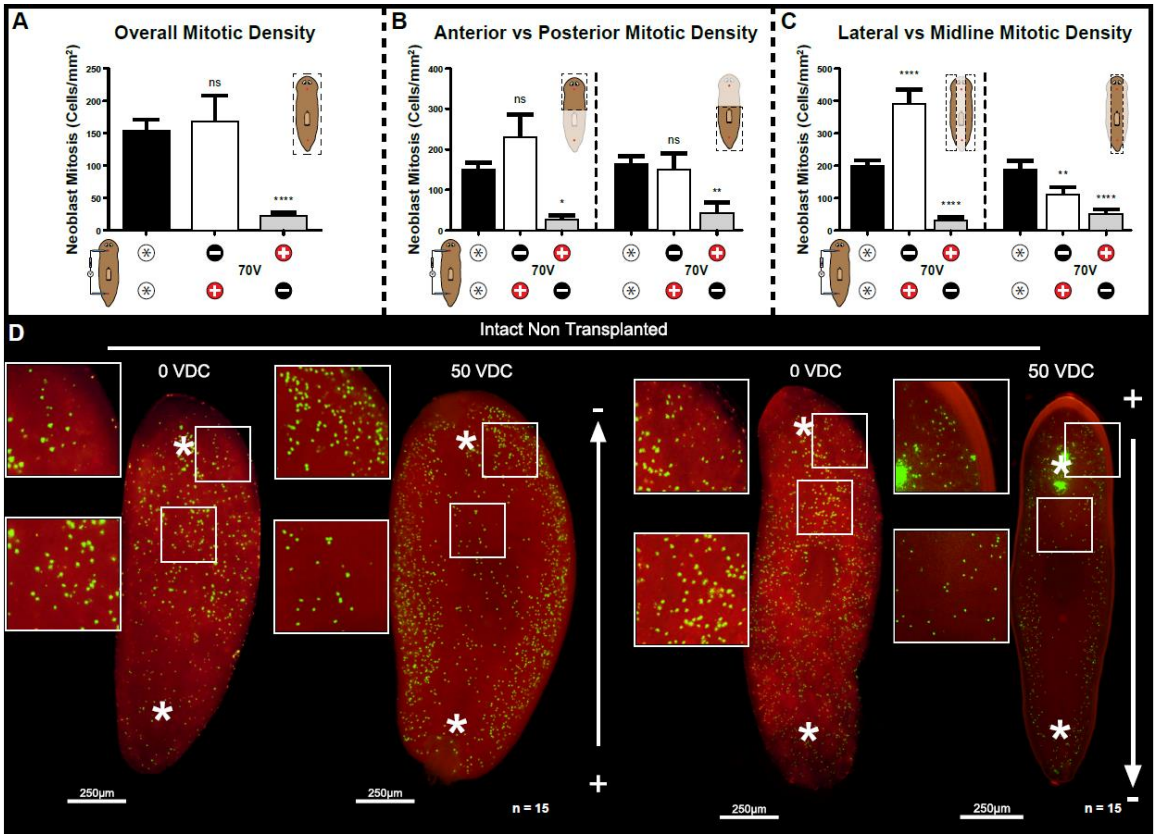

Figure 13. pDCS^S application in homeostatic intact planaria leads to symmetric redistribution of mitosis along the lateral-mediolateral (LM) axis while simultaneously influencing overall mitosis density in a polarity dependent manner. **A)** Overall mitotic density of pDCS^S planaria, both polarities, compared to sham control. **B)** Mitotic density along the anterior-posterior (AP) axis in pDCS^S planaria compared to sham control. **C)** Mitotic density along the LM axis in pDCS^S planaria compared to sham control. **D)** Representative immunostainings for H3P in pDCS^S planaria ([+]H [-]T, [-]H [+]T) compared to sham control. Enhanced images showing increased mitotic density in lateral tissues compared to mediolateral tissues. P<0.005**, P<0.0005***, P<0.0001**** and ns= no significance, One/Two-Way ANOVA. Three independent replicates 5 animals/experiment.

bioelectric polarity ([-]H [+]T) the overall density of proliferating neoblasts is not significantly impacted but, the distribution of dividing neoblasts within the body plan is drastically modified by after pDCS^S exposure (Fig 13 C, E). In this model, the distribution of proliferative neoblasts appears to be cut across the sagittal plane, becoming highly concentrated in the lateral tissues (Fig 13 C, D). When quantified, it was found that cell division in the lateral tissues was 4-fold increase than that found in the medial tissues and

a 2-fold increase compared to control lateral tissues (Fig 13 C). Interestingly, medial cell division decreased 2-fold compared to control medial proliferative density (Fig 13 C).

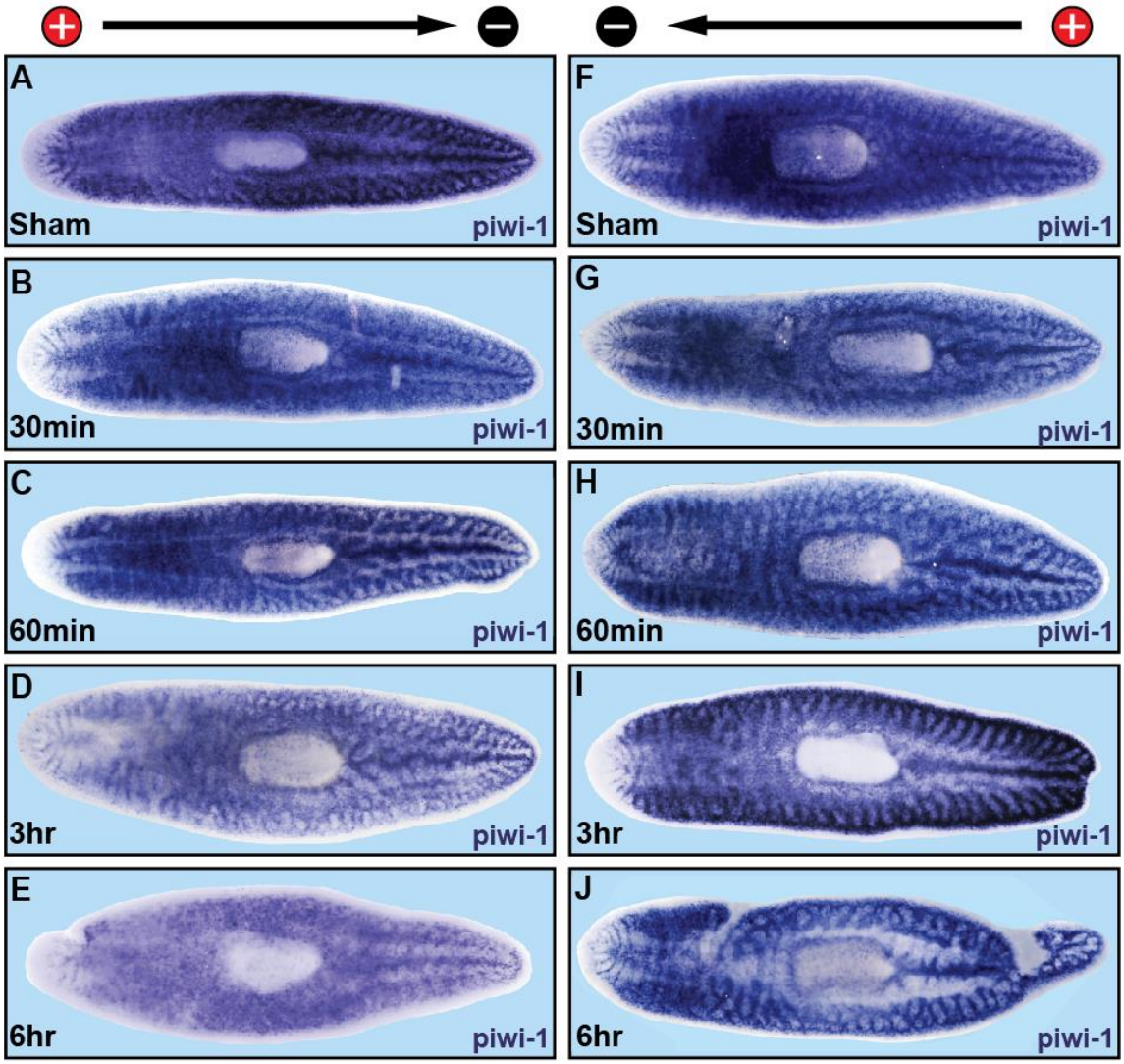

Figure 14. pDCS^S application causes redistribution of neoblast specific piwi-1 gene expression. Intact planaria were exposed to 30min, 60min, 3hrs, and 6hrs of pDCS^S and then fixed for in-situ hybridization. **A – E)** pDCS^S application with [+]H [-]T showed progressive decreased expression of *smed-piwi-1+* cells with the most prominent effect at 6hrs pDCS^S. **F – J)** pDCS^S application with [-]H [+]T showed progressive increases in piwi-1$^+$ cells within the lateral tissues while decreasing piwi-1$^+$ in the mediolateral tissues, this effect was strongest at 3 and 6hrs.

This display of mitotic control was not restricted to one pDCS^S polarity. Exposure to pDCS^S which combats the planarians endogenous polarity ([+]H [-]T pDCS^S polarity) demonstrated profound effects on neoblast proliferation. After 6hrs of pDCS^S, neoblast proliferative density decreased nearly 7-fold compared to control (Fig 13 A, G). This effect was accompanied by a similar, less potent redistribution effect, exhibited by planaria subjected to complimentary endogenous pDCS^S treatments ([-]H [+]T), with very strong reduction in lateral and medial neoblast proliferative density when compared to control Fig (13 C, G). Interestingly, neither polarity exhibited significant redistribution of neoblast

mitosis across the anterior-posterior axis (Fig 13 B). However, the ability to rapidly regulate neoblast proliferation with applied electric fields is evident and illustrated clearly with these results. To further explore this $pDCS^S$-mediated regulation of neoblast cellular division within the homeostatic model, we addressed the effect of $pDCS^S$ and the regulation of neoblast specific gene expression.

5.2.2 pDCS regulates *smed-piwi-1* expression in a polarity specific manner

To qualitatively address the effect of $pDCS^S$ on the expression of neoblast specific gene *smed-piwi-1*, we performed in-situ hybridization on intact planaria subjected to $pDCS^S$ for different time periods. *Smed-piwi-1* expression responded periodically to $pDCS^S$, following the expected outcome developed through the activity of neoblast proliferation shown previously. It was observed that application of complimentary $pDCS^S$ ([-]H [+]T) appears to have little to no effect on the qualitative distribution of *smed-piwi-1* throughout the body until about 3hrs of $pDCS^S$ exposure (Fig 14 A-D). However, at 3hrs of $pDCS^S$ exposure, *smed-piwi-1* expression becomes moderately distributed across the sagittal axis of the planarian body plan; subsequently at 6hrs of $pDCS^S$ exposure *smed-piwi-1* is strongly polarized across the sagittal axis, becoming concentrated in lateral tissues (Fig 14 D, E). This result is consistent with the neoblast proliferative distribution found within the body of planaria exposed to equivalent $pDCS^S$ (Fig 14 C, E). Moreover, planaria subjected to counter endogenous $pDCS^S$ ([+]H [-]T) exhibited reduced *smed-piwi-1* expression levels at 3hrs of $pDCS^S$ exposure; becoming more severe at 6hrs of $pDCS^S$ exposure (Fig 14 H, I). Changes in *smed-piwi-1* expression, for either $pDCS^S$ polarity condition, within intact planaria exposed to $pDCS^S$ were not qualitatively evident until 3hrs of $pDCS^S$ (Fig 14 A-D, F-H).

5.3 Discussion

Planarian neoblasts have the capacity to give rise to all tissues within the planaria. Additionally, neoblasts are required to support homeostatic turnover replacing dead or dying cells on a regular basis. This homeostatic process of cellular turnover is central to the longevity of the planaria and is something shared among all complex organisms. Neoblasts tasked with the replacement of aging cells must properly recognize cellular identity, physiological whereabouts, and need for a cellular successor. With such reaching responsibilities in the planaria, understanding how $pDCS^S$ effect homeostatic neoblasts is central to the investigation of potential bioelectric regulatory networks governing the behavior of naïve planarian neoblasts. Recent advancements in the understanding of bioelectricity suggests that cells may use the innate bioelectric properties of tissues as ‘topological maps’ to maneuver and recognize the complexities of the endogenous body plan[209,291,335]. Endogenous bioelectrical properties of tissues rely greatly on the landscape of collective cellular RMPs. Collective changes in cellular RMP can impede large scale biological processes leading to developmental abnormalities, regenerative impotence, and other undesirable outcomes[579,586,587,589,590]. Cellular RMP is dynamic and changes with differing stages of the cells life cycle[13,512]. Dysregulation of cellular RMP is destructive in nature and has been discovered to be indicative to various forms of cancer[511,537]. Understanding how $pDCS^S$ influence body wide bioelectrical signaling and how $pDCS^S$ influence tissue homeostasis within the planaria can provide insight into exactly how these currents interact with different cell populations and how they may impact their normal behavior.

The planaria maintains an asymmetric endogenous bioelectric difference across its anterior-posterior axis; with anterior tissues being significantly depolarized with respect to the posterior tissues[585,586]. These stark differences in bioelectric potential have been shown act as signaling mechanisms encoding positional information coordinating the proper regeneration of missing tissues[586]. Planarian tissue amputation immediately causes membrane potential depolarization in tissues adjacent to the amputated region, a common outcome of injury in many invertebrate and vertebrate organisms including humans[564,579,585,586]. However, depolarization experienced in the anterior tissue amputation region is greater than that experienced in the posterior amputation region. Ultimately, magnitude and persistence of depolarizing signals, following amputation, dictate the endogenous anterior-posterior axis in regenerating planaria, resulting in full scale regeneration of complex tissues such as the brain and intestinal branches[586]. In planaria, wound healing/regeneration is characterized by the rapid induction of 'wound response genes', followed by increased neoblast mitosis both systemically (at 6hrs post-amputation), and locally within tissues undergoing regeneration (seen 36-48hrs post-amputation)[477]. As cellular RMP is dynamic and changes with cellular state (proliferative or quiescent), the endogenous bioelectric landscape may regulate said wound induced neoblast activities while exogenous manipulation of this landscape may provide insight into the bioelectric underpinnings of the planarian neoblast.

5.3.1 pDCS^S leads to changes in mitotic distribution in the homeostatic planaria

Exogenous manipulation of endogenous bioelectrical properties is a growing field with immense therapeutic potential. In planaria, alike many other model organisms, the study of bioelectric regulation of stem cells is largely overlooked. More recent studies have shown promising evidence supporting bioelectric regulation of planarian neoblasts[335,512,586]. However, much is lacking in the knowledge of bioelectric manipulation of stem cells especially in the context of homeostatic regulation. Planarian neoblasts are the only dividing cells within the planaria making them the sole proprietors of planarian regeneration, and in their absence, regeneration cannot occur[359,477]. Moreover, planarian regeneration is guided by endogenous bioelectric potentials, as such, neoblasts must directly respond to the bioelectric properties of the tissues in which they replenish. Low magnitude pDCS^S application for a period of 6hrs results in a significant neoblast response at both the transcriptional and proliferative level. Interestingly, neoblast responses to pDCS^S differ greatly with respect to the polarity of the applied stimulus. pDCS^S oriented such that the cathode is placed within the anterior tissues results in mitotic redistribution favoring lateral tissues while leaving overall mitotic density unchanged. However, when the cathode is placed within the posterior tissues, 6-hour pDCS^S results in both lateral redistribution of mitosis as well as an overall reduction in mitotic density throughout the body (Fig 13 A, C, D). No difference was observed in the distribution of dividing neoblasts across the anterior-posterior axis following pDCS^S application (Fig 13 B). Consistent among pDCS^S is this medial-lateral redistribution of dividing neoblasts within the planarian body. This phenotypic mitotic re-distribution has not been observed in other experimental procedures performed within planarian biology to date.

The bioelectric landscape of tissues can directly influence nascent proliferative activity. Generally speaking, differentiated cells tend to have a more hyperpolarized RMP while dividing cells (stem cells, embryonic, and cancerous) tend to have more depolarized RMPs[6,12,511,512]. Imposing changes to the endogenous bioelectrical landscape through pDCS^S directly perturbs neoblast mitosis. The observed reduction in overall neoblast

proliferation was polarity dependent only occurring when the pDCS^S orientation resembled [+]H [-]T. However, this pDCS^S orientation amplifies the constructed polarity of the endogenous potential landscape of planarian tissues. As such, pDCS^S enforces a slight hyperpolarization to the posterior while further depolarizing anterior tissues. The imbalance in endogenous bioelectrical topology, enhanced by pDCS^S, effectively downregulated normal neoblast mitosis. In contrast to this result, pDCS^S orientation resembling [-]H [+]T did not result in any significant change in overall neoblast mitosis. These data suggest there may exist a differential bioelectric range imposed across the anterior-posterior axis by which the homeostatic body employs to dictate body-wide neoblast proliferation and deviations from the baseline result in drastic mitotic differences.

Overall complexity of the planarian tissues may directly influence the observed medial-lateral mitotic redistribution following pDCS^S. During pDCS^S application, microelectrodes are used to penetrate the planarian epithelia to ensure current stimulation within the planarian body. However, microelectrode current delivery will pass through tissues at different magnitudes. The anterior microelectrode is placed directly below the eyes on the ventral surface of the planaria, the tip of the microelectrode is thus likely to be found either adjacent or within the anterior intestinal branches. Additionally, the posterior microelectrode is also placed ventrally past the epithelial membranes but due to the anatomical structure of the planarian intestinal system, the electrode is likely to be found within the lose mesenchymal tissue adjacent to the lateral ventral nerve cords and posterior intestinal branches. As a result of this electrode placement, in order for the current to complete the circuit it must travel both through the intestinal cavity as well as through the mesenchymal tissue (Fig 4 B). However, the pass into the mesenchymal regions, current must traverse the epithelial barrier lining the intestinal branches. Moreover, the intestinal cavity is not occupied by cells in a starving planaria and as such its resistivity is dictated by the intestinal luminal fluid present in homeostatic planaria. Mesenchymal resistivity can be estimated to be greater than that found within the intestinal cavity, leading to an overall decreased induced current density during pDCS^S as a function of relative resistivity ($E = J\rho$)[65,581,591]. Mathematical modeling of current densities during transcranial direct current stimulation reveal differential intensities in current proportional to tissue resistivity[592–594]; supporting the premise of differential current densities within tissues of variable resistivity's. This purposed decreased current density experienced by mesenchymal tissues may account for the differences in mitotic activity across the medial-lateral axis, imposing more pronounced effects on resident neoblasts. However, the relative currents passing through each region of the planaria during pDCS^S require further quantification.

5.3.2 pDCS^S restricts neoblast gene expression markers to tissues experiencing elevated mitotic events

pDCS^S redistribute dividing neoblasts within the homeostatic planaria within 6hrs of stimulation. To investigate whether this proliferative restriction corresponded to changes in the distribution of neoblasts within the planarian body we used the neoblast marker piwi-1 to label all planarian neoblasts. Over the course of 6 hour pDCS^S piwi-1$^+$ cells begin to concentrate in lateral tissues ([-]H [+]T) or exhibit a dramatic decrease ([+]H [-]T) within 3hrs of pDCS^S (Fig 14 A). piwi-1+ redistribution progress further at 6hrs pDCS^S exhibiting dramatic medial-lateral differences ([-]H [+]T) and a significant systemic piwi-1$^+$ reduction ([+]H [-]T). The observed piwi-1+ redistribution is in agreement with our mitotic observations showing enhanced lateral neoblast proliferation ([-]H [+]T) and a systemic

reduction in neoblast mitosis ([+]H [-]T) at 6hrs pDCS^S (Fig 13 A, C). It is evident from that body wide pDCS^S has the potential to influence planarian neoblast activity in the realm of both proliferation and cellular gene expression within homeostatic planaria. These effects occur over time showing significant differences influence on neoblast activity within 3hrs to 6hrs of pDCS^S.

The observed phenotypes following body wide pDCS^S within homeostatic planaria is both polarity specific and time dependent. The polarity of pDCS^S results in two distinct phenotypes regarding neoblast density throughout the planarian body. Cathodal electrode placement within the anterior results in planaria with neoblast dense lateral tissues in both mitotic levels and neoblast gene expression. However, simply reversing the polarity of pDCS^S, without changing magnitude or duration, results in planaria with a significantly reduced neoblast presence in all tissues. The phenotypic response neoblasts display towards pDCS^S is both proliferative and transcriptional in nature. Capacity to regulate stem cell behavior, enriching or diminishing neoblast presence and activity within specific tissues is a powerful tool exhibited in pDCS^S. More research is needed to explore the capacity and utility of direct current stimulation in modulating neoblast behavior exploring molecular mechanisms by which pDCS^S govern neoblast behavior.

CHAPTER SIX

FINDING

Effects of detergent-mediated membrane depolarization on cellular activity, with respect to gene expression and cell division

6.1 Introduction

Wound healing is a complex process involving many different cell types working in harmony towards the singular goal of tissue reconstitution. Cellular processes such as migration, proliferation, and differentiation are undertaken during wound healing; processes which operate through an array of signaling cascades with unique genetic regulators[561,564,581]. In planaria, characteristics of the wound response has been a focus of research for decades. With recent advances in molecular and genomic tools, researchers have found definitive evidence for both proliferative and transcriptomic wound induced responses onset but tissue injury each having district characteristics which are dependent on the magnitude of injury received[319,359,477]. In response to injury, planarian neoblasts experience robust systemic increased proliferation 4-6hrs post-injury followed by redistribution of active mitosis restricted to regions adjacent to injury/amputation site 36-48hrs post-injury[595]. These proliferative dynamics alter slightly when responding to small scale injuries as neoblasts will terminate their proliferative responses at its systemic 6hr post-injury stage without progressing towards localized mitosis[359]. Similar to the injury induced mitotic responses, recent work in planaria have identified groups of genes within injured tissues which experience distinct transcriptomic changes following injury[319,477]. More specifically, three distinct waves of gene expression have been identified and characterized as the phenotypic transcriptomic response to wounding in planaria; these three groups are known as “early”, “late”, and “sustained” wound response genes[319]. Interestingly, some genes within the early response category can be seen upregulated as early as 30 minutes post-injury[319,477]. Although the molecular/genetic responses associated with wound healing are shown to possess impressive temporal kinetics, signals initiating these responses remain obscure. However, a promising candidate for initiating the wound response, in planaria and other models alike, are the changes in electrical properties induced by physical trauma naturally occurring at the injury site immediately following tissue damage. These electrical changes come about through the ionic leakage caused by the destruction of endogenous electrogenic ionic barriers, the epithelium[3,5,581]. The loss of endogenous potential and subsequent ionic leakage is a known phenomenon occurring in all epithelialized tissues following injury and has been shown to have to potential to act as a bioelectric signaling mechanism for cells tasked with wound healing[354,564,581,596].

Electrical potential is the bioelectric currency of excitable and non-excitable cells. A collective of coupled cells, for instance an epithelium, generates a potential difference spanning across its layer(s). In the case of an epithelium, this is known as the transepithelial potential difference (TEPD)[597–599]. Organisms with integrated organ

systems use epithelial layers to separate and compartmentalize organs within the body plan. Disruption of TEPD within the adult organ system can lead to disease such as what occurs in cystic fibrosis which is characterized by an increased hyperpolarization of TEPD or respiratory epithelium[597]. Disruption of TEPD can occur in a number of ways, one of which occurs immediately at the onset of a wound or injury[333,349,564,581,600,601]. Destruction of a region of epithelial tissue upon injury disrupts its capacity to maintain its TEPD, allowing for differentially transported charges to then travel down their electrochemical gradients, depolarizing tissues at injury site. Current passing through injury induced pathways have been measured in a multitude of model organisms, demonstrating its native presence across the animal kingdom[333,334,579,581]. Depolarizing injury potentials have been well characterized and have been demonstrated to influence the behavior of a wide array of cells across a multitude of model organisms[6,292,564,581]. Moreover, proper wound healing within these diverse model organisms is greatly dependent on bioelectrical signals; allowing researchers to influence wound healing processes by artificially modulating bioelectric properties at the site of injury[333,584,586,587]. In planaria, wounding of any type can be properly regenerated and healed within 7 days following injury.

Planarian regeneration has been shown to be influenced by endogenous changed in local TEPDs at the site of injury/amputation[586]. Neoblasts, being the sole proprietor of planarians innate regenerative capabilities, must properly respond and mobilize an appropriate response to all forms of injury. These responses include but are not restricted too: regenerate proportionality to body size, tissue identity, recognition of lost or damaged organs, and proper regulation of magnitude of the proliferative response required by a specific injury type. It has been shown that disrupting the bioelectrical response within the planarian model organism leads to an inappropriate regenerative outcomes in the planarian model[512,585,586]. Proper planarian regeneration is characterized by distinct waves of neoblast-related gene expression alongside distinct mitotic activity[359,477]. Many of these studies focus primarily on either 1) planarian bioelectricity or 2) changes in cellular transcriptomics in response to wounding. Surprisingly, many of these studies fail to address the potential for cross talk between these two profound wound healing responses. To address this fundamental gap in knowledge, we developed a technique to locally depolarize regions of the dorsal epithelium without introducing physical injury and dissect the effects of depolarizing potentials on planarian neoblast behavior.

Physical injury or amputation initiates a multitude of responses, some of which influence wound healing but are not directly associated with injury induced depolarization. This local tissue depolarization occurring at the wound interface is the most immediate response elicited by injured tissue. We believe wound induced ionic leakage and subsequent tissue depolarization is a bioelectric signal that initiates characteristic wound healing signaling cascades and acts as a signaling mechanisms for organisms to effectively recognize and mount characteristic wound responses. To focus on ionic leakage/tissue depolarization and their capacity to induce characteristic planarian wound response and drive wound healing and regeneration initiation independent of physical injury, we implemented local administration of amphipathic surfactants to microscopically permeabilize the dorsal epithelium and permit local TEPD depolarization. Amphipathic surfactants, used at low concentrations, create micropores within cell membranes of epithelial cells and disrupt the TEPD by short circuiting the cellular RMP[602]. Using fire polished glass capillaries, we locally administered chosen surfactant at specific concentrations to the surface of the dorsal epithelium for a given exposure time. To ensure local administration, treated tissue is suctioned into the polished capillary during exposure, created a seal at the epithelial capillary junction (Fig 15 A). This method for local and

precise exposer of planarian epithelial tissue to low levels of surfactant, namely trtx, was used to disrupt the TEPD and generate localized regions of depolarized tissues.

6.2.1 Detergent induced epithelial depolarization leads to distinct mitotic responses along the Planarian anterior-posterior axis

Trtx was diluted with planarian water (1.00%, 2.50% Tx) and administered to the anterior or posterior of chilled planaria, for 10-15s, using fire polished glass capillaries (Fig 15 A). Planaria were then rinsed with planarian water and placed in pH_2O filled petri dishes until their appropriate fixation times. As illustrated by high resolution cross sectional analysis of the planarian epithelial monolayer, administration of trtx did not damage or rupture the planarian epithelial (Fig 15 D, E). Thus, subsequent cellular responses following trtx application are rooted in detergent induced plasma membrane permeabilization. As the plasma membranes primary role is to separate ions between extracellular and cytosolic fluids, introduction of trtx disrupts cellular V_{mem} and consequently induces local depolarization of the TEP. First, we investigated the mitotic responses of neoblasts within the planaria following trtx-mediated tissue depolarization.

In the planaria only neoblasts undergo cellular proliferation[324,577]. In addition to this, mounting evidence has shown that cell division is tightly regulated by changes in the V_{mem} of dividing cells[12,512]. Therefore, we asses neoblast proliferation following trtx induced TEPD. We found that the planarian neoblasts exhibited very interesting mitotic responses following regional trtx induced TEPD. Initially there was no mitotic response to regional TEPD however, 3hrs and 6hrs post-trtx application neoblast proliferation changed drastically along the AP axis. In planaria exposed to both 1.00% and 2.50% trtx mitotic events decreased within regions exposed to trtx and increased within tissues opposite that of the exposed region (Fig 16 A - C). This effect was consistent within planaria subjected to anteriorized trtx application or posteriorized trtx application (Fig 16 D - F). Surprisingly, 6hrs post-trtx application the mitotic response was opposite that found at 3hrs exhibiting increased proliferation within tissues exposed to trtx and decreased mitosis within tissues opposite trtx treatment (Fig 16 I, L). From these experiments, it was

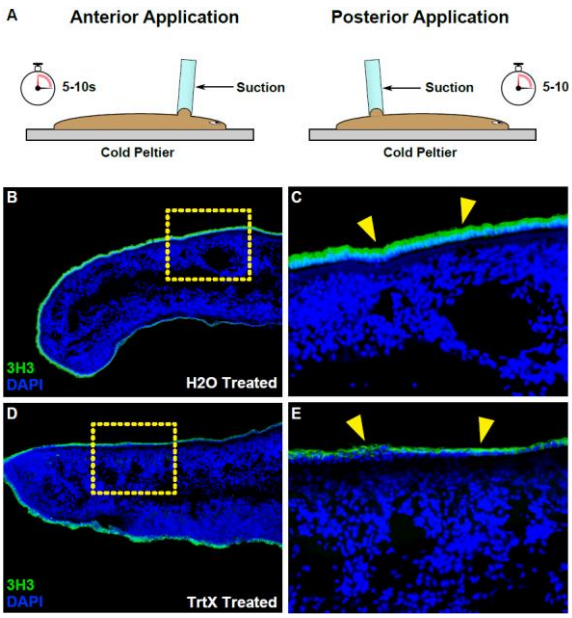

Figure 15. Low concentration localized triton X-100 (trtx) application does not damage planarian epithelial layer at the application site. **A)** Schematic representation for localized triton X-100 treatment depicting both anterior and posterior tissue specific triton X-100 treatment. Borosilicate glass capillaries were flame polished, filled with mineral oil and triton X-100, placed at the region of interest and then suction was applied to isolate the tissue-triton interface. **B)** Cross sections immunostaining labeling nuclei (DAPI) and epithelial junctions (3H3) of planaria exposed to H_2O (sham). **C)** Enhanced image of hashed rectangular area in (**B**) clearly depicting an intact dorsal epithelial layer. **D)** Cross sections immunostaining labeling nuclei and epithelial junctions of planaria exposed to 15s of triton X-100. **E)** Enhanced image of hashed rectangular area in (D) clearly depicting an intact dorsal epithelial layer despite triton X-100 exposure.

illustrated that trtx induced TEPD in the planaria generated a systemic proliferative response from neoblasts (Fig 16 G- L). Interestingly, this response was biphasic in nature, shifting the mitotic distribution of neoblasts along the AP axis to become concerted within distal tissues 3hrs post-trtx application and then shifting again at 6hrs post-trtx application to treated regions. These effects were seen across varying trtx concentrations and were consistent across anterior vs posterior treated planaria.

6.2.2 Distinct transcriptional responses follow detergent induced TEPD resembling the characteristics of a planarian wound response

Planaria have the unique regenerative capacity to heal and replace any lost or missing tissues. Additionally, it has been shown that planarian cells involved in the regenerative process exhibit a distinct gene expression response following injury and/or amputation. Specifically, the transcriptomic response observed during planarian wounding is consistent across different injury types with unique temporal kinetics with respect to specific groups of genes which are dependent on the severity and type of injury experienced. There are 3 distinct waves of gene expression that are responsible for coordinating proper regeneration for all injury types. These 3 waves are characterized as early, late, and sustained wound response[319]. The most immediate response to wounding is the early response which initiates within 30mins, reaches its climax within a few hours and then drops to basal levels 12hrs following injury. This early response is consistent across all injury and amputation types and is associated with mounting the most immediate response to injury.

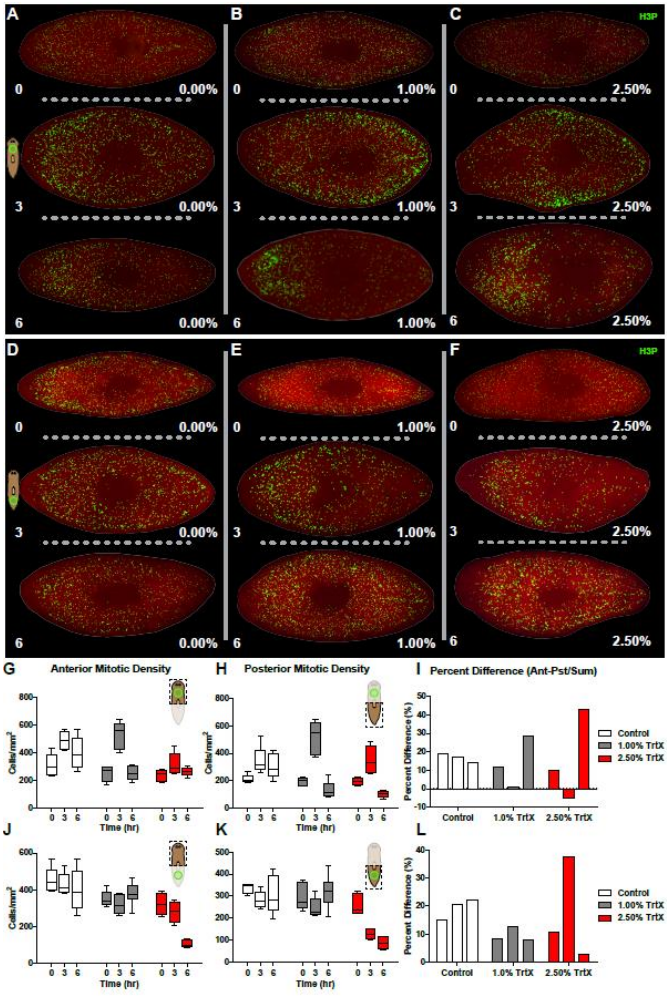

Figure 16. Local trtx application redistributes neoblasts mitosis by inducing temporal oscillatory mitotic responses along the planarian AP axis. **A-C)** the effects of incremental increases of trtx application to anterior planarian tissues representing by distributions of mitotic neoblasts represented by H3P immunostaing. **D-F)** the effects of incremental increases of trtx application to posterior planarian tissues representing by distributions of mitotic neoblasts represented by H3P immunostaing. **G, H)** Mitotic density at 0, 3, 6hrs post-anterior trtx application of increasing trtx concentration with respect to the anterior (**G**) and posterior (**H**) tissues. **I)** Percent difference of cellular mitotic density in anterior exposed trtx planaria with increasing trtx concentrations. **J, K)** Mitotic density at 0, 3, 6hrs post-posterior trtx application of increasing trtx concentration with respect to the anterior (**J**) and posterior (**K**) tissues. **I)** Percent difference of cellular mitotic density in posterior exposed trtx planaria with increasing trtx concentrations.

Interestingly, when assessing specific sets of genes found within these 3 distinct wound response waves we found that planaria treated with triton X-100 exhibit gene expression profiles with striking similarities to the actual wound healing response.

To address the distribution of neoblasts following trtx induced regional TEPD we performed whole body in-situ hybridization for the pan neoblast marker *smed-piwi-1*. This was done in planaria exposed to trtx in both the anterior and posterior region. Consistent with the observed biphasic response in neoblast mitosis, *smed-piwi-1* gene expression shifted asymmetrically along the AP axis at both 3hrs and 6hrs post-trtx application (Fig 17 A, B). When quantified using qPCR, *smed-piwi-1* gene expression exhibited distinct tissue specific responses to regional trtx application. When planaria were exposed to trtx in the anterior, *smed-piwi-1* gene expression levels decreased initially and at 3hrs within the anterior and returned to basal levels 6hrs post-triton application (Fig 17 C, E). Conversely, in the posterior tissues, *smed-piwi-1* gene expression decreased immediately at 0hrs and then rapidly increased at 3hrs showing a 2-fold increase in gene expression with respect to the control. This is consistent with the observed increase in neoblast mitosis within the posterior tissues of anterior treated planaria at 3hrs post-trtx application (Fig 16 A). Finally, at 6hrs post- anterior trtx application *smed-piwi-1* returned to near basal levels within the posterior (Fig 17 C, E) complimenting the observed attenuation of mitosis within these regions at 6hrs post-trtx application. Planaria treated with 1.00% trtx within the posterior region exhibited complimentary *smed-piwi-1* gene expression patterns consistent with the asymmetric mitosis observed in these same planaria. Specifically, *smed-piwi-1* gene expression initially decreased within the posterior treated tissues (0hr) and then subsequently

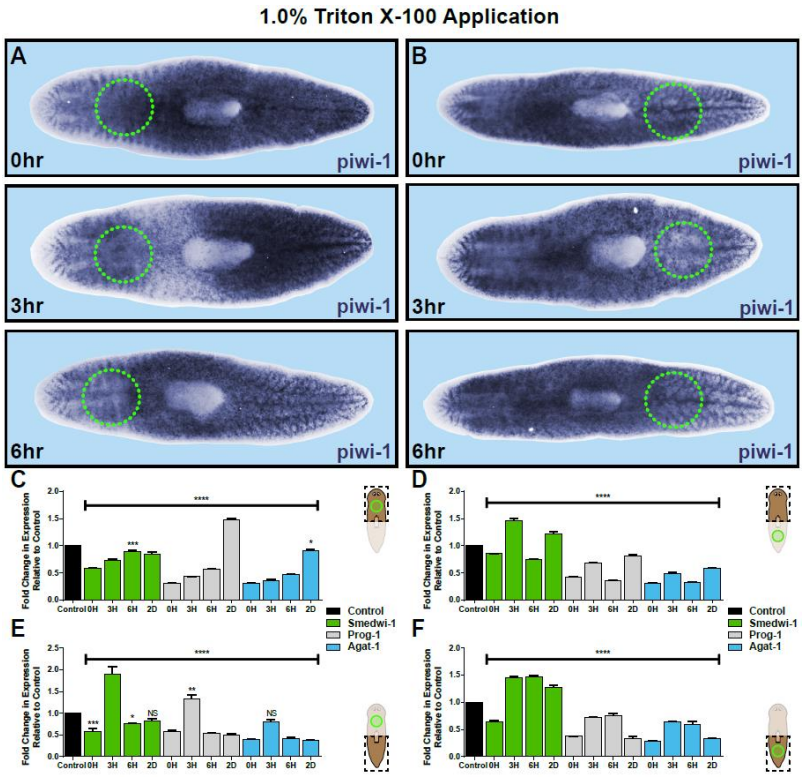

Figure 17. Local application of triton X-100 (trtx) in anterior or posterior planarian tissues leads to unique oscillatory responses in neoblast specific gene expression density across the AP axis. **A)** *smed-piwi-1* gene expression levels in anterior trtx^{+} planaria at 0, 3, and 6hrs post-trtx showing dynamic changes in *smed-piwi-1* expression along the AP axis. **B)** *smed-piwi-1* gene expression levels in posterior trtx^{+} planaria at 0, 3, and 6hrs post-trtx showing dynamic changes in *smed-piwi-1* expression along the AP axis. **C-F)** Relative gene expression of *smed-piwi-1*, *smed-prog-1*, and *smed-agat-1* normalized against housekeeping gene UDP glucose within the anterior tissue of anterior trtx planaria at 0, 3, 6, and 2days within the anterior tissue of anterior (C)/posterior (D) treated planaria; and posterior tissues of anterior (E)/posterior (F) treated planaria. P<0.005**, P<0.0005***, P<0.0001**** and ns= no significance, One/Two-Way ANOVA. Three independent replicates 5 animals/experiment.

increased within the anterior region at 3hrs following posterior trtx application (Fig 17 B, D, F). At 6hrs post-posterior trtx treatment, *smed-piwi-1* gene expression decreased at 6hrs within the anterior. This decrease in *smed-piwi-1* gene expression was complimented by an increase in posterior *smed-piwi-1* gene expression (Fig 17 D, F). Interestingly, *smed-piwi-1* gene expression within the posterior tissues exhibited a persistent increase at both 3 and 6hrs post-triton application (Fig 17 F). This elevation in neoblast specific *smed-piwi-1* at 6hrs within the posterior tissues at 3hrs does not align with the exhibited decrease in proliferation within these same tissues at 3hrs. This disconnect between neoblast density and implied neoblast proliferation. This demonstrates the capacity for changes in the bioelectric properties of tissues can directly influence the mitotic density of tissues and their respective behavior of stem cells.

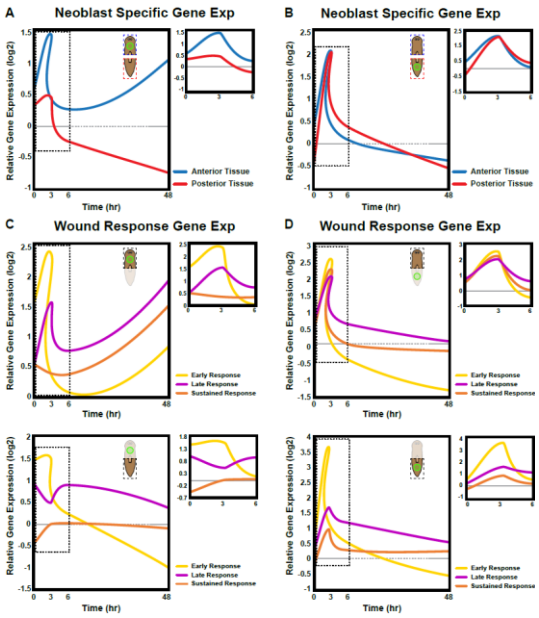

Figure 18. Trtx induces characteristic 'wound-like' gene expression patterns in both exposed and distal planarian tissues following trtx application. Average gene expression profile of **A)** neoblast specific genes (*smed-CKS2, smed- egr1, smed-frz-D, smed-runt-1, smed-piwi-1*) and **C)** wound response genes (*smed-BAG3, smed-CKS2, smed-egr-1, smed-egr-2, smed-egr-3, smed-frz-D, smed-inx-13, smed-KCNK18, smed-noggin-1, smed-notch, smed-notum, smed-runt-1, smed-wntP-1*) assessed at 0, 3, 6, and 48hrs post-anterior trtx application in anterior and posterior tissues. Added graph showing increased time resolution between 0 and 6hrs post-trtx application. Average gene expression profile of **B)** neoblast specific genes and **D)** wound response genes assessed at 0, 3, 6, and 48hrs post-posterior trtx application in anterior and posterior tissues. Added graphs showing increased time resolution between 0 and 6hrs post-trtx application.

To address mechanisms underlying the planarian wound response in the context of regional tissue depolarization we measured several known wound response genes in planarian exposed to trtx. When investigating the characteristic wound response in trtx exposed planaria we found that induced TEPD was sufficient in mounting a wound response similar to that characterized by physical amputation/injury. We addressed gene expression within both anterior and posterior tissues at 0, 3, and 6 hrs post-triton exposure and found that wound associated gene expression responded in ways very similar to that seen within normal regenerating planarian tissues. More specifically there are three characteristic waves of gene expression following injury/amputation: early response genes, late response genes, and sustained response genes[319]. When assessing several genes within each of the three characteristic wound responses we found that trtx-mediated depolarization consistently induced a strong response within the known early wound response genes (Fig 18 C, D). This finding is consistent with planarian wounding were early wound response genes exhibit rapid increases following injury. Interestingly, in many most forms of trtx application late and sustained wound response genes exhibited rapid increases in expression following trtx application. This increase in expression of these two

wound-related responses may be caused by a lack of need in planarian regeneration in which the planaria recognizes tissue lost has not occurred as thus shuts down gene expression of late and sustained gene expression which have been shown to be most related to active regeneration and tissue differentiation in late stages of wound repair. The capacity for local trtx-mediated tissue depolarization to induce fundamental aspects of the characteristic planarian wound response demonstrates importance of bioelectric signaling in wound healing and regeneration. Moreover, there was a systemic increase in neoblast specific genes upon tissue depolarization which are known to respond specifically to wounding (Fig 18 A-D). These increases reflect consistently with the characterized neoblast specific changes in gene expression following wounding. To better understand the bioelectric properties of epithelial tissues we used the potentiometric dye di-8-ANEPPS to measure the bioelectric response to induced depolarization.

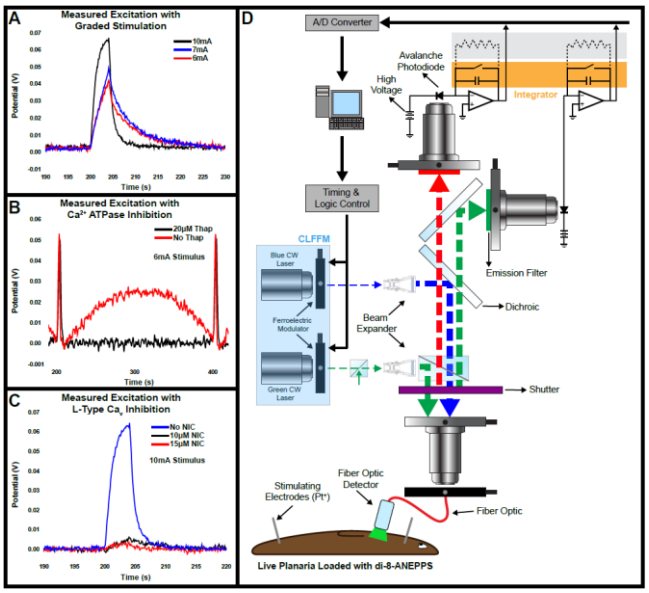

Figure 19. Potentiometric dyes are used to effectively measure potential differences following electric stimulation in epithelial tissues. **A)** Graded electrical stimuli (6, 7, and 10mA) is passed through platinum wire electrodes and the respective electrical response is measured with di-8-ANEEPS potentiometric dye detected via 500µm diameter optic fibers. **B)** Electrical response of planaria following 20µM thapsigargin incubation, inhibiting SERCA activity shutting down muscle gross muscle contraction. This is illustrated by a clear reduction in signal bowing caused by muscle contraction following stimulus caused by changes in distance between the tissue and fiber optic cross section. **C)** Electrical responses following graded nicardipine (NIC) incubation demonstrating large 10mA stimulations are insufficient to overcome NIC inhibition of L-Type Ca_v resulting in an overall nullification of cellular electric sensitivity. **D)** Schematic representation of optic configuration for potentiometric recordings of stimulated planaria.

6.2.3 Potentiometric recording of planarian epithelia implicate L-Type Ca_vs as key contributors to the passive electrical properties of epithelial cells

Ca^{2+} flux is a key regulator of a multitude of biological processes effecting nearly every tissue and cell type in the body. Influx of calcium through L-type Ca_vs is responsible for what is known as excitation-contraction coupling, found in invertebrate and vertebrate muscle cells, leading to the release of intracellular stores of Ca^{2+} from the sarcoplasmic reticulum[287]. In planarian muscle cells, Ca^{2+} influx has been shown to be solely responsible for the depolarization-induced contraction of muscle cells, permitting function and response to depolarizing stimuli[491]. Planarian muscle cells have also been shown to play critical roles in regulating the fate of local neoblasts, coordinating the regeneration of lost tissues and organs[320]. Together with this data it has been shown that modulating Ca^{2+} flux through L-type Ca_v within regenerating planaria has profound consequences on the reconstitution of planarian tissue; resulting in planaria with complete anatomical disarray[468,470]. Together these data present striking evidence of the importance of muscle

cells in the function of neoblasts and moreover calcium's governance over neoblast form and function within the planarian body.

Measuring cellular bioelectrical responses to a depolarizing pulsing currents is key for characterizing bioelectric properties of planarian cells however, performing this *in-vivo*, using the planarian model, is challenging. To overcome the complexity of measuring bioelectrical responses to delivered stimuli within the planarian model, of whom is an invertebrate, mucous covered, non-compliant model system we using di-8-ANEPPS; a potentiometric dye that is membrane permeant and capable of high resolution cellular recordings of electrical events[603,604]. To record these electrical events, we implemented CLLFM technology and measured these bioelectric phenomena *in-vivo* in real time[604]. Thus, planaria were incubated for 72hrs in 1µg/mL di-8-ANEPPS dissolved in planarian water (containing 4% v/v pluronic and 1µg/mL di-8-ANEPPS), refreshing di-8-ANEPPS solution every 24hrs. Following di-8-ANEPPS incorporation, planaria were then mounted atop sylgard pads, punctured with stimulating electrodes, and stimulated with pulsing current of varying magnitudes and frequencies. We were capable of accurately measure the passive properties of epithelial cells exposed to currents ranging from 0 – 10mA with a frequency of 5hz and pulse duration of 4ms (Fig 19 A). Loaded epithelial cells exhibited a graded response to pulsed currents (Fig 19 A). It was evidenced that these passive responses are Ca^{2+}-mediated, more specifically, through L-type Ca_vs as the introduction of known L-type Ca_v inhibitor nicardipine (10µM and 15µM) completely abolished electrical responses under all magnitudes of pulsed currents conditions (Fig 19 B).

6.3 Discussion

Tissue depolarization is an immediate, persistent, and pivotal conserved wound response that has been shown, time and again, to relay crucial information to cells participating in wound healing. In addition to tissue depolarization, other injury induced stimuli such as: mechanical stress, tissue absence, and inflammation play roles in the signaling of regenerative cells during wound healing[561,601]. To study the independent effects of tissue depolarization and its role in the governance of regenerative stem cells, we designed a model in which amphipathic surfactants are used to selectively depolarize planarian tissues without the introduction of other wound associated responses caused by physical injury.

Tissue depolarization following amputation can be quite considerable, with measured current densities ranging from 1 - 50µA/cm^2 leaving the amputation site[11,334,579,581]. Injury induced currents are temporal and tend to decrease in magnitude as wound healing progresses, followed by proper tissue regeneration[11,334,605]. Injury induced currents are conserved phenomena found among vertebrates and invertebrates alike, occurring in a variety of injury types[10,457,606,607]. The key component generating injury induced currents is the disruption of the epithelial barrier allowing for unimpeded ionic currents at the site of injury. These changes in trans-epithelial ion transport dynamics caused by tissue ablation is an immediate bioelectric signal that elicits an effect both locally at the injury site and within adjacent tissues. Using various amphipathic surfactants to compromise the epithelial ion barrier, consequentially disrupting the transepithelial ion transport system, allow us to study the effects of artificial 'injury induced-like' currents, caused by unrestrained ion leakage from epithelial tissues, on characteristic wound healing processes.

Low doses of nonionic detergents causes cell membrane permeabilization without perturbing overall tissue structure or morphology and result in cell membrane

depolarization[602,608–611]. This technique of membrane depolarization has been shown to be effective in a wide variety of cell types using various nonionic detergents, including trtx[612–615]. However, the effects of local detergent induced depolarization within an adult organism has yet to be investigated in the context of wound healing response initiation. Moreover, understanding the systemic responses organisms experience when confronted with large local membrane depolarizations will provide insight into the potential mechanisms governed by injury induced bioelectric tissue depolarizations. In the planarian model, we observed distinct transcriptomic and mitotic responses to localized trtx-mediated tissue depolarization. Trtx treated planaria did not experience epithelial injury/damage (Fig 15 B-E) suggesting changes in planarian neoblast dynamics is due to changes in the subsequent changes in bioelectric properties of treated tissues. These responses were systemic and changed inherently depending treatment position along the AP axis.

6.3.1 Local depolarization induces neoblast specific genetic expression

Planarian regeneration is one of the few times in which the planaria experiences large scale, localized, tissue depolarization. Proper planarian regeneration relies on the functional orchestration of neoblast specific gene expression and proliferation. Due to the clear importance of neoblasts and their regulation during the planarian wound response, we chose to investigate the behavior of neoblasts following brief periods of trtx exposure. Moreover, neoblast specific *smed-piwi-1* expression has been shown to be susceptible to bioelectric regulation, induced within irradiated and intact tissues following brief or extended periods of pDCS respectively (Fig 7, 14). Additionally, L-type Ca_v activity, a key regulator of Ca^{2+} influx, has been implicated in a vast number of gene regulatory. Along with established evidence for L-type Ca^{2+} flux and transcriptional regulation, we demonstrated that associated pDCS gene expression changes are susceptible to inhibition of L-Type Ca_v suggesting Ca^{2+} as a mediator of pDCS gene induction (Fig 8). Interestingly, trtx has been evidenced to influence the activity of L-type Ca_vs. In rat vascular smooth muscle cells, trtx has been found to reversibly inhibit the activity of L-type Ca_vs[616]. This inhibitory function of trtx may contribute to the oscillatory gene expression phenotypes observed following trtx-mediated TEP depolarization (Fig 17). In line with this hypothesis, as trtx is first introduced to the planarian tissue, initiating local depolarization and L-Type Ca_v inhibition, *smed-piwi-1* expression is reduced in those areas immediately following exposure. As tissues recover from trtx exposure, *smed-piwi-1* gene expression begins to return, showing elevated levels at both 3hrs and 6hrs post-permeabilization (Fig 17). As this initial response to regional specific trtx is shared between anterior and posterior trtx treated planaria alike, the overall tissue specific responses observed within each treatment population are quite distinct. These differences in gene expression responses demonstrate differences in the way planaria respond bioelectric TEP disruption at the anatomical level.

A unique component of the neoblast specific gene expression response following local trtx were expression differences observed along the AP axis. Depending on the anatomical placement of trtx treatment along the anterior-posterior axis (anterior treated vs posterior treated), unique differences were observed in the gene expression response within treated and untreated regions of planarian tissues between treatment types (Fig 17, 18). However, two consistencies were found in both treatment conditions. Firstly, immediately following treatment, the tissue region which experienced trtx membrane depolarization responded with a reduced expression of *smed-piwi-1*, *smed-prog-1*, and *smed-agat-1* (Fig 17 C-F). Secondly, 3hrs after trtx treatment, all three of these genes

showed elevated expression levels within tissues distal of the treated region compared to that of 0hrs. Notably, naïve neoblast marker *smed-piwi-1* exhibited a strong expressive response within these distal tissues 3hrs post-treatment with levels 3 – 4 times greater then found within treated tissues and even 1.5 – 2 times greater than basal piwi -1 levels within control tissues (Fig 17 C-F).

Initial decreases in neoblast specific gene expression within treated tissues may be representative of malfunctioning sub-epidermal muscle cell stimulation as a result of local trtx treatment. It has been shown that nonionic detergents effectively attenuate action potentials of excitable cells[614,615,617]. In addition to this, trtx has been shown to decrease the effectiveness of neuropeptides to innervate target cells by reducing currents passing through target receptors and increasing receptor desensitization rates[618,619]. Excitable cells in planaria, notable muscle and nervous cells, have been shown to regulate neoblast behavior guiding neoblast plasticity in both homeostasis and regeneration[320,481]. As such, dysregulation of these cells resulting from brief trtx application is expected to influence neoblast specific gene expression, as illustrated with rapid downregulation within both regions of exposed tissues (Fig 17). Once trtx is removed, the distinct tissue specific temporal changes in gene expression may reflect large scale responses in the bioelectric landscape across the planarian AP axis as a result of brief trtx treatment. More specifically, temporal changes in gene expression may be due to interference with planarians innate, collective, topographical tissue electric potential which naturally maintains depolarized regions in the anterior and hyperpolarized regions in the posterior with respect to one another[331,585,586]. Tissues exposed to trtx will experience rapid depolarization which may either accentuate natural AP differences in bioelectric potential or attenuate these differences leading to two bioelectrically distinct outcomes.

As explained previously, planaria possess a natural bioelectric landscape representing depolarized tissues in the anterior with more hyperpolarized tissues in the posterior. When trtx exposure is performed in anterior tissues, these tissues will then become further depolarized resulting in even larger disparities across the planarians AP axis. Within this model, distal tissues express exceptionally high levels of *smed-piwi-1* being 3 times greater than what is found in the anterior and 2 times greater than control planaria 3hrs after exposure (Fig 17 C, E). This increase in bioelectric potential difference across the AP axis may be promoting both neoblast and progenitor specific gene expression within thee distal tissues, as *prog-1* expression is also elevated at this time (Fig 17 C, E). Interestingly, gene expression within these planaria attenuates at 6hrs, returning to near basal levels (Fig 17 C, E). In contrast to these results, trtx treatment within posterior tissues elicits a system increase in *smed-piwi-1* gene expression 3hrs post-application. Moreover, gene expression within the treated posterior tissue remains elevated 48hrs post-application (Fig 17 D, F). Bioelectrically speaking, these planaria should experience a state of bioelectric attenuation across the AP axis as the posterior tissue becomes depolarized due to trtx exposure; similar to what is observed when perturbing proton pumps in the planaria[586]. This bioelectric leveling across the AP axis may prompt these temporal changes in neoblast specific gene expression however, further experiments are required to fully display bioelectric dysregulation as the conveyor of these systemic responses in neoblast specific gene expression.

Regional depolarization leads to rapid transcriptomic changes locally within treated tissues. In addition, tissues far from the depolarized regions responded in distinct ways to depolarization despite the shear distance away. This data suggests changes in regional membrane polarization, caused by epithelial membrane disruption, induces both local and systemic neoblast responses within the homeostatic planarian model. Interestingly,

transcriptomic flexibility within the homeostatic planaria is a trait readily observed throughout the various stages of planarian wound healing in response to injury and amputation[319,327,477]. Moreover, planarian amputation generates both a local and systemic changes in neoblast specific gene expression profiles following injury[319,477]. These wound-related changes in neoblast-related gene expression exhibit temporal dynamics as the process of wound healing progresses[319]. To address the possibility that tissue depolarization alone could elicit transcriptomic changes characteristic of wounding in planaria, we sought to characterize several wound induced transcriptomic changes within the tissues of our trtx and contrast them with those previously characterized[319].

6.3.2 Local tissue depolarization is sufficient to initiate fundamental aspects portraying the planarian wound response

Tissue regeneration within various regenerative organisms is preceded by distinct transcriptional responses. In the planarian model, tissues regeneration initiates both a generic and distinct gene expression response. The generic wound response is engaged by all forms of injury and regeneration however the distinct wound response that follows injury is more specific and is based within the type of regeneration required. These wound-related gene expression responses have been split into 3 categories: early, late, and sustained responses. The generic wound response is primarily the early wound response and is consistent across all injury types. Both sustained and late wound response genes are more specific to the injury types encompassing genes required for tissue specific regeneration and cellular differentiation. When injury occurs without the need for large scale regeneration the generic wound response initiates and upregulates within the first 6-12hrs and then normalizes within 24hrs following injury. If regeneration is required, late and sustained wound response genes will initiate and carry out their roles in tissue specific regeneration. Additionally, there are specific responses within neoblasts following wounding which are consistent across injury types, similar to the early response genes. We assessed these four characteristic populations of wound response genes and addressed them within tissues of exposed trtx planaria. Interestingly we found that genes within the generic planarian wound response were characteristically initiated by trtx-mediated epithelial depolarization, closely resembled the generic planarian wound response.

Trtx-mediated epithelial depolarization induced a rapid generic early wound response within all tissues. This early response is the generic gene response which is engaged by all forms of injury and forms of wounding. Tissues exposed directly to brief trtx epithelial depolarization exhibited a robust engagement of these early response genes. Even tissues distal trtx depolarized tissues exhibited a clear initiation of the early wound response however it was not as robust as those observed within the depolarized tissue (Fig 18 C, D). This suggests that trtx induced TEPD is sufficient in engaging the generic wound response. This finding illustrates that bioelectric signals can directly regulate the planarian wound response and when manipulated, can systemically induce a robust generic wound response. Interestingly, anterior and posterior tissues, regardless of site of trtx treatment region, exhibited rapid upregulation which attenuated over time to basal levels. The generic wound response and neoblast response are both associated the inherent reaction to planarian wounding.

In addition to the generic transcriptional response to wounding, planaria respond to wounding with robust mitotic events at various stages of planaria regeneration[359]. Similarly, trtx treatment induces robust and rapid changes in local mitotic distribution of

neoblasts (Fig 16). In normal planarian wound healing neoblasts first respond with systemic increases in mitosis 6hrs post-amputation and then with local increases in mitosis at the injury site 36-48hrs post-amputation[359]. However, trtx induced changes in neoblast mitosis are both local and biphasic as exhibited by distinct oscillations across the planarian AP axis. Trtx induced changes in proliferation have two distinct temporal changes in mitosis, one occurring at 3hrs and another at 6hrs. Mitotic increases at 3hrs post-trtx application are both systemic and local at the site of trtx application. For example, in anterior treated planaria mitosis increases systemically yet in addition to this mitosis increases locally in posterior tissues, opposite that of trtx application (Fig 16 A-C). The local effect occurs in both low and high levels of trtx application in planaria treated anywhere along the AP axis. The second unique changes in planaria mitosis in trtx treated planaria occur at 6hrs post-treatment. At this time planaria mitosis decreases systemically yet shifts to tissues initially exposed to trtx (Fig 16 A-F, I, L). These effects closely resemble standard mitotic responses to wounding on a much shorter time scale. Systemic increases in mitosis are only evident in anterior treated planaria suggesting anterior TEP dynamics are largely involved in regulating systemic neoblast mitosis. The dynamic changes along the planarian AP axis are most evident when reflect as percent difference between the anterior and posterior tissues at these distinct time points. As anticipated, mitotic distribution largely favors tissues opposite trtx treatment at 3hrs while shifting back to trtx treated regions at 6hrs. These local changes are generally observed 36-48hrs post-amputation however we observed these local changes rapidly in trtx treated planaria suggesting regional largescale TEPD is a powerful driver for regulating neoblast mitosis (Fig 16). Further research is required to assess the connected between TEP and systemic neoblast mitosis. Moreover, changes neoblast mitosis along the AP axis may also be largely influenced by changes in topographic collective cellular V_{mem}. Collectively, these results show clear evidence that ionic leakage drives early planarian wound healing and regeneration responses and supporting the hypothesis that the immediate bioelectric response to injury acts to induce signaling cascades which initiate characteristic wound healing responses.

Current limitations in the presented work are can be found when addresses tissue depolarization itself in the planaria. Despite our best efforts, measuring tissue depolarization in planaria using common microelectrode techniques is a challenging endeavor as planaria are encapsulated in a thick mucosal layer. This mucosal layer, along with a firm yet malleable epidermis makes accurate microelectrode recordings of TEP nearly impossible. However, labs have used the potentiometric dye DiBAC to measure collective V_{mem} in planaria in the past[331,586]. The use of potentiometric staining to observe detergent induced TEPD would be an effective data set quantify the severity of TEPD following detergent exposure and to address systemic temporal changes in TEP induced following initial treatment. Moreover, increased robustness in the number of characterized wound induced genes analyzed in these works would help increase resolution in the observed wound induced response with respect to more robust bodies of work addressing characteristic planarian wound responses[319,477]. In addition to increases genomic resolution, FACS analysis eluding to changes in cell cycle dynamics in detergent treated planaria will provide insight into potential cell cycle regulation onset by distinct temporal changes in collective tissue V_{mem}. The use of different nonionic (NP-40, Tween-20), ionic detergents (SDS), or saponins would add robustness to this work and elucidate whether this response is detergent specific or if all membrane permeabilizing agents can induce similar responses.

CHAPTER SEVEN

FINDING

Pulsing direct current stimulation redistributes neoblast mitosis and predictively overrides normal tissue specification along the planarian AP axis

7.1.1 Introduction

The lipid bilayer surrounding cells is a well-designed, insulating, dielectric. These dielectric properties of the lipid membrane allow it to respond to changes in extracellular electrical potential without allowing the passage of electrical current to the intracellular space. However, when changes in extracellular electrical potential are rapid, the membrane dielectric can no longer keep pace with the rapid electrical fluctuations, leading to unrestricted flow of electrical current through the cell. The resulting permeance pulsed currents allows for intracellular interaction with polar molecules, including a wide array of proteins (cytosolic and/or membrane bound), ionic secondary messengers, seemingly anything polar in nature. These vast interactions with pulsing currents have led to the discovery of a wide variety of effects underlining the application of pulsing currents to living cells and tissues.

7.1.2 Pulsing electrical current stimulation elicits distinct cellular responses within a variety of cell types

Proper regeneration of lost tissues requires complex orchestration of migration, proliferation, and differentiation of stem cells at the site of injury. Several vertebrate and invertebrate organisms can perform large scale regeneration being able to regrow lost limbs, appendages, and for some even heads. To achieve this level of tissue regeneration requires the participation of diverse cell populations in the areas surrounding the injury. Depending on the anatomical location where regeneration is taking place, a multitude of cell types can be implicated in the regenerative process. For this reason, many therapies focused on improving wound healing and regeneration are narrowly specialized to treat specific types of injuries[601,620]. Interestingly, electrotherapies are showing promise with substantial effectiveness in a number of wound healing and regeneration applications[31,620]. A vary flexible form of therapeutic electric stimulation is pulsed direct current stimulation (DCS^P). Fundamental changes in the magnitudes and frequencies of DCS^P have been shown to result in different cellular responses allowing researchers to modify techniques to reach a desired effect. Cellular responses to DCS^P are inherently based on the physical properties of the stimulation and how these properties interact with the native electrical properties of the cell. For example, the cell membrane has a resistance and capacitance of $\cong 200M\Omega$ and $\cong 1\mu F/cm^2$ respectively[58,59,65]. As such, steady-state direct currents interact primarily with proteins on the outer membrane as these currents do not penetrate through the strong resistance of the membrane. However, as discussed previously, the

dielectric nature of the membrane will pass direct current when they are presented in a pulsating manner. The conductance of the membrane in the presence of a pulsing current is inversely proportional to the frequency, with smaller frequencies the membrane permeates larger amounts of current[58,59]. These permeating currents then depolarize the membrane, interact with intracellular components and thus carry the potential to activate a multitude of signaling cascades[9,564,620]. The permeating nature of DCS^P provide unique opportunities to interact with a wide array of cell types in novel and effective ways.

A fundamental cell involved in wound healing and regeneration is the mesenchymal stem cell (MSCs). Both vertebrates and invertebrates require MSCs throughout the course of regeneration. In vertebrate systems, MSCs differentiate and give rise to a multitude of cell types during regenerative wound healing (e.g. bone, muscle, adipose, etc)[621,622]. However, post-natal mammalian wound healing focuses around reepithelialization and wound closure to secure interstitial components behind the epithelial barrier, forming characteristic scar tissue. In stark contrast to this, invertebrate wound healing typically results in complete robust regeneration absent scaring. Invertebrates MSCs, like complex mammalian systems, contribute enormously to regenerative wound healing; replacing epithelium, nervous, and muscle tissues to name a few. It comes to no surprise that researchers have sought techniques to regulate and control the behavior of MSCs for therapeutic means. One such method which has borne fruit in the regulation of fundamental cellular processes of MSCs are pulsed direct currents[39,623].

Electric stimulation has shown promise as a therapeutic tool to control various behaviors of MSCs across a variety of model systems. For decades researchers have seen potential in the use of pulsed currents to enhance the healing of bone fractures *in-vivo*[624]. However, the mechanisms behind enhanced healing and bone reconstitution have remained elusive. As such, understanding the mechanisms dictating differential outcome of MSCs is paramount in developing methods to predictively control and enhance MSC therapies. A known mediator of MSC differentiation is intracellular Ca^{2+}[621]. Recently, oscillations in intracellular Ca^{2+} have been shown to play a significant role in the maturation of MSCs; including osteoblast differentiation[622]. Interestingly, application of pulsing electric fields allow researchers to control and induce Ca^{2+} oscillations in MSCs[622,625]. Moreover, implementation of pulsing electric fields has been effective in guiding MSCs towards osteoblast differentiation[622,626–628]. Such techniques involve periodic application of pulsing currents throughout the MSC differentiation time span; usually administered for several hours over the course of several days[32,624]. In contrast to physical application of pulsing currents, directed MSC osteoblast differentiation has been predominantly achieved by the administration of growth factors to MSC cultures. Osteogenesis through growth factor inoculation is found to readily involve intracellular Ca^{2+} signaling[629]. Interestingly, increases in intracellular Ca^{2+} concentration suppress cyclic adenosine monophosphate (cAMP) synthesis by inhibiting adenylyl cyclase and upregulate cAMP phosphodiesterase, further inhibiting cAMP signaling. Moreover, increased cAMP signaling was found to reduce osteogenic differentiation suggesting cAMP negatively inhibits osteoblast differentiation[630]. Additionally, Ca^{2+} activation of extracellular signal regulated kinase (ERK1/2) pathway is known to positively influence osteoblast differentiation[627,631]. As such, it has been shown that application of pulsing currents can enhance ERK1/2 activation, further cementing their utility as potential regulators of cellular differentiation[596,627,632–634]. Such evidence brings insight into the possible mechanisms by which pulsing currents guide the differentiation of stem cells.

Neuronal cell types have long been known to be sensitive to application of exogenous currents[234,236,564,581]. Thus, investigation into applied currents and their therapeutic potential for neuronal regeneration is ongoing. Researchers have found that application of electric fields are capable of stimulating neuronal galvanotropism, guided migration, and selective differentiation of neuronal stem cells[19,20,234,236,248,562,635]. Neuronal stem cells (NSCs) are destined to mature into distinct cell types: neuronal cells, astrocytes, or oligodendrocytes[636]. However, the fate of a NSC can be influenced by the application of an electric field. Interestingly, researchers have found that changing the electrical properties of the applied currents (type [AC vs DC], magnitude, frequency) can predictively influence NSC maturation[19,20,562,635,637]. Specifically, using various applied currents, differentiation rates and fates could be controlled *in-vitro*[20,562,635,638]. Researchers discovered that electrically induced differentiation of NSCs was dependent on influx of Ca^{2+} and Ca^{2+} signaling[20]. These results agreed with findings illustrating that neuronal differentiation is contingent on Ca^{2+} signaling via Ca^{2+} influx through Ca_vs. Furthermore, although NSCs do not inherently express Ca_vs, upon the onset of differentiation NSCs begin to express Ca_vs allowing for influx of Ca^{2+} thus, permitting the necessary Ca^{2+} signaling to take place[639].

Substantial research has been done illustrating the effectiveness of pulsed currents in the guidance of stem cell differentiation. A wide array of stem cells, from various model organisms, displayed sensitivity to cellular maturation while undergoing electric current application, in a predictive manner[19,32,39,562,635,640]. The ability to control cellular fate of regenerative stem cells is powerful therapeutic tool with immeasurable potential in the field of wound healing and regeneration. In addition to cellular differentiation, application of pulsing currents has been shown to influence cellular mitosis within various populations of exposed cells and tissues. Necessary for all wound healing and regeneration is the presence of healthy dividing stem cells to serve as the cellular supply for newly growing tissues. Fortunately for researchers, pulsed current stimulation has demonstrated to have significant influence over the proliferative behavior of various mitotically capable cells. Even though the reasons behind these effects are still being investigated, some of these effects may be attributed to the bioelectrical nature of a dividing cell. When a cell progresses through various stages of the cell cycle its membrane potential changes simultaneously in a very distinct and consistent way[12,512,513]. In fact, interrupting these changes in membrane potential can singlehandedly send a dividing cell into arrest and potentially programmed cell death[12,512,514]. Thus, the state of the resting membrane potential can serve as a bioelectric regulator of cellular mitosis. This has been supported by various findings of dividing stem cells, including cancer stem cells, maintaining significantly depolarized membrane potentials while in their mitotic state[511,515]. As mentioned previously, membrane depolarization can be induced by imposing exogenous pulsed current to cells; a practice which has been employed to study properties and mechanisms of membranes, particularly in excitable cells, well before its effects on cell division were personified[58,60]. Nonetheless, pulsed current stimulation has proven to have significant impacts on the proliferative activity of many cell types[641,642] and have been used to improve wound healing and regenerative processes[30,31,643,644]. To elaborate on the effects of electrical stimulation on the planarian model, we developed techniques to imposed pulsed direct currents directly to immobilized planaria ($pDCS^P$) undergoing both regeneration and normal non-regenerative cellular turnover. Using the planaria we were able to probe specific effects of $pDCS^P$, at both the cellular and organismal level, while planarian stem cells heed to the demands of fundamental cellular turnover and large-scale tissue regeneration.

7.2.1 Brief application of whole body pulsing electric current stimulation reduces overall mitosis while simultaneously initiating proliferation in otherwise dormant tissues

Brief application of $pDCS^P$ to intact planaria had profound effects on the normal behavior of planarian neoblasts and differentiated tissues. Planaria were immobilized for the duration (6hrs) of $pDCS^P$ using a specially designed chamber to deliver fresh planarian water and pulsing current (Fig 20 A). Pulsing current was delivered for 6hrs at a frequency of 5Hz, with a 4ms pulse duration, and a 10V amplitude; the measured magnitude of $pDCS^P$ was ~200mV/mm. Planaria exposed to $pDCS^P$ displayed minor pulsatory muscle contractions which subsided after 30s-120s. Control planaria were immobilized in the same manner without the introduction of pulsing current (Fig 20 B). Planaria exposed to $pDCS^P$ inherited a distorted brain morphology, increasing its surface area and decreasing its curvature (Fig 20 B, C). Photoreceptors appeared to distance themselves from the brain, elongating the optical neurons connecting the photoreceptors to the medial optic chiasma (Fig 20 B, C). This displacement of the photo receptors was quantified and found to be nearly 40µm in front of its normal physiological location (Fig 20 F). Interestingly, instances of neoblast cell division in the brain region was found to be induced under the influence of $pDCS^P$ (Fig 20 B, C, E). Proliferative density in these regions, of which are normally found to be extremely low or non-existent, enriched 6-fold to levels only found within the body of the planaria (Fig 20 E). However, proliferative activity throughout the body plan decreased dramatically from 200cell/mm^2 to 60cells/mm^2, a near 3-fold decrease (Fig 20 D). Similar to non-pulsing steady state $pDCS^S$ applications, $pDCS^P$ applications rearranges neoblast cell division, reducing it dramatically, and even leads to

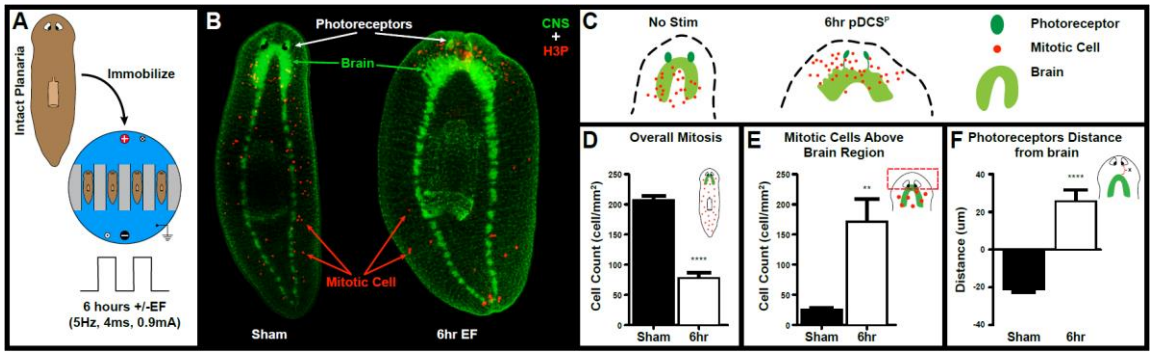

Figure 20. $pDCS^P$ induces largescale morphological and mitotic differences within homeostatic planaria leading to a significant downregulation in neoblast mitosis, concurrent mitotic stimulation within otherwise dormant tissues, and architectural changes to planarian CNS. **A)** Schematic representation of planarian agar immobilization used for 6hrs of $pDCS^P$. **B)** Immunostaining of planarian CNS (VC1+Synapsin) overlaid with neoblast mitosis (H3P) comparing sham and 6hr $pDCS^P$ planaria. **C)** Illustration highlighting morphological changes in brain structure induced by 6hr $pDCS^P$ along with dramatic increases in neoblast mitosis in and around planarian brain tissue. **D)** Quantification of overall neoblast mitotic density in sham and 6hr $pDCS^P$ planaria showing significant decreases in $pDCS^P$ planaria. **E)** Quantification of neoblast mitotic density with regional boundaries starting at the anterior most tip and ending at the base of the optic chiasma. Results clearly show significant increases in $pDCS^P$ planaria compared to sham control. **F)** Assessment of morphological changes through the measurement of optic nerve length demonstrating $pDCS^P$ planaria exhibit increased distance between photoreceptor and brain with increased optic nerve extensions protruding into distal anterior tissues when compared to sham controls. P<0.005**, P<0.0005***, P<0.0001**** and ns= no significance, One/Two-Way ANOVA. Three independent replicates 8 animals/experiment.

drastic morphological changes in differentiated organs. All of this is observed within a 6hr period of pDCS^{P} exposure lending to its rapid and profound effects on planarian homeostasis. Due to the nature of ubiquitous anatomical exposure experienced by these planaria, the mechanisms behind these responses may lead to novel and significant realizations of pDCS^{P} and their potent impacts, spanning a multitude of tissues and organs, *in-vivo*.

7.2.2 DCS^{P} modulates identity and morphology of planarian tissues

Planarian regeneration is led by the early expression of genes that mandate the identity newly forming tissues[324,326,328,359,477,645]. Polar identity of regenerating tissue is determined very early on in planaria; within the first 24hrs[326,328]. The primary genes responsible for the determination of head and tail within regenerating planaria are known as *notum* and *wnt-1* respectively. Interestingly, both *notum* and *wnt* are part of the fibroblast growth factor receptor like-Wnt pathway (FGFLR-Wnt)[329,330]. These genes are expressed homeostatically at their respective regions in which they favor regeneration and silencing of these genes via RNAi leads to planaria with bipolar heads or tails, respectively[326,328]. These genes are both indicators and regulators of planarian regeneration. Previous work has shown that modulation of Ca^{2+} flux directly influences the expression of FGFLR-Wnt family genes, including Wnt-1[468,470]. Interestingly, the expression of planarian L-type Ca_vs coincide with FGFLR-Wnt family genes throughout the regeneration process; beginning as early as 18hrs post-amputation[469]. Additionally, Ca^{2+} flux through L-Type Cavs has the capacity to govern large scale tissue identity across the AP axis in regenerating planaria[468,469], further supported by the discovery of multiple families of Ca^{2+} channels in planaria[470]. Furthermore, Ca^{2+} flux, likely through L-type Ca_vs, is playing a significant role in proper dictation of tissue identity and regeneration in planaria subjected to pDCS^{P}.

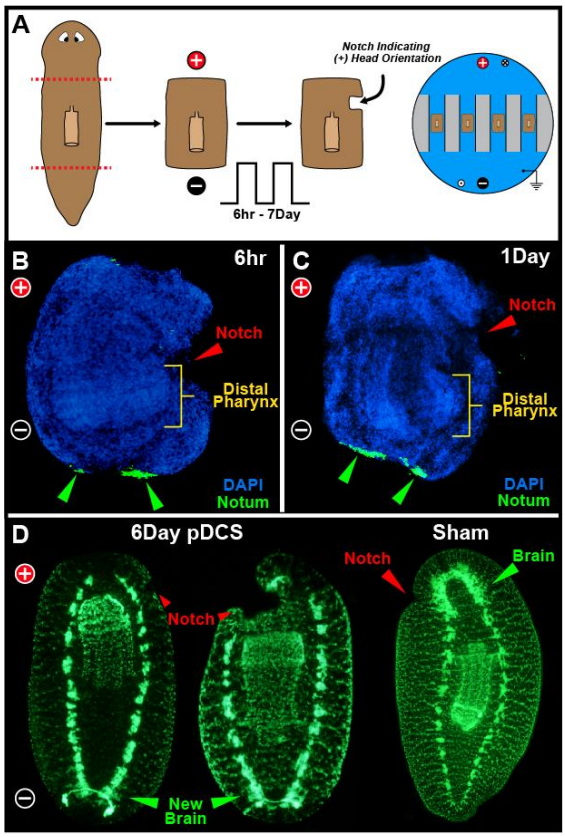

Figure 21. pDCS^{P} override tissue identity and polarity signaling early on in planarian regeneration. **A)** Heads and tails were removed, and regenerating trunk fragments were exposed to pDCS^{P} (hours to days) with the anterior facing wound toward the positive pole; with application parameters of 0.9mA current magnitude, 5hz frequency, 4ms pulse duration. **B, C)** Tissue notch to keep track of original body polarity after fragment is removed from chamber; FISH of notum shows reversal of AP polarity as early as 6hrs persisting to 24hrs in pDCS^{P} trunk fragments compared to sham control. **D)** Resultant of 6Day pDCS^{P} exposed regenerating animals showing reversed AP polarity as identified by the notch as in contrast to the anatomical brain. This is compared to sham control whose regeneration proceeded normally.

To test this hypothesis, we subjected regenerating planaria to pDCS^{P}, known to stimulate Ca^{2+} flux (Fig 19 A), and qualitatively addressed the expression of known

FGFLR-Wnt tissue identity markers throughout the course of regeneration. Planaria were amputated at the post- and pre-pharyngeal, immobilized in current delivery chambers, and subjected to pulsing depolarizing $pDCS^P$ for up to 7 days (Fig 21 A). During encapsulation, planaria were oriented such that their natural anterior faced the positive pole of the $pDCS^P$, indicated by a surgical notch created immediately after concluding $pDCS^P$ treatment (Fig 21 B). Once the $pDCS^P$ was terminated, regenerating planaria were removed from their chambers and immediately fixed to assess gene expression profiles via in-situ hybridization. Nuclear labeling via DAPI showed additional detail and morphology of tissues such as the polar morphology of the pharynx, which was not amputated or removed for the duration of these experiments (Fig 22 B, C). It was found that application of monophasic pulsing currents, generating $pDCS^P$ with magnitudes reaching ~200mV/mm (at 5Hz and 4ms duration), was adequate to reverse the natural expression of head identity marker *notum* within 6hrs of $pDCS^P$ application, compared to control (Fig 21 B). This is clearly evidenced by the remaining polarization of the planarian pharynx (Fig 21 B). This phenotype persists for over 24hrs of regeneration (Fig 21 C). At the termination of regeneration, the reversal of anatomical structures is clearly shown as the anterior specific structure (i.e. the brain) is clearly formed within native posterior tissue as indicated by the notch (Fig 21 D). It is important to note the endogenous polarity of the anatomical pharynx, which has also reversed during $pDCS^P$-mediated regeneration. This clearly indicates the ability for applied $pDCS^P$ to dictate the identity of regenerating tissues. It remains unclear whether this mechanism is mediated through L-type Ca_vs or by other means and this question should be further investigated.

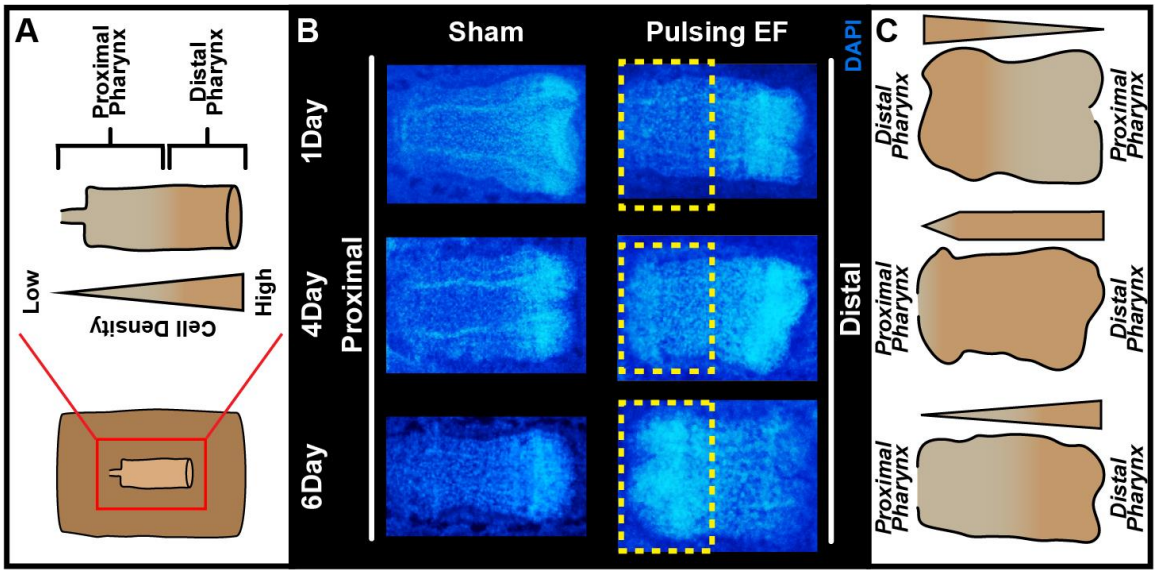

Figure 22 $pDCS^P$ override polarity of the pre-existing pharynx in regenerating trunk leading to large scale remodeling. **A)** Schematic representation of pharynx showing differences in cellular densities along its endogenous AP axis with respect to cellular nuclei. As mentioned previously, pDCSP application parameters were 0.9mA current magnitude, 5hz frequency, 4ms pulse duration. **B)** Pre-existing pharynx in regenerating trunk at different time points after amputation with or without $pDCS^P$ application. Reorientation of pharynx polarity occurs after day 4-post amputation and is visible by day 6 when cellular density is increased in the original proximal region. Proximal region is to the top. **C)** Graphical illustration depicting the progression of morphological changes with time showing increased cellular density across the endogenous AP axis at day 3 with resulting reversal in density and overall pharynx anatomical structures such as esophagus and mouth at 6 days of regeneration.

During pulsing electric field induced tissue reversal differentiated tissues change morphologically to resemble proper orientation along the AP axis. When assessing tissue identity using whole body FISH we realized the pharynx changed its anatomical orientation through what appears to be large scale morphological remodeling within non-regenerating tissues (Fig 22). The pharynx has a distinct nuclear density across its own AP axis, being denser at the mouth [distal pharynx]and less dense at the esophagus [proximal pharynx] (Fig 22 A). Over the course of head/tail regeneration in planarian trunk fragments, no distinguishable changes in nuclear density or pharynx morphology occur along the pharynx's AP axis. However, when regenerating in the presence of pulsing electric fields pharynx morphology rearranges along its AP axis mirroring the large-scale tissue reversal observed in the resulting head and tail regenerates (Fig 22 B). This is evidenced by increased proximal nuclear density in 4-day regenerates followed by persistent increased proximal nuclear density and decreased distal nuclear density (Fig 22 B). Additionally, overall pharynx morphology appears to resemble large scale shift along the AP axis resembling a distal esophagus and proximal mouth (Fig 22 B). This can be more clearly seen in a summarized schematic representation which resembles observed phenotypes in pulsing regenerating fragments (Fig 22 B). Changes in regenerates and large scale morphology observed within regenerating tissues and non-regenerating pharynx's resemble anatomical redistributions across the AP axis experienced as a result of genetic or pharmacological manipulation[327,329,330] using solely pulsing electric fields. These results clearly demonstrate the overriding power of bioelectric signals to guide planarian regeneration and even control tissue morphology.

7.3.1 Discussion

In contrast to DCS^S in which the magnitude of delivered current is felt at the cell membrane of exposed cells, DCS^P effectively transmits currents through cells, bypassing their highly resistive plasma membranes. This form of stimulation is widely used in various medical and commercial devices designed for specialized therapeutic applications from muscle stimulation, bone healing, and neurodegeneration[31,644,646,647]. Despite wide spread commercial availability of such devices[647], much remains unknown regarding the effects these electrical stimulations have on the diverse array of cells in which these currents interact while traveling through various tissues. Using planaria we subject the entire body, and all anatomical organs, to pulsing electric fields both during normal tissue homeostasis and regeneration. The parameters of $pDCS^P$ exposure in planaria are 5hz frequency, 4ms pulse width, and 10V amplitude. Frequency of pulsating currents dictate their capacity to short circuit the highly resistive membrane through the induction of capacitive currents. Various studies have shown that cellular excitation by membrane depolarization occurs at frequencies of 5Hz[35,490,648,649]. We have also demonstrated this using potentiometric recordings of planarian epithelial tissue (Fig 19 A). Our planarian-based approach allows us to observe the effects of $pDCS^P$ on specific cell populations housed in various organ systems of the adult planaria. Our major findings resulting from $pDCS^P$ exposure were observed during both planarian homeostasis and regeneration. Moderate (6hrs) $pDCS^P$ exposure times in homeostatic planaria garnered distinct effects on proliferating neoblasts (i.e. decreased and restricted mitosis) and morphology of differentiated tissues (i.e. distinct broadening of brain and photoreceptors). Additionally, extended periods (several days) of $pDCS^P$ subjected to regenerating planaria rewired endogenous AP polarity of regenerating trunk fragments resulting in complete systemic AP reversal. Although physical changes (i.e. photoreceptor location) in reversed planaria were only observable in the later stages

of regeneration, molecular analysis of known AP determinant genes revealed pDCS^{P} influence began in the very early stages of regeneration (<24hrs). These results demonstrate both the potency and versatility of pulsing DCS and reiterates their standing as biomedical tools with immense governing potential.

7.3.2 pDCS^{P} promotes neoblast cell division in characteristically mitotically dormant tissues

As it stands, mitosis readily occurs just below the optic chiasma in tissues adjacent the proximal brain structure. In normal planaria, these proximal brain anterior tissues mark absolute delineation of tissue containing mitotic neoblasts within the distal anterior of the planaria. This is further certified by studies demonstrating consistent neoblast distribution within homeostatic planaria inhibits proliferation in these areas; even surgical planarian eye resection does not mount a neoblast response, mitotic or otherwise[314,358,365,650]. However, pDCS^{P} planaria exhibit rampant mitosis within these anterior most tissues (Fig 20 E). As such, for the planaria to gain mitotic capacity in these tissues, following pDCS^{P}, there lie several possibilities: 1) pDCS^{P} stimulates quiescent cells to reenter the cell cycle, reaching G_2/M phase and 2) pDCS^{P} modulates endogenous restricted gradients of known position control genes (PCGs) greatly differentially influencing neoblasts within modified tissues. However, it is important to note that these two explanations together may paint a full picture of the observed effects and are not contradictory. As the effects of pDCS^{P} are still largely mysterious, multilayered regulation and signaling mechanisms may be at play during pDCS^{P} leading to diverse responses.

Pulsing direct current stimulation has been shown to influence proliferative events of other cells and tissues through a variety of modalities. Pulsed direct current stimulation has been shown to enhance proliferation in a variety of cell types such as prostate cancer spheroids[459], canine and human mesenchymal stem cells[651–653], adipose derived stromal cells[32], and several others[12,461,620,654–656]. Pulsed direct current stimulation has been shown to enhance hair growth in balding patients suggesting electrical stimulation promotes mitotic activity in quiescent hair follicles[641]; with other studies reporting increases in cellular plasticity following DCS^{P} [657,658]. Many of these reports attribute these effects to activated calcium flux through Ca_vs triggering downstream cellular cascades capable of prompting such phenotypic observations. During pDCS^{P}, overall mitosis decreased nearly 2-fold while simultaneously stimulating mitosis in characteristically quiescent anterior most tissues (Fig 20 B, D, E). Various studies have investigated the cellular composition of these planarian tissues determining they contain a mixture of neoblast and progenitor cells while lacking in active dividing neoblasts[314,359,365,577]. Reasons behind the mitotic quiescence in these anterior most neoblasts remains unknown. However, it has been shown that the bioelectric landscape of these distal anterior tissues are highly depolarized[331,586]. Additionally, the bioelectric properties of perimeter epithelial tissues exhibit high depolarization along with characteristic mitotic quiescence[331,359]. The concept of topographical bioelectric regulation of systemic cellular mitosis is gaining traction in the field of organismal development[8,13,589,659] but in the context of adult tissues topographic bioelectric signaling is largely overlooked. However, we demonstrate the moderate pDCS^{P} induce neoblasts in quiescent tissues to overcome environmental constraints and engage in active cell division. We believe pDCS^{P} application changes the inherent bioelectric landscape of these anterior most tissues allowing them to harbor mitotic neoblasts. We have demonstrated the capacity for pDCS^{P} to rapidly and consistently change the bioelectric properties of tissues (Fig 19 A) supporting the notion of bioelectric meddling

altering the mitotic properties of these tissues. Moreover, $pDCS^P$ induced cellular depolarization shows significant sensitivity to nicardipine inhibition (L-Type Ca_v blocker), nullifying $pDCS^P$ induced depolarization in the presence of nicardipine. Therefore, the observed increases in mitosis found within quiescent tissues may operate through Ca^{2+} signaling, increasing cellular plasticity and cellular capacity to enter mitosis. These mechanisms are focused on the observed increase in mitosis in distal most anterior tissues but do not properly address the overall observed reduction in neoblast mitosis.

Planarian form and function is largely dependent on positional guidance cues from specific populations of mesodermal muscle cells spanning the planarian body, demonstrated during planarian regeneration[320,321]. In fact, one of the first differentiated cell types to arise within regenerating blastema tissue of the planaria, tissue which facilitates ample neoblast cell division, are muscle cells[320,660,661]. Muscle based PCGs store positional information, respond dynamically to tissue loss, and guide neoblasts during regeneration. Planarian muscle cells, like all excitable cells, are susceptible to external electrical stimuli to induce excitation. Interestingly, excitation of planarian muscle cells is dependent on Ca^{2+} flux and can be abrogated by various Ca^{2+} current blockers[491]. Not only is Ca^{2+} implicated as a large-scale determinant of tissue identity during regeneration[468–470], it is responsible for producing muscle cell depolarization ushering activity; the same muscle cells establishing PCG topography and guiding neoblast behavior during tissue renewal. Excitation-transcription coupling, a process exhibiting significant Ca^{2+} dependency, has been established in neurons[300,429,432,433] (whose activity regulates muscle), muscle cells themselves[288,289], and may play a role in the purposed changes in muscle-neoblast signaling within $pDCS^P$ planaria. Therefore, changes in the signaling paradigms and PCG distributions across these orthogonal muscle fibers, onset by $pDCS^P$, may dictate the unique behavior of dividing neoblasts observed in $pDCS^P$ planaria. Moreover, the diverse array of signaling muscle cell subsets (PCG specific groups), spanning the planarian AP axis, may respond differently to $pDCS^P$ producing unique tissue specific neoblast signaling modalities leading to planaria with unusual mitotic distributions across the AP axis. The diversity in neoblast signaling cascades demonstrated by orthogonal muscle fibers and repeated Ca^{2+} dependence creates the possibility of equally diverse mitotic responses in nearby neoblasts following excitation inducing stimuli such as $pDCS^P$.

Both the transcriptomic and bioelectric response to $pDCS^P$ may vary across tissues, explaining the drastic differences in mitotic activity across tissues and provide insight into mechanisms leading to mitotic redistribution within anterior most tissues. Key instances of known topographical diversity in planaria can be seen both bioelectrically and genetically in the form of tissue specific resting membrane potentials[331,585,586] and muscle based PCGs[320,321] respectively. Planarian PCGs are found in restricted patterns which is reminiscent of morphogen gradients established during embryonic development[662]. Several morphogens have been shown to regulate cellular mitosis[663–666]. In addition to known morphogen regulators of proliferation, pulsing DCS have also shown consistent influence in cell cycle dynamics and overall proliferation[13–15,654]. Moreover, pulsed DCS has shown time and again to influence expression profiles of various cell types[288,490,640,651,653,658,667] culminating in overall cell regulation. Thus, planarian PCGs may administer mechanisms similar to embryonic morphogen signaling with distinct regulatory patterns and thus regional neoblast regulation. Altogether, systemic exposure to $pDCS^P$ may influence endogenous bioelectric and genetic topography; influencing these cellular regulators leading to the observed changes in neoblast response and its apparent tissue specific restriction in neoblast activity. However, more experiments must be performed to

better address either stipulation and reach conclusive results about pDCS^{P} influence on both bioelectric and PCG topography.

7.3.3 pDCS^{P} morphogenic regulation of adult tissue form and cellular processes

Tissue remodeling is most evident when addressing morphological changes in non-regenerating planaria exposed to pDCS^{P}. Specifically, disruption of proper optic cup distance from the planarian optic chiasma leading to a lengthening of the optic nerve (Fig 20 B, F). This effect is accompanied by dramatic changes in brain shape. The appearance of the planarian brain resembles a shape of two concentric ellipses connected at their equator (Fig 20 B). Brain shape in planaria exposed to pDCS^{P} change dramatically, widening at the base of the brain and elongating its distal ganglia; adopting a broad flattened shape (Fig 20 B). These changes all occur in the small window of 6hrs pDCS^{P}; suggesting large scale rapid remodeling of differentiated cells composing form and function of the brain and photoreceptors. During embryonic development, signaling molecules known as morphogens create restricted expression gradients whose distinct patterns determine form of specific anatomical structures[662,668]. Morphogens have been shown to exhibit specific feedback mechanisms to create very unique and predictable patterns in the embryo[668]. Collectively, morphogen signaling is a complex process which ultimately leads to overall organismal development and morphogen interference can lead to predictable changes in various anatomical structures[662]. Over the course of morphogen signaling analysis many different mechanisms have been purposed to regulate and maintain various morphogen gradients (fundamental aspect of morphogen signaling are their distinct gradients); one of which is a mechanism governed by bioelectric regulation[337,338,669]. In planaria, even though no proteins have been specifically tested to fit the criteria of morphogens due to limitations in molecular tools, high levels of evolutionary conservation among known morphogen genes[326,328–330] as well as the discovery of distinct PCG patterns and their impact on tissue identity during regeneration[320,326,329,330,645] strongly suggests that these organisms display signaling mechanisms closely resembling morphogen signaling tasked with guiding tissue patterning.

Neural cells are excitable and thus have been shown to elicit a variety of responses to pulsing DCS procedures, morphological or otherwise. Pulsing DCS has been shown to stimulate nerves resulting in a variety of differing responses. In humans, *in-vivo* transcranial DCS has shown to enhance or reduce neural activity in a polarity specific manner[27,594,670]. In cultured neural cell lines, pulsing DCS has shown to direct neurite outgrowth while also enhancing neurite length[246,671,672], enhance neurotransmitter release and growth factor response[646,673], modulate neuroinflammation[22,674], enhance neural differentiation (neurogenesis)[19,638,675,676], and accelerate neural regeneration[22,22,606]. Neurogenesis is responsible for post-natal development and brain growth in growing organisms and adults[677]. The vast majority of planarian research is performed on adult organisms and studies neurogenesis in the context of regeneration following loss of head and brain tissue[678,679]. Nevertheless, our results demonstrate significant morphological changes in non-regenerating planarian brain tissue following pDCS^{P} (Fig 20 B), signifying interplay between pDCS^{P} and homeostatic neurogenesis and/or collective neuronal growth. Some studies investigate homeostatic regulation of neurogenesis in non-regenerating planaria. Interestingly, a regulatory neuronal network identified by the expression of neural transcription factors *smed-nkx2.2* and *smed-arx* were found to maintain unique populations of neural cells tasked with producing planarian *hedgehog*

(Hh) ligand[680]. In addition, it was discovered that *smed-Hh* is a crucial regulator of planarian neurogenesis[680]. Sonic hedgehog (SHH) signaling is a well-known morphogenic signaling cascade with distinct regulatory roles during embryonic development and proper pattern regulation[681]. In planaria, disruption of this neurogenic regulatory network led to decreased neurogenesis and maintenance of brain tissue[680]. Research has shown ion channel activity and subsequent increases in cellular ion currents (Ca^{2+}, K^{+}, etc) enhance SHH signaling resulting in increased protein levels[40,682,683]. Many of these ion fluxes can be stimulated through DCS^{P} in a voltage dependent manner. Moreover, some ion fluxes, conducted through ATP dependent ion channels, can be influenced by DCS^{P} as it is shown to modulate ATP/cAMP intracellular concentration[32,180,353,357,684]. The known regulatory role of SHH signaling during planarian neurogenesis and previously described DCS^{P} interaction with SHH signaling suggests $pDCS^{P}$ increases SHH signaling which in turn offsets planarian neurogenic homeostasis ultimately resulting in increased brain size (Fig 20 B). More experiments are required to secure $pDCS^{P}$ interaction with SHH signaling to see if $pDCS^{P}$ are in fact modifying planarian neurogenesis in a SHH dependent manner.

For new growing tissues to occupy space in adult organisms who are not experiencing growth, preexisting tissues must undergo large scale programmed cell death to create space for new growth. This holds true for changes in large scale tissue morphology which characteristically remodels preexisting tissue to give rise to new organ architectures[535]. Pulsing direct current stimulation has been documents to have varying effects on cells. In planaria, head regression is a hallmark of planarian health, typically occurring from widespread cell death[325,367,535]. This phenotype can be induced in a number of gene knockdown models as well as in planaria exposed to lethal or sublethal doses of γ-irradiation, all of which induce cell death[308,359,482,535,536]. Pulsing direct current stimulation has been used to effectively induce cell death in a number of models and cell types[14,539,540,654]. However, apoptosis inducing pulsed currents are generally several orders of magnitude more intense with significantly higher frequencies then what we chose for $pDCS^{P}$ [5hz, 0.9mA, 10V] (Fig 20). $pDCS^{P}$ induced apoptosis has yet to be addressed and as such it is unknown if cell death driven head regression occurs during $pDCS^{P}$. Additionally, this is one of the first instances of pulsed current stimulation in the planarian field and as such much is unknown in terms of the planarian specific responses to $pDCS^{P}$. Cell death in these planaria needs to be addressed as it may elude important information as to the dynamic effects $pDCS^{P}$ have on tissue remodeling and neoblast homeostasis in non-regenerating organisms.

7.3.4 Persistent $pDCS^{P}$ exposure to regenerating trunks reverses natural AP polarity at both the genetic and organismal level

Pulsing DCS has been used in therapeutic practices to enhance various forms of wound healing and regeneration. This form of stimulation has been shown to enhance repair of spinal cord injury[22,22,606,607], general nervous tissues[646,671], nonunion bone fractures[31,630,685], chronic ulcers[643,644,686], and more[620]. In the 1950s, applied DCSS were used to predictively modulate body axis polarity in the planaria, *Dugesia Tigrina*[585]. However, since these early experiments, applied currents and planarian regeneration have not been revisited, leaving a plethora of questions unanswered. To address this long-standing gap in fundamental knowledge of bioelectric regulation of large scale regeneration we used the *Schmidtea mediterranea*, a species with established genomic

and molecular tools, to understand how applied electric currents can be used to fundamentally regulate large scale tissue regeneration.

As anticipated, application of $pDCS^P$ can control regenerative outcome of amputated trunk fragment planaria with respect to their endogenous AP axis. Effects of $pDCS^P$ in recoding of the endogenous AP axis are observed as early as 6hrs following amputation and DCS^P application and persist throughout the course of regeneration (Fig 21 B, C). Change in endogenous expression of known planarian AP axis determinant genes demonstrated that $pDCS^P$ elicits its effects rapidly, controlling the most rapid endogenous anterior determinant *notum*[326,328] (Fig 21 B, C). This member of the planarian FGFRL-Wnt signaling pathway, *notum*, is an amputation induced gene that, using a positive feedback mechanism, enhances its expression in anteriorized amputations to inhibit the expression of known posterior identity gene *wnt-1*, remaining highly expressed in the anterior throughout regeneration, securing its identity[326,328]. Interestingly, it has been shown that planarian AP polarity can be modified bioelectrically using various approaches. Most recently it has been shown that induced cellular hyperpolarization by means of Ivermectin dosing causes regenerating trunks to become completely anteriorized (double headed)[586]. Additionally, this anteriorization of trunk fragments can be achieved with the drug Praziquantel which acts to induce Ca^{2+} influx in planaria[469]. Moreover, inhibition of planarian Ca_vs by either $Ca_v1\beta$ subunit RNAi or by nicardipine inhibition proved sufficient to attenuate the effects of Praziquantel anteriorization[468]. With the later discovery that a subset of muscle cells, whose activity is Ca^{2+} current dependent[491], are responsible for conferring patterning information during regeneration through known PCGs[320,321] solidifies the importance of Ca^{2+} flux and tissue specification during regeneration. Moreover, considerable Ca^{2+} membrane currents were measured upon muscle depolarization of only 50mV[491]. In our work we demonstrated we can achieve similar depolarization potentials in epithelial cells with magnitudes of 6mA $pDCS^P$ (Fig 19 B). As such, prolonged $pDCS^P$ exposure to 0.9mA magnitude currents throughout the course of regeneration is expected to modify the membrane depolarization dynamics likely enhancing Ca^{2+} flux by lowering the muscle activation threshold. Changes in muscle activity may influence PCG distribution changing overall neoblast signaling and subsequent tissue identity during regeneration which may ultimately lead to the rewiring of endogenous AP tissue specification during regeneration causing the observed AP reversal (Fig 21 D). This mechanism is supported by the rapid and persistent changes in *notum* gene expression in the induced by $pDCS^P$ (Fig 21 B, C). In addition to this, Ca^{2+} induced changes in regenerative tissue identity consistently induced the regeneration of an additional pharynx oriented to compliment the newly regenerated head[468]. Consistent with this emphasis on pharynx orientation, planaria exposed to $pDCS^P$ experiencing AP reversal also exhibited complete anatomical reversal of the preexisting pharynx to compliment the newly reversed $pDCS^P$ planaria (Fig 22 B). Together, these results suggest $pDCS^P$ influence orthogonal muscle activity to reprogram planarian neoblasts during regeneration through a Ca^{2+} dependent mechanism. However, more experiments are needed to adequately convey $pDCS^P$ influence on Ca^{2+} dynamics.

Limitations to the current body of work regarding $pDCS^P$ fall within the breadth of current results provided. Albeit, there are many speculative purposed mechanisms by which $pDCS^P$ may elicit its domain over neoblast behavior, namely Ca^{2+} kinetics and control over PCG signaling. To quell such gaps, experiments using fluorescent Ca^{2+}

indicators such as Fluo-4 AM can be used to measure both qualitative Ca^{2+} flux during $pDCS^P$ exposure revealing changes in cytosolic Ca^{2+} in various tissues systems. This work may provide insight into tissue types experiencing changes in Ca^{2+} flux during $pDCS^P$ (i.e. neural, muscular, epithelial, or intestinal) allowing us to further assess the role of these cells in neoblast regulation during $pDCS^P$. In addition to a fluorescent Ca^{2+} indicator, the role of Ca^{2+} can be addressed with the use of Ca^{2+} chelators to sequester changes in rapid cytosolic Ca^{2+} through local membrane flux (BAPTA-AM; NIC) and intracellular stores (EGTA-AM; thapsigargin). These Ca^{2+} signaling inhibition mechanisms are better suited for small windows of time as exposing the planaria to such Ca2+ signaling inhibitors over several days is likely to prove lethal. For this reason, both homeostatic and regenerative influence of $pDCS^P$ can be addressed in the context of the first 24hrs permitting the assessment mitosis, PCG topology, and overall CNS morphology as well as early regenerate identity markers such as *notum* and *wntP-1*. In addition to Ca2+ dynamics, evaluation of cell cycle progression during 6-hour $pDCS^P$ exposure to homeostatic planaria would provide insight into the various stages by which neoblasts are becoming either silenced or stimulated with respect to various tissue fractions. For example, FACS analysis of anterior most tissue fractions (above the photoreceptors) comparing both $pDCS^P$ and sham control planaria will compliment IHC clearly demonstrating how $pDCS^P$ promotes cellular mitosis within these tissues with the converse being true for the remainder of planarian tissue.

Implicating PCG signaling in both homeostatic and regenerative $pDCS^P$ phenotypes calls for in-situ hybridization to evaluate PCG patterning following treatment compared to sham control. Implementation of multi-fluorescent whole mount in-situ hybridization will display changes in PCG topology, if any, prompted by $pDCS^P$ exposure. Specific genes which exhibit sensitivity to $pDCS^P$ can be further investigated via RNAi knockdown to show their impact on $pDCS^P$-mediated phenotypes. Similar experiments can be performed during $pDCS^P$-mediated tissue polarity reversal during regeneration. Temporal changes in PCG topology can be evaluated via fluorescent in-situ at various stages of regenerative reversal. In addition to these experiments, RNA sequencing analysis of regenerative fractions exposed to $pDCS^P$ may reveal potential genetic regulators of PCG topological distribution and provide insight on how these molecular regulators and utilized via $pDCS^P$ to elicit change. Along with PCG signaling, $pDCS^P$ influence over SHH signaling can be addressed using approaches described previously. All in all, much work can be done to further evaluate neoblast regulation mediated through $pDCS^P$. However, this work provides clear merit for further exploration into the potential of $pDCS^P$ in regulating systemic neoblast behavior in the context of both homeostatic and regenerative functions.

CHAPTER EIGHT

CONCLUSION

Recapitulation of damaged cells and tissues is a challenging problem facing many patients undergoing harsh therapeutics targeting harmful cancer cells by means of chemotherapy. In addition to damaging chemotherapies, patients with cancerous melanomas caused by sustained exposure to damaging ultraviolet rays, people suffering from type 2 induced diabetic ulcers, and neurodegenerative diseases, all of which introduce significant DNA stress on healthy cells, characteristic features in numerous health complications. Bioelectric manipulation of cellular behavior has been studied extensively both *in-vitro* and ex vitro which have provided the field with exciting and ground-breaking discoveries. However, the conditions in which these studies are performed are far from comprehensive with respect to the complexity of an *in-vivo* micro-environment. To overcome challenges of *in-vivo* study in mammalian model organisms *we introduce a new novel model organism, Schmidtea mediterranea planaria, whose hardiness and significant evolutionary conservation make them exceptional organisms to address fundamental biological questions concerning bioelectric regulation, using various electrical modalities, at both the systemic and cellular level.* In addition, we provide new and effective techniques for immobilization, bioelectric quantification, and current administration in the planaria allowing us to administer various forms of electrical stimulation making these models useful in addressing bioelectric signaling in fundamentally unique contexts.

Here we illustrate the potential for applied low magnitude direct current stimulation to influence stem cell-specific transcription, reconstitution of stem cells within lethally irradiated tissues, and increased levels of active DNA repair all of which are exhibited *in-vivo* within the adult body using an approach that dissects these responses with organismal and cellular resolution. Moreover, many DCS responses are visible within astonishingly short intervals of application, highlighting the potency of this form of cellular manipulation. Although much work remains to unveil detailed mechanisms underlying our observed electric stimulation induced phenomena, **our data clearly illustrates pDCS$^{S/P}$ as proficient tools that can be used enhance DNA integrity within irradiated tissues, and exhibit domain over normal planarian regeneration through a FGFRL-Wnt-mediated mechanisms, likely downstream of planarian SHH signaling, collectively demonstrating the capacity for exogenous currents to override and recode neoblast behavior in a predictive manner. Additionally, we show evidence for bioelectric initiation of wound healing responses, in the form of mounted proliferative and genomic responses, in the absence of physical injury.** Altogether, these findings establish fundamental evidence for bioelectric regulation over various cellular processes which have potentially far reaching implications in regenerative medicine and other cell-based therapies.

The planarian model, with an abundance of pluripotent stem cells[325,358,365], recent advancements in molecular and genetic tools[317,687–689], comprehensive genome[690], evolutionarily conserved signaling mechanisms[329,330,481], and pliable tissue engraftment procedures[366,370,650,691] enables researchers to approach difficult biological questions from

unique, otherwise impossible, perspectives. Planaria are bioelectrically adept, using fundamentally conserved ion channels and transporters to establish diverse bioelectric tissue topographies[331,586], similar to those seen in vertebrates[8,13,589,692], that can be altered to influence normal physiological functions. Using the planaria, we found many powerful effects of applied $DCS^{S/P}$ on planarian neoblasts and differentiated tissues both during homeostatic tissue turnover and large-scale regeneration. These observed effects differ with changing physiological contexts. For example, *in-vivo* DCS^{S} within transplanted irradiated tissues effectively enhance neoblastic presence within distal irradiated tissues in as little as 15mins while simultaneously enhance endogenous DDR leading to increased DNA integrity within 60mins and increased cellular mitosis despite copious amounts of DNA DSBs prior to treatment. These DCS^{S}-mediated responses show clear sensitivity to L-type Ca_v activity illustrating the instructive role of Ca^{2+} signaling governing fundamental aspects of DCS^{S} responses within irradiated tissues. Interestingly, these data suggest novel mechanisms involving IEG transcription given both Ca^{2+} sensitivity, a known evolutionarily conserved IEG signaling mechanism, and the rapid temporal nature in which these mRNA expression changes are observed in the context of DNA damage and bioelectric signaling; results which may shed light on undiscovered connections between bioelectric induction of IEG transcription and DNA damage repair responses. Additionally, intact/homeostatic planaria subjected to DCS^{S} experience unique proliferative responses which are polarity dependent and appear to be superseded by similar neoblast specific responses observed at the mRNA level. It is abundantly clear that bioelectric signals conferred through DCS^{S} have the potential to enhance fundamental aspects of neoblast behavior regarding cellular mitosis, DNA damage repair, and newly observed rapid transcription; all of which occurs *in-vivo* in the adult organism.

Pulsed direct current stimulation was addressed in both the homeostatic and regenerating planaria. Firstly, we demonstrate the capacity to quantitatively measure tissue depolarization using fluorescent optics and the potentiometric dye, di-8-ANNEPS. This quantitative assessment of DCS^{P} tissue depolarization is the first quantitative evaluation of bioelectric stimulation in planaria to date. Moreover, using comparable pulsed stimulation currents we demonstrate their capacity to regulate neoblast behavior during both homeostatic and regenerative conditions. Specifically, 6 hour DCS^{P} application lead to distinct downregulation in neoblast proliferation while simultaneously stimulating robust mitosis within distinct anterior tissues which, under normal conditions, do not experience active proliferation[365,576]. We believe these responses may be mediated through Ca^{2+} signaling as DCS^{P}-mediated epithelial depolarization was attenuated through inhibition of planarian L-type Ca_vs. Interestingly, DCS^{P} exposure significantly impacted native tissue morphology of the planarian CNS in intact planaria suggesting the signaling mechanisms governing changes in neoblastic behavior are concurrently influencing native morphology of organ structures containing excitable cells (i.e. neurons in the CNS). These observed changes may be attributed to the notion that DCS^{P}-mediated Ca^{2+} signaling has broader implications in excitable tissues like muscle and nervous tissue. Moreover, DCS^{P} had overriding effects on planarian tissue regeneration resulting in consistent AP reversal at throughout regeneration. AP reversal through $pDCS^{P}$ was observed within 6hrs of exposure indicated by the clear reversal of known anterior genetic identity marker *notum*[326,328] heralding the formation of a posturized head and anteriorized tail. It has been shown that planarian L-type Ca_v activity/flux regulates neurogenesis, tissue specification along the AP axis[468–470], and body wall muscle excitation-contraction initiation[491]. With the discover that planarian orthogonal muscles fibers are tasked with neoblast regulation via PCG signaling[320,321] we purpose these same mechanisms are being hijacked during

pDCS^{P} culminating in many of these observed responses. Thus, DCS-mediated Ca^{2+} signaling mechanisms are likely to be responsible for observed morphological changes in intact and non-regenerating planaria subjected to DCS^{P}.

DCS has become a growing therapeutic technique to treat a number of human conditions. However, these devices have been more recently designed and marketed for use at home without medical supervision, as solutions for things such as improved mental focus, concentration, increased endurance, improved gaming, enhanced muscle growth, depression, anxiety, and many more. The vast array of purposed benefits marketed affect a broad spectrum of individuals making the market for such devices far reaching. Since these devices have hit the market, there has been an increasing number of people who create *"do it yourself"* DCS devices in which they use freely and frequently[693]. Here we provide robust techniques using a novel model organism, with highly conserved signaling mechanisms, to study the intricacies of DCS exposure to tissues, in-vivo, in the context of the adult organism. As we have demonstrated, various types of DCS have unique significant effects at both the cellular and organismal level with different forms of DCS garnering novel cellular responses. It is for these reasons that work such as this is important in progressing the understanding of electrical regulation over essential cellular processes. Addressing gaps in our understanding of the mechanistic underpinnings of DCS inducing cellular behavior is vital to both educate the consumer in the accurate benefits and risks when partaking in such procedures and drive research in developing powerful and effective tools to treat challenging human disabilities.

CHAPTER NINE

METHODS

Planarian Tissue Transplantation

Transplantation Tool Fabrication

In order to transplant tissue from one planaria to another, a cylindrical tool was fabricated to cut precise disks from the planaria body to be removed and replaced between donor and host planaria. Transplantation tools were fabricated from 19-18$\frac{1}{2}$ gauge syringe that was bored out to an inner diameter of 750µm using a dremel drill bit. The outer diameter was polished using 500-1000grit wet sand paper until the edges were paper thin and smooth to reduce friction during transplantation procedures. Using this procedure, a variety of transplantation tools were fabricated with sizes ranging from 600-850µm ID. Transplantation tools fabricated in this way last years and can be cleaned in boiling water or 10% NAC to remove mucous buildup around the tools edge. For smaller tool sizes (<700µm) 20 gauge syringes were used. Syringe column was clipped and placed directly into the Dremel bit for high speed sanding and boring throughout the production of the transplantation tools. When the desired size and edge thickness was reached, the Dremel was used to carefully remove the polished section of the syringe allowing for ~2mm of cylindrical space from tip to base.

Planarian Transplantation

Planaria were transplanted as described in Guedelhoefer OC 4th et al. 2012[366] with modification to the transplantation tool used to generate tissue sections. Briefly, large planaria (8-12mm) were selected for transplantation. Host planaria were first lethally irradiated with 6Krads (γ-irradiation) 6-24hrs prior to transplantation. Donor planaria, of comparable size, where chosen from colonies of planaria that had been starved for a minimum of 4 days. Both donor and host planaria were anesthetized using chilled 0.2% chloretone. Once anesthetized, planaria were placed atop damp, chilled black Whatman filter paper for complete immobilization. Tissue sections were then cut from both host and donor planaria (700µm and 800µm respectively), host tissue sections were discarded and replaced with donor tissue sections. Forceps were used to lift the Whatman filter paper to transfer the transplanted planaria to a holtfreters hydrated petri dish. Transplanted planaria were then encapsulated in damp hemp paper and further surrounded with a combination of Whatman paper and folded Kim Wipes. Transplanted planaria were given 18Hrs at 10°C to allow proper tissue grafting. Successfully transplanted planaria were then transferred to petri dishes filled with pH_2O. After 1Hr all Whatman paper was removed from pH_2O dishes and planaria were placed at 16°C until they were utilized for experiments.

Planarian Immobilization

Planarian Immobilization for Electrode Penetration

Planaria were immobilized to perform experiments in which microelectrodes were used to penetrate and deliver current through planarian tissue. Large planaria were first anesthetized by soaking in chilled 0.2% chloretone (Sigma 112054) for 5 minutes. Once sedated, planaria were rinsed with chilled planaria water and then laid out atop a glass slide. Residual planarian water was removed from the relaxed planaria and then the planaria were submersed in 1.0-1.5% low melting point agarose (dissolved in pH_2O) (Sigma A9414). Once the agarose solidified it was trimmed closely around the relaxed planaria forming a tight-fitting agar box. Trimmed agar planaria were then placed ventral side up into 35mm petri dishes, pre-filled halfway with solidified 1.0% agarose (dissolved in pH_2O) (Sigma A9539). 1.0% agarose (at 37°C) was used to surround the LMP agar box, without covering its top, securing it in the center of the petri dish. Fresh planarian water was used to fill the remaining volume of the dish.

Planarian Immobilization for Pulsing Electric Field Chambers

Pulsing EF experiments were performed primarily on small planaria ranging from 3-4mm in length. Pulsing EF experiments, in some instances, required several day long durations and therefore effective planarian immobilization was paramount. Similar to immobilization of large planaria, pulsing EF planaria were first anesthetized in 0.2% chloretone for 3minutes (or until pharynx was relaxed and visible). Anesthetized planaria were then transferred to their respective channels using a 10µL tip that had to be cut back to properly fit the planaria. Once transferred, the planaria were rinsed with pH2O to remove any residual chloretone, placed parallel with respect to the channel, and then covered with 7-12µL of 1.5% LMP agarose. Quickly, precut glass coverslips were pressed onto the still gelatinous agar creating a flush level surface over the planaria. Small ice shavings were then placed on the glass coverslip to rapidly cool and solidify the agar. Once solidified, a small razor was used to trim agar away from the glass coverslip. 5µL of chilled pH_2O was then placed at each end of the glass coverslip. The glass coverslip was then carefully removed, using microdissection forceps, exposing the agar encapsulated planaria. A small ~500µm channel was then cut on the left side of the planaria to allow adequate water flow through the agar section of the channel. Vacuum grease was then spread across the sylgar wall on either side, just underneath the portion covered by the glass coverslip. A small droplet (~3µL) of pH_2O was placed on top of the encapsulated planaria then the glass coverslip was cleaned with optical microfilament cleaning cloth. The cleaned coverslip was then gently pressed atop the encapsulated planaria, being careful to not introduce any air, creating sealed edges atop the vacuum grease.

Planarian Chamber Fabrication

Planarian EF chambers were fabricated using primarily Sylgard 184 (Sigma 761036). To create the mold for the sylgard 184, corning glass coverslips (Sigma CLS285022) were cut using a diamond tip pen to 2mm x 22mm x 0.1mm and then glued to a larger glass slide 3mm apart parallel to one another. Another layer of cut glass coverslips were added on top of the previously glued slips making a final thickness of ~0.2mm thick canals (clear nail polish was used as a glue). Glass slides were placed upright around the center of the channels forming a box and secured with epoxy. Sylgard 184 was mixed (10:1), clarified

via centrifugation at 5000rpm for 1min, and poured into the fabrication chamber and baked the following day at 100°C for 45min. Prior to baking, the sylgard 184 was further clarified within a desiccator for 10-45min to ensure no air was trapped within the mold. Once the sylgard 184 solidified within the mold, its perimeter was cut using a blade and the sylgard chamber was gently removed using forceps, being sure to not puncture or tear the planarian channels.

A 35mm petri dish was prepared with a thin layer of sylgard 184 at its base, the solidified sylgard chamber was then carefully placed atop the liquid sylgard layer as to not introduce any bubbles. The sylgard petri dish was then backed for 45minutes at 80°C until sylgard solidified, securing the newly fabricated sylgard chamber at its center. Glass coverslips were then cut to the proper length and width, inserted within the sylgard base using razor cut slits, and placed perpendicularly at either end of the sylgard rectangle in order to create electrically isolated wells. Epoxy was then used to permanently secure the glass coverslips at either end of the sylgard rectangle.

Planarian EF chambers included specially designed lids to facilitate pH_2O flow/suction as well as exogenous EF quantification. Within the lid, two 1mm diameter Ag/AgCl electrodes were fixed 20mm apart to measure the magnitude of the applied EF. Two 1.2mm glass capillaries were passed through (~2mm) and fixed at either end of the lid to allow for pH_2O flow/suction. Hydration was maintained through 2mm O.D. polycarbonate tubing allowing for the constant flow/suction of pH_2O at opposing ends of the EF chamber. Flow rate was restricted prior to capillary junction while suction rate was dependent on well volume. Ag/AgCl electrodes were electrically coupled to a digital recording device (National Instruments USB-6210) which delivered real-time potential measurements via LabView 2017 software.

Administration of $pDCS^{P/S}$

Current Injection for Transplanted Planaria

Large planaria were first immobilized as described for electrode penetration. Once immobilization was achieved, the electrodes and current delivering tools were prepared. Borosilicate (Drummond #3-000-203-G/X) electrodes were pulled using a Sutter P-97 electrode puller. Microelectrode, once pulled, had thin 20mm tips that were cut back 3mm to slightly enlarge the electrode outlet. Microelectrodes were then filled with 3M KCl and connected to 2mm diameter, 15cm long polycarbonate tubing filled with 3% 3M KCl agar. These agar bridges were connected to 3M baths where Ag/AgCl electrodes supplied current to the system. Circuit current was clamped with a 100MΩ resistor.

Immobilized planaria were then placed at the center of the microscope field of view in a specially fabricated holding station for 35mm petri dishes. The petri dish was then cooled, underneath, with a thermo-electric cooler; reaching temperatures between 8 and 11°C. Chilled, immobilized planaria, and were then penetrated ventrally, with positive and negative electrified microelectrodes, at both post- and pre-pharyngeal areas. Once the planaria was properly penetrated with each electrode, current was established to 7µA-10µA generating an internal EF across the planarian body.

Localized Triton Application

Triton Application to Planarian Epithelia

Triton X-100 was diluted in planarian water (pH_2O_{tx}) to a concentration of 1.0% and locally administered to dorsal planarian epithelial tissue. Precise exposure to pH_2O_{tx} was achieved through capillary tissue suction. Glass capillaries (Drummond #3-000-203-G/X) were flame polished at their ends, filled with mineral oil, and attached to a micro-manipulator injection apparatus. Once proper capillary attachment was achieved, pH_2O_{tx} was loaded into capillaries via suction. Planaria were then placed dorsal side up, atop chilled black Whatman paper (Sigma WHA1001325), and all excess planaria water was removed using a KimWipe. Using the injection tool, air was removed from the tip of the loaded capillary while maintaining an upward facing liquid meniscus; at this point the outlet of the loaded capillary was carefully placed onto the pre- or post-pharyngeal epithelia of the planaria and 3 sequential suction actions were performed gently pulling the desired tissue into the polished capillary inlet. The tissue was given 5-10 seconds of contact with the pH_2O_{tx} until the suction was removed and the tissue released from the capillary inlet. Following pH_2O_{tx} exposure, planaria were quickly rinsed 2x with pH_2O and placed back into clean 35mm petri dishes.

Planarian Fixations Methods

Methacarn Fixation

Methacarn Fixation was used primarily for large (>8mm), intact or transplanted, planaria destined for whole mount in-situ hybridization as previously described[694]. First, 0.66M $MgCl_2$ was used to relax planaria (20s) followed by 1xPBS dilution to 0.25M $MgCl_2$ until planaria bodies settled to bottom of vial (20s). Planarian mucous was removed using 10% NAC in 1xPBS for 8 minutes at room temperature. NAC solution was replaced with methacarn solution (6:3:1 methanol, chloroform, acetic acid) for 30 minutes on ice with gentle agitation. Methacarn solution was replaced with 100% methanol for 30 minutes. Fresh methanol was added to vials and sampled were placed at -20°C for minimum of 1hr or stored for long-term. Planarian samples were then placed in bleaching solution (5% Formamide, 1.2% H_2O_2, and 0.5% Triton X-100 in 1xPBS) overnight.

Formamide Fixation

Formamide fixation was used for IHC of large planaria (>8mm) as described previously[366]. Planarian mucous was removed using 5.7% HCl on ice for 8min. HCl solution was washed 3x with 1xPBS and then formamide fixative was added to vials for 20 minutes at room temperature. Fixative is then replaced with bleaching solution (6% H_2O_2, 0.5%Triton X-100 in 1xPBS) overnight, under light, at room temperature.

Carnoys Fixation

Carnoys fixation was used to prepare small planaria for IHC (<5mm) and was performed as described in previous work[574,694,695]. Planarian mucous was removed using 5.7% HCl on ice for 8min. HCL solution was then replaced with fixative (6:3:1 ethanol, chloroform, acetic acid) for 2hrs on ice with gentle agitation. Fixative was discarded, and fresh methanol was added to vials and sampled were placed at -20°C for minimum of 1hr or

stored for long-term. Samples were removed from -20°C and allowed to reach room temperature before bleaching solution was added to the vials. Once equilibrated, methanol was replaced with bleaching solution (6% H_2O_2 in methanol) overnight, under light, at room temperature.

NAC Fixation

Traditional NAC fixation was used for preparation of small planaria for whole mount in-situ hybridization (WISH). Planarian mucous was removed using 5% NAC in 1xPBS for 5-7 minutes at room temperature. NAC solution was replaced with 4% formalin solution (4% formaldehyde, 0.1%Triton X-100 in 1XPBS) for 15-20 minutes at room temperature. Following formalin fixing, samples were washed with 1XPBS and then placed in preheated reduction solution (50mM DTT, 1% NP-40, 0.5% SDS, in 1XPBS) for 5-10min at 37°C. Following reduction, samples were rinsed 1x with PBSTx and then dehydrated to 100% methanol using serial dilutions of methanol:PBS from 50%-100% methanol. Fresh methanol was added to each sample and samples were placed at -20°C for minimum of 1hr or stored for long-term. Samples were then brought to room temperature and placed in bleaching solution (6% H_2O_2 in methanol) overnight, under light, at room temperature.

Planarian Tissue Cryosectioning

Planaria are fixed using either carnoys, formaldehyde, or NAC fixation techniques depending on the desired signal. As described in 2014 Forsthoefel et al. fixed planaria are gently hydrated by immersion in increasing concentrations of sucrose:PBS; 1XPBS is replaced with 10% sucrose:PBS for 1 hour and then 30% sucrose:PBS overnight at 4°C. Planaria are then placed in tissue imbedding molds, the 30% sucrose is removed and replaced with optimal cutting temperature (OCT) medium. Planaria are then situated to the desired position/orientation within the OCT and molds are quickly placed at -80°C. Once frozen, samples were ejected from their imbedding molds and mounted onto lieca cutting fixtures using excess OCT to effectively ‘glue’ each sample to a cutting fixture. The prepared fixtures were then mounted into the lieca machine where 15µm samples were cut and placed atop fisherbrand superfrost plus microscope slides (Cat # 22-037-246). Once the microscope slide was full of cut tissue sections the slide was either placed back into the -80˚C to be stored for long periods of time or prepared for immunostaining/in-situ hybridization.

Planarian cultivation

Planarian cultivation was performed as previously described[575], with slight modification. Planaria are raised in large Ziploc Tupperware containers housed in temperature regulated incubators devoid of light. Planaria cultivated at 16°C and 10°C, similar to our 20°C planaria, are fed once a week on a designated day/time with organic bovine liver devoid of connective tissue. Planarian containers are cleaned twice a week, once when fed and again two days after feeding. During cleaning planaria are forced to a designated corner of the container, pH_2O is removed from the container, and the containers surface is wiped down with untreated paper towels to remove all mucous from the containers surface.

Planarian destined for tissue transplantation were cultivated in a unique manner. Transplantation requires planaria to be large enough across to harbor a circular transplant 700µm in diameter. Along with the size restraint, transplanted planaria had to be conditioned to withstand lower temperatures of 10°C for extended periods of time to facilitate transplantation processes. Thus, large planaria, ranging between 5-15mm, were selected from the normal culture conditions (20°C) and placed at 16°C culture incubators for 2 or more weeks. Once they had spent a minimum of two weeks at 16°C planaria containers were fed liver and transferred to 10°C incubators. Planaria that were recently transferred had to be watched closely for the first week as they would quickly regurgitate their food and became increasingly susceptible to stress and illness. However, if planaria were not fed before being transferred to 10°C they seemed to be at even higher risk to illness and death at these lower temperatures. It took at least 1.5 weeks for planaria to acclimate to 10°C and resume normal feeding behavior. It is important to note that planaria cultured at 10°C exhibit a dramatic reduction in locomotion, a necessary trait for transplantation, which subsides once they are returned to 20°C pH_2O. All other planaria used in experiments were cultivated using our standard planarian culturing methods (). Size of planaria used in experiments varied greatly for reasons unique to each experimental procedure.

Molecular Fluorescent Tools

Planarian Immunostaining

Immunohistochemistry (IHC) was performed primarily for visualization of H3P, VC1, and Synapsin antibodies. Standard tyramide signal amplification (TSA) reactions were performed for all IHC staining as described previously[694,695]. Primary antibodies H3P (1:500), VC1 (1:800), and Synapsin (1:1000) were incubated overnight. All secondary antibodies, conjugated horse radish peroxidase (HRP), were incubated overnight. Prior to primary and secondary antibody incubation, planarian samples were blocked for 2-4hrs (1.0% bovine serum albumin (BSA) in 1XPBS; 0.3% triton X-100) at room temperature. Tyramide substrate was diluted 1:1000 Fluorescein or 1:2000 Rhodamine in PBSTI (0.1M Imidazole, 0.3% Triton X-100, 1xPBS) and used for TSA reaction. TSA reaction was activated using 0.0015% H_2O_2 PBSTI for 45min at room temperature followed by 10min quenching in 2% H_2O_2 PBSTI. Samples were then washed, mounted on glass slides, and imaged with a Nikon AZ-100 upright fluorescent microscope. Larger planaria required more washing to remove non-specific signal. Cell quantification was done using NIH ImageJ cell counter plugin and all data analysis was performed in GraphPad Prism.

Planarian Whole Mount In-Situ hybridization

The procedure for whole mount in-situ hybridization of planaria utilized in this body of work was developed by Pearson et al. 2009[687]. However, in-situ hybridization for larger planaria (< 5mm) slightly deviated from the standard in-situ procedure in several critical ways. Larger planaria were fixed and bleached using the methacarn based fixation technique described previously. After fixation, sample preparation for hybridization (day 1 of in-situ hybridization) was modified to suite larger planaria. Proteinase K treatment was administered for 10min however, concentration was doubled from 1µg/mL to 2µg/mL for larger planaria. Hybridization was performed at 56˚C and allotted a full 18hrs to ensure thorough hybridization. The remainder of the in-situ protocol was not modified in any way.

In general, larger samples were treated with 100% ethanol to remove background created by extended periods of development with the NBT development buffer as larger planaria required much longer developing times. All samples were imaged on a Nikon AZ-100 multizoom upright microscope equipped with NIS Elements AR 3.2 software for imaging.

Planarian Fluorescent In-Situ hybridization

Fluorescent in-situ hybridization (FISH) done in this work followed previously established techniques described previously in King et al. 2013[688]. No modification was made to the protocol as animal size was restricted to <5mm. FISH on larger animals was possible however, portions of tissue displayed undesirable low resolution and noise and for those reasons WISH was primarily used for larger planaria.

Whole mount Immunostaining

Immunostaining techniques used for this work were based on techniques performed in Peiris et al. 2012[574] and Guedelhoefer OC 4th et al. 2012[366] for larger planaria. Planarian immunostaining and fixation procedures differed depending on the size of the planaria being assessed. Small planaria (<4mm) were fixed and bleached using the standard carnoys fixation protocol and then placed at -20˚C until immunostaining was to take place. Immunostaining for small planaria was as follows; samples were removed from -20˚C and given 15 minutes to return to room temperature. Using a methanol:PBSTx gradient (75%, 50%, 25%, 0% MeOH), planaria were rehydrated and subsequently blocked in PBSTB (1xPBS, 0.3%Tx, 0.25% BSA) for 4hrs prior to primary antibody incubation. Blocking solution was removed and replaced with primary antibody solution and given 12-16hrs to incubate. In this study, the primary antibodies were diluted with PBSTB at concentrations appropriate for each antibody (1:500 H3P-rabbit: Millipore, 05-817R, 1:250 activated caspase3-rabbit: Abcam, ab13847, 1:250 Rad51-mouse: Abcam, ab109107, 1:250 VC1-mouse: Developmental Studies Hybridoma Bank, 1:800 Synapsin-mouse: Developmental Studies Hybridoma Bank). Primary antibodies were retrieved from samples to be reused in future experiments. Washes with PBSTx (1xPBS, 0.3%Tx) were performed for 3hrs/20min each along with 1hr of 20min washes with blocking solution. Once washes were complete, secondary antibody was placed with each sample and given 12-16hrs to incubate. Secondary antibodies were conjugated with horse radish peroxidase (HRP) to perform standard tyramide signal amplification (TSA) reaction, concentrations were (1:500 for anti-rabbit HRP: Millipore, 12-348 and 1:500 for anti-mouse HRP: Millipore, 12-349). Secondary antibodies were retrieved for use with future experiments. Secondary antibody was washed with 4hrs/20min washes followed by TSA reaction with either tyramide-NHS rhodamine or tyramide-FITC.

Planarian immunostaining with large animals (<4mm) was different than immunostaining with small planaria in several ways. Large planaria were fixed and bleached using the formamide based fixation technique and were therefore never dehydrated with methanol nor stored for extended periods of time. If storage was necessary, planaria were placed in 1xPBS at 4˚C for up to 2 weeks. Blocking solution (1xPBS, 0.05%Tx, 1%BSA) and PBSTx (1xPBS, 0.05%Tx) was modified for large planaria. Following fixation and bleaching, planaria were washed 3X with PBSTx and then placed in blocking solution for 4hrs. The remainder of the procedure mirrored that of which was used for small planaria completely.

All samples were imaged on a Nikon AZ-100 multizoom upright microscope equipped with NIS Elements AR 3.2 software for imaging.

Cryosection Immunostaining

Sectioned slides were retrieved from -80˚C and given 1hr to acclimate to room temperature and dry. Samples were then placed in specially fabricated slide chambers, designed for frequent solution exchange, and were rehydrated with 1xPBS for 5 minutes. PBS was then replaced with blocking solution (1xPBS 0.05%Tx, 1%BSA) for 1hr. After blocking was complete, slides were removed from these wash chambers, placed sample side up atop a dry kim wipe, and transferred to a specially designed humidified chamber for antibody incubation. These humidity chambers were made from old tip boxes in which damp paper towels were placed at the base, underneath the perforated tip holding layer while the slides rest atop the perforated tip holding layer. The lid of these humidity chambers was painted black as to minimize light exposure. Once slides were placed within the humidity chambers, 15-20µL of antibody was administered at the top of the slide. Parafilm, cut to the exact size of tissue containing area, was gently laid atop the sample slide, starting where the antibody was placed to ensure not air was introduced during the laying of the parafilm. With this technique, very little antibody was needed to address many samples at a time. Once the humidity chamber was at capacity, the lid was closed and sealed with masking tape. Primary antibody incubation was done for 2hrs at room temperature or overnight at 4˚C. Following incubation, parafilm was gently lifted with dissection tweezers and primary antibody was retrieved and placed into a fresh 1.5mL Eppendorf tube for later use. Slides were then quickly placed back into washing chambers, filled with PBSTx, and washed 3x 15min with PBSTx and 3x 15min with PBSTB. Secondary antibody was administered, incubated, and retrieved as described previously. Secondary antibody was washed 6x 15min with PBSTx. Standard TSA reaction was performed within the washing chambers. Following TSA, samples were washed another 3x 15min with PBSTx and then incubated for 30min with DAPI diluted 1:1000 in 1xPBS. DAPI solution was then washed away with 3x15min 1xPBS washes. Slides were then mounted using ProLong Gold Antifade Mountant (Cat# P36930 ThermoFisher). All samples were imaged on a Nikon AZ-100 multizoom upright microscope equipped with NIS Elements AR 3.2 software for imaging.

Immunostaining and Fixation of dissociated planarian cells

Planarian tail portions were separated and homogenized following EF application. Homogenate was suspended in calcium and magnesium free media (CMF) and placed on ice. Cell density was quantified using glass hemocytometer and cells were plated at 1mill/cm^2 onto glass coverslips. Cells were given 1hour to adhere to the surface and were then fixed with Carnoys solution for 2hrs on ice. IHC was performed according to Peiris et al. 2016[481] specifically labeling Rad51 (Cat#) and γH2AX (Cat#).

RNA Extraction

Extracting the RNA from planarian cells is done with a well-established protocol[696]. First, planarian tissue of interest is diced with a razor and placed into a 1.5mL Eppendorf tube with as little planarian water as possible. Then, 1mL of trizol is added to the tube and allowed several minutes to sit on ice. Samples are then placed in the -80˚C to freeze until

extraction is to take place. Samples set for extraction are retrieved from the -80˚C and then are homogenized using either a standard upright homogenizer or tissue is homogenized by vigorous vortexing for 30-60 seconds until there is no trace of planarian tissue within the tube. Once the sample has been homogenized, 266.6µL of chloroform is added to each sample, vortexed, and then allowed to sit for 3 minutes at room temperature. Samples are then spun down at 5000G at 4˚C for 15 minutes to allow for separation of digested RNA and trizol. Once centrifugation is complete, each sample should have 2 distinct layers, the colorless top layer is retrieved and placed in a fresh 1.5mL Eppendorf tube; the pink trizol layer is discarded along with its corresponding tube. 666µL of isopropanol is then added and then samples are inverted for 10-20seconds for mixing. Samples are given 10 minutes to rest at room temperature and then spun down at 5000G for 15 minutes at 4˚C. RNA is in the pellet form as a black pellet at the bottom of each Eppendorf tube. The supernatant is decanted, being careful not to disturb the pellet; then 1mL of chilled 75% ethanol is added. Samples are then spun down again at 5000G for 5 minutes. The ethanol step is repeated once again and then all the ethanol is carefully removed (this may require further centrifugation with a benchtop centrifuge). The RNA pellet is then dissolved in 15µL of nuclease free water on ice. Extracted RNA is then assed for purity and concentration using a Nanodrop.

Riboprobe Synthesis

Riboprobes were synthesized using T3 and T7 polymerase along with digoxigenin-labeled ribonucleotides mix or fluorescein ribonucleotide labeling mix. Synthesis of riboprobes was done against specific PCR templates of desired gene targets as previously described in Reddien et al. 2005[363] and Peiris et al. 2012[574].

Planarian RNAi Experiments

RNAi was carried out via dsRNA micro-injection as described previously[363]. *Smed-piwi-1* RNAi consisted of 3 consecutive injection days. Injections were administered to the pre-pharyngeal regions and, due to the size of the planaria (8-12mm), each planaria was given 6-8 pulses of dsRNA 37nL each. Following 3 consecutive injections, dsRNA was injected once a week to maintain RNAi efficiency. Due to the size constraint for planarian transplantation, injected planaria were fed liver once a week to maintain appropriate transplantation size.

dsRNA synthesis

Asexual S. mediterranea RNA was extracted from homogenate and used to create cDNA using the Thermo Scientific VERSO cDNA synthesis kit (cat#). The gene of interest was then targeted using attB flanking primers and subsequently cloned into pPR244 vector using BP Clonase II kit. The pPR244 vector was then transformed into NEB5a bacteria and later into HT115 bacteria. Glycerol stocks were made for each gene using a 1:1 dilution of glycerol and cultured bacteria and stored at -80°C. Ligated vectors were then isolated using MiniPrep kit (cat#). Isolated vectors were diluted 1:10 and used to generate gene PCR products using T3 T7 primers. dsRNA for injection was produced as described in Oviedo et al. 2008[575].

Quantitative Real Time PCR

Quantitative real-time PCR was performed as described previously[481]. The ubiquitously expressed gene H.55.12e was used as a control. Experiments were conducted with triplicates for each condition. Each qPCR experiment was conducted independently at least two times. For EF and non-EF transplanted planaria, RNA was exclusively extracted from the post-pharyngeal tail region (n > 4 per condition). RNA from EF and non-EF Intact planarian was extracted from both the whole planaria or from the sagittal and midline tissues independently. Extracted RNA was then converted to cDNA using the Verso cDNA synthesis kit. Gene expression is expressed in fold change in comparison to the control, normalized against the H.55.12e control gene.

Flow cytometry

FACS analysis was performed as previously described in Peiris et al. 2016[481]

Comet Assay

Comet assay was performed as previously described in Peiris et al. 2016[481].

Statistical analysis

All data is presented as mean ± SEM (Standard error of the margin) or foldchange ± SEM. Statistical analysis of all quantitative data presented was performed with GraphPad Prism 6.0 (www.graphpad.com/scientific-software/prism/).

References

1. Nuccitelli, R. Endogenous electric fields in embryos during development, regeneration and wound healing. *Radiat. Prot. Dosimetry* 106, 375–383 (2003).
2. Tosti, E., Boni, R. & Gallo, A. Ion currents in embryo development: Ion Current in Embryo. *Birth Defects Res. Part C Embryo Today Rev.* 108, 6–18 (2016).
3. Zhao, M. Electrical fields in wound healing—An overriding signal that directs cell migration. *Semin. Cell Dev. Biol.* 20, 674–682 (2009).
4. Nuccitelli, R. A role for endogenous electric fields in wound healing. 58, 1–26 (2003).
5. Jaffe, L. F. & Vanable, J. W. Electric fields and wound healing. *Clin. Dermatol.* 2, 34–44 (1984).
6. Levin, M. Molecular bioelectricity: how endogenous voltage potentials control cell behavior and instruct pattern regulation in vivo. *Mol. Biol. Cell* 25, 3835–3850 (2014).
7. Wang, E. & Zhao, M. Regulation of tissue repair and regeneration by electric fields. *Chin. J. Traumatol. Zhonghua Chuang Shang Za Zhi Chin. Med. Assoc.* 13, 55–61 (2010).
8. Levin, M. Endogenous bioelectrical networks store non-genetic patterning information during development and regeneration: Bioelectric networks as epi-genetic controls of growth and form. *J. Physiol.* 592, 2295–2305 (2014).
9. Hormuzdi, S. G., Filippov, M. A., Mitropoulou, G., Monyer, H. & Bruzzone, R. Electrical synapses: a dynamic signaling system that shapes the activity of neuronal networks. *Biochim. Biophys. Acta BBA - Biomembr.* 1662, 113–137 (2004).
10. Khan, T., Myklebust, J., Swiontek, T., Sayers, S. & Dauzvardis, M. Electrical field distribution within the injured cat spinal cord: injury potentials and field distribution. *J. Neurotrauma* 11, 699–710 (1994).
11. Jenkins, L. S., Duerstock, B. S. & Borgens, R. B. Reduction of the Current of Injury Leaving the Amputation Inhibits Limb Regeneration in the Red Spotted Newt. *Dev. Biol.* 178, 251–262 (1996).
12. Sundelacruz, S., Levin, M. & Kaplan, D. L. Role of membrane potential in the regulation of cell proliferation and differentiation. *Stem Cell Rev.* 5, 231–246 (2009).
13. Blackiston, D. J., McLaughlin, K. A. & Levin, M. Bioelectric controls of cell proliferation: Ion channels, membrane voltage and the cell cycle. *Cell Cycle* 8, 3527–3536 (2009).
14. Kim, E. H. *et al.* Biological effect of an alternating electric field on cell proliferation and synergistic antimitotic effect in combination with ionizing radiation. *Oncotarget* 7, 62267–62279 (2016).
15. Fitzsimmons, R. J., Strong, D. D., Mohan, S. & Baylink, D. J. Low-amplitude, low-frequency electric field-stimulated bone cell proliferation may in part be mediated by increased IGF-II release. *J. Cell. Physiol.* 150, 84–89 (1992).
16. Stump, R. F. & Robinson, K. R. Xenopus neural crest cell migration in an applied electrical field. *J. Cell Biol.* 97, 1226–1233 (1983).
17. Lin, B. *et al.* Lipid rafts sense and direct electric field-induced migration. *Proc. Natl. Acad. Sci.* 114, 8568–8573 (2017).
18. Zhang, J. *et al.* Electrically guiding migration of human induced pluripotent stem cells. *Stem Cell Rev.* 7, 987–996 (2011).

19. Thrivikraman, G., Madras, G. & Basu, B. Electrically driven intracellular and extracellular nanomanipulators evoke neurogenic/cardiomyogenic differentiation in human mesenchymal stem cells. *Biomaterials* 77, 26–43 (2016).
20. Zhao, H., Steiger, A., Nohner, M. & Ye, H. Specific Intensity Direct Current (DC) Electric Field Improves Neural Stem Cell Migration and Enhances Differentiation towards βIII-Tubulin+ Neurons. *PLOS ONE* 10, e0129625 (2015).
21. Vines, S. H. *Lectures on the Physiology of Plants*. (WENTWORTH Press, 2016).
22. Ross, C. L., Syed, I., Smith, T. L. & Harrison, B. S. The regenerative effects of electromagnetic field on spinal cord injury. *Electromagn. Biol. Med.* 1–14 (2016). doi:10.3109/15368378.2016.1160408
23. Wallace, M. C., Tator, C. H. & Piper, I. Recovery of spinal cord function induced by direct current stimulation of the injured rat spinal cord. *Neurosurgery* 20, 878–884 (1987).
24. Potter-Baker, K. A. *et al.* Transcranial direct current stimulation (tDCS) Paired with massed practice training to promote adaptive plasticity and motor recovery in chronic incomplete tetraplegia: a pilot study. *J. Spinal Cord Med.* 1–15 (2017). doi:10.1080/10790268.2017.1361562
25. Thakral, G. *et al.* Electrical stimulation to accelerate wound healing. *Diabet. Foot Ankle* 4, (2013).
26. Ud-Din, S. & Bayat, A. Electrical Stimulation and Cutaneous Wound Healing: A Review of Clinical Evidence. *Healthc. Basel Switz.* 2, 445–467 (2014).
27. Fregni, F. *et al.* Noninvasive cortical stimulation with transcranial direct current stimulation in Parkinson's disease. *Mov. Disord. Off. J. Mov. Disord. Soc.* 21, 1693–1702 (2006).
28. Benninger, D. H. *et al.* Transcranial direct current stimulation for the treatment of Parkinson's disease. *J. Neurol. Neurosurg. Psychiatry* 81, 1105–1111 (2010).
29. Tortella, G. *et al.* Transcranial direct current stimulation in psychiatric disorders. *World J. Psychiatry* 5, 88–102 (2015).
30. Wang, Z., Clark, C. C. & Brighton, C. T. Up-regulation of bone morphogenetic proteins in cultured murine bone cells with use of specific electric fields. *J. Bone Joint Surg. Am.* 88, 1053–1065 (2006).
31. Schemitsch, E. & Kuzyk, P. The science of electrical stimulation therapy for fracture healing. *Indian J. Orthop.* 43, 127 (2009).
32. Hammerick, K. E., James, A. W., Huang, Z., Prinz, F. B. & Longaker, M. T. Pulsed direct current electric fields enhance osteogenesis in adipose-derived stromal cells. *Tissue Eng. Part A* 16, 917–931 (2010).
33. Pedrotty, D. M. *et al.* Engineering skeletal myoblasts: roles of three-dimensional culture and electrical stimulation. *Am. J. Physiol. Heart Circ. Physiol.* 288, H1620-1626 (2005).
34. Leon-Salas, W. D. *et al.* A dual mode pulsed electro-magnetic cell stimulator produces acceleration of myogenic differentiation. *Recent Pat. Biotechnol.* 7, 71–81 (2013).
35. Ewertowska, E. *et al.* Effect of applied voltage, duration and repetition frequency of RF pulses for pain relief on temperature spikes and electrical field: a computer modelling study. *Int. J. Hyperthermia* 34, 112–121 (2018).

36. Hurley, M. V. & Bearne, L. M. Non-exercise physical therapies for musculoskeletal conditions. *Best Pract. Res. Clin. Rheumatol.* 22, 419–433 (2008).
37. Côté, P. *et al.* Management of neck pain and associated disorders: A clinical practice guideline from the Ontario Protocol for Traffic Injury Management (OPTIMa) Collaboration. *Eur. Spine J. Off. Publ. Eur. Spine Soc. Eur. Spinal Deform. Soc. Eur. Sect. Cerv. Spine Res. Soc.* 25, 2000–2022 (2016).
38. Page, M. J. *et al.* Electrotherapy modalities for adhesive capsulitis (frozen shoulder). *Cochrane Database Syst. Rev.* CD011324 (2014). doi:10.1002/14651858.CD011324
39. Bai, F., Gusbeth, C., Frey, W. & Nick, P. Nanosecond pulsed electric fields trigger cell differentiation in Chlamydomonas reinhardtii. *Biochim. Biophys. Acta BBA - Biomembr.* 1859, 651–661 (2017).
40. Matsumoto, K. *et al.* Low-intensity pulsed ultrasound stimulation promotes osteoblast differentiation through hedgehog signaling. *J. Cell. Biochem.* 119, 4352–4360 (2018).
41. Stryer, L. Cyclic GMP cascade of vision. *Annu. Rev. Neurosci.* 9, 87–119 (1986).
42. Hagins, W. A., Penn, R. D. & Yoshikami, S. Dark Current and Photocurrent in Retinal Rods. *Biophys. J.* 10, 380–412 (1970).
43. Kaupp, U. B. & Koch, K. W. Role of cGMP and Ca2+ in vertebrate photoreceptor excitation and adaptation. *Annu. Rev. Physiol.* 54, 153–175 (1992).
44. Hausser, M. Diversity and Dynamics of Dendritic Signaling. *Science* 290, 739–744 (2000).
45. Haydon, P. G. GLIA: listening and talking to the synapse. *Nat. Rev. Neurosci.* 2, 185–193 (2001).
46. Ibáñez, C. F. Message in a bottle: long-range retrograde signaling in the nervous system. *Trends Cell Biol.* 17, 519–528 (2007).
47. Bers, D. M. Cardiac excitation-contraction coupling. *Nature* 415, 198–205 (2002).
48. Wahler, G. M. Cardiac Action Potentials. in *Cell Physiology Source Book* 887–898 (Elsevier, 2001). doi:10.1016/B978-012656976-6/50144-X
49. Cajavilca, C. & Varon, J. Willem Einthoven: The development of the human electrocardiogram. *Resuscitation* 76, 325–328 (2008).
50. Catterall, W. A. Excitation-contraction coupling in vertebrate skeletal muscle: a tale of two calcium channels. *Cell* 64, 871–874 (1991).
51. Delbono, O. Neural control of aging skeletal muscle. *Aging Cell* 2, 21–29 (2003).
52. Hall, Z. W. & Sanes, J. R. Synaptic structure and development: The neuromuscular junction. *Cell* 72, 99–121 (1993).
53. Fernie, A. R., Carrari, F. & Sweetlove, L. J. Respiratory metabolism: glycolysis, the TCA cycle and mitochondrial electron transport. *Curr. Opin. Plant Biol.* 7, 254–261 (2004).
54. Ashcroft, F. M. *Ion channels and disease: channelopathies*. (Academic Press, 2000).
55. Hatta, S., Sakamoto, J. & Horio, Y. Ion channels and diseases. *Med. Electron Microsc. Off. J. Clin. Electron Microsc. Soc. Jpn.* 35, 117–126 (2002).
56. Pilewski, J. M. & Frizzell, R. A. Role of CFTR in Airway Disease. *Physiol. Rev.* 79, S215–S255 (1999).

57. Wright, S. H. Generation of resting membrane potential. *Adv. Physiol. Educ.* 28, 139–142 (2004).
58. Hille, B. *Ionic channels of excitable membranes*. (Sinauer Associates, 1992).
59. Plonsey, R. & Barr, R. C. *Bioelectricity: a quantitative approach*. (Springer, 2007).
60. Hodgkin, A. L. & Huxley, A. F. A quantitative description of membrane current and its application to conduction and excitation in nerve. *J. Physiol.* 117, 500–544 (1952).
61. Amir, R., Michaelis, M. & Devor, M. Membrane potential oscillations in dorsal root ganglion neurons: role in normal electrogenesis and neuropathic pain. *J. Neurosci. Off. J. Soc. Neurosci.* 19, 8589–8596 (1999).
62. Carpenter, D. O. A Contribution of an Electrogenic Na+ Pump to Membrane Potential in Aplysia Neurons. *J. Gen. Physiol.* 52, 1–21 (1968).
63. Bilbrey, G. L., Herbin, L., Carter, N. W. & Knochel, J. P. Skeletal Muscle Resting Membrane Potential in Potassium Deficiency. *J. Clin. Invest.* 52, 3011–3018 (1973).
64. Pethig, R. & Kell, D. B. The passive electrical properties of biological systems: their significance in physiology, biophysics and biotechnology. *Phys. Med. Biol.* 32, 933–970 (1987).
65. Clausen, C., Lewis, S. A. & Diamond, J. M. Impedance analysis of a tight epithelium using a distributed resistance model. *Biophys. J.* 26, 291–317 (1979).
66. Tan, S. C. & Yiap, B. C. DNA, RNA, and Protein Extraction: The Past and The Present. *J. Biomed. Biotechnol.* 2009, 1–10 (2009).
67. *Medical physiology: a cellular and molecular approach*. (Saunders/Elsevier, 2009).
68. Goldup, A., Ohki, S. & Danielli, J. F. Black Lipid Films. in *Recent Progress in Surface Science* 3, 193–260 (Elsevier, 1970).
69. Ringer, S. A further Contribution regarding the influence of the different Constituents of the Blood on the Contraction of the Heart. *J. Physiol.* 4, 29-42.3 (1883).
70. Ringer, S. Regarding the Action of Hydrate of Soda, Hydrate of Ammonia, and Hydrate of Potash on the Ventricle of the Frog's Heart. *J. Physiol.* 3, 195-202.6 (1882).
71. Mann, P. J., Tennenbaum, M. & Quastel, J. H. Acetylcholine metabolism in the central nervous system: The effects of potassium and other cations on acetylcholine liberation. *Biochem. J.* 33, 822–835 (1939).
72. Heilbrunn, L. V. & Wiercinski, F. J. The action of various cations on muscle protoplasm. *J. Cell. Comp. Physiol.* 29, 15–32 (1947).
73. Li, Z. & Langhans, S. A. Transcriptional regulators of Na,K-ATPase subunits. *Front. Cell Dev. Biol.* 3, 66 (2015).
74. McBride, B. W. & Early, R. J. Energy expenditure associated with sodium/potassium transport and protein synthesis in skeletal muscle and isolated hepatocytes from hyperthyroid sheep. *Br. J. Nutr.* 62, 673 (1989).
75. Kramer, I. M. *Signal transduction*. (Elsevier/AP, 2016).
76. Catterall, W. A. Voltage-Gated Calcium Channels. *Cold Spring Harb. Perspect. Biol.* 3, a003947–a003947 (2011).
77. Clairfeuille, T., Xu, H., Koth, C. M. & Payandeh, J. Voltage-gated sodium channels viewed through a structural biology lens. *Curr. Opin. Struct. Biol.* 45, 74–84 (2017).

78. Catterall, W. A. From ionic currents to molecular mechanisms: the structure and function of voltage-gated sodium channels. *Neuron* 26, 13–25 (2000).
79. Catterall, W. A., Perez-Reyes, E., Snutch, T. P. & Striessnig, J. International Union of Pharmacology. XLVIII. Nomenclature and structure-function relationships of voltage-gated calcium channels. *Pharmacol. Rev.* 57, 411–425 (2005).
80. Brehm, P., Okamura, Y. & Mandel, G. Ion channel evolution. *Semin. Neurosci.* 3, 355–367 (1991).
81. Moran, Y., Barzilai, M. G., Liebeskind, B. J. & Zakon, H. H. Evolution of voltage-gated ion channels at the emergence of Metazoa. *J. Exp. Biol.* 218, 515–525 (2015).
82. Cuello, L. G., Cortes, D. M. & Perozo, E. The gating cycle of a K+ channel at atomic resolution. *eLife* 6, (2017).
83. Lenaeus, M. J. *et al.* Structures of closed and open states of a voltage-gated sodium channel. *Proc. Natl. Acad. Sci.* 114, E3051–E3060 (2017).
84. Yu, F. H. Overview of Molecular Relationships in the Voltage-Gated Ion Channel Superfamily. *Pharmacol. Rev.* 57, 387–395 (2005).
85. Adair, R. K. Noise and stochastic resonance in voltage-gated ion channels. *Proc. Natl. Acad. Sci.* 100, 12099–12104 (2003).
86. O'Donnell, C. & van Rossum, M. C. W. Systematic analysis of the contributions of stochastic voltage gated channels to neuronal noise. *Front. Comput. Neurosci.* 8, 105 (2014).
87. O'Donnell, C. & Nolan, M. F. Stochastic Ion Channel Gating and Probabilistic Computation in Dendritic Neurons. in *The Computing Dendrite* (eds. Cuntz, H., Remme, M. W. H. & Torben-Nielsen, B.) 11, 397–414 (Springer New York, 2014).
88. Maki, B. A., Cummings, K. A., Paganelli, M. A., Murthy, S. E. & Popescu, G. K. One-channel cell-attached patch-clamp recording. *J. Vis. Exp. JoVE* (2014). doi:10.3791/51629
89. Pérez, C. G. *et al.* Ryanodine receptor function in newborn rat heart. *Am. J. Physiol.-Heart Circ. Physiol.* 288, H2527–H2540 (2005).
90. Shaya, D. *et al.* Voltage-gated sodium channel (NaV) protein dissection creates a set of functional pore-only proteins. *Proc. Natl. Acad. Sci.* 108, 12313–12318 (2011).
91. Catterall, W. A. Structure and Function of Voltage-Gated Ion Channels. *Annu. Rev. Biochem.* 64, 493–531 (1995).
92. Jensen, M. Ø. *et al.* Mechanism of voltage gating in potassium channels. *Science* 336, 229–233 (2012).
93. Almers, W. Gating currents and charge movements in excitable membranes. in *Reviews of Physiology, Biochemistry and Pharmacology, Volume 82* 82, 96–190 (Springer-Verlag, 1978).
94. Chanda, B., Kwame Asamoah, O., Blunck, R., Roux, B. & Bezanilla, F. Gating charge displacement in voltage-gated ion channels involves limited transmembrane movement. *Nature* 436, 852–856 (2005).
95. Ishida, I. G., Rangel-Yescas, G. E., Carrasco-Zanini, J. & Islas, L. D. Voltage-dependent gating and gating charge measurements in the Kv1.2 potassium channel. *J. Gen. Physiol.* 145, 345–358 (2015).
96. Adrian, R. H. Conduction Velocity and Gating Current in the Squid Giant Axon. *Proc. R. Soc. B Biol. Sci.* 189, 81–86 (1975).

97. Toombes, G. E. S. & Swartz, K. J. Twists and turns in gating ion channels with voltage. *Science* 353, 646–647 (2016).
98. Jiang, Y. *et al.* X-ray structure of a voltage-dependent K+ channel. *Nature* 423, 33–41 (2003).
99. Jiang, Y. *et al.* Crystal structure and mechanism of a calcium-gated potassium channel. *Nature* 417, 515–522 (2002).
100. Doyle, D. A. *et al.* The structure of the potassium channel: molecular basis of K+ conduction and selectivity. *Science* 280, 69–77 (1998).
101. Noda, M. *et al.* Primary structure of Electrophorus electricus sodium channel deduced from cDNA sequence. *Nature* 312, 121 (1984).
102. Tanabe, T. *et al.* Primary structure of the receptor for calcium channel blockers from skeletal muscle. *Nature* 328, 313–318 (1987).
103. Ertel, E. A. *et al.* Nomenclature of voltage-gated calcium channels. *Neuron* 25, 533–535 (2000).
104. Yellen, G. The voltage-gated potassium channels and their relatives. *Nature* 419, 35–42 (2002).
105. Hoshi, T., Zagotta, W. N. & Aldrich, R. W. Biophysical and molecular mechanisms of Shaker potassium channel inactivation. *Science* 250, 533–538 (1990).
106. Hoshi, T., Zagotta, W. N. & Aldrich, R. W. Two types of inactivation in Shaker K+ channels: effects of alterations in the carboxy-terminal region. *Neuron* 7, 547–556 (1991).
107. López-Barneo, J., Hoshi, T., Heinemann, S. H. & Aldrich, R. W. Effects of external cations and mutations in the pore region on C-type inactivation of Shaker potassium channels. *Receptors Channels* 1, 61–71 (1993).
108. Cordero-Morales, J. F. *et al.* Molecular determinants of gating at the potassium-channel selectivity filter. *Nat. Struct. Mol. Biol.* 13, 311–318 (2006).
109. Cuello, L. G., Jogini, V., Cortes, D. M. & Perozo, E. Structural mechanism of C-type inactivation in K(+) channels. *Nature* 466, 203–208 (2010).
110. Rettig, J. *et al.* Inactivation properties of voltage-gated K+ channels altered by presence of beta-subunit. *Nature* 369, 289–294 (1994).
111. Murrell-Lagnado, R. D. & Aldrich, R. W. Interactions of amino terminal domains of Shaker K channels with a pore blocking site studied with synthetic peptides. *J. Gen. Physiol.* 102, 949–975 (1993).
112. Murrell-Lagnado, R. D. & Aldrich, R. W. Energetics of Shaker K channels block by inactivation peptides. *J. Gen. Physiol.* 102, 977–1003 (1993).
113. Zagotta, W. N., Hoshi, T. & Aldrich, R. W. Restoration of inactivation in mutants of Shaker potassium channels by a peptide derived from ShB. *Science* 250, 568–571 (1990).
114. Labro, A. J. *et al.* Kv channel gating requires a compatible S4-S5 linker and bottom part of S6, constrained by non-interacting residues. *J. Gen. Physiol.* 132, 667–680 (2008).
115. Aryal, P., Sansom, M. S. P. & Tucker, S. J. Hydrophobic Gating in Ion Channels. *J. Mol. Biol.* 427, 121–130 (2015).
116. Jensen, M. O. *et al.* Principles of conduction and hydrophobic gating in K+ channels. *Proc. Natl. Acad. Sci.* 107, 5833–5838 (2010).

117.Catterall, W. A. Structure and function of voltage-gated sodium channels at atomic resolution: Voltage-gated sodium channels at atomic resolution. *Exp. Physiol.* 99, 35–51 (2014).
118.West, J. W. *et al.* A cluster of hydrophobic amino acid residues required for fast Na(+)-channel inactivation. *Proc. Natl. Acad. Sci. U. S. A.* 89, 10910–10914 (1992).
119.Armstrong, C. M. Sodium channels and gating currents. *Physiol. Rev.* 61, 644–683 (1981).
120.Kellenberger, S., West, J. W., Catterall, W. A. & Scheuer, T. Molecular analysis of potential hinge residues in the inactivation gate of brain type IIA Na+ channels. *J. Gen. Physiol.* 109, 607–617 (1997).
121.Vassilev, P. M., Scheuer, T. & Catterall, W. A. Identification of an intracellular peptide segment involved in sodium channel inactivation. *Science* 241, 1658–1661 (1988).
122.Vassilev, P., Scheuer, T. & Catterall, W. A. Inhibition of inactivation of single sodium channels by a site-directed antibody. *Proc. Natl. Acad. Sci. U. S. A.* 86, 8147–8151 (1989).
123.Leipold, E., Lu, S., Gordon, D., Hansel, A. & Heinemann, S. H. Combinatorial interaction of scorpion toxins Lqh-2, Lqh-3, and LqhalphaIT with sodium channel receptor sites-3. *Mol. Pharmacol.* 65, 685–691 (2004).
124.Sheets, M. F., Kyle, J. W., Kallen, R. G. & Hanck, D. A. The Na channel voltage sensor associated with inactivation is localized to the external charged residues of domain IV, S4. *Biophys. J.* 77, 747–757 (1999).
125.Rogers, J. C., Qu, Y., Tanada, T. N., Scheuer, T. & Catterall, W. A. Molecular determinants of high affinity binding of alpha-scorpion toxin and sea anemone toxin in the S3-S4 extracellular loop in domain IV of the Na+ channel alpha subunit. *J. Biol. Chem.* 271, 15950–15962 (1996).
126.Srinivasan, J., Schachner, M. & Catterall, W. A. Interaction of voltage-gated sodium channels with the extracellular matrix molecules tenascin-C and tenascin-R. *Proc. Natl. Acad. Sci. U. S. A.* 95, 15753–15757 (1998).
127.Ratcliffe, C. F. *et al.* A sodium channel signaling complex: modulation by associated receptor protein tyrosine phosphatase beta. *Nat. Neurosci.* 3, 437–444 (2000).
128.Ratcliffe, C. F., Westenbroek, R. E., Curtis, R. & Catterall, W. A. Sodium channel beta1 and beta3 subunits associate with neurofascin through their extracellular immunoglobulin-like domain. *J. Cell Biol.* 154, 427–434 (2001).
129.Kazarinova-Noyes, K. *et al.* Contactin associates with Na+ channels and increases their functional expression. *J. Neurosci. Off. J. Soc. Neurosci.* 21, 7517–7525 (2001).
130.Malhotra, J. D. *et al.* Structural requirements for interaction of sodium channel beta 1 subunits with ankyrin. *J. Biol. Chem.* 277, 26681–26688 (2002).
131.Wallace, R. H. *et al.* Febrile seizures and generalized epilepsy associated with a mutation in the Na+-channel beta1 subunit gene SCN1B. *Nat. Genet.* 19, 366–370 (1998).
132.Reuter, H. Properties of two inward membrane currents in the heart. *Annu. Rev. Physiol.* 41, 413–424 (1979).
133.Tsien, R. W. Calcium channels in excitable cell membranes. *Annu. Rev. Physiol.* 45, 341–358 (1983).

134.Tanabe, T. *et al.* Structure and function of voltage-dependent calcium channels from muscle. *Ann. N. Y. Acad. Sci.* 707, 81–86 (1993).
135.Yang, S.-N. & Berggren, P.-O. The role of voltage-gated calcium channels in pancreatic beta-cell physiology and pathophysiology. *Endocr. Rev.* 27, 621–676 (2006).
136.Tsien, R. W., Lipscombe, D., Madison, D. V., Bley, K. R. & Fox, A. P. Multiple types of neuronal calcium channels and their selective modulation. *Trends Neurosci.* 11, 431–438 (1988).
137.Catterall, W. A. & Few, A. P. Calcium channel regulation and presynaptic plasticity. *Neuron* 59, 882–901 (2008).
138.Dunlap, K., Luebke, J. I. & Turner, T. J. Exocytotic Ca2+ channels in mammalian central neurons. *Trends Neurosci.* 18, 89–98 (1995).
139.Flavell, S. W. & Greenberg, M. E. Signaling mechanisms linking neuronal activity to gene expression and plasticity of the nervous system. *Annu. Rev. Neurosci.* 31, 563–590 (2008).
140.Snutch, T. P. & Reiner, P. B. Ca2+ channels: diversity of form and function. *Curr. Opin. Neurobiol.* 2, 247–253 (1992).
141.Mori, Y. *et al.* Primary structure and functional expression from complementary DNA of a brain calcium channel. *Nature* 350, 398–402 (1991).
142.Starr, T. V., Prystay, W. & Snutch, T. P. Primary structure of a calcium channel that is highly expressed in the rat cerebellum. *Proc. Natl. Acad. Sci. U. S. A.* 88, 5621–5625 (1991).
143.Perez-Reyes, E. *et al.* Molecular characterization of a neuronal low-voltage-activated T-type calcium channel. *Nature* 391, 896–900 (1998).
144.Bean, B. P. Classes of calcium channels in vertebrate cells. *Annu. Rev. Physiol.* 51, 367–384 (1989).
145.Carbone, E. & Lux, H. D. A low voltage-activated, fully inactivating Ca channel in vertebrate sensory neurones. *Nature* 310, 501–502 (1984).
146.Nowycky, M. C., Fox, A. P. & Tsien, R. W. Three types of neuronal calcium channel with different calcium agonist sensitivity. *Nature* 316, 440–443 (1985).
147.Hagiwara, S., Ozawa, S. & Sand, O. Voltage clamp analysis of two inward current mechanisms in the egg cell membrane of a starfish. *J. Gen. Physiol.* 65, 617–644 (1975).
148.Iftinca, M. C. Neuronal T-type calcium channels: what's new? Iftinca: T-type channel regulation. *J. Med. Life* 4, 126–138 (2011).
149.Perez-Reyes, E. Molecular physiology of low-voltage-activated t-type calcium channels. *Physiol. Rev.* 83, 117–161 (2003).
150.Molderings, G. J., Likungu, J. & Göthert, M. N-Type calcium channels control sympathetic neurotransmission in human heart atrium. *Circulation* 101, 403–407 (2000).
151.Hayashi, K. *et al.* Ca2+ channel subtypes and pharmacology in the kidney. *Circ. Res.* 100, 342–353 (2007).
152.Llinás, R. & Yarom, Y. Electrophysiology of mammalian inferior olivary neurones in vitro. Different types of voltage-dependent ionic conductances. *J. Physiol.* 315, 549–567 (1981).

153.Llinás, R. R., Sugimori, M. & Cherksey, B. Voltage-dependent calcium conductances in mammalian neurons. The P channel. *Ann. N. Y. Acad. Sci.* 560, 103–111 (1989).
154.Randall, A. & Tsien, R. W. Pharmacological dissection of multiple types of Ca2+ channel currents in rat cerebellar granule neurons. *J. Neurosci. Off. J. Soc. Neurosci.* 15, 2995–3012 (1995).
155.Nimmrich, V. & Gross, G. P/Q-type calcium channel modulators: P/Q-type calcium channel blockers. *Br. J. Pharmacol.* 167, 741–759 (2012).
156.Soong, T. W. *et al.* Structure and functional expression of a member of the low voltage-activated calcium channel family. *Science* 260, 1133–1136 (1993).
157.Parajuli, L. K. *et al.* Quantitative regional and ultrastructural localization of the Ca(v)2.3 subunit of R-type calcium channel in mouse brain. *J. Neurosci. Off. J. Soc. Neurosci.* 32, 13555–13567 (2012).
158.Wolfe, J. T., Wang, H., Howard, J., Garrison, J. C. & Barrett, P. Q. T-type calcium channel regulation by specific G-protein betagamma subunits. *Nature* 424, 209–213 (2003).
159.Wang, M.-C. *et al.* 3D structure of the skeletal muscle dihydropyridine receptor. *J. Mol. Biol.* 323, 85–98 (2002).
160.Serysheva, I. I., Ludtke, S. J., Baker, M. R., Chiu, W. & Hamilton, S. L. Structure of the voltage-gated L-type Ca2+ channel by electron cryomicroscopy. *Proc. Natl. Acad. Sci. U. S. A.* 99, 10370–10375 (2002).
161.Curtis, B. M. & Catterall, W. A. Purification of the calcium antagonist receptor of the voltage-sensitive calcium channel from skeletal muscle transverse tubules. *Biochemistry* 23, 2113–2118 (1984).
162.Flockerzi, V. *et al.* Purified dihydropyridine-binding site from skeletal muscle t-tubules is a functional calcium channel. *Nature* 323, 66–68 (1986).
163.Hosey, M. M. *et al.* Photoaffinity labelling and phosphorylation of a 165 kilodalton peptide associated with dihydropyridine and phenylalkylamine-sensitive calcium channels. *Biochem. Biophys. Res. Commun.* 147, 1137–1145 (1987).
164.Leung, A. T., Imagawa, T. & Campbell, K. P. Structural characterization of the 1,4-dihydropyridine receptor of the voltage-dependent Ca2+ channel from rabbit skeletal muscle. Evidence for two distinct high molecular weight subunits. *J. Biol. Chem.* 262, 7943–7946 (1987).
165.Striessnig, J. *et al.* Photoaffinity labelling of the phenylalkylamine receptor of the skeletal muscle transverse-tubule calcium channel. *FEBS Lett.* 212, 247–253 (1987).
166. Takahashi, M., Seagar, M. J., Jones, J. F., Reber, B. F. & Catterall, W. A. Subunit structure of dihydropyridine-sensitive calcium channels from skeletal muscle. *Proc. Natl. Acad. Sci. U. S. A.* 84, 5478–5482 (1987).
167. Ruth, P. *et al.* Primary structure of the beta subunit of the DHP-sensitive calcium channel from skeletal muscle. *Science* 245, 1115–1118 (1989).
168. Arikkath, J. & Campbell, K. P. Auxiliary subunits: essential components of the voltage-gated calcium channel complex. *Curr. Opin. Neurobiol.* 13, 298–307 (2003).
169. De Jongh, K. S., Warner, C. & Catterall, W. A. Subunits of purified calcium channels. Alpha 2 and delta are encoded by the same gene. *J. Biol. Chem.* 265, 14738–14741 (1990).

170. Chen, Y.-H. *et al.* Structural basis of the alpha1-beta subunit interaction of voltage-gated Ca2+ channels. *Nature* 429, 675–680 (2004).
171. Van Petegem, F., Clark, K. A., Chatelain, F. C. & Minor, D. L. Structure of a complex between a voltage-gated calcium channel beta-subunit and an alpha-subunit domain. *Nature* 429, 671–675 (2004).
172. Pragnell, M. *et al.* Calcium channel beta-subunit binds to a conserved motif in the I-II cytoplasmic linker of the alpha 1-subunit. *Nature* 368, 67–70 (1994).
173. Lacerda, A. E. *et al.* Normalization of current kinetics by interaction between the alpha 1 and beta subunits of the skeletal muscle dihydropyridine-sensitive Ca2+ channel. *Nature* 352, 527–530 (1991).
174. Singer, D. *et al.* The roles of the subunits in the function of the calcium channel. *Science* 253, 1553–1557 (1991).
175. Davies, A. *et al.* Functional biology of the alpha(2)delta subunits of voltage-gated calcium channels. *Trends Pharmacol. Sci.* 28, 220–228 (2007).
176. Peterson, B. Z., DeMaria, C. D., Adelman, J. P. & Yue, D. T. Calmodulin is the Ca2+ sensor for Ca2+ -dependent inactivation of L-type calcium channels. *Neuron* 22, 549–558 (1999).
177. Qin, N., Olcese, R., Bransby, M., Lin, T. & Birnbaumer, L. Ca2+-induced inhibition of the cardiac Ca2+ channel depends on calmodulin. *Proc. Natl. Acad. Sci. U. S. A.* 96, 2435–2438 (1999).
178. Zühlke, R. D., Pitt, G. S., Deisseroth, K., Tsien, R. W. & Reuter, H. Calmodulin supports both inactivation and facilitation of L-type calcium channels. *Nature* 399, 159–162 (1999).
179. Hulme, J. T., Yarov-Yarovoy, V., Lin, T. W.-C., Scheuer, T. & Catterall, W. A. Autoinhibitory control of the CaV1.2 channel by its proteolytically processed distal C-terminal domain. *J. Physiol.* 576, 87–102 (2006).
180. Emrick, M. A., Sadilek, M., Konoki, K. & Catterall, W. A. Beta-adrenergic-regulated phosphorylation of the skeletal muscle Ca(V)1.1 channel in the fight-or-flight response. *Proc. Natl. Acad. Sci. U. S. A.* 107, 18712–18717 (2010).
181. Fuller, M. D., Emrick, M. A., Sadilek, M., Scheuer, T. & Catterall, W. A. Molecular mechanism of calcium channel regulation in the fight-or-flight response. *Sci. Signal.* 3, ra70 (2010).
182. Hofmann, F., Biel, M. & Flockerzi, V. Molecular basis for Ca2+ channel diversity. *Annu. Rev. Neurosci.* 17, 399–418 (1994).
183. Dolphin, A. C. Beta subunits of voltage-gated calcium channels. *J. Bioenerg. Biomembr.* 35, 599–620 (2003).
184. Ye, S., Li, Y. & Jiang, Y. Novel insights into K+ selectivity from high-resolution structures of an open K+ channel pore. *Nat. Struct. Mol. Biol.* 17, 1019–1023 (2010).
185. Heginbotham, L., Lu, Z., Abramson, T. & MacKinnon, R. Mutations in the K+ channel signature sequence. *Biophys. J.* 66, 1061–1067 (1994).
186. Heginbotham, L., Abramson, T. & MacKinnon, R. A functional connection between the pores of distantly related ion channels as revealed by mutant K+ channels. *Science* 258, 1152–1155 (1992).
187. Payandeh, J., Scheuer, T., Zheng, N. & Catterall, W. A. The crystal structure of a voltage-gated sodium channel. *Nature* 475, 353–358 (2011).

188. Lipkind, G. M. & Fozzard, H. A. Voltage-gated Na channel selectivity: the role of the conserved domain III lysine residue. *J. Gen. Physiol.* 131, 523–529 (2008).
189. Zhang, X. *et al.* Analysis of the selectivity filter of the voltage-gated sodium channel Na(v)Rh. *Cell Res.* 23, 409–422 (2013).
190. Yang, J., Ellinor, P. T., Sather, W. A., Zhang, J. F. & Tsien, R. W. Molecular determinants of Ca2+ selectivity and ion permeation in L-type Ca2+ channels. *Nature* 366, 158–161 (1993).
191. Tang, S. *et al.* Molecular localization of ion selectivity sites within the pore of a human L-type cardiac calcium channel. *J. Biol. Chem.* 268, 13026–13029 (1993).
192. Heinemann, S. H., Terlau, H., Stühmer, W., Imoto, K. & Numa, S. Calcium channel characteristics conferred on the sodium channel by single mutations. *Nature* 356, 441–443 (1992).
193. van Meer, G., Voelker, D. R. & Feigenson, G. W. Membrane lipids: where they are and how they behave. *Nat. Rev. Mol. Cell Biol.* 9, 112–124 (2008).
194. Hulbert, A. J. Life, death and membrane bilayers. *J. Exp. Biol.* 206, 2303–2311 (2003).
195. Hulbert, A. J. & Else, P. L. Mechanisms underlying the cost of living in animals. *Annu. Rev. Physiol.* 62, 207–235 (2000).
196. Hulbert, A. J. & Else, P. L. Membranes as possible pacemakers of metabolism. *J. Theor. Biol.* 199, 257–274 (1999).
197. Koushik, A. B., Powell, R. R. & Temesvari, L. A. Localization of Phosphatidylinositol 4,5-Bisphosphate to Lipid Rafts and Uroids in the Human Protozoan Parasite Entamoeba histolytica. *Infect. Immun.* 81, 2145–2155 (2013).
198. Hou, Q. *et al.* Regulation of AMPA receptor localization in lipid rafts. *Mol. Cell. Neurosci.* 38, 213–223 (2008).
199. Head, B. P., Patel, H. H. & Insel, P. A. Interaction of membrane/lipid rafts with the cytoskeleton: Impact on signaling and function. *Biochim. Biophys. Acta BBA - Biomembr.* 1838, 532–545 (2014).
200. Levin, M., Thorlin, T., Robinson, K. R., Nogi, T. & Mercola, M. Asymmetries in H+/K+-ATPase and cell membrane potentials comprise a very early step in left-right patterning. *Cell* 111, 77–89 (2002).
201. Mañes, S., Ana Lacalle, R., Gómez-Moutón, C. & Martínez-A, C. From rafts to crafts: membrane asymmetry in moving cells. *Trends Immunol.* 24, 319–325 (2003).
202. Neumüller, R. A. & Knoblich, J. A. Dividing cellular asymmetry: asymmetric cell division and its implications for stem cells and cancer. *Genes Dev.* 23, 2675–2699 (2009).
203. Emoto, K. & Umeda, M. An essential role for a membrane lipid in cytokinesis. Regulation of contractile ring disassembly by redistribution of phosphatidylethanolamine. *J. Cell Biol.* 149, 1215–1224 (2000).
204. Streb, H., Irvine, R. F., Berridge, M. J. & Schulz, I. Release of Ca2+ from a nonmitochondrial intracellular store in pancreatic acinar cells by inositol-1,4,5-trisphosphate. *Nature* 306, 67–69 (1983).
205. Creba, J. A. *et al.* Rapid breakdown of phosphatidylinositol 4-phosphate and phosphatidylinositol 4,5-bisphosphate in rat hepatocytes stimulated by vasopressin and other Ca2+-mobilizing hormones. *Biochem. J.* 212, 733–747 (1983).

206. Hokin, M. R. & Hokin, L. E. Enzyme secretion and the incorporation of P32 into phospholipides of pancreas slices. *J. Biol. Chem.* 203, 967–977 (1953).
207. Nishizuka, Y. Intracellular signaling by hydrolysis of phospholipids and activation of protein kinase C. *Science* 258, 607–614 (1992).
208. Taylor, C. W., da Fonseca, P. C. A. & Morris, E. P. IP(3) receptors: the search for structure. *Trends Biochem. Sci.* 29, 210–219 (2004).
209. Tuszynski, J., Tilli, T. M. & Levin, M. Ion Channel and Neurotransmitter Modulators as Electroceutical Approaches to the Control of Cancer. *Curr. Pharm. Des.* 23, 4827–4841 (2017).
210. Atlas, D. The voltage-gated calcium channel functions as the molecular switch of synaptic transmission. *Annu. Rev. Biochem.* 82, 607–635 (2013).
211. Bachnoff, N., Cohen-Kutner, M., Trus, M. & Atlas, D. Intra-membrane signaling between the voltage-gated Ca2+-channel and cysteine residues of syntaxin 1A coordinates synchronous release. *Sci. Rep.* 3, 1620 (2013).
212. Chapman, E. R. How does synaptotagmin trigger neurotransmitter release? *Annu. Rev. Biochem.* 77, 615–641 (2008).
213. Stevens, C. F. & Sullivan, J. M. The synaptotagmin C2A domain is part of the calcium sensor controlling fast synaptic transmission. *Neuron* 39, 299–308 (2003).
214. Südhof, T. C. A molecular machine for neurotransmitter release: synaptotagmin and beyond. *Nat. Med.* 19, 1227–1231 (2013).
215. Südhof, T. C. & Rothman, J. E. Membrane fusion: grappling with SNARE and SM proteins. *Science* 323, 474–477 (2009).
216. Honigmann, A. *et al.* Phosphatidylinositol 4,5-bisphosphate clusters act as molecular beacons for vesicle recruitment. *Nat. Struct. Mol. Biol.* 20, 679–686 (2013).
217. Gianaroli, L. *et al.* Fertilization current in the human oocyte. *Mol. Reprod. Dev.* 38, 209–214 (1994).
218. Dale, B., Santella, L. & Tosti, E. Gap-junctional permeability in early and cleavage-arrested ascidian embryos. *Dev. Camb. Engl.* 112, 153–160 (1991).
219. Parrington, J. *et al.* Expression of inositol 1,4,5-trisphosphate receptors in mouse oocytes and early embryos: the type I isoform is upregulated in oocytes and downregulated after fertilization. *Dev. Biol.* 203, 451–461 (1998).
220. Levin, M. & Mercola, M. Gap junctions are involved in the early generation of left-right asymmetry. *Dev. Biol.* 203, 90–105 (1998).
221. Levin, M. & Mercola, M. Gap junction-mediated transfer of left-right patterning signals in the early chick blastoderm is upstream of Shh asymmetry in the node. *Dev. Camb. Engl.* 126, 4703–4714 (1999).
222. Jaffe, L. F. & Stern, C. D. Strong electrical currents leave the primitive streak of chick embryos. *Science* 206, 569–571 (1979).
223. Winkel, G. K. & Nuccitelli, R. Large Ionic Currents Leave the Primitive Streak of the 7.5-Day Mouse Embryo. *Biol. Bull.* 176, 110–117 (1989).
224. Yan, T. *et al.* Electric field-induced suppression of PTEN drives epithelial-to-mesenchymal transition via mTORC1 activation. *J. Dermatol. Sci.* 85, 96–105 (2017).

225. Liu, J. *et al.* Electric field exposure promotes epithelial-mesenchymal transition in human lens epithelial cells via integrin β1-FAK signaling. *Mol. Med. Rep.* 16, 4008–4014 (2017).
226. Morokuma, J., Blackiston, D. & Levin, M. KCNQ1 and KCNE1 K+ channel components are involved in early left-right patterning in Xenopus laevis embryos. *Cell. Physiol. Biochem. Int. J. Exp. Cell. Physiol. Biochem. Pharmacol.* 21, 357–372 (2008).
227. Hatayama, M., Mikoshiba, K. & Aruga, J. IP3 signaling is required for cilia formation and left-right body axis determination in Xenopus embryos. *Biochem. Biophys. Res. Commun.* 410, 520–524 (2011).
228. Metcalf, M. E. M., Shi, R. & Borgens, R. B. Endogenous ionic currents and voltages in amphibian embryos. *J. Exp. Zool.* 268, 307–322 (1994).
229. Cooper, M. S. & Keller, R. E. Perpendicular orientation and directional migration of amphibian neural crest cells in dc electrical fields. *Proc. Natl. Acad. Sci. U. S. A.* 81, 160–164 (1984).
230. Gruler, H. & Nuccitelli, R. Neural crest cell galvanotaxis: new data and a novel approach to the analysis of both galvanotaxis and chemotaxis. *Cell Motil. Cytoskeleton* 19, 121–133 (1991).
231. Le Douarin, N. & Kalcheim, C. *The neural crest*. (Cambridge University Press, 1999).
232. Metcalf, M. E. M. & Borgens, R. B. Weak applied voltages interfere with amphibian morphogenesis and pattern. *J. Exp. Zool.* 268, 323–338 (1994).
233. Hotary, K. B. & Robinson, K. R. Evidence of a role for endogenous electrical fields in chick embryo development. *Dev. Camb. Engl.* 114, 985–996 (1992).
234. Patel, N. & Poo, M. M. Orientation of neurite growth by extracellular electric fields. *J. Neurosci. Off. J. Soc. Neurosci.* 2, 483–496 (1982).
235. Bedlack, R. S., Wei, M. & Loew, L. M. Localized membrane depolarizations and localized calcium influx during electric field-guided neurite growth. 9, 393–403 (1992).
236. McCaig, C. D. & Rajnicek, A. M. Electrical fields, nerve growth and nerve regeneration. *Exp. Physiol.* 76, 473–494 (1991).
237. Poo, M. & Robinson, K. R. Electrophoresis of concanavalin A receptors along embryonic muscle cell membrane. 265, 602–605 (1977).
238. Meng, X. *et al.* PI3K mediated electrotaxis of embryonic and adult neural progenitor cells in the presence of growth factors. 227, 210–217 (2011).
239. Rajnicek, A. M. Bacterial galvanotropism: mechanisms and applications. *Sci. Prog.* 77 (Pt 1–2), 139–151 (1993).
240. Rajnicek, A. M., McCaig, C. D. & Gow, N. A. Electric fields induce curved growth of Enterobacter cloacae, Escherichia coli, and Bacillus subtilis cells: implications for mechanisms of galvanotropism and bacterial growth. *J. Bacteriol.* 176, 702–713 (1994).
241. BAYLISS, J. S. On the Galvanotropism of Roots. *Ann. Bot.* 21, 387–405 (1907).
242. Navez, A. E. 'GALVANOTROPISM' OF ROOTS. *J. Gen. Physiol.* 10, 551–558 (1927).

243. Wolverton, C., Mullen, J. L., Ishikawam, H. & Evans, M. L. Two distinct regions of response drive differential growth in Vigna root electrotropism. *Plant Cell Environ.* 23, 1275–1280 (2000).
244. Kral, N., Hanna Ougolnikova, A. & Sena, G. Externally imposed electric field enhances plant root tip regeneration. *Regen. Oxf. Engl.* 3, 156–167 (2016).
245. VAN HARREVELD, A. On Galvanotropism and Oscillotaxis in Fish. *J. Exp. Biol.* 15, 197 (1938).
246. Patel, N. B., Xie, Z., Young, S. H. & Poo, M. Response of nerve growth cone to focal electric currents. *J. Neurosci. Res.* 13, 245–256 (1985).
247. Yamashita, M. Electric axon guidance in embryonic retina: Galvanotropism revisited. *Biochem. Biophys. Res. Commun.* 431, 280–283 (2013).
248. Yamashita, M. Weak electric fields serve as guidance cues that direct retinal ganglion cell axons in vitro. *Biochem. Biophys. Rep.* 4, 83–88 (2015).
249. Viaud, G. [Galvanotropism, excitatory anisotropy and electrical anisotropy in a planarian (Planaria Dugesia lugubris O. Schm.)]. *J. Physiol. (Paris)* 44, 343–345 (1952).
250. Robinson, K. R. & Messerli, M. A. Left/right, up/down: The role of endogenous electrical fields as directional signals in development, repair and invasion. *BioEssays* 25, 759–766 (2003).
251. Zhao, M. Membrane lipids, EGF receptors, and intracellular signals colocalize and are polarized in epithelial cells moving directionally in a physiological electric field. (2002). doi:10.1096/fj.01-0811fje
252. Brown, M. J. & Loew, L. M. Electric field-directed fibroblast locomotion involves cell surface molecular reorganization and is calcium independent. 127, 117–128 (1994).
253. Cooper, M. S. & Schliwa, M. Transmembrane Ca2+ fluxes in the forward and reversed galvanotaxis of fish epidermal cells. 210, 311–318 (1986).
254. Trollinger, D. R., Isseroff, R. R. & Nuccitelli, R. Calcium channel blockers inhibit galvanotaxis in human keratinocytes. 193, 1–9 (2002).
255. Lever, M. C. *et al.* pH and Ca2+ dependent galvanotropism of filamentous fungi: implications and mechanisms. *Mycol. Res.* 98, 301–306 (1994).
256. Palmer, A. M., Messerli, M. A. & Robinson, K. R. Neuronal galvanotropism is independent of external Ca2+ entry or internal Ca2+ gradients. *J. Neurobiol.* 45, 30–38 (2000).
257. Zhao, M., Jin, T., McCaig, C. D., Forrester, J. V. & Devreotes, P. N. Genetic analysis of the role of G protein–coupled receptor signaling in electrotaxis. *J. Cell Biol.* 157, 921–928 (2002).
258. McCaig, C. D., Rajnicek, A. M., Song, B. & Zhao, M. Has electrical growth cone guidance found its potential? *Trends Neurosci.* 25, 354–359 (2002).
259. Steavenson, W. E. *Medical electricity*. (P. Blakiston, Son & Company, 1892).
260. Licht, S. *Therapeutic electricity and ultraviolet radiation*. (Elizabeth Licht, New Haven, Conn, 1967).
261. Burton, C. Instrumentation for dorsal column stimulator implantation. *Surg. Neurol.* 2, 39–40 (1974).

262. Wu, L.-C. *et al.* Literature Review and Meta-Analysis of Transcutaneous Electrical Nerve Stimulation in Treating Chronic Back Pain: *Reg. Anesth. Pain Med.* 1 (2018). doi:10.1097/AAP.0000000000000740
263. Almeida, C. C. de, Silva, V. Z. M. da, Júnior, G. C., Liebano, R. E. & Durigan, J. L. Q. Transcutaneous electrical nerve stimulation and interferential current demonstrate similar effects in relieving acute and chronic pain: a systematic review with meta-analysis. *Braz. J. Phys. Ther.* (2018). doi:10.1016/j.bjpt.2017.12.005
264. Sarzi-Puttini, P. *et al.* Osteoarthritis: an overview of the disease and its treatment strategies. *Semin. Arthritis Rheum.* 35, 1–10 (2005).
265. Sim, J. & Adams, N. Physical and other non-pharmacological interventions for fibromyalgia. *Baillieres Best Pract. Res. Clin. Rheumatol.* 13, 507–523 (1999).
266. Vélez-Díaz-Pallarés, M. *et al.* Nonpharmacologic Interventions to Heal Pressure Ulcers in Older Patients: An Overview of Systematic Reviews (The SENATOR-ONTOP Series). *J. Am. Med. Dir. Assoc.* 16, 448–469 (2015).
267. Reddy, M. Pressure ulcers. *BMJ Clin. Evid.* 2011, (2011).
268. Aziz, Z. & Cullum, N. Electromagnetic therapy for treating venous leg ulcers. *Cochrane Database Syst. Rev.* CD002933 (2015). doi:10.1002/14651858.CD002933.pub6
269. Sauer, H., Stanelle, R., Hescheler, J. & Wartenberg, M. The DC electrical-field-induced Ca(2+) response and growth stimulation of multicellular tumor spheroids are mediated by ATP release and purinergic receptor stimulation. 115, 3265–3273 (2002).
270. Pullar, C. E. & Isseroff, R. R. Cyclic AMP mediates keratinocyte directional migration in an electric field. 118, 2023–2034 (2005).
271. Zhao, M. Electrical stimulation directly induces pre-angiogenic responses in vascular endothelial cells by signaling through VEGF receptors. 117, 397–405 (2003).
272. Orida, N. & Poo, M. M. Electrophoretic movement and localisation of acetylcholine receptors in the embryonic muscle cell membrane. 275, 31–35 (1978).
273. McLaughlin, S. & Poo, M. M. The role of electro-osmosis in the electric-field-induced movement of charged macromolecules on the surfaces of cells. 34, 85–93 (1981).
274. Groves, J. T., Wülfing, C. & Boxer, S. G. Electrical manipulation of glycan-phosphatidyl inositol-tethered proteins in planar supported bilayers. 71, 2716–2723 (1996).
275. Han, X. *et al.* Manipulation and charge determination of proteins in photopatterned solid supported bilayers. 1, 205–211 (2009).
276. Daniel, S. *et al.* Separation of membrane-bound compounds by solid-supported bilayer electrophoresis. 129, 8072–8073 (2007).
277. Stelzle, M., Miehlich, R. & Sackmann, E. Two-dimensional microelectrophoresis in supported lipid bilayers. 63, 1346–1354 (1992).
278. Allen, G. M., Mogilner, A. & Theriot, J. A. Electrophoresis of Cellular Membrane Components Creates the Directional Cue Guiding Keratocyte Galvanotaxis. 23, 560–568 (2013).
279. Andreev, V. P. Cytoplasmic Electric Fields and Electroosmosis: Possible Solution for the Paradoxes of the Intracellular Transport of Biomolecules. 8, e61884 (2013).

280. Hart, F. X. Cytoskeletal forces produced by extremely low-frequency electric fields acting on extracellular glycoproteins. 31, 77–84 (2010).
281. Hart, F. X., Laird, M., Riding, A. & Pullar, C. E. Keratinocyte galvanotaxis in combined DC and AC electric fields supports an electromechanical transduction sensing mechanism. 34, 85–94 (2013).
282. Barry, P. H. & Hope, A. B. Electroosmosis in Membranes: Effects of Unstirred Layers and Transport Numbers. 9, 729–757 (1969).
283. Palese, P., Tobita, K., Ueda, M. & Compans, R. W. Characterization of temperature sensitive influenza virus mutants defective in neuraminidase. 61, 397–410 (1974).
284. Finkelstein, E. I., Chao, P. G., Hung, C. T. & Bulinski, J. C. Electric field-induced polarization of charged cell surface proteins does not determine the direction of galvanotaxis. 64, 833–846 (2007).
285. Hart, F. X. Integrins may serve as mechanical transducers for low-frequency electric fields. 27, 505–508 (2006).
286. Hart, F. X. The mechanical transduction of physiological strength electric fields. 29, 447–455 (2008).
287. Fabiato, A. & Fabiato, F. Calcium-induced release of calcium from the sarcoplasmic reticulum of skinned cells from adult human, dog, cat, rabbit, rat, and frog hearts and from fetal and new-born rat ventricles. *Ann. N. Y. Acad. Sci.* 307, 491–522 (1978).
288. Barlow, C. A., Rose, P., Pulver-Kaste, R. A. & Lounsbury, K. M. Excitation-transcription coupling in smooth muscle: Excitation-transcription coupling in smooth muscle. *J. Physiol.* 570, 59–64 (2006).
289. Gundersen, K. Excitation-transcription coupling in skeletal muscle: the molecular pathways of exercise. *Biol. Rev.* 86, 564–600 (2011).
290. Morgan, J. I. & Curran, T. Stimulus-Transcription Coupling in the Nervous System: Involvement of the Inducible Proto-Oncogenes *fos* and *jun*. *Annu. Rev. Neurosci.* 14, 421–451 (1991).
291. Levin, M., Pezzulo, G. & Finkelstein, J. M. Endogenous Bioelectric Signaling Networks: Exploiting Voltage Gradients for Control of Growth and Form. *Annu. Rev. Biomed. Eng.* 19, 353–387 (2017).
292. Levin, M. & Stevenson, C. G. Regulation of cell behavior and tissue patterning by bioelectrical signals: challenges and opportunities for biomedical engineering. *Annu. Rev. Biomed. Eng.* 14, 295–323 (2012).
293. Banks, T. A., Luckman, P. S. B., Frith, J. E. & Cooper-White, J. J. Effects of electric fields on human mesenchymal stem cell behaviour and morphology using a novel multichannel device. *Integr Biol* 7, 693–712 (2015).
294. Saha, R. N. & Dudek, S. M. Splitting Hares and Tortoises: A classification of neuronal immediate early gene transcription based on poised RNA polymerase II. *Neuroscience* 247, 175–181 (2013).
295. Jayaraman, R. Transcription of bacteriophage T4 DNA by Escherichia coli RNA polymerase in vitro: Identification of some immediate-early and delayed-early genes. *J. Mol. Biol.* 70, 253–263 (1972).

296. Park, J. A. & Koh, J.-Y. Induction of an Immediate Early Gene egr-1 by Zinc Through Extracellular Signal-Regulated Kinase Activation in Cortical Culture: Its Role in Zinc-Induced Neuronal Death. *J. Neurochem.* 73, 450–456 (2002).
297. Brennan, P. A., Hancock, D. & Keverne, E. B. The expression of the immediate-early genes c-fos, egr-1 and c-jun in the accessory olfactory bulb during the formation of an olfactory memory in mice. *Neuroscience* 49, 277–284 (1992).
298. Bahrami, S. & Drabløs, F. Gene regulation in the immediate-early response process. *Adv. Biol. Regul.* 62, 37–49 (2016).
299. Greer, P. L. & Greenberg, M. E. From Synapse to Nucleus: Calcium-Dependent Gene Transcription in the Control of Synapse Development and Function. *Neuron* 59, 846–860 (2008).
300. Murphy, T. H., Worley, P. F. & Baraban, J. M. L-type voltage-sensitive calcium channels mediate synaptic activation of immediate early genes. *Neuron* 7, 625–635 (1991).
301. Bading, H. *et al.* N-methyl-D-aspartate receptors are critical for mediating the effects of glutamate on intracellular calcium concentration and immediate early gene expression in cultured hippocampal neurons. *Neuroscience* 64, 653–664 (1995).
302. Reddien, P. W. SMEDWI-2 Is a PIWI-Like Protein That Regulates Planarian Stem Cells. *Science* 310, 1327–1330 (2005).
303. Randolph, H. Observations and experiments on regeneration in Planarians. *Arch. Für Entwicklungsmechanik Org.* 5, 352–372 (1897).
304. Guedelhoefer, O. C. & Alvarado, A. S. Amputation induces stem cell mobilization to sites of injury during planarian regeneration. *Development* 139, 3510–3520 (2012).
305. Eisenhoffer, G. T., Kang, H. & Alvarado, A. S. Molecular Analysis of Stem Cells and Their Descendants during Cell Turnover and Regeneration in the Planarian Schmidtea mediterranea. *Cell Stem Cell* 3, 327–339 (2008).
306. Zhu, S. J., Hallows, S. E., Currie, K. W., Xu, C. & Pearson, B. J. A mex3 homolog is required for differentiation during planarian stem cell lineage development. *eLife* 4, (2015).
307. Hayashi, T., Asami, M., Higuchi, S., Shibata, N. & Agata, K. Isolation of planarian X-ray-sensitive stem cells by fluorescence-activated cell sorting. *Dev. Growth Differ.* 48, 371–380 (2006).
308. Guo, T., Peters, A. H. F. M. & Newmark, P. A. A bruno-like Gene Is Required for Stem Cell Maintenance in Planarians. *Dev. Cell* 11, 159–169 (2006).
309. Labbé, R. M. *et al.* A comparative transcriptomic analysis reveals conserved features of stem cell pluripotency in planarians and mammals. *Stem Cells Dayt. Ohio* 30, 1734–1745 (2012).
310. Newmark, P. A. & Sánchez Alvarado, A. Bromodeoxyuridine Specifically Labels the Regenerative Stem Cells of Planarians. *Dev. Biol.* 220, 142–153 (2000).
311. Reddien, P. W. Specialized progenitors and regeneration. *Development* 140, 951–957 (2013).
312. Collins, J. J. *et al.* Adult somatic stem cells in the human parasite Schistosoma mansoni. *Nature* 494, 476–479 (2013).

313. Wagner, D. E., Wang, I. E. & Reddien, P. W. Clonogenic Neoblasts Are Pluripotent Adult Stem Cells That Underlie Planarian Regeneration. *Science* 332, 811–816 (2011).
314. Scimone, M. L., Kravarik, K. M., Lapan, S. W. & Reddien, P. W. Neoblast Specialization in Regeneration of the Planarian Schmidtea mediterranea. *Stem Cell Rep.* 3, 339–352 (2014).
315. Lapan, S. W. & Reddien, P. W. dlx and sp6-9 Control Optic Cup Regeneration in a Prototypic Eye. *PLoS Genet.* 7, e1002226 (2011).
316. Lapan, S. W. & Reddien, P. W. Transcriptome Analysis of the Planarian Eye Identifies ovo as a Specific Regulator of Eye Regeneration. *Cell Rep.* 2, 294–307 (2012).
317. van Wolfswinkel, J. C., Wagner, D. E. & Reddien, P. W. Single-cell analysis reveals functionally distinct classes within the planarian stem cell compartment. *Cell Stem Cell* 15, 326–339 (2014).
318. Barberán, S., Fraguas, S. & Cebrià, F. The EGFR signaling pathway controls gut progenitor differentiation during planarian regeneration and homeostasis. *Development* 143, 2089–2102 (2016).
319. Wurtzel, O. *et al.* A Generic and Cell-Type-Specific Wound Response Precedes Regeneration in Planarians. *Dev. Cell* 35, 632–645 (2015).
320. Scimone, M. L., Cote, L. E. & Reddien, P. W. Orthogonal muscle fibres have different instructive roles in planarian regeneration. *Nature* (2017). doi:10.1038/nature24660
321. Witchley, J. N., Mayer, M., Wagner, D. E., Owen, J. H. & Reddien, P. W. Muscle cells provide instructions for planarian regeneration. *Cell Rep.* 4, 633–641 (2013).
322. Beane, W. S., Morokuma, J., Adams, D. S. & Levin, M. A Chemical Genetics Approach Reveals H,K-ATPase-Mediated Membrane Voltage Is Required for Planarian Head Regeneration. *Chem. Biol.* 18, 77–89 (2011).
323. Marsh, G. & Beams, H. W. Electrical control of morphogenesis in regenerating Dugesia tigrina. I. Relation of axial polarity to field strength. *J. Cell. Physiol.* 39, 191–213 (1952).
324. Newmark, P. A. & Alvarado, A. S. NOT YOUR FATHER'S PLANARIAN: A CLASSIC MODEL ENTERS THE ERA OF FUNCTIONAL GENOMICS. *Nat. Rev. Genet.* 3, 210–219 (2002).
325. Rink, J. C. Stem cell systems and regeneration in planaria. *Dev. Genes Evol.* 223, 67–84 (2013).
326. Hill, E. M. & Petersen, C. P. Wnt/Notum spatial feedback inhibition controls neoblast differentiation to regulate reversible growth of the planarian brain. *Development* 142, 4217–4229 (2015).
327. Petersen, C. P. & Reddien, P. W. A wound-induced Wnt expression program controls planarian regeneration polarity. *Proc. Natl. Acad. Sci.* 106, 17061–17066 (2009).
328. Petersen, C. P. & Reddien, P. W. Polarized notum Activation at Wounds Inhibits Wnt Function to Promote Planarian Head Regeneration. *Science* 332, 852–855 (2011).

329. Scimone, M. L., Cote, L. E., Rogers, T. & Reddien, P. W. Two FGFRL-Wnt circuits organize the planarian anteroposterior axis. *eLife* 5, (2016).
330. Lander, R. & Petersen, C. P. Wnt, Ptk7, and FGFRL expression gradients control trunk positional identity in planarian regeneration. *eLife* 5, (2016).
331. Beane, W. S., Morokuma, J., Lemire, J. M. & Levin, M. Bioelectric signaling regulates head and organ size during planarian regeneration. *Development* 140, 313–322 (2013).
332. Lange, C. S. & Steele, V. E. The mechanism of anterior-posterior polarity control in planarians. *Differ. Res. Biol. Divers.* 11, 1–12 (1978).
333. Reid, B., Graue-Hernandez, E. O., Mannis, M. J. & Zhao, M. Modulating Endogenous Electric Currents in Human Corneal Wounds—A Novel Approach of Bioelectric Stimulation Without Electrodes: *Cornea* 30, 338–343 (2011).
334. Borgens, R. B., McGinnis, M. E., Vanable, J. W. & Miles, E. S. Stump currents in regenerating salamanders and newts. *J. Exp. Zool.* 231, 249–256 (1984).
335. Pietak, A. & Levin, M. Exploring Instructive Physiological Signaling with the Bioelectric Tissue Simulation Engine. *Front. Bioeng. Biotechnol.* 4, (2016).
336. Taghian, T., Narmoneva, D. A. & Kogan, A. B. Modulation of cell function by electric field: a high-resolution analysis. *J. R. Soc. Interface* 12, 20150153–20150153 (2015).
337. Esser, A. T., Smith, K. C., Weaver, J. C. & Levin, M. Mathematical model of morphogen electrophoresis through gap junctions. *Dev. Dyn.* 235, 2144–2159 (2006).
338. Cervera, J., Meseguer, S. & Mafe, S. The interplay between genetic and bioelectrical signaling permits a spatial regionalisation of membrane potentials in model multicellular ensembles. *Sci. Rep.* 6, (2016).
339. Nuccitelli, R. Physiological Electric Fields can Influence Cell Motility, Growth, and Polarity. *Adv. Mol. Cell Biol.* 2, 213–233 (1988).
340. Chiang, M. C., Cragoe, E. J. & Vanable, J. W. Intrinsic electric fields promote epithelization of wounds in the newt, Notophthalmus viridescens. *Dev. Biol.* 146, 377–385 (1991).
341. Chiang, M., Robinson, K. R. & Vanable, J. W. Electrical fields in the vicinity of epithelial wounds in the isolated bovine eye. *Exp. Eye Res.* 54, 999–1003 (1992).
342. Nuccitelli, R., Smart, T. & Ferguson, J. Protein kinases are required for embryonic neural crest cell galvanotaxis. *Cell Motil. Cytoskeleton* 24, 54–66 (1993).
343. Nuccitelli, R. & Smart, T. Extracellular Calcium Levels Strongly Influence Neural Crest Cell Galvanotaxis. 176, 130 (1989).
344. Zhao, M. *et al.* Electrical signals control wound healing through phosphatidylinositol-3-OH kinase-γ and PTEN. *Nature* 442, 457–460 (2006).
345. Erickson, C. A. & Nuccitelli, R. Embryonic fibroblast motility and orientation can be influenced by physiological electric fields. *J. Cell Biol.* 98, 296–307 (1984).
346. Eaglstein, W. H. & Falanga, V. Chronic wounds. *Surg. Clin. North Am.* 77, 689–700 (1997).
347. Singer, A. J. & Clark, R. A. Cutaneous wound healing. *N. Engl. J. Med.* 341, 738–746 (1999).

348. Reid, B., Song, B. & Zhao, M. Electric currents in Xenopus tadpole tail regeneration. *Dev. Biol.* 335, 198–207 (2009).
349. Reid, B. Wound healing in rat cornea: the role of electric currents. *FASEB J.* 19, 379–386 (2005).
350. Wang, E., Zhao, M., Forrester, J. V. & McCaig, C. D. Electric fields and MAP kinase signaling can regulate early wound healing in lens epithelium. *Invest. Ophthalmol. Vis. Sci.* 44, 244–249 (2003).
351. Meng, X. *et al.* PI3K mediated electrotaxis of embryonic and adult neural progenitor cells in the presence of growth factors. *Exp. Neurol.* 227, 210–217 (2011).
352. Sato, M. J. *et al.* Switching direction in electric-signal-induced cell migration by cyclic guanosine monophosphate and phosphatidylinositol signaling. *Proc. Natl. Acad. Sci. U. S. A.* 106, 6667–6672 (2009).
353. Pullar, C. E., Isseroff, R. R. & Nuccitelli, R. Cyclic AMP-dependent protein kinase A plays a role in the directed migration of human keratinocytes in a DC electric field. *Cell Motil. Cytoskeleton* 50, 207–217 (2001).
354. Huttenlocher, A. & Horwitz, A. R. Wound healing with electric potential. *N. Engl. J. Med.* 356, 303–304 (2007).
355. Kolsch, V., Charest, P. G. & Firtel, R. A. The regulation of cell motility and chemotaxis by phospholipid signaling. *J. Cell Sci.* 121, 551–559 (2008).
356. Eberle, M., Traynor-Kaplan, A. E., Sklar, L. A. & Norgauer, J. Is there a relationship between phosphatidylinositol trisphosphate and F-actin polymerization in human neutrophils? *J. Biol. Chem.* 265, 16725–16728 (1990).
357. Pullar, C. E. & Isseroff, R. R. Cyclic AMP mediates keratinocyte directional migration in an electric field. *J. Cell Sci.* 118, 2023–2034 (2005).
358. Wagner, D. E., Wang, I. E. & Reddien, P. W. Clonogenic Neoblasts Are Pluripotent Adult Stem Cells That Underlie Planarian Regeneration. *Science* 332, 811–816 (2011).
359. Wenemoser, D. & Reddien, P. W. Planarian regeneration involves distinct stem cell responses to wounds and tissue absence. *Dev. Biol.* 344, 979–991 (2010).
360. Morgan, T. H. Experimental studies of the regeneration of Planaria maculata. *Arch. Für Entwickelungsmechanik Org.* 7, 364–397 (1898).
361. Adell, T., Cebria, F. & Salo, E. Gradients in Planarian Regeneration and Homeostasis. *Cold Spring Harb. Perspect. Biol.* 2, a000505–a000505 (2010).
362. Wolff, E. & Dubois, F. Sur la migration des cellules de régénération chez les Planaires. *Rev. Suisse Zool.* 55, 218–227 (1948).
363. Reddien, P. W. SMEDWI-2 Is a PIWI-Like Protein That Regulates Planarian Stem Cells. *Science* 310, 1327–1330 (2005).
364. Palakodeti, D., Smielewska, M., Lu, Y.-C., Yeo, G. W. & Graveley, B. R. The PIWI proteins SMEDWI-2 and SMEDWI-3 are required for stem cell function and piRNA expression in planarians. *RNA* 14, 1174–1186 (2008).
365. Eisenhoffer, G. T., Kang, H. & Alvarado, A. S. Molecular Analysis of Stem Cells and Their Descendants during Cell Turnover and Regeneration in the Planarian Schmidtea mediterranea. *Cell Stem Cell* 3, 327–339 (2008).
366. Guedelhoefer, O. C. & Sánchez Alvarado, A. Planarian immobilization, partial irradiation, and tissue transplantation. *J. Vis. Exp. JoVE* (2012). doi:10.3791/4015

367. Reddien, P. W., Bermange, A. L., Murfitt, K. J., Jennings, J. R. & Sánchez Alvarado, A. Identification of Genes Needed for Regeneration, Stem Cell Function, and Tissue Homeostasis by Systematic Gene Perturbation in Planaria. *Dev. Cell* 8, 635–649 (2005).
368. Oviedo, N. J. *et al.* Long-range neural and gap junction protein-mediated cues control polarity during planarian regeneration. *Dev. Biol.* 339, 188–199 (2010).
369. Jenrow, K. A., Smith, C. H. & Liboff, A. R. Weak extremely-low-frequency magnetic field-induced regeneration anomalies in the planarian Dugesia tigrina. *Bioelectromagnetics* 17, 467–474 (1996).
370. Rand, H. W. & Browne, A. Inhibition of Regeneration in Planarians by Grafting: Technique of Grafting. *Proc. Natl. Acad. Sci. U. S. A.* 12, 575–581 (1926).
371. Coward, S. J. Planarian Regeneration. H. V. Brondsted. Pergamon, New York, 1969. viii + 280 pp. + plates. $13.50. International Series of Monographs in Pure and Applied Biology: Zoology, vol. 42. *Science* 167, 1117–1118 (1970).
372. Stevenson, C. G. & Beane, W. S. A Low Percent Ethanol Method for Immobilizing Planarians. *PLoS ONE* 5, e15310 (2010).
373. Agata, K. & Umesono, Y. Brain regeneration from pluripotent stem cells in planarian. *Philos. Trans. R. Soc. B Biol. Sci.* 363, 2071–2078 (2008).
374. Oviedo, N. J., Nicolas, C. L., Adams, D. S. & Levin, M. Live Imaging of Planarian Membrane Potential Using DiBAC4(3). *Cold Spring Harb. Protoc.* 2008, pdb.prot5055-pdb.prot5055 (2008).
375. Agata, K. *et al.* Structure of the planarian central nervous system (CNS) revealed by neuronal cell markers. *Zoolog. Sci.* 15, 433–440 (1998).
376. Collins, J. J. *et al.* Genome-Wide Analyses Reveal a Role for Peptide Hormones in Planarian Germline Development. *PLoS Biol.* 8, e1000509 (2010).
377. Chin, J. H. & Goldstein, D. B. Effects of low concentrations of ethanol on the fluidity of spin-labeled erythrocyte and brain membranes. *Mol. Pharmacol.* 13, 435–441 (1977).
378. Goldstein, D. B. & Chin, J. H. Interaction of ethanol with biological membranes. *Fed. Proc.* 40, 2073–2076 (1981).
379. Silveira, M. G., Baumgartner, M., Rombouts, F. M. & Abee, T. Effect of Adaptation to Ethanol on Cytoplasmic and Membrane Protein Profiles of Oenococcus oeni. *Appl. Environ. Microbiol.* 70, 2748–2755 (2004).
380. Harris, R. A. & Schroeder, F. Ethanol and the physical properties of brain membranes: fluorescence studies. *Mol. Pharmacol.* 20, 128–137 (1981).
381. Local and Regional Anesthesia, with Chapters on Spinal, Epidural, PARAVERTEBRAL, AND Parasacral Analgesia, AND on OTHER Applications of Local and Regional Anesthesia to the Surgery of the Eye, Ear, Nose and Throat, and to Dental Practice. *JAMA J. Am. Med. Assoc.* 71, 1243 (1918).
382. Sharma, B. K. *Analytical Chemistry: (Comprehensively Covering the UGC Syllabus)*. (Krishna Prakashan).
383. Paskin, T. R., Jellies, J., Bacher, J. & Beane, W. S. Planarian Phototactic Assay Reveals Differential Behavioral Responses Based on Wavelength. *PLoS ONE* 9, e114708 (2014).

384. Narayanan, J., Xiong, J.-Y. & Liu, X.-Y. Determination of agarose gel pore size: Absorbance measurements vis a vis other techniques. *J. Phys. Conf. Ser.* 28, 83–86 (2006).
385. Schantz, E. J. & Lauffer, M. A. Diffusion measurements in agar gel. *Biochemistry* 1, 658–663 (1962).
386. Davies, E. *et al.* Dynamics of water in agar gels studied using low and high resolution 1H NMR spectroscopy: Water relaxation and diffusion in agar gels. *Int. J. Food Sci. Technol.* 45, 2502–2507 (2010).
387. Currie, J. D. *et al.* Live Imaging of Axolotl Digit Regeneration Reveals Spatiotemporal Choreography of Diverse Connective Tissue Progenitor Pools. *Dev. Cell* 39, 411–423 (2016).
388. Kornblihtt, A. R. *et al.* Alternative splicing: a pivotal step between eukaryotic transcription and translation. *Nat. Rev. Mol. Cell Biol.* 14, 153–165 (2013).
389. Iborra, F. J. Coupled Transcription and Translation Within Nuclei of Mammalian Cells. *Science* 293, 1139–1142 (2001).
390. Jackson, R. J., Hellen, C. U. T. & Pestova, T. V. The mechanism of eukaryotic translation initiation and principles of its regulation. *Nat. Rev. Mol. Cell Biol.* 11, 113–127 (2010).
391. Eddy, S. R. Non-coding RNA genes and the modern RNA world. *Nat. Rev. Genet.* 2, 919–929 (2001).
392. Palazzo, A. F. & Lee, E. S. Non-coding RNA: what is functional and what is junk? *Front. Genet.* 6, 2 (2015).
393. Roeder, R. G. The complexities of eukaryotic transcription initiation: regulation of preinitiation complex assembly. *Trends Biochem. Sci.* 16, 402–408 (1991).
394. Black, D. L. Mechanisms of Alternative Pre-Messenger RNA Splicing. *Annu. Rev. Biochem.* 72, 291–336 (2003).
395. Keren, H., Lev-Maor, G. & Ast, G. Alternative splicing and evolution: diversification, exon definition and function. *Nat. Rev. Genet.* 11, 345–355 (2010).
396. Matera, A. G. & Wang, Z. A day in the life of the spliceosome. *Nat. Rev. Mol. Cell Biol.* 15, 108–121 (2014).
397. William Roy, S. & Gilbert, W. The evolution of spliceosomal introns: patterns, puzzles and progress. *Nat. Rev. Genet.* 7, 211–221 (2006).
398. Porrua, O. & Libri, D. Transcription termination and the control of the transcriptome: why, where and how to stop. *Nat. Rev. Mol. Cell Biol.* 16, 190–202 (2015).
399. Jonkers, I. & Lis, J. T. Getting up to speed with transcription elongation by RNA polymerase II. *Nat. Rev. Mol. Cell Biol.* 16, 167–177 (2015).
400. Abascal-Palacios, G., Ramsay, E. P., Beuron, F., Morris, E. & Vannini, A. Structural basis of RNA polymerase III transcription initiation. *Nature* 553, 301–306 (2018).
401. Krishnamurthy, S. & Hampsey, M. Eukaryotic transcription initiation. *Curr. Biol.* 19, R153–R156 (2009).
402. Lavut, A. & Raveh, D. Sequestration of Highly Expressed mRNAs in Cytoplasmic Granules, P-Bodies, and Stress Granules Enhances Cell Viability. *PLoS Genet.* 8, e1002527 (2012).
403. Aragon, A. D., Quiñones, G. A., Thomas, E. V., Roy, S. & Werner-Washburne, M. Release of extraction-resistant mRNA in stationary phase Saccharomyces

cerevisiae produces a massive increase in transcript abundance in response to stress. *Genome Biol.* 7, R9 (2006).
404. Hoyle, N. P. & Ashe, M. P. Subcellular localization of mRNA and factors involved in translation initiation. *Biochem. Soc. Trans.* 36, 648–652 (2008).
405. Anderson, P. & Kedersha, N. Stressful initiations. *J. Cell Sci.* 115, 3227–3234 (2002).
406. Kedersha, N. *et al.* Dynamic shuttling of TIA-1 accompanies the recruitment of mRNA to mammalian stress granules. *J. Cell Biol.* 151, 1257–1268 (2000).
407. Balagopal, V. & Parker, R. Polysomes, P bodies and stress granules: states and fates of eukaryotic mRNAs. *Curr. Opin. Cell Biol.* 21, 403–408 (2009).
408. Hoyle, N. P., Castelli, L. M., Campbell, S. G., Holmes, L. E. A. & Ashe, M. P. Stress-dependent relocalization of translationally primed mRNPs to cytoplasmic granules that are kinetically and spatially distinct from P-bodies. *J. Cell Biol.* 179, 65–74 (2007).
409. Parker, R. & Sheth, U. P Bodies and the Control of mRNA Translation and Degradation. *Mol. Cell* 25, 635–646 (2007).
410. Brengues, M. Movement of Eukaryotic mRNAs Between Polysomes and Cytoplasmic Processing Bodies. *Science* 310, 486–489 (2005).
411. Saha, R. N. *et al.* Rapid activity-induced transcription of Arc and other IEGs relies on poised RNA polymerase II. *Nat. Neurosci.* 14, 848–856 (2011).
412. Sorenson, R. & Bailey-Serres, J. Selective mRNA sequestration by OLIGOURIDYLATE-BINDING PROTEIN 1 contributes to translational control during hypoxia in *Arabidopsis*. *Proc. Natl. Acad. Sci.* 111, 2373–2378 (2014).
413. Merret, R. *et al.* Heat Shock Protein HSP101 Affects the Release of Ribosomal Protein mRNAs for Recovery after Heat Shock. *Plant Physiol.* 174, 1216–1225 (2017).
414. Herschman, H. R. Primary Response Genes Induced by Growth Factors and Tumor Promoters. *Annu. Rev. Biochem.* 60, 281–319 (1991).
415. Greenberg, M. E., Greene, L. A. & Ziff, E. B. Nerve growth factor and epidermal growth factor induce rapid transient changes in proto-oncogene transcription in PC12 cells. *J. Biol. Chem.* 260, 14101–14110 (1985).
416. Mulcahy, L. S., Smith, M. R. & Stacey, D. W. Requirement for ras proto-oncogene function during serum-stimulated growth of NIH 3T3 cells. *Nature* 313, 241–243 (1985).
417. Cochran, B. H., Reffel, A. C. & Stiles, C. D. Molecular cloning of gene sequences regulated by platelet-derived growth factor. *Cell* 33, 939–947 (1983).
418. Curran, T. & Morgan, J. I. Superinduction of c-fos by nerve growth factor in the presence of peripherally active benzodiazepines. *Science* 229, 1265–1268 (1985).
419. Curran, T., Bravo, R. & Müller, R. Transient induction of c-fos and c-myc in an immediate consequence of growth factor stimulation. *Cancer Surv.* 4, 655–681 (1985).
420. West, A. E. & Greenberg, M. E. Neuronal Activity-Regulated Gene Transcription in Synapse Development and Cognitive Function. *Cold Spring Harb. Perspect. Biol.* 3, a005744–a005744 (2011).

421. Kandel, E. R. The molecular biology of memory: cAMP, PKA, CRE, CREB-1, CREB-2, and CPEB. *Mol. Brain* 5, 14 (2012).
422. Minatohara, K., Akiyoshi, M. & Okuno, H. Role of Immediate-Early Genes in Synaptic Plasticity and Neuronal Ensembles Underlying the Memory Trace. *Front. Mol. Neurosci.* 8, 78 (2015).
423. Kim, T.-K. *et al.* Widespread transcription at neuronal activity-regulated enhancers. *Nature* 465, 182–187 (2010).
424. Wu, C.-H. *et al.* NELF and DSIF cause promoter proximal pausing on the hsp70 promoter in Drosophila. *Genes Dev.* 17, 1402–1414 (2003).
425. Peterlin, B. M. & Price, D. H. Controlling the elongation phase of transcription with P-TEFb. *Mol. Cell* 23, 297–305 (2006).
426. Helmchen, F., Imoto, K. & Sakmann, B. Ca2+ buffering and action potential-evoked Ca2+ signaling in dendrites of pyramidal neurons. *Biophys. J.* 70, 1069–1081 (1996).
427. Yuste, R. & Denk, W. Dendritic spines as basic functional units of neuronal integration. *Nature* 375, 682–684 (1995).
428. Schiller, J., Schiller, Y., Stuart, G. & Sakmann, B. Calcium action potentials restricted to distal apical dendrites of rat neocortical pyramidal neurons. *J. Physiol.* 505, 605–616 (1997).
429. Dolmetsch, R. Excitation-Transcription Coupling: Signaling by Ion Channels to the Nucleus. *Sci. Signal.* 2003, pe4–pe4 (2003).
430. Hardingham, G. E., Chawla, S., Johnson, C. M. & Bading, H. Distinct functions of nuclear and cytoplasmic calcium in the control of gene expression. *Nature* 385, 260–265 (1997).
431. Okamura, H. & Rao, A. Transcriptional regulation in lymphocytes. *Curr. Opin. Cell Biol.* 13, 239–243 (2001).
432. Wheeler, D. G., Barrett, C. F., Groth, R. D., Safa, P. & Tsien, R. W. CaMKII locally encodes L-type channel activity to signal to nuclear CREB in excitation–transcription coupling. *J. Cell Biol.* 183, 849–863 (2008).
433. Ma, H., Groth, R. D., Wheeler, D. G., Barrett, C. F. & Tsien, R. W. Excitation–transcription coupling in sympathetic neurons and the molecular mechanism of its initiation. *Neurosci. Res.* 70, 2–8 (2011).
434. Muller, C. S. *et al.* Quantitative proteomics of the Cav2 channel nano-environments in the mammalian brain. *Proc. Natl. Acad. Sci.* 107, 14950–14957 (2010).
435. Jenkins, M. A. *et al.* Ca2+-dependent facilitation of Cav1.3 Ca2+ channels by densin and Ca2+/calmodulin-dependent protein kinase II. *J. Neurosci. Off. J. Soc. Neurosci.* 30, 5125–5135 (2010).
436. Hudmon, A. *et al.* CaMKII tethers to L-type Ca2+ channels, establishing a local and dedicated integrator of Ca2+ signals for facilitation. *J. Cell Biol.* 171, 537–547 (2005).
437. Kovács, K. J. Invited review c-Fos as a transcription factor: a stressful (re)view from a functional map. *Neurochem. Int.* 33, 287–297 (1998).
438. Ch'ng, T. H. *et al.* Activity-Dependent Transport of the Transcriptional Coactivator CRTC1 from Synapse to Nucleus. *Cell* 150, 207–221 (2012).

439. Fang, M. *et al.* Evidence of EGR1 as a differentially expressed gene among proliferative skin diseases. *Genomic Med.* 1, 75–85 (2007).
440. Trinh, N.-T. *et al.* Increased Expression of EGR-1 in Diabetic Human Adipose Tissue-Derived Mesenchymal Stem Cells Reduces Their Wound Healing Capacity. *Stem Cells Dev.* 25, 760–773 (2016).
441. van den Akker, G. G. H. *et al.* EGR1 controls divergent cellular responses of distinctive nucleus pulposus cell types. *BMC Musculoskelet. Disord.* 17, 124 (2016).
442. Atar, D., Backx, P. H., Appel, M. M., Gao, W. D. & Marban, E. Excitation-Transcription Coupling Mediated by Zinc Influx through Voltage-dependent Calcium Channels. *J. Biol. Chem.* 270, 2473–2477 (1995).
443. Fahmy, R. G., Dass, C. R., Sun, L.-Q., Chesterman, C. N. & Khachigian, L. M. Transcription factor Egr-1 supports FGF-dependent angiogenesis during neovascularization and tumor growth. *Nat. Med.* 9, 1026–1032 (2003).
444. Tu, K. C. *et al. Egr-5* is a post-mitotic regulator of planarian epidermal differentiation. *eLife* 4, (2015).
445. Davis, S., Bozon, B. & Laroche, S. How necessary is the activation of the immediate early gene zif268 in synaptic plasticity and learning? *Behav. Brain Res.* 142, 17–30 (2003).
446. Cheng, L.-C. *et al.* Cellular, ultrastructural and molecular analyses of epidermal cell development in the planarian Schmidtea mediterranea. *Dev. Biol.* 433, 357–373 (2018).
447. Teves, S. S. & Henikoff, S. DNA torsion as a feedback mediator of transcription and chromatin dynamics. *Nucleus* 5, 211–218 (2014).
448. Ma, J., Bai, L. & Wang, M. D. Transcription Under Torsion. *Science* 340, 1580–1583 (2013).
449. Chow, L. T., Gelinas, R. E., Broker, T. R. & Roberts, R. J. An amazing sequence arrangement at the 5’ ends of adenovirus 2 messenger RNA. *Cell* 12, 1–8 (1977).
450. Berget, S. M., Moore, C. & Sharp, P. A. Spliced segments at the 5’ terminus of adenovirus 2 late mRNA. *Proc. Natl. Acad. Sci. U. S. A.* 74, 3171–3175 (1977).
451. Thomas, M., White, R. L. & Davis, R. W. Hybridization of RNA to double-stranded DNA: formation of R-loops. *Proc. Natl. Acad. Sci.* 73, 2294–2298 (1976).
452. Sollier, J. & Cimprich, K. A. Breaking bad: R-loops and genome integrity. *Trends Cell Biol.* 25, 514–522 (2015).
453. Bonnet, A. *et al.* Introns Protect Eukaryotic Genomes from Transcription-Associated Genetic Instability. *Mol. Cell* 67, 608-621.e6 (2017).
454. Bunch, H. *et al.* Transcriptional elongation requires DNA break-induced signalling. *Nat. Commun.* 6, 10191 (2015).
455. Madabhushi, R. *et al.* Activity-Induced DNA Breaks Govern the Expression of Neuronal Early-Response Genes. *Cell* 161, 1592–1605 (2015).
456. Zhao, M. *et al.* Electrical signals control wound healing through phosphatidylinositol-3-OH kinase-γ and PTEN. 442, 457–460 (2006).
457. Zhao, M., Dick, A., Forrester, J. V. & McCaig, C. D. Electric Field-directed Cell Motility Involves Up-regulated Expression and Asymmetric Redistribution of the Epidermal Growth Factor Receptors and Is Enhanced by Fibronectin and Laminin. *Mol. Biol. Cell* 10, 1259–1276 (1999).

458. Bai, H., Forrester, J. V. & Zhao, M. DC electric stimulation upregulates angiogenic factors in endothelial cells through activation of VEGF receptors. *Cytokine* 55, 110–115 (2011).
459. Sauer, H. *et al.* DC electrical field-induced c-fos expression and growth stimulation in multicellular prostate cancer spheroids. *Br. J. Cancer* 75, 1481–1488 (1997).
460. Jennings, J., Chen, D. & Feldman, D. Transcriptional response of dermal fibroblasts in direct current electric fields. *Bioelectromagnetics* 29, 394–405 (2008).
461. Hronik-Tupaj, M. & Kaplan, D. L. A Review of the Responses of Two- and Three-Dimensional Engineered Tissues to Electric Fields. *Tissue Eng. Part B Rev.* 18, 167–180 (2012).
462. Wartenberg, M., Hescheler, J. & Sauer, H. Electrical fields enhance growth of cancer spheroids by reactive oxygen species and intracellular Ca2+. *Am. J. Physiol.-Regul. Integr. Comp. Physiol.* 272, R1677–R1683 (1997).
463. Davis, S., Bozon, B. & Laroche, S. How necessary is the activation of the immediate early gene zif268 in synaptic plasticity and learning? *Behav. Brain Res.* 142, 17–30 (2003).
464. Chan, J. D., Zarowiecki, M. & Marchant, J. S. Ca^{2+} channels and praziquantel: a view from the free world. *Parasitol. Int.* 62, 619–628 (2013).
465. Tikhonov, D. B. & Zhorov, B. S. Structural model for dihydropyridine binding to L-type calcium channels. *J. Biol. Chem.* 284, 19006–19017 (2009).
466. Peterson, B. Z. *et al.* Analysis of the dihydropyridine receptor site of L-type calcium channels by alanine-scanning mutagenesis. *J. Biol. Chem.* 272, 18752–18758 (1997).
467. Lin, M., Aladejebi, O. & Hockerman, G. H. Distinct properties of amlodipine and nicardipine block of the voltage-dependent Ca2+ channels Cav1.2 and Cav2.1 and the mutant channels Cav1.2/dihydropyridine insensitive and Cav2.1/dihydropyridine sensitive. *Eur. J. Pharmacol.* 670, 105–113 (2011).
468. Nogi, T., Zhang, D., Chan, J. D. & Marchant, J. S. A Novel Biological Activity of Praziquantel Requiring Voltage-Operated Ca2+ Channel β Subunits: Subversion of Flatworm Regenerative Polarity. *PLoS Negl. Trop. Dis.* 3, e464 (2009).
469. Zhang, D., Chan, J. D., Nogi, T. & Marchant, J. S. Opposing Roles of Voltage-Gated Ca2+ Channels in Neuronal Control of Regenerative Patterning. *J. Neurosci.* 31, 15983–15995 (2011).
470. Chan, J. D. *et al.* Utilizing the planarian voltage-gated ion channel transcriptome to resolve a role for a Ca 2+ channel in neuromuscular function and regeneration. *Biochim. Biophys. Acta BBA - Mol. Cell Res.* 1864, 1036–1045 (2017).
471. Brennan, P. A., Hancock, D. & Keverne, E. B. The expression of the immediate-early genes c-fos, egr-1 and c-jun in the accessory olfactory bulb during the formation of an olfactory memory in mice. *Neuroscience* 49, 277–284 (1992).
472. Molnar, G., Crozat, A. & Pardee, A. B. The immediate-early gene Egr-1 regulates the activity of the thymidine kinase promoter at the G0-to-G1 transition of the cell cycle. *Mol. Cell. Biol.* 14, 5242–5248 (1994).
473. Ouellette, A. J., Malt, R. A., Sukhatme, V. P. & Bonventre, J. V. Expression of two 'immediate early' genes, Egr-1 and c-fos, in response to renal ischemia and during compensatory renal hypertrophy in mice. *J. Clin. Invest.* 85, 766–771 (1990).

474. Zhu, S. J. & Pearson, B. J. (Neo)blast from the past: new insights into planarian stem cell lineages. *Curr. Opin. Genet. Dev.* 40, 74–80 (2016).
475. Scimone, M. L., Kravarik, K. M., Lapan, S. W. & Reddien, P. W. Neoblast Specialization in Regeneration of the Planarian Schmidtea mediterranea. *Stem Cell Rep.* 3, 339–352 (2014).
476. Levin, M. Large-scale biophysics: ion flows and regeneration. *Trends Cell Biol.* 17, 261–270 (2007).
477. Wenemoser, D., Lapan, S. W., Wilkinson, A. W., Bell, G. W. & Reddien, P. W. A molecular wound response program associated with regeneration initiation in planarians. *Genes Dev.* 26, 988–1002 (2012).
478. Stewart, G. S., Wang, B., Bignell, C. R., Taylor, A. M. R. & Elledge, S. J. MDC1 is a mediator of the mammalian DNA damage checkpoint. *Nature* 421, 961–966 (2003).
479. Fernandez-Capetillo, O. *et al.* DNA damage-induced G2-M checkpoint activation by histone H2AX and 53BP1. *Nat. Cell Biol.* 4, 993–997 (2002).
480. Vermeulen, K., Van Bockstaele, D. R. & Berneman, Z. N. The cell cycle: a review of regulation, deregulation and therapeutic targets in cancer. *Cell Prolif.* 36, 131–149 (2003).
481. Peiris, T. H. *et al.* Regional signals in the planarian body guide stem cell fate in the presence of genomic instability. *Development* 143, 1697–1709 (2016).
482. Lei, K. *et al.* Egf Signaling Directs Neoblast Repopulation by Regulating Asymmetric Cell Division in Planarians. *Dev. Cell* 38, 413–429 (2016).
483. Wagner, D. E., Ho, J. J. & Reddien, P. W. Genetic regulators of a pluripotent adult stem cell system in planarians identified by RNAi and clonal analysis. *Cell Stem Cell* 10, 299–311 (2012).
484. Ahel, D. *et al.* Poly(ADP-ribose)-dependent regulation of DNA repair by the chromatin remodeling enzyme ALC1. *Science* 325, 1240–1243 (2009).
485. Mortusewicz, O., Amé, J.-C., Schreiber, V. & Leonhardt, H. Feedback-regulated poly(ADP-ribosyl)ation by PARP-1 is required for rapid response to DNA damage in living cells. *Nucleic Acids Res.* 35, 7665–7675 (2007).
486. Hinz, M. *et al.* A Cytoplasmic ATM-TRAF6-cIAP1 Module Links Nuclear DNA Damage Signaling to Ubiquitin-Mediated NF-κB Activation. *Mol. Cell* 40, 63–74 (2010).
487. Fonfria, E. *et al.* TRPM2 channel opening in response to oxidative stress is dependent on activation of poly(ADP-ribose) polymerase. *Br. J. Pharmacol.* 143, 186–192 (2004).
488. Masumoto, K., Tsukimoto, M. & Kojima, S. Role of TRPM2 and TRPV1 cation channels in cellular responses to radiation-induced DNA damage. *Biochim. Biophys. Acta BBA - Gen. Subj.* 1830, 3382–3390 (2013).
489. Bentle, M. S., Reinicke, K. E., Bey, E. A., Spitz, D. R. & Boothman, D. A. Calcium-dependent Modulation of Poly(ADP-ribose) Polymerase-1 Alters Cellular Metabolism and DNA Repair. *J. Biol. Chem.* 281, 33684–33696 (2006).
490. Kerfant, B.-G. *et al.* Altered Nuclear Calcium Signaling in Tachycardia-Induced Remodeling in Rabbit Atria: A Mechanism of Altered Excitation-Transcription Coupling in Atrial Fibrillation? *Biophys. J.* 100, 517a (2011).

491. Cobbett, P. & Day, T. A. Functional voltage-gated Ca2+ channels in muscle fibers of the platyhelminth Dugesia tigrina. *Comp. Biochem. Physiol. A. Mol. Integr. Physiol.* 134, 593–605 (2003).
492. Hanahan, D. & Weinberg, R. A. The Hallmarks of Cancer. *Cell* 100, 57–70 (2000).
493. Pajonk, F., Vlashi, E. & McBride, W. H. Radiation resistance of cancer stem cells: the 4 R's of radiobiology revisited. *Stem Cells Dayt. Ohio* 28, 639–648 (2010).
494. Huber, S. M. *et al.* Role of ion channels in ionizing radiation-induced cell death. *Biochim. Biophys. Acta* 1848, 2657–2664 (2015).
495. Heise, N. *et al.* Non-selective cation channel-mediated Ca2+-entry and activation of Ca2+/calmodulin-dependent kinase II contribute to G2/M cell cycle arrest and survival of irradiated leukemia cells. *Cell. Physiol. Biochem. Int. J. Exp. Cell. Physiol. Biochem. Pharmacol.* 26, 597–608 (2010).
496. Kühn, F. J. P., Heiner, I. & Lückhoff, A. TRPM2: a calcium influx pathway regulated by oxidative stress and the novel second messenger ADP-ribose. *Pflugers Arch.* 451, 212–219 (2005).
497. Perraud, A.-L. *et al.* Accumulation of Free ADP-ribose from Mitochondria Mediates Oxidative Stress-induced Gating of TRPM2 Cation Channels. *J. Biol. Chem.* 280, 6138–6148 (2005).
498. Orfanelli, U. *et al.* Identification of novel sense and antisense transcription at the TRPM2 locus in cancer. *Cell Res.* 18, 1128–1140 (2008).
499. Scully, R. & Xie, A. Double strand break repair functions of histone H2AX. *Mutat. Res.* 750, 5–14 (2013).
500. Palme, D. *et al.* Kv3.4 potassium channel-mediated electrosignaling controls cell cycle and survival of irradiated leukemia cells. *Pflüg. Arch. - Eur. J. Physiol.* 465, 1209–1221 (2013).
501. Aten, J. A. *et al.* Dynamics of DNA double-strand breaks revealed by clustering of damaged chromosome domains. *Science* 303, 92–95 (2004).
502. Stucki, M. & Jackson, S. P. gammaH2AX and MDC1: anchoring the DNA-damage-response machinery to broken chromosomes. *DNA Repair* 5, 534–543 (2006).
503. Rogakou, E. P., Pilch, D. R., Orr, A. H., Ivanova, V. S. & Bonner, W. M. DNA double-stranded breaks induce histone H2AX phosphorylation on serine 139. *J. Biol. Chem.* 273, 5858–5868 (1998).
504. Carney, J. P. *et al.* The hMre11/hRad50 protein complex and Nijmegen breakage syndrome: linkage of double-strand break repair to the cellular DNA damage response. *Cell* 93, 477–486 (1998).
505. Nakamura, T. M., Du, L.-L., Redon, C. & Russell, P. Histone H2A phosphorylation controls Crb2 recruitment at DNA breaks, maintains checkpoint arrest, and influences DNA repair in fission yeast. *Mol. Cell. Biol.* 24, 6215–6230 (2004).
506. Keogh, M.-C. *et al.* A phosphatase complex that dephosphorylates gammaH2AX regulates DNA damage checkpoint recovery. *Nature* 439, 497–501 (2006).
507. Rossi, L. *et al.* Insight into stem cell regulation from sub-lethally irradiated worms. *Gene* 662, 37–45 (2018).
508. Sperka, T., Wang, J. & Rudolph, K. L. DNA damage checkpoints in stem cells, ageing and cancer. *Nat. Rev. Mol. Cell Biol.* 13, 579–590 (2012).
509. Schafer, K. A. The Cell Cycle: A Review. *Vet. Pathol.* 35, 461–478 (1998).

510. Tyson, J. J., Csikasz-Nagy, A. & Novak, B. The dynamics of cell cycle regulation. *BioEssays* 24, 1095–1109 (2002).
511. Soto-Cerrato, V. *et al.* Facilitated Anion Transport Induces Hyperpolarization of the Cell Membrane That Triggers Differentiation and Cell Death in Cancer Stem Cells. *J. Am. Chem. Soc.* 137, 15892–15898 (2015).
512. Barghouth, P. G., Thiruvalluvan, M. & Oviedo, N. J. Bioelectrical regulation of cell cycle and the planarian model system. *Biochim. Biophys. Acta BBA - Biomembr.* 1848, 2629–2637 (2015).
513. Cone, C. D. & Cone, C. M. Induction of mitosis in mature neurons in central nervous system by sustained depolarization. *Science* 192, 155–158 (1976).
514. Cone, C. D. & Tongier, M. Contact inhibition of division: involvement of the electrical transmembrane potential. *J. Cell. Physiol.* 82, 373–386 (1973).
515. Cone, C. D. Unified theory on the basic mechanism of normal mitotic control and oncogenesis. *J. Theor. Biol.* 30, 151–181 (1971).
516. Ouadid-Ahidouch, H. & Ahidouch, A. K+ Channel Expression in Human Breast Cancer Cells: Involvement in Cell Cycle Regulation and Carcinogenesis. *J. Membr. Biol.* 221, 1–6 (2008).
517. MacFarlane, S. N. & Sontheimer, H. Changes in ion channel expression accompany cell cycle progression of spinal cord astrocytes. *Glia* 30, 39–48 (2000).
518. Morgan, D. O. Cyclin-dependent kinases: engines, clocks, and microprocessors. *Annu. Rev. Cell Dev. Biol.* 13, 261–291 (1997).
519. Mercer, W. E. Checking on the cell cycle. *J. Cell. Biochem. Suppl.* 30–31, 50–54 (1998).
520. Fischer, M. & Müller, G. A. Cell cycle transcription control: DREAM/MuvB and RB-E2F complexes. *Crit. Rev. Biochem. Mol. Biol.* 52, 638–662 (2017).
521. Goodrich, D. W., Wang, N. P., Qian, Y. W., Lee, E. Y. & Lee, W. H. The retinoblastoma gene product regulates progression through the G1 phase of the cell cycle. *Cell* 67, 293–302 (1991).
522. Frolov, M. V. & Dyson, N. J. Molecular mechanisms of E2F-dependent activation and pRB-mediated repression. *J. Cell Sci.* 117, 2173–2181 (2004).
523. Wu, C. L., Zukerberg, L. R., Ngwu, C., Harlow, E. & Lees, J. A. In vivo association of E2F and DP family proteins. *Mol. Cell. Biol.* 15, 2536–2546 (1995).
524. Zhang, Y., Venkatraj, V. S., Fischer, S. G., Warburton, D. & Chellappan, S. P. Genomic cloning and chromosomal assignment of the E2F dimerization partner TFDP gene family. *Genomics* 39, 95–98 (1997).
525. Saló, E. & Baguñà, J. Cell movement in intact and regenerating planarians. Quantitation using chromosomal, nuclear and cytoplasmic markers. *J. Embryol. Exp. Morphol.* 89, 57 (1985).
526. Halazonetis, T. D., Gorgoulis, V. G. & Bartek, J. An Oncogene-Induced DNA Damage Model for Cancer Development. *Science* 319, 1352–1355 (2008).
527. Phillips, D. H., Hewer, A., Martin, C. N., Garner, R. C. & King, M. M. Correlation of DNA adduct levels in human lung with cigarette smoking. *Nature* 336, 790–792 (1988).
528. Ciccia, A. & Elledge, S. J. The DNA damage response: making it safe to play with knives. *Mol. Cell* 40, 179–204 (2010).

529. Bartkova, J. *et al.* Oncogene-induced senescence is part of the tumorigenesis barrier imposed by DNA damage checkpoints. *Nature* 444, 633–637 (2006).
530. d'Adda di Fagagna, F. Living on a break: cellular senescence as a DNA-damage response. *Nat. Rev. Cancer* 8, 512–522 (2008).
531. Pazolli, E. & Stewart, S. A. Senescence: the good the bad and the dysfunctional. *Curr. Opin. Genet. Dev.* 18, 42–47 (2008).
532. Lord, C. J. & Ashworth, A. The DNA damage response and cancer therapy. *Nature* 481, 287–294 (2012).
533. Medema, J. P. Escape from senescence boosts tumour growth. *Nature* 553, 37–38 (2018).
534. Yang, L., Fang, J. & Chen, J. Tumor cell senescence response produces aggressive variants. *Cell Death Discov.* 3, 17049 (2017).
535. Pellettieri, J. *et al.* Cell death and tissue remodeling in planarian regeneration. *Dev. Biol.* 338, 76–85 (2010).
536. Peiris, T. H., García-Ojeda, M. E. & Oviedo, N. J. Alternative flow cytometry strategies to analyze stem cells and cell death in planarians. *Regen. Oxf. Engl.* 3, 123–135 (2016).
537. Lansu, K. & Gentile, S. Potassium channel activation inhibits proliferation of breast cancer cells by activating a senescence program. *Cell Death Dis.* 4, e652–e652 (2013).
538. Nuccitelli, R. *et al.* Optimized nanosecond pulsed electric field therapy can cause murine malignant melanomas to self-destruct with a single treatment. *Int. J. Cancer* 127, 1727–1736 (2010).
539. Stacey, M. *et al.* Differential effects in cells exposed to ultra-short, high intensity electric fields: cell survival, DNA damage, and cell cycle analysis. *Mutat. Res. Toxicol. Environ. Mutagen.* 542, 65–75 (2003).
540. Nuccitelli, R. *et al.* Nanosecond pulsed electric fields cause melanomas to self-destruct. *Biochem. Biophys. Res. Commun.* 343, 351–360 (2006).
541. Mah, L.-J., El-Osta, A. & Karagiannis, T. C. gammaH2AX: a sensitive molecular marker of DNA damage and repair. *Leukemia* 24, 679–686 (2010).
542. D'Arco, M. & Dolphin, A. C. L-type calcium channels: on the fast track to nuclear signaling. *Sci. Signal.* 5, pe34 (2012).
543. Mazina, O. M. & Mazin, A. V. Human Rad54 protein stimulates DNA strand exchange activity of hRad51 protein in the presence of Ca2+. *J. Biol. Chem.* 279, 52042–52051 (2004).
544. Bugreev, D. V. & Mazin, A. V. Ca2+ activates human homologous recombination protein Rad51 by modulating its ATPase activity. *Proc. Natl. Acad. Sci.* 101, 9988–9993 (2004).
545. Sakai, H. *et al.* Intracellular Ca2+ concentration change of T24 cell under irradiation in the presence of TiO2 ultrafine particles. *Biochim. Biophys. Acta* 1201, 259–265 (1994).
546. Gafter, U., Malachi, T., Ori, Y. & Breitbart, H. The role of calcium in human lymphocyte DNA repair ability. *J. Lab. Clin. Med.* 130, 33–41 (1997).

547. Spielberg, H. *et al.* UV irradiation of lymphocytes triggers an increase in intracellular Ca2+ and prevents lectin-stimulated Ca2+ mobilization: evidence for UV- and nifedipine-sensitive Ca2+ channels. *Exp. Hematol.* 19, 742–748 (1991).
548. Ristic, D. *et al.* Human Rad51 filaments on double- and single-stranded DNA: correlating regular and irregular forms with recombination function. *Nucleic Acids Res.* 33, 3292–3302 (2005).
549. Petukhova, G., Stratton, S. & Sung, P. Catalysis of homologous DNA pairing by yeast Rad51 and Rad54 proteins. *Nature* 393, 91–94 (1998).
550. Petukhova, G., Van Komen, S., Vergano, S., Klein, H. & Sung, P. Yeast Rad54 promotes Rad51-dependent homologous DNA pairing via ATP hydrolysis-driven change in DNA double helix conformation. *J. Biol. Chem.* 274, 29453–29462 (1999).
551. Liu, C., Vyas, A., Kassab, M. A., Singh, A. K. & Yu, X. The role of poly ADP-ribosylation in the first wave of DNA damage response. *Nucleic Acids Res.* 45, 8129–8141 (2017).
552. Yamanaka, H., Penning, C. A., Willis, E. H., Wasson, D. B. & Carson, D. A. Characterization of human poly(ADP-ribose) polymerase with autoantibodies. *J. Biol. Chem.* 263, 3879–3883 (1988).
553. Ludwig, A., Behnke, B., Holtlund, J. & Hilz, H. Immunoquantitation and size determination of intrinsic poly(ADP-ribose) polymerase from acid precipitates. An analysis of the in vivo status in mammalian species and in lower eukaryotes. *J. Biol. Chem.* 263, 6993–6999 (1988).
554. Barton, M. B. *et al.* Estimating the demand for radiotherapy from the evidence: A review of changes from 2003 to 2012. *Radiother. Oncol.* 112, 140–144 (2014).
555. Barton, M. B., Frommer, M. & Shafiq, J. Role of radiotherapy in cancer control in low-income and middle-income countries. *Lancet Oncol.* 7, 584–595 (2006).
556. Shahidi, M., Mozdarani, H. & Mueller, W.-U. Radiosensitivity and repair kinetics of gamma-irradiated leukocytes from sporadic prostate cancer patients and healthy individuals assessed by alkaline comet assay. *Iran. Biomed. J.* 14, 67–75 (2010).
557. Shahidi, M., Mozdarani, H. & Bryant, P. E. Radiation sensitivity of leukocytes from healthy individuals and breast cancer patients as measured by the alkaline and neutral comet assay. *Cancer Lett.* 257, 263–273 (2007).
558. Mohseni-Meybodi, A., Mozdarani, H. & Mozdarani, S. DNA damage and repair of leukocytes from Fanconi anaemia patients, carriers and healthy individuals as measured by the alkaline comet assay. *Mutagenesis* 24, 67–73 (2009).
559. McCaig, C. D. & Rajnicek, A. M. Electrical fields, nerve growth and nerve regeneration. *Exp. Physiol.* 76, 473–494 (1991).
560. Zhao, M., Forrester, J. V. & McCaig, C. D. A small, physiological electric field orients cell division. *Proc. Natl. Acad. Sci.* 96, 4942–4946 (1999).
561. Gonzalez, A. C. de O., Costa, T. F., Andrade, Z. de A. & Medrado, A. R. A. P. Wound healing - A literature review. *An. Bras. Dermatol.* 91, 614–620 (2016).
562. Lim, J.-H., McCullen, S. D., Piedrahita, J. A., Loboa, E. G. & Olby, N. J. Alternating Current Electric Fields of Varying Frequencies: Effects on Proliferation and Differentiation of Porcine Neural Progenitor Cells. *Cell. Reprogramming* 15, 405–412 (2013).

563. Maziarz, A. *et al.* How electromagnetic fields can influence adult stem cells: positive and negative impacts. *Stem Cell Res. Ther.* 7, (2016).
564. Zhao, M. Electrical fields in wound healing—An overriding signal that directs cell migration. *Semin. Cell Dev. Biol.* 20, 674–682 (2009).
565. Wang, E. Physiological electric fields control the G1/S phase cell cycle checkpoint to inhibit endothelial cell proliferation. *FASEB J.* (2003). doi:10.1096/fj.02-0510fje
566. Sebastian, A., Iqbal, S. A., Colthurst, J., Volk, S. W. & Bayat, A. Electrical Stimulation Enhances Epidermal Proliferation in Human Cutaneous Wounds by Modulating p53–SIVA1 Interaction. *J. Invest. Dermatol.* 135, 1166–1174 (2015).
567. Morris, E. J. & Dyson, N. J. Retinoblastoma protein partners. *Adv. Cancer Res.* 82, 1–54 (2001).
568. Boynton, A. L., Whitfield, J. F., Isaacs, R. J. & Tremblay, R. G. Different extracellular calcium requirements for proliferation of nonneoplastic, preneoplastic, and neoplastic mouse cells. *Cancer Res.* 37, 2657–2661 (1977).
569. Boynton, A. L., Whitfield, J. F., Isaacs, R. J. & Tremblay, R. The control of human WI-38 cell proliferation by extracellular calcium and its elimination by SV-40 virus-induced proliferative transformation. *J. Cell. Physiol.* 92, 241–247 (1977).
570. Berridge, M. J. Calcium signalling and cell proliferation. *BioEssays News Rev. Mol. Cell. Dev. Biol.* 17, 491–500 (1995).
571. Santella, L. The role of calcium in the cell cycle: facts and hypotheses. *Biochem. Biophys. Res. Commun.* 244, 317–324 (1998).
572. Piõl, M. R., Berchtold, M. W., Bachs, O. & Heizmann, C. W. Increased calmodulin synthesis in the pre-replicative phase of rat liver regeneration. *FEBS Lett.* 231, 445–450 (1988).
573. Rasmussen, C. D., Means, R. L., Lu, K. P., May, G. S. & Means, A. R. Characterization and expression of the unique calmodulin gene of Aspergillus nidulans. *J. Biol. Chem.* 265, 13767–13775 (1990).
574. Peiris, T. H. *et al.* TOR signaling regulates planarian stem cells and controls localized and organismal growth. *J. Cell Sci.* 125, 1657–1665 (2012).
575. Oviedo, N. J., Pearson, B. J., Levin, M. & Sanchez Alvarado, A. Planarian PTEN homologs regulate stem cells and regeneration through TOR signaling. *Dis. Model. Mech.* 1, 131–143 (2008).
576. Sánchez Alvarado, A. Stem cells and the Planarian Schmidtea mediterranea. *C. R. Biol.* 330, 498–503 (2007).
577. Newmark, P. A. & Sánchez Alvarado, A. Bromodeoxyuridine Specifically Labels the Regenerative Stem Cells of Planarians. *Dev. Biol.* 220, 142–153 (2000).
578. Reddien, P. W. Specialized progenitors and regeneration. *Development* 140, 951–957 (2013).
579. Reid, B., Song, B. & Zhao, M. Electric currents in Xenopus tadpole tail regeneration. *Dev. Biol.* 335, 198–207 (2009).
580. Zhang, J. *et al.* Electrically guiding migration of human induced pluripotent stem cells. 7, 987–996 (2011).
581. Nuccitelli, R. A role for endogenous electric fields in wound healing. 58, 1–26 (2003).
582. Nuccitelli, R. Physiological Electric Fields can Influence Cell Motility, Growth, and Polarity. *Adv. Mol. Cell Biol.* 2, 213–233 (1988).

583. Erickson, C. A. & Nuccitelli, R. Embryonic fibroblast motility and orientation can be influenced by physiological electric fields. *J. Cell Biol.* 98, 296–307 (1984).
584. Chiang, M. C., Cragoe, E. J. & Vanable, J. W. Intrinsic electric fields promote epithelization of wounds in the newt, Notophthalmus viridescens. *Dev. Biol.* 146, 377–385 (1991).
585. Marsh, G. & Beams, H. W. Electrical control of morphogenesis in regenerating Dugesia tigrina. I. Relation of axial polarity to field strength. *J. Cell. Physiol.* 39, 191–213 (1952).
586. Beane, W. S., Morokuma, J., Adams, D. S. & Levin, M. A Chemical Genetics Approach Reveals H,K-ATPase-Mediated Membrane Voltage Is Required for Planarian Head Regeneration. *Chem. Biol.* 18, 77–89 (2011).
587. Tseng, A.-S., Beane, W. S., Lemire, J. M., Masi, A. & Levin, M. Induction of Vertebrate Regeneration by a Transient Sodium Current. *J. Neurosci.* 30, 13192–13200 (2010).
588. BAGUNA, J. Mitosis in the Intact and Regenerating Planarian Dugesia mediterranea n.sp. *J. Exp. Zoöl.* 195, 53–64 (1976).
589. Pai, V. P. *et al.* HCN2 Rescues brain defects by enforcing endogenous voltage pre-patterns. *Nat. Commun.* 9, (2018).
590. Moore, D., Walker, S. I. & Levin, M. Cancer as a disorder of patterning information: computational and biophysical perspectives on the cancer problem. *Converg. Sci. Phys. Oncol.* 3, 043001 (2017).
591. Mossop, B. J., Barr, R. C., Zaharoff, D. A. & Yuan, F. Electric fields within cells as a function of membrane resistivity–a model study. 3, 225–231 (2004).
592. Miranda, P. C., Lomarev, M. & Hallett, M. Modeling the current distribution during transcranial direct current stimulation. *Clin. Neurophysiol.* 117, 1623–1629 (2006).
593. Holdefer, R. N., Sadleir, R. & Russell, M. J. Predicted current densities in the brain during transcranial electrical stimulation. *Clin. Neurophysiol.* 117, 1388–1397 (2006).
594. Wagner, T. *et al.* Transcranial direct current stimulation: A computer-based human model study. *NeuroImage* 35, 1113–1124 (2007).
595. Wenemoser, D. & Reddien, P. W. Planarian regeneration involves distinct stem cell responses to wounds and tissue absence. *Dev. Biol.* 344, 979–991 (2010).
596. Liu, Q. & Song, B. Electric field regulated signaling pathways. *Int. J. Biochem. Cell Biol.* 55, 264–268 (2014).
597. Hay, J. G. & Geddes, D. M. Transepithelial potential difference in cystic fibrosis. 40, 493–496 (1985).
598. Clausell, M., Fang, Z. & Chen, W. In Vivo Study of Transepithelial Potential Difference (TEPD) in Proximal Convoluted Tubules of Rat Kidney by Synchronization Modulation Electric Field. 247, 601–609 (2014).
599. Dietz, T. H., Kirschner, L. B. & Porter, D. The roles of sodium transport and anion permeability in generating transepithelial potential differences in larval salamanders. 46, 85–96 (1967).
600. Huttenlocher, A. & Horwitz, A. R. Wound healing with electric potential. 356, 303–304 (2007).

601. Singer, A. J. & Clark, R. A. Cutaneous wound healing. *N. Engl. J. Med.* 341, 738–746 (1999).
602. Koley, D. & Bard, A. J. Triton X-100 concentration effects on membrane permeability of a single HeLa cell by scanning electrochemical microscopy (SECM). *Proc. Natl. Acad. Sci.* 107, 16783–16787 (2010).
603. Loew, L. M. Design and Use of Organic Voltage Sensitive Dyes. in *Membrane Potential Imaging in the Nervous System* (eds. Canepari, M. & Zecevic, D.) 13–23 (Springer New York, 2010). doi:10.1007/978-1-4419-6558-5_2
604. Aguilar-Sanchez, Y., Fainstein, D., Mejia-Alvarez, R. & Escobar, A. L. Local Field Fluorescence Microscopy: Imaging Cellular Signals in Intact Hearts. *J. Vis. Exp.* (2017). doi:10.3791/55202
605. Borgens, R. B., Vanable, J. W. & Jaffe, L. F. Bioelectricity and regeneration: large currents leave the stumps of regenerating newt limbs. *Proc. Natl. Acad. Sci.* 74, 4528–4532 (1977).
606. Zuberi, M., Liu-Snyder, P., ul Haque, A., Porterfield, D. M. & Borgens, R. B. Large naturally-produced electric currents and voltage traverse damaged mammalian spinal cord. *J. Biol. Eng.* 2, 17 (2008).
607. Borgens, R. B., Jaffe, L. F. & Cohen, M. J. Large and persistent electrical currents enter the transected lamprey spinal cord. *Proc. Natl. Acad. Sci. U. S. A.* 77, 1209–1213 (1980).
608. Depenbusch, J. W., Bricker, C. S., Bennett, J. L. & Pax, R. A. Effect of Triton X-100 on tegument and muscle in Schistosoma mansoni. *J. Parasitol.* 68, 884–891 (1982).
609. Heerklotz, H. Interactions of surfactants with lipid membranes. *Q. Rev. Biophys.* 41, 205 (2008).
610. Vaidyanathan, S., Orr, B. G. & Banaszak Holl, M. M. Detergent Induction of HEK 293A Cell Membrane Permeability Measured under Quiescent and Superfusion Conditions Using Whole Cell Patch Clamp. *J. Phys. Chem. B* 118, 2112–2123 (2014).
611. Ahyayauch, H., Bennouna, M., Alonso, A. & Goñi, F. M. Detergent Effects on Membranes at Subsolubilizing Concentrations: Transmembrane Lipid Motion, Bilayer Permeabilization, and Vesicle Lysis/Reassembly Are Independent Phenomena. *Langmuir* 26, 7307–7313 (2010).
612. Herzyk, E. & Minc, S. Modification of human erythrocyte membrane potentials by the action of the polyoxyethylene detergent Triton X-100. *Bioelectrochem. Bioenerg.* 15, 7–18 (1986).
613. Grossmann, G., Opekarová, M., Malinsky, J., Weig-Meckl, I. & Tanner, W. Membrane potential governs lateral segregation of plasma membrane proteins and lipids in yeast. *EMBO J.* 26, 1–8 (2007).
614. Kishimoto, U. Effect of Detergent on Electrical Properties of Squid Axon Membrane. *J. Gen. Physiol.* 47, 975–986 (1964).
615. Wasano, T., Ogata, M. & Goto, M. THE EFFECT OF SURFACE-ACTIVE AGENTS ON THE RESTING POTENTIAL OF MUSCLE. *Jpn. J. Physiol.* 6, 137–149 (1956).
616. Narang, D. *et al.* Triton X-100 inhibits L-type voltage-operated calcium channels. *Can. J. Physiol. Pharmacol.* 91, 316–324 (2013).

617. Ottoson, D. & Rydqvist, B. The effects of Triton-detergents on the stretch receptor of the crayfish. *Acta Physiol. Scand.* 103, 9–18 (1978).
618. Søgaard, R., Ebert, B., Klaerke, D. & Werge, T. Triton x-100 inhibits agonist-induced currents and suppresses benzodiazepine modulation of GABAA receptors in Xenopus oocytes. *Biochim. Biophys. Acta BBA - Biomembr.* 1788, 1073–1080 (2009).
619. Søgaard, R. *et al.* GABA(A) receptor function is regulated by lipid bilayer elasticity. *Biochemistry* 45, 13118–13129 (2006).
620. Hunckler, J. & de Mel, A. A current affair: electrotherapy in wound healing. *J. Multidiscip. Healthc.* 10, 179–194 (2017).
621. Pittenger, M. F. Multilineage Potential of Adult Human Mesenchymal Stem Cells. *Science* 284, 143–147 (1999).
622. Titushkin, I., Sun, S., Shin, J. & Cho, M. Physicochemical Control of Adult Stem Cell Differentiation: Shedding Light on Potential Molecular Mechanisms. *J. Biomed. Biotechnol.* 2010, 1–14 (2010).
623. Hronik-Tupaj, M., Rice, W. L., Cronin-Golomb, M., Kaplan, D. L. & Georgakoudi, I. Osteoblastic differentiation and stress response of human mesenchymal stem cells exposed to alternating current electric fields. *Biomed. Eng. OnLine* 10, 9 (2011).
624. McLeod, K. J. & Rubin, C. T. The effect of low-frequency electrical fields on osteogenesis. *J. Bone Joint Surg. Am.* 74, 920–929 (1992).
625. Titushkin, I. & Cho, M. Regulation of cell cytoskeleton and membrane mechanics by electric field: role of linker proteins. *Biophys. J.* 96, 717–728 (2009).
626. Hronik-Tupaj, M., Rice, W. L., Cronin-Golomb, M., Kaplan, D. L. & Georgakoudi, I. Osteoblastic differentiation and stress response of human mesenchymal stem cells exposed to alternating current electric fields. *Biomed. Eng. OnLine* 10, 9 (2011).
627. Aaron, R. K., Boyan, B. D., Ciombor, D. M., Schwartz, Z. & Simon, B. J. Stimulation of growth factor synthesis by electric and electromagnetic fields. *Clin. Orthop.* 30–37 (2004).
628. Sun, S., Liu, Y., Lipsky, S. & Cho, M. Physical manipulation of calcium oscillations facilitates osteodifferentiation of human mesenchymal stem cells. *FASEB J. Off. Publ. Fed. Am. Soc. Exp. Biol.* 21, 1472–1480 (2007).
629. Hughes, F. J., Turner, W., Belibasakis, G. & Martuscelli, G. Effects of growth factors and cytokines on osteoblast differentiation. *Periodontol. 2000* 41, 48–72 (2006).
630. Siddappa, R. *et al.* cAMP/PKA signaling inhibits osteogenic differentiation and bone formation in rodent models. *Tissue Eng. Part A* 15, 2135–2143 (2009).
631. Raucci, A., Bellosta, P., Grassi, R., Basilico, C. & Mansukhani, A. Osteoblast proliferation or differentiation is regulated by relative strengths of opposing signaling pathways. *J. Cell. Physiol.* 215, 442–451 (2008).
632. Hoare, J. I., Rajnicek, A. M., McCaig, C. D., Barker, R. N. & Wilson, H. M. Electric fields are novel determinants of human macrophage functions. *J. Leukoc. Biol.* 99, 1141–1151 (2016).
633. Cao, L. *et al.* Polarizing intestinal epithelial cells electrically through Ror2. *J. Cell Sci.* 127, 3233–3239 (2014).

634. Sheikh, A. Q. *et al.* Regulation of endothelial MAPK/ERK signalling and capillary morphogenesis by low-amplitude electric field. *J. R. Soc. Interface* 10, 20120548 (2013).
635. Matos, M. A. & Cicerone, M. T. Alternating current electric field effects on neural stem cell viability and differentiation. *Biotechnol. Prog.* 26, 664–670 (2010).
636. Okabe, S., Forsberg-Nilsson, K., Spiro, A. C., Segal, M. & McKay, R. D. Development of neuronal precursor cells and functional postmitotic neurons from embryonic stem cells in vitro. *Mech. Dev.* 59, 89–102 (1996).
637. Ariza, C. A. *et al.* The influence of electric fields on hippocampal neural progenitor cells. *Stem Cell Rev.* 6, 585–600 (2010).
638. Chang, H.-F., Lee, Y.-S., Tang, T. K. & Cheng, J.-Y. Pulsed DC Electric Field–Induced Differentiation of Cortical Neural Precursor Cells. *PLOS ONE* 11, e0158133 (2016).
639. D'Ascenzo, M. *et al.* Role of L-type Ca2+ channels in neural stem/progenitor cell differentiation. *Eur. J. Neurosci.* 23, 935–944 (2006).
640. Feng, Y., Luo, S., Yang, P. & Song, Z. Electric pulse current stimulation increases electrophysiological properties of If current reconstructed in mHCN4-transfected canine mesenchymal stem cells. *Exp. Ther. Med.* 11, 1323–1329 (2016).
641. Maddin, W. S., Bell, P. W. & James, J. H. M. The Biological Effects of a Pulsed Electrostatic Field with Specific Reference to Hair Electrotrichogenesis. *Int. J. Dermatol.* 29, 446–450 (1990).
642. Brighton, C. T., Unger, A. S. & Stambough, J. L. In vitro growth of bovine articular cartilage chondrocytes in various capacitively coupled electrical fields. *J. Orthop. Res. Off. Publ. Orthop. Res. Soc.* 2, 15–22 (1984).
643. Peters, E. J., Lavery, L. A., Armstrong, D. G. & Fleischli, J. G. Electric stimulation as an adjunct to heal diabetic foot ulcers: a randomized clinical trial. *Arch. Phys. Med. Rehabil.* 82, 721–725 (2001).
644. Wood, J. M. *et al.* A multicenter study on the use of pulsed low-intensity direct current for healing chronic stage II and stage III decubitus ulcers. *Arch. Dermatol.* 129, 999–1009 (1993).
645. Iglesias, M., Almuedo-Castillo, M., Aboobaker, A. A. & Saló, E. Early planarian brain regeneration is independent of blastema polarity mediated by the Wnt/β-catenin pathway. *Dev. Biol.* 358, 68–78 (2011).
646. Sisken, B. F., Kanje, M., Lundborg, G. & Kurtz, W. Pulsed electromagnetic fields stimulate nerve regeneration in vitro and in vivo. *Restor. Neurol. Neurosci.* 1, 303–309 (1990).
647. Miller, G. Inside the Strange New World of DIY Brain Stimulation. *Wired Magazine* (2014).
648. Hu, X. D., Huang, Q., Roadcap, D. W., Shenolikar, S. S. & Xia, H. Actin-associated neurabin-protein phosphatase-1 complex regulates hippocampal plasticity: Neurabin-PP1 regulates hippocampal plasticity. *J. Neurochem.* 98, 1841–1851 (2006).
649. Silberberg, G., Wu, C. & Markram, H. Synaptic dynamics control the timing of neuronal excitation in the activated neocortical microcircuit: Synaptic dynamics shape cross-correlations. *J. Physiol.* 556, 19–27 (2004).

650. LoCascio, S. A., Lapan, S. W. & Reddien, P. W. Eye Absence Does Not Regulate Planarian Stem Cells during Eye Regeneration. *Dev. Cell* 40, 381-391.e3 (2017).
651. Wen, L., Zhang, C., Nong, Y., Yao, Q. & Song, Z. Mild Electrical Pulse Current Stimulation Upregulates S100A4 and Promotes Cardiogenesis in MSC and Cardiac Myocytes Coculture Monolayer. *Cell Biochem. Biophys.* 65, 43–55 (2013).
652. Hess, R. *et al.* Synergistic effect of defined artificial extracellular matrices and pulsed electric fields on osteogenic differentiation of human MSCs. *Biomaterials* 33, 8975–8985 (2012).
653. Tsai, M.-T., Li, W.-J., Tuan, R. S. & Chang, W. H. Modulation of osteogenesis in human mesenchymal stem cells by specific pulsed electromagnetic field stimulation. *J. Orthop. Res. Off. Publ. Orthop. Res. Soc.* 27, 1169–1174 (2009).
654. Schoenbach, K. H., Peterkin, F. E., Alden, R. W. & Beebe, S. J. The effect of pulsed electric fields on biological cells: experiments and applications. *IEEE Trans. Plasma Sci.* 25, 284–292 (1997).
655. Markx, G. H. The use of electric fields in tissue engineering: A review. *Organogenesis* 4, 11–17 (2008).
656. Teissié, J., Escoffre, J., Rols, M. & Golzio, M. Time dependence of electric field effects on cell membranes. A review for a critical selection of pulse duration for therapeutical applications. *Radiol. Oncol.* 42, (2008).
657. Smith, S. D., Thomas, C. L. & Frasch, S. F. 209 - Lanthanum Inhibition of Electrically Induced Dedifferentiation in Frog Erythrocytes. *Bioelectrochem. Bioenerg.* 5, 177–184 (1978).
658. Jansen, J. H. *et al.* Stimulation of osteogenic differentiation in human osteoprogenitor cells by pulsed electromagnetic fields: an in vitro study. *BMC Musculoskelet. Disord.* 11, (2010).
659. Mustard, J. & Levin, M. Bioelectrical Mechanisms for Programming Growth and Form: Taming Physiological Networks for Soft Body Robotics. *Soft Robot.* 1, 169–191 (2014).
660. Cebrià, F., Vispo, M., Newmark, P., Bueno, D. & Romero, R. Myocyte differentiation and body wall muscle regeneration in the planarian Girardia tigrina. *Dev. Genes Evol.* 207, 306–316 (1997).
661. Cebrià, F. Planarian Body-Wall Muscle: Regeneration and Function beyond a Simple Skeletal Support. *Front. Cell Dev. Biol.* 4, 8 (2016).
662. Tabata, T. Morphogens, their identification and regulation. *Development* 131, 703–712 (2004).
663. Rogulja, D. & Irvine, K. D. Regulation of Cell Proliferation by a Morphogen Gradient. *Cell* 123, 449–461 (2005).
664. Ulloa, F. & Briscoe, J. Morphogens and the Control of Cell Proliferation and Patterning in the Spinal Cord. *Cell Cycle* 6, 2640–2649 (2007).
665. Zecca, M., Basler, K. & Struhl, G. Direct and Long-Range Action of a Wingless Morphogen Gradient. *Cell* 87, 833–844 (1996).
666. Brennecke, J., Hipfner, D. R., Stark, A., Russell, R. B. & Cohen, S. M. bantam Encodes a Developmentally Regulated microRNA that Controls Cell Proliferation and Regulates the Proapoptotic Gene hid in Drosophila. *Cell* 113, 25–36 (2003).

667. Hart, R. A. & Gandhi, O. P. Comparison of cardiac-induced endogenous fields and power frequency induced exogenous fields in an anatomical model of the human body. *Phys. Med. Biol.* 43, 3083–3099 (1998).
668. Cotterell, J. & Sharpe, J. An atlas of gene regulatory networks reveals multiple three-gene mechanisms for interpreting morphogen gradients. *Mol. Syst. Biol.* 6, (2010).
669. Fosslien, E. Hormetic Electric Field Theory of Pattern Formation. *Dose-Response* 8, dose-response.1 (2010).
670. George, M. S. & Aston-Jones, G. Noninvasive techniques for probing neurocircuitry and treating illness: vagus nerve stimulation (VNS), transcranial magnetic stimulation (TMS) and transcranial direct current stimulation (tDCS). *Neuropsychopharmacology* 35, 301–316 (2010).
671. Macias, M. Y., Battocletti, J. H., Sutton, C. H., Pintar, F. A. & Maiman, D. J. Directed and enhanced neurite growth with pulsed magnetic field stimulation. *Bioelectromagnetics* 21, 272–286 (2000).
672. Zhang, Y., Ding, J., Duan, W. & Fan, W. Influence of pulsed electromagnetic field with different pulse duty cycles on neurite outgrowth in PC12 rat pheochromocytoma cells. *Bioelectromagnetics* 26, 406–411 (2005).
673. Sisken, B. F., Midkiff, P., Tweheus, A. & Markov, M. Influence of static magnetic fields on nerve regeneration in vitro. *The Environmentalist* 27, 477–481 (2007).
674. Luo, X.-D. *et al.* Energy controllable steep pulse (ECSP) treatment suppresses tumor growth in rats implanted with Walker 256 carcinosarcoma cells through apoptosis and an antitumor immune response. *Oncol. Res.* 20, 31–37 (2012).
675. Park, J.-E. *et al.* Electromagnetic fields induce neural differentiation of human bone marrow derived mesenchymal stem cells via ROS mediated EGFR activation. *Neurochem. Int.* 62, 418–424 (2013).
676. Kim, H.-J. *et al.* Extremely low-frequency electromagnetic fields induce neural differentiation in bone marrow derived mesenchymal stem cells. *Exp. Biol. Med.* 238, 923–931 (2013).
677. Fuchs, E. & Flügge, G. Adult neuroplasticity: more than 40 years of research. *Neural Plast.* 2014, 541870 (2014).
678. Seebeck, F. *et al.* Integrins are required for tissue organization and restriction of neurogenesis in regenerating planarians. *Development* 144, 795–807 (2017).
679. Bonar, N. A. & Petersen, C. P. Integrin suppresses neurogenesis and regulates brain tissue assembly in planarian regeneration. *Development* 144, 784–794 (2017).
680. Currie, K. W., Molinaro, A. M. & Pearson, B. J. Neuronal sources of hedgehog modulate neurogenesis in the adult planarian brain. *eLife* 5, (2016).
681. Lee, R. T. H., Zhao, Z. & Ingham, P. W. Hedgehog signalling. *Development* 143, 367–372 (2016).
682. Paulis, L. *et al.* Activation of Sonic hedgehog signaling in ventricular cardiomyocytes exerts cardioprotection against ischemia reperfusion injuries. *Sci. Rep.* 5, (2015).
683. Belgacem, Y. H. & Borodinsky, L. N. Sonic hedgehog signaling is decoded by calcium spike activity in the developing spinal cord. *Proc. Natl. Acad. Sci.* 108, 4482–4487 (2011).

684. Seegers, J. C. *et al.* A pulsed DC electric field affects P2-purinergic receptor functions by altering the ATP levels in in vitro and in vivo systems. *Med. Hypotheses* 58, 171–176 (2002).
685. Aleem, I. S. *et al.* Efficacy of Electrical Stimulators for Bone Healing: A Meta-Analysis of Randomized Sham-Controlled Trials. *Sci. Rep.* 6, (2016).
686. Lawson, D. & Petrofsky, J. S. A randomized control study on the effect of biphasic electrical stimulation in a warm room on skin blood flow and healing rates in chronic wounds of patients with and without diabetes. *Med. Sci. Monit. Int. Med. J. Exp. Clin. Res.* 13, CR258-263 (2007).
687. Pearson, B. J. *et al.* Formaldehyde-based whole-mount in situ hybridization method for planarians. *Dev. Dyn.* 238, 443–450 (2009).
688. King, R. S. & Newmark, P. A. In situ hybridization protocol for enhanced detection of gene expression in the planarian Schmidtea mediterranea. *BMC Dev. Biol.* 13, 8 (2013).
689. Fincher, C. T., Wurtzel, O., de Hoog, T., Kravarik, K. M. & Reddien, P. W. Cell type transcriptome atlas for the planarian Schmidtea mediterranea. *Science* eaaq1736 (2018). doi:10.1126/science.aaq1736
690. Grohme, M. A. *et al.* The genome of Schmidtea mediterranea and the evolution of core cellular mechanisms. *Nature* 554, 56–61 (2018).
691. Atabay, K. D., LoCascio, S. A., de Hoog, T. & Reddien, P. W. Self-organization and progenitor targeting generate stable patterns in planarian regeneration. *Science* 360, 404–409 (2018).
692. Adams, D. S., Masi, A. & Levin, M. H+ pump-dependent changes in membrane voltage are an early mechanism necessary and sufficient to induce Xenopus tail regeneration. *Development* 134, 1323–1335 (2007).
693. Miller, G. Inside the Strange New World of DIY Brain Stimulation. *Wired Magazine* (2014).
694. Forsthoefel, D. J., Waters, F. A. & Newmark, P. A. Generation of cell type-specific monoclonal antibodies for the planarian and optimization of sample processing for immunolabeling. *BMC Dev. Biol.* 14, (2014).
695. Ross, K. G. *et al.* Novel monoclonal antibodies to study tissue regeneration in planarians. *BMC Dev. Biol.* 15, 2 (2015).
696. Liu, S.-Y. & Rink, J. C. Total RNA Isolation from Planarian Tissues. in *Planarian Regeneration* (ed. Rink, J. C.) 1774, 259–265 (Springer New York, 2018).